SINGLE POLYMER COMPOSITES MADE OF SLOWLY CRYSTALLIZING POLYMERS

A Dissertation
Presented to
The Academic Faculty

by

Ruihua Li

In Partial Fulfillment
of the Requirements for the Degree
Doctor of Philosophy in the
School of Polymer, Textile and Fiber Engineering

Georgia Institute of Technology
May 2009

COPYRIGHT 2009 BY RUIHUA LI

SINGLE POLYMER COMPOSITES MADE OF

SLOWLY CRYSTALLIZING POLYMERS

Approved by:

Dr. Donggang Yao, Advisor
School of Polymer, Textile and Fiber Engineering
Georgia Institute of Technology

Dr. W. Steven Johnson
School of Materials Science and Engineering
Georgia Institute of Technology

Dr. Karl Jacob
School of Polymer, Textile and Fiber Engineering
Georgia Institute of Technology

Dr. Rina Tannenbaum
School of Materials Science and Engineering
Georgia Institute of Technology

Dr. Youjiang Wang
School of Polymer, Textile and Fiber Engineering
Georgia Institute of Technology

Date Approved: November 24, 2008

ACKNOWLEDGEMENTS

I am deeply indebted to my thesis advisor, Dr. Donggang Yao, for his great guidance, support and encouragement during my PhD study and research. I wish to sincerely thank him for his extreme patience in helping me through different aspects of my graduate study.

I would like to thank my committee members, Dr. Karl Jacob, Dr. Youjiang Wang, Dr. Steven Johnson, and Dr. Rina Tannenbaum, for their valuable inputs to my thesis. Their comments have indeed helped in improving the quality of this work.

I wish to express my appreciation to Dr. Shanjun Zhang, for his useful suggestions on morphological studies. I would like to thank Dr. Radhakrishnaiah Parachuru for his warmhearted help for the experiments.

I would like to thank my group members, Pratapkumar Nagarajan, Jun Jia, Wei Zhang, Ramasubramani Kuduva-Raman-Thanumoorthy, Sarang Deodhar, Ian Winters and Yutong Pan, for their understanding and constant encouragement. I would also like to thank Xuxia Yao, Vibhor Jain, and Sudhakar Jagannathan for their kind help during my research.

Last, but most certainly not the least, I would like to take this opportunity to thank my parents, Ying Li and Shufan Liu, my sister, Jinling Li, my brother-in-law Jiyu Yuan, my husband, Jian Zhu, my parents-in-law, Huaguang Zhu and Lijin Feng for their endless love and support.

TABLE OF CONTENTS

LIST OF TABLES

Page

LIST OF FIGURES

Page

LIST OF SYMBOLS AND ABBREVIATIONS

AFM	Atomic force microscopy
A-PET	Amorphous poly (ethylene terephthalate)
DSC	Differential scanning calorimetry
ΔHc	Enthalpy of cold crystallization of the sample
ΔHm	Melt enthalpy of the sample
ΔHm*	Ideal crystalline melt enthalpy of the sample
HDPE	High-density polyethylene
LDPE	Low-density polyethylene
PET	Poly (ethylene terephthalate)
PLA	Poly (lactic acid)
PMMA	Poly (methyl methacrylate)
PP	Polypropylene
SEM	Scanning electron microscopy
SPCs	Single polymer composites
Tg	Glass transition temperature
Tm	Melting temperature
TEM	Transmission electron microscope
TGA	Thermo-gravimetric analysis
UHMWPE	Ultra-high molecular weight polyethylene
WAXS	Wide-angle X-ray scattering
XRD	X-ray diffraction

SUMMARY

Composites are widely used in an increasing number of applications in diverse fields. However, most traditional composite materials are difficult to recycle. Because of their enhanced recyclability, thermoplastic single-polymer composites (SPCs), i.e., composites with fiber and matrix made from the same thermoplastic polymer, have attracted much attention in the recent years. High-performance polymer fibers in combination with same polymer matrices would lead to a fully recyclable single polymer composite that has major ecological advantages. However, because a single polymer is involved in the composite, thermoplastic SPCs manufacturing presents a unique set of technical problems, and different approaches from those in standard composites manufacturing are frequently needed. Two specific issues in SPCs manufacturing are how to produce distinct forms of the same polymer and how to consolidate them. So far, most investigations have been reported on a single-component hot compaction method and two-component molecular methods. However, in these methods, either the processing window is too narrow or some impure materials are introduced into the system. The key issue in thermoplastic SPCs processing is how to melt-process the matrix without significantly annealing or even melting the fiber. To overcome the above drawbacks in existing SPCs processing, particularly to widen the SPCs processing temperature window and to purify the SPCs, a novel SPCs manufacturing process utilizing the characteristics of slowly crystallizing polymers was developed and investigated. Highly oriented and highly crystalline fibers made of a slowly crystallizing polymer are mixed with the amorphous form of the same polymer and then consolidated

together under heat and pressure. In this dissertation research, two slowly crystallizing polymers, poly(ethylene terephthalate) (PET) and poly(lactic acid) (PLA), were used as model systems for SPCs processing.. To study the deformation and failure mechanisms of PET and PLA SPCs, the SPCs were characterized using tensile test, tearing test, impact test, SEM, optical microscopy, and other methods. The change of crystallinity and orientation of the material forms during SPCs processing were characterized by DSC and XRD. The effects of major process conditions on the performance of the SPCs were studied. It was found that the processing temperature played a profound role in affecting the fiber-matrix bonding property. The compression molded SPCs exhibited enhanced mechanical properties. For the PET SPCs with 45% by weight fiber content the tensile strength is four folds of that of non-reinforced PET. After reinforcement, the tearing strength of the PLA SPCs is almost an order higher than that of the non-reinforced PLA.

The fusion bonding behavior of two crystallizable amorphous PET sheets was also studied. Several characterization methods including SEM, TEM and polarized microscopy (either on etched or on non-etched samples) were used to observe interfacial bonding morphology of the crystallizable amorphous PET sheets. For a bonded sample, a layer of transcrystals with a thickness of 1-2 μm was found right at the interface. A secondary but much larger zone with a distinct morphology was observed outside the transcrystal layer. With increase of the heating time, the width of the whole interfacial region decreases. The interfacial morphology was found to significantly affect the interfacial bonding quality. The testing results further indicated that high bonding temperature with an appropriate holding time promotes interfacial bonding of two crystallizable amorphous PET.

CHAPTER 1

INTRODUCTION

1.1 Single polymer composites

Polymer composites are being used in steadily increasing quantities in diverse fields, e.g., aerospace, automotive, electrical, microelectronics, infrastructure and construction, medical, and chemical industries, as a result of improved material performance, cost-effective production, and manufacturing flexibility (especially with thermoplastics as matrix materials). Compared to the widespread and widely documented activities on polymer recycling, the work on recycling of composites is still modest. However, as composites are more widely used in an increasing number of commodity products, the issue of composites recycling is becoming ever more important. Unfortunately, not all polymer composites are equally easy to recycle. Since thermoplastics can in theory be re-melted and cooled to solidify for an infinite number of times, recycling of thermoplastic composites through material recovery is easier than that for thermosets. While this is generally the case, each re-melting unfortunately causes the material to gradually degrade. More notably, the presence of additives or inclusions such as glass fibers greatly limits the recyclability of the composite and the application of the recyclate. Hence, there is a need for systems consisting of a minimum number of different polymers. This in the ideal case means mono-component systems or in other words single polymer composites.

The concept of single polymer composites is not new. The original concept was proposed by Mead and Porter almost 30 years ago [1]. Since then, different methods have been proposed for formulating and processing single polymer composites, referring

mainly to polyethylene (PE) and polypropylene (PP). In order to increase the potential of single polymer composites, it is essential to have polymer fibers and matrices optimized in structure, properties, and processing performance. Isotropic polymers have relatively low mechanical properties because of the relatively weak interactions that exist between the polymer chains. Therefore, high-strength and high-modulus fibers are needed in order to reinforce the matrix material. The development of high-performance polymer fibers has been highly achieved for more than 40 years in the past, and most approaches are based on forming the polymers into filaments and post-drawing them uniaxially in the solid state in order to orient the molecules in the direction of the applied load [2]. A high degree of chain-extension in combination with a high molar mass is needed for high-performance fibers. Since the molecular chains of thermoplastic polymers have a finite length, chain overlap is needed for load transfer through the system. Thus, in practice, the use of high molecular weight polymers is preferred. In the literature various processes have been described to orient the chains directly in the molten state. The problem of chain orientation and extension in the melt is that extensive relaxation occurs, i.e., the chains resist deformation and retract back to a random coil conformation. Consequently, in order to obtain a high degree of chain extension, drawing should be performed in a separate step, after processing and below the melting point, viz. in the (semi)solid state. Next, to achieve good mechanical properties a clear difference in the melting temperatures of the fiber- and matrix-materials is required for manufacturing single polymer composites. This problem is generally tackled by using different polymer grades for the fiber and the matrix, e.g., ultra high molecular weight polyethylene (UHMPE) for the fiber and high density polyethylene (HDPE) for the matrix [3, 4]. However, for true

single polymer composites, the matrix and the fiber should originate from the same polymer grade, and hence should have similar melting temperatures. In this case, it is difficult to combine the fiber with the matrix, without melting the oriented fiber and thus losing stiffness and strength developed in the drawing process.

One of the important rules in ‘designing for recycling’ is based on selecting the smallest possible number of different constituents in a material system or, alternatively, in the case of plastics, selecting compatible polymers, which in practice means the use of monomaterials. Automotive manufacturers are forced to make every component recyclable, resulting in decreasing use of traditional fiber reinforced plastics in vehicles. The inclusion of any ‘foreign’ fillers, including natural fibers, are in conflict with the basic idea behind ‘designing for recycling’. Instead, an appealing reinforcing element for matrix would be a high-performance polymer fiber made of the same polymer as the matrix.

High-performance polymer fibers in combination with same polymer matrices will lead to a fully recyclable, single polymer composite that has major ecological advantages. Besides recyclability, the use of single polymer composites has a number of other ecological and technological advantages compared with glass fibers. Polymer fibers are nonabrasive to processing equipment, can be thermally recycled at the end of their lifetime for energy recovery, and have a very low density, which can potentially lead to lightweight parts, lowering fuel consumption and gas emissions. Another advantage of using a more flexible and ductile fiber will be improved crash behavior. Single polymer composites will not splinter, but fail in a more ductile manner. Such ‘soft’ crash behavior

is of significant interest for various inner-trim parts as well as for external panels, bumper bars, etc., since it will lead to safer automobiles.

1.2 Need of the research

Single-polymer composites (SPCs) are composites with matrix and reinforcement made of the same polymer. They are environmentally benign materials and can be recycled following the standard single polymer recycling practice. The recently growing number of investigations in SPCs manufacturing is driven by the increasing use of composites in consumer products and thus the need of fully recyclable materials. Because a single polymer is involved in the composite, SPCs manufacturing present a unique set of technical problems and different approaches from those in standard composites manufacturing are frequently needed. The specific issues in SPCs manufacturing are how to produce distinct forms of the same polymer and how to consolidate them. So far, most investigations have been reported on a single-component hot compaction method and two-component molecular methods. For the single-component hot compaction method, the fibers are heated near its melting temperature. The fiber surface will melt and recrystallize to serve as a matrix to glue these fibers together. However, the processing temperature window is very narrow, less than 5°C. The later method can overcome the limitation of a small process window in the former process, but it is not a true SPCs approach. Some impurities are introduced into the system. Besides the fiber hot compaction method and two-component molecular methods, over heating of constrained fibers, solution imbedding and other methods have been used to manufacture single polymer composites. Although some of these methods can effectively enlarge the process window, they are difficult to implement in practice. In particular, the constrained fiber

over heating method requires a special and complex tool during processing and is limited to simple sample geometries. Solution involved methods, on the other hand, is a slow process and is also an environmental unfriendly process. Hence, there emerges a great need for the development of economically more viable and environmentally more friendly methods for true SPCs processing and manufacturing.

1.3 Objectives and technical approach

The previous work on SPCs mainly involved fast crystallizing polymers such as polyethylene and polypropylene. However, for these polymers, the proximity in the melting temperatures between the fiber and the matrix poses a considerable difficulty during SPCs processing. To enlarge the processing temperature window, a new approach to SPCs processing utilizing the unique characteristics of slowly crystallizing polymers was proposed, with PET and PLA as model systems. With a slowly crystallizing polymer, distinct physical forms having a large difference in melting/softening temperatures can be created. These single-polymer entities can then be consolidated into a composite material. In the SPCs, the reinforcement can be highly oriented, highly crystalline fibers, and the matrix can be a more amorphous and less orientated material entity made from the same grade of slowly crystallizing polymer. Because of its slow crystallization rate, a slowly crystallizing polymer can be processed into a low-crystallinity or amorphous material entity, more easily than a fast crystallizing polymer. To prepare an amorphous material, the slowly crystallizing polymer is heated above its melting temperature (Tm) and then rapidly quenched below its glass transition temperature (Tg) to suppress crystallization. Upon reheating above Tg, the amorphous material becomes viscous and can glue together to form a matrix for the reinforcing material. Since the processing temperature is only

above Tg but well below Tm, the reinforcements can keep their high orientation and high crystallinity in the final SPCs product. The processing temperature window in this case ranges from Tg to Tm, much wider than those reported in the literature. There are also no impurities introduced into the SPCs material. During recycling, the composites just need to be heated above Tm; the fiber and the matrix will melt together and become the single polymer.

Therefore, to address the drawbacks in traditional SPCs processing, specifically, to widen the processing temperature window and to purify the material, we proposed to use slowly crystallizing polymers for SPCs processing and manufacturing. High-strength fabrics of a slowly crystallizing polymer such as PET or PLA are laminated with amorphous sheets of the same-grade polymer and consolidated together under heat and pressure. The specific tasks of the research included:

1) To test the technical feasibility of the proposed method using two slowly crystallizing polymers, PET and PLA, and determine the optimum processing conditions for PET and PLA SPCs processing.
2) To study the deformation and failure mechanisms of PET and PLA SPCs under different mechanical testing conditions and conduct morphological characterizations of the fracture interface.
3) To characterize the interfacial morphology at the fusion bond formed by two crystallizable amorphous PET films and understand the fusion bonding mechanism.

1.4 Overview of following chapters

A detailed literature survey on the current methods for SPCs formulation and manufacturing are provided in Chapter 2. From materials perspectives, the reinforcement and the matrix of SPCs can be the same polymer with the same chemical composition but different molecular structures or the same polymer with the same chemical structure but different physical states. These material formulation methods may involve variation of molecular weight, chain configuration, tacticity, molecular orientation, crystallinity, and others. Known methods for processing these material forms into SPCs are then described. Chapter 2 further provides a literature survey on the consolidation mechanism and the crystallization mechanism of thermoplastic polymers. Typical methods used for etching-based morphological studies are also surveyed.

The mechanism for SPCs manufacture utilizing the unique crystallization kinetics of slowly crystallizing polymers is introduced in Chapter 3. The Concept development is discussed and the results on experimental verification are presented.

To make SPCs using slowly crystallizing polymer and investigate the processing and concepts of this new method, two types of common slowly crystallizing polymers, PET and PLA, were tested. The results on PET SPCs are given in Chapter 4. The effects of processing conditions on the performance of PET SPCs were explored. The PET SPCs processed by the new method were compared with two commercially available single polymer composites. The effects of heat treatment on the orientation and crystallinity of PET fibers were also studied.

The fusion bonding behavior of crystallizable amorphous polymers is discussed in Chapter 5. Upon reheating above Tg, a crystallizable amorphous polymer experiences

two competing processes; fusion bonding and crystallization compete with each other. Thus the fusion bonding behavior of a crystallizable amorphous polymer is more complex than that of a non-crystallizable amorphous polymer. It was found that the interfacial bonding quality is significantly affected by the state of crystallization and the morphological development at the bonding interface. It was also found that, at different processing temperature, the fusion bonding behavior is different. At low temperature, with the increase of heating time, the bonding strength decreases monotonically. At higher temperature, the bonding strength increases first and then decreases. At the temperature near the melting temperature, the fusion bonding behavior is similar with amorphous polymer.

Chapter 6 deals with the morphological studies at the bonding interface of two crystallizable amorphous PET films. When the heating time is short, the growth of the crystal of slowly crystallizing polymer is limited. Thus the crystals are small, and it is difficult to observe such crystals using standard protocols. To enhance the contrast in microscopy, the samples were properly etched first and then observed under high-resolution SEM and TEM to identify the unique morphology formed at the bonding interface. Double interfacial regions were observed at the bonding interface, and their appearance was found to be significantly affected by the processing conditions, particularly by the heating temperature and the holding time.

The findings from the focused study on PLA SPCs are provided in Chapter 7. The optimum processing conditions for PLA SPCs manufacturing were determined. The mechanical properties of PLA SPCs were evaluated. To test the formability into 3-D shapes, a case study involving a PLA SPCs dome was preformed.

CHAPTER 2

LITERATURE SURVEY

2.1 Single polymer composites

In traditional heterogeneous composites, the matrix and the reinforcement have very different physical and chemical properties. Manufacturing of these composites can be simply treated as liquid-state deformation of the matrix material. Through the flow and solidification of the matrix material, the reinforcement is encapsulated evenly in the composite. The situation becomes more complicated in SPCs manufacturing. Since they are derived from a single polymer, the matrix and the reinforcement in SPCs are subjected to strong physical and chemical coupling effects during manufacturing. For example, they tend to undergo transitions, either chemical or physical, under the same condition. Therefore, means for decoupling such coupling effects and enlarge the difference in processing conditions between the matrix and the reinforcement are needed in SPCs manufacturing. The polymer in SPCs manufacturing cannot be simply treated as a plastic. Instead, material-aware approaches are needed and the method may differ from one polymer to another.

It should be mentioned that there have been much parallel work on self-reinforcing polymer processing. In self-reinforcing polymer processing, the polymer is deformed as a solid or a semi-solid, rather than a liquid as in processes such as extrusion and injection molding. The resulting part is self-reinforced by preferred molecular orientations. Although solid-state forming is also intended to obtain a stronger single polymer, it does not involve a composite approach for forming a strengthened polymer as

in SPCs manufacturing. Further, solid-phase forming in most cases only works for objects with small diameters or thickness, e.g. fibers and films.

Different approaches have been developed for formation of SPCs, including hot compaction of fibers [5, 6], hot compaction of two components [7, 8], solution impregnation of two components [9], constrained fiber processing [10], copolymer approach [11], variation of molecular weight [7, 9], variation of chain configuration [12], and others. Different physical states and material forms of raw polymers have been used in SPCs manufacturing, including melts, solutions, powders, films, tapes, unidirectional lay-ups, chopped fiber, and fabrics. It is noted that although these different methods were developed for different materials and applications, some of them share certain commonality and may thus be categorized based on their similar characteristics. With appropriate classification, different processes may be studied in the same group with a focus on understanding the basic material formulation and/or manufacturing problem and the commonality of these processes, which would in turn facilitate the development of more effective methods. A unified classification framework for SPCs formulation and manufacturing has been summarized in Figure 2.1 by the author. Because in a single polymer composite reinforcement and matrix are made from the same polymer, their melting temperatures are close to each other. Thus, SPCs manufacturing presents a unique set of technical problems, needing to be specifically addressed for successful applications.

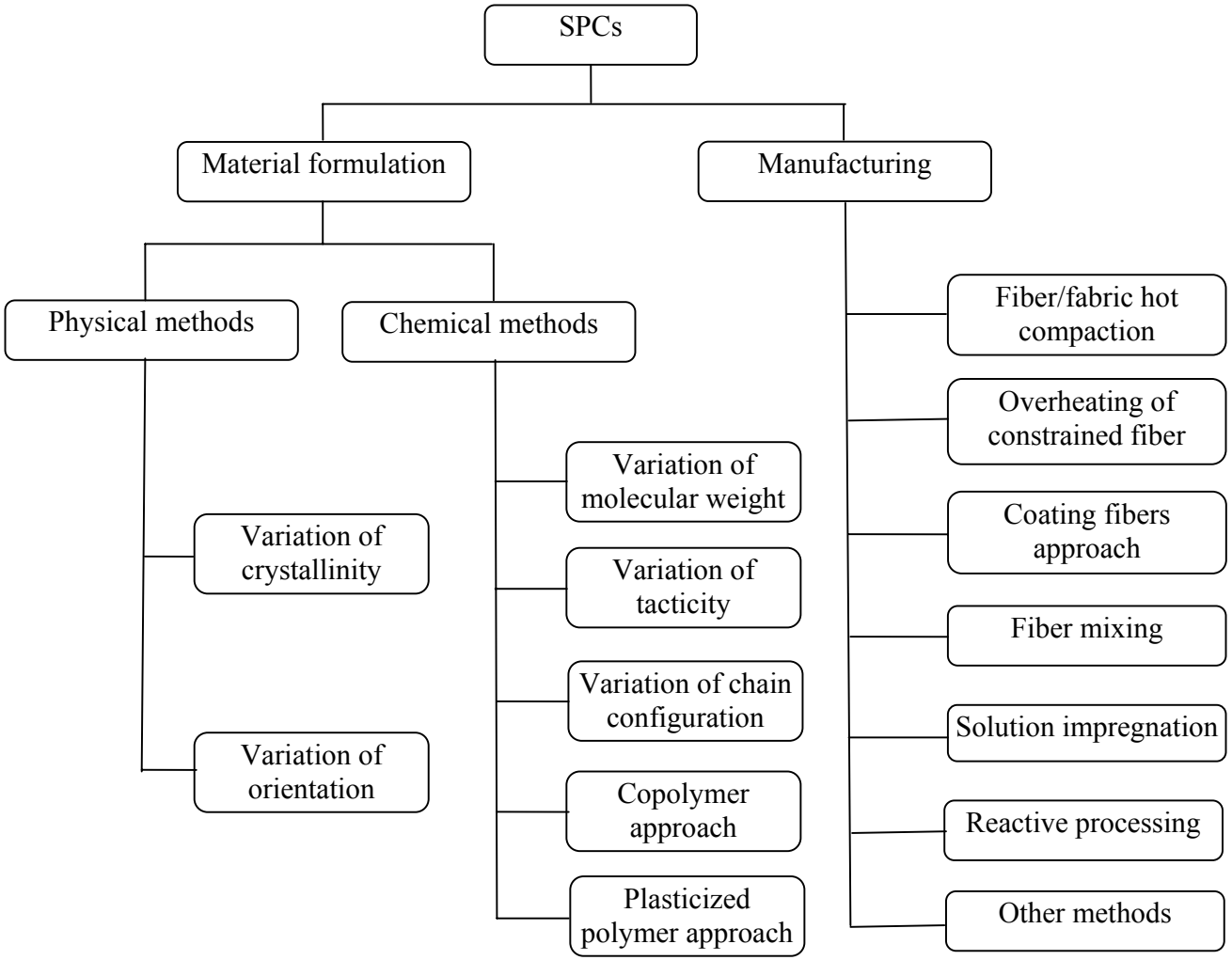

Figure 2.1 A framework for SPCs manufacturing

2.1.1 Material formulation

From materials perspectives, SPCs can be formulated both by chemical methods and by physical methods.

2.1.1.1 Chemical methods

To enlarge the process window, the original SPCs concept may be relaxed and extended to the incorporation of polymers with the same chemical composition but different chemical structures [9-12]. Examples are HDPE matrix reinforced by UHMWPE fibers [7, 9] and low-density PE (LDPE) matrix reinforced by HDPE fibers [1]. In both cases, a process window of about 20°C is resulted. When LDPE is reinforced by UHMWPE fibers, the process window can be further enlarged to about 40°C [12].

In general, for the same molecular composition, the melting/softening temperature of the polymer can be varied by varying the molecular weight and the chain configuration. For the "variation of molecular weight" method, HDPE matrix reinforced by UHMWPE fibers [7, 9] is a good example. The crystallization kinematics and thus the melting temperature of a polymer can also be altered by employment of chain branches. For example, LDPE, a branched polymer, has a much lower melting temperature than HDPE, a linear polymer, and thus can be reinforced by the latter [1]. In addition, the tacticity of the polymer chain can be varied to control crystallization. It is well known that from atatic to syndiotactic and further to isotactic, the ease in crystallization increases. Thus, syndiotactic polystyrene (PS) may be used as reinforcement for atatic PS, and isotatic PP (iPP) can be used as reinforcement for a more atatic PP.

The copolymer approach is another molecular method. A so-called "PURE® Technology" process, utilizing co-polyolefins or co-polyesters, is commercially available. This process was developed by two Universities: Eindhoven University of Technology (SKT) in the Netherlands and Queen Mary and University of London in the UK, and four industrial partners, all from the Netherlands: Lankhorst-Indutech, BW Industrial, Polynorm Plastics and DSM [11]. Two types of PP with different melting temperature were coextruded (Figure 2.2). The core is made of highly oriented pure PP, while the skin is made of a PP copolymer with a lower melting temperature. The coextruded tapes were cold drawn to increase the mechanical properties. At final stage, these tapes were welded together under heat. The oriented PP core provides strength and stiffness, and the thin copolymer skin with a lower melting temperature than the core material forms the matrix. One of the advantages of using tapes instead of fibers is the more effective packing that flat tapes enable compared with circular fibers, leading to higher reinforcement contents in the final product. Consolidation is achieved by simply welding the tapes together, thus avoiding the typical impregnation problems encountered in traditional thermoplastic composite manufacturing. By using this method, the processing window can be widened to 20-40°C. This copolymer process has been commercialized by Lankhorst-Indutech in the Netherlands under the trade name PURE® [13]. With this process, laminates made from woven fabrics have been shown to exhibit a typical stiffness of 6-8 GPa and a tensile strength of around 200-250 MPa [14]. However, since copolymers were introduced into the system, the resulting material is not a real single polymer composite.

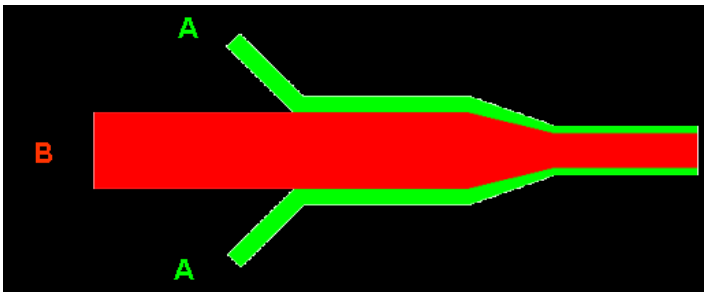

Co-extrusion and cold drawing

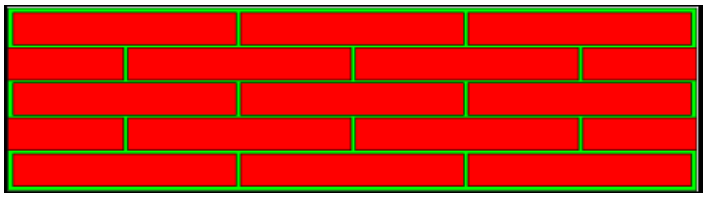

Consolidation

Figure 2.2 Co-extrusion technology is used for the development of high-performance polypropylene tapes. These tapes consist of a highly oriented core (B) and a thin co-polymer skin (A) to weld the tapes together in a subsequent consolidation process. This process results in a PP-based composite with very high reinforcement content (>80%) [11].

2.1.1.2 Physical methods

Traditional composites manufacturing adopts a two-component approach, in which the reinforcement and the matrix are two distinct components at the beginning of manufacturing. The feasibility of composites manufacturing is established on the basis that the reinforcement will be affected little during the flow and deformation of the matrix. Likewise, the reinforcement and the matrix of SPCs manufacturing should bear distinct properties in order to successfully produce SPCs. From a fundamental standpoint, SPCs processing can be resolved into two elementary steps: 1) preparation of two

different phases, and 2) consolidation of the two distinct phases. Each fundamental step has its own objectives to fulfill and questions to answer and may be realized using different technical approaches.

One approach for preparation of different phases of the same polymer is to vary the physical structure of the polymer. It is well known that the melting or softening temperature of the polymer depend on its physical state, i.e., amorphous state, crystalline state and amount of crystallinity. With appropriate control of processing conditions, different physical forms having a significant difference in melting temperature may be produced. For instance, a low-crystallinity unoriented film of polyamide may be produced using a combined relaxation and rapid quenching approach, i.e., relaxation of the molecular orientation caused by deformation followed by rapid quenching to reduce crystallinity. On the other hand, highly oriented and highly crystalline fibers of the same polyamide can be produced using a self-reinforcing fiber processing method, e.g. solid-state drawing, high temperature heat setting, gel spinning, etc. Similarly, highly oriented fibers with a higher softening temperature than a more isotropic matrix material can be prepared for an amorphous polymer. In this case the SPCs are made from the same grade of amorphous polymer with different molecular orientations. For examples, the fibers are highly orientated PMMA fibers, and the matrix is made of lightly orientated or unorientated PMMA. Hot compaction can be used to consolidate the matrix for this SPCs material.

2.1.2 Manufacturing methods

Although the SPCs approach did not attract much attention from the composites research community in the earlier days following Capiati and Porter's pioneering work, there has been consistently growing interest in manufacturing of new SPCs after the 1990s. SPCs have been successfully manufactured for a variety of different polymers, including PE [8, 15-19], PP [20-24], PET [25], poly(ethylene naphthalate) (PEN) [29], PLA [10, 30-33], polyamides [10], PMMA [34-36], etc. This trend in technological development in composites manufacturing is primarily driven by the increasing concern on the environment and thus the need of recyclable materials. As composites are more widely used in an increasing number of commodity products, the issue of composites recycling is becoming ever more important [37].

A major challenge in the development of single polymer composites is the creation of a processing window where fibers and matrix resin, made of the same polymer, can be combined. This is of eminent importance, as one has to combine two materials with basically the same chemical structure and, thus, similar melting temperatures. To make single polymer composites, different manufacturing methods can be used, such as hot compaction, solution impregnation, film stacking, fibers mixing and others. Hot compaction is the most widely used method for making single polymer composites. With this method, the material preforms are simply consolidated into SPCs by applying heat and pressure. A possible alternative to hot compaction is a solvent-assisted process. In this case, minor solvent can be applied as a binding agent at the surface of the fiber through vapor treating or other methods, resulting in a significant reduction in softening temperature for the fiber surface portion. Amorphous polymer fibers may be easily treated with an appropriate solvent. Some semicrystalline polymer,

such as PLA and nylon may also be effectively treated using solvents. With solvent treatment, compaction may be carried out at room temperature. After consolidation, the solvent can be extracted in a coagulation bath. Several SPCs manufacturing methods mentioned in the literature are summarized below.

2.1.2.1 Fiber hot compaction route

The fiber hot-compaction route for SPCs manufacturing was initially developed by Ward et al. at the Polymer IRC (Interdisciplinary Research Center) at University of Leeds in the UK [26]. It is now the most popular method for manufacturing single polymer composites. In fiber hot compaction, when the temperature is close to, but below Tm, the polymer fiber surface can be partially melted without melting the inner material of the fiber. The melted surface can be fused together, and the fibers are converted into a solid plaque. The essence of the process is to melt only a surface fraction of each fiber under a comparatively low contact pressure, and then to apply a substantially higher pressure for a short time to achieve excellent consolidation of the structure [27-29]. Upon cooling this molten surface material recrystallizes to form a matrix, which binds the fibers together [5, 38-42]. A combination of mechanical measurements and structural studies, such as wide-angle X-ray scattering (WAXS), (DSC) and electron microscopy [5, 43, 44], has been used to investigate the properties of single polymer composites made by hot compaction. The matrix phase creates molecular continuity between the original oriented fiber phase and the matrix phase.

The initial studies of hot compaction used melt spun polyethylene fibers to make single polymer composites. Later, this method was successfully adopted to a wide range of oriented fibers and tapes, such as gel spun polyethylene fibers (both Dyneema [45] and

Spectra [34]), PET fibers [39, 45], liquid crystalline polymer fibers [46], fibrillated polypropylene tapes [41] and a new highly oriented melt spun polyethylene tape (Tensylon manufactured by Synthetic Industries) [47]. Currently, hot compaction is the main commercial processing method for manufacturing SPCs. By hot compaction of high strength polymer fibers, SPCs have been successfully fabricated for different semicrystalline polymers including PE, PP, nylon, PET, PEN, and PLA. The method was also found useful for amorphous polymer fibers including PMMA fibers [35-55]. PP SPCs [48] made using the hot compaction method have been commercialized by Propex Fabrics under the trade name Curve®.

Although the fiber hot-compaction method is an elegant manufacturing method for single polymer composites, the processing window is very narrow, typically only a few degrees of Celsius. The material has to be processed in a well-controlled environment, since overheating will degrade the useful fiber properties [40, 41].

2.1.2.2 Overheating of constrained fibers

To address the problem of small processing temperature window in fiber hot compaction, a method called "overheating of constrained fibers" was developed, utilizing the overheating effect of constrained fibers [49]. Compared to the bulk material, drawn fibers exhibit an increased melting temperature and an increased enthalpy of melting [50]. Thus, a "constraint fibers" concept was introduced to enlarge the process window. During the process, a load is applied to prevent oriented molecules to adopt their random-coil conformation [37]. Oriented fibrous polymeric structures can be overheated significantly above their standard melting temperature. For PP, a difference of 26°C in the melting temperature between unconstrained and constrained fibers can be obtained, which is

fairly high and illustrates the efficiency of constraining on PP fibers. PET fibers show 10°C of overheating while PA6 fibers exhibit a shift of 7°C under constraining [6]. The degree of overheating for PE, PET, and PA6 is not as high as for iPP but may still be large enough to create single polymer composites.

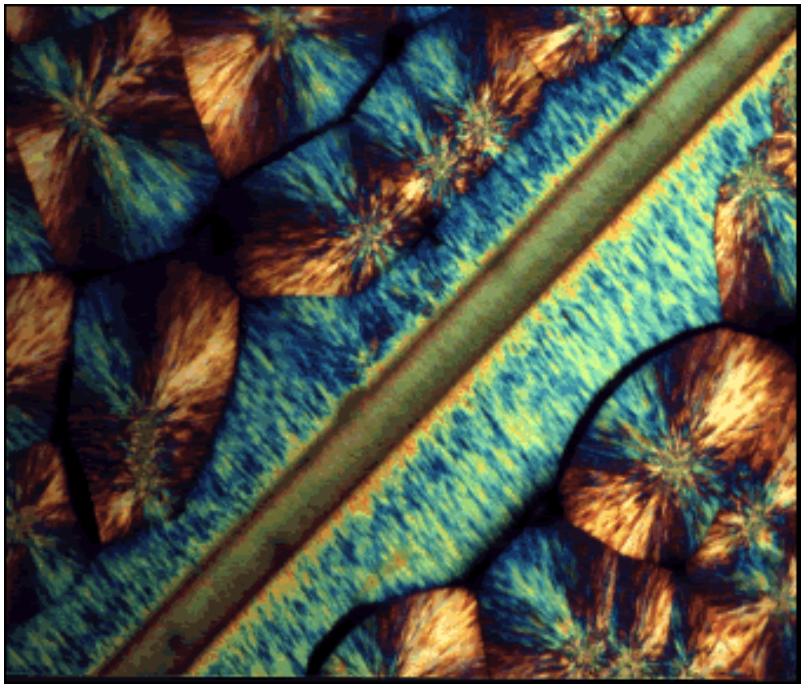

Figure 2.3 Optical micrograph (Loos et al.), showing transcrystalline interfacial regions in between a PP fiber and a PP matrix. Both fiber and matrix are of the same polymer grade and show the potential of constrained overheating of the fiber to impregnate PP fibers with the same PP matrix [50].

Figure 2.3 showed that constrained fibers were embedded in thin films of the same polymer to make a single polymer composite. There are three different regions in the composites morphology: 1) the iPP fiber partially embedded in 2) a transcrystalline layer, surrounded by 3) the iPP matrix material consisting of spherulitic superstructures.

Thus, the concept of constraining can be used to prepare single polymer composites. However, for this method a load must be applied along the fibers direction to keep the high orientation of fibers. Thus only unidirectional fiber reinforced composites can be acquired.

2.1.2.3 Solution imbedding method

Theoretically, it should be possible to impregnate polymer fibers with the same polymer matrix using traditional solution or powder impregnation routes. Impregnation of fiber bundles with highly viscous resins is, however, one of the main bottlenecks in the cost-effective manufacturing of thermoplastic composites [51]. There are some difficulties using melt processing method to make single polymer composites. The temperature window to make single polymer composites without damaging fibers is very narrow. The viscosity of polymer in this temperature region is very high too. Thus, impregnation of fiber bundles by melt impregnation technique is relatively difficult [52].

Solution imbedding methods may be used to make single polymer composites [52, 53]. In the study by Schulz and Hirte [53], an oriented polyethylene substrate was dipped into a saturated polyethylene solution. Crystals were found to nucleate on the fiber surface and grow into an oriented layer around the substrate. In the experiment by Lacroix et al. [52], UHMPE fibers were dipped into a LDPE-xylene solution, and then the impregnated bundles were dried in an oven. Heating the parallel arranged impregnated fibers or fiber bundles and compacting them above the melting temperature of the matrix material leads to single polymer composites [52]. However, since solvents are involved, this method is not an environmentally friendly method.

From the above survey of the state of art, it can be seen that the major issue in SPCs manufacturing is on how to process the matrix material in its liquid state without significantly degrading the useful engineering properties of the reinforcement. So far, most investigations have been reported on the fiber hot compaction method and the two-component molecular method. The later method can overcome the limitation of a small process window in the former process but is subjected to other problems. For instance, it is known that the difference in chain configurations, particularly the length of branched chains, could significantly affect the compatibility and miscibility of different grades of polyethylene [36, 55]. In a rigorous sense, composites resulting from molecular methods are not true single-polymer composites.

Looking at SPCs manufacturing in terms of two elementary steps are useful. The first step is to create two distinct phases from a same polymer and the second is to consolidate the two phases. The steps may be considered independently in the development of new processes. Particularly, new SPCs manufacturing processes could result if new practical approaches for creating distinct physical forms of the same polymer should be uncovered. Likewise, new processes could be created if new consolidation methods should be found.

It would also be interesting to develop amorphous layer coated crystalline fibers, because the resulting fiber will offer a great flexibility in manufacturing. This may be achieved using a rapid coagulation method to precipitate a thin layer on the highly crystalline fiber. Similarly, it would also be interesting to see other new processes which could result in differentiation of the fiber structure from the skin to the core.

2.2 Consolidation mechanism and crystallization kinetics

2.2.1 Consolidation mechanism

Fusion bonding plays a major role in processing of thermoplastics and thermoplastic-based composites, including inter-ply consolidation, repair, and new manufacturing techniques such as integrated processing [56, 57]. Processing conditions have great influence on the efficiency of the bonding process. Generally, fusion bonding of semicrystalline polymers requires the interfacial temperature above the melting temperature. For amorphous polymer, the interfacial temperature must be higher than the glass transition temperature. High contact pressures and elevated processing temperatures can induce strong bonding between identical or miscible amorphous polymers. Under such conditions, the polymer chains can interdiffuse across the interface [58-64]. Consolidation in fusion bonding is mainly characterized by a polymer-polymer interface healing process [65].

When two pieces of polymer are heated above the glass transition temperature or melting temperature, the interface gradually disappears through a healing process [65]. Wool and O'Connor [66, 67] described the healing process at a polymer-polymer interface using five sequential stages: (1) surface rearrangement, (2) surface approaching, (3) wetting, (4) diffusion, and (5) randomisation. Ageorges and Ye [68] used an intimate contact model and an autohesion model to describe the fusion bonding process. Prager [69] illustrated the healing of a polymer-polymer interface considering the formation of an intimate contact and the subsequent interdiffusion process, as shown in Figure 2.4. First the polymer surface rearranges and approaches each other. In this stage, two distinct faces still exist. Then the two surfaces begin to approach and wet. The stages of surface

approaching and wetting have been described by the intimate contact concept [70-73]. The completion of the wetting stage marks the achievement of intimate contact. [69]. At an autohesion process, the potential barriers at the interface are disappeared; molecular chains can move across the interface freely. The two surfaces interdiffuse each other. The reptation theory [74] can be used to explain the autohesion process. Figure 2.5 described the polymer chain migration from its initial tube in the reputation theory. At the beginning, the polymer chain is confined inside a tube having a similar shape to the random coil configuration of the chain. Then the polymer chain exhibits Brownian motion back and forth in the tube. Because the chain ends are free to move in any directions away from the tube, the memory of the initial tube position in space is gradually lost as shown at times t_2 and t_3 in Figure 2.5. Finally, when the reptation time, t_τ, has elapsed, the chain has escaped and forgotten its original configuration [75].

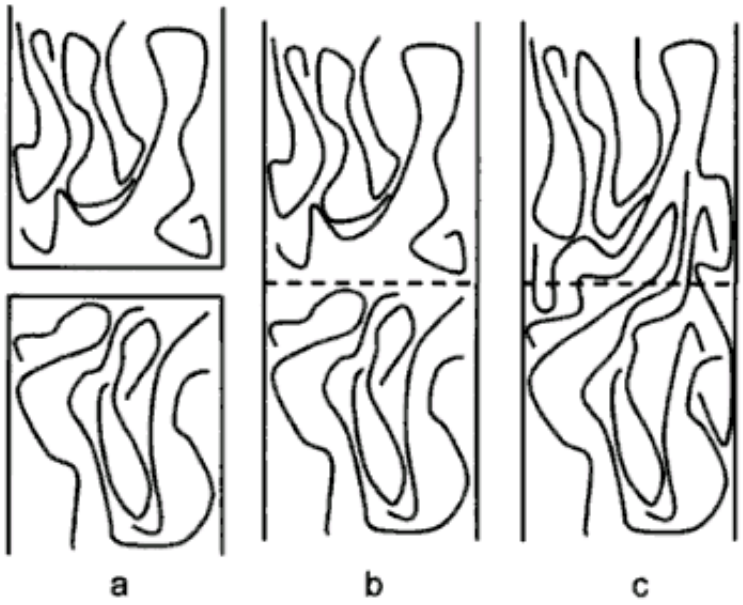

Figure 2.4 Healing of a polymer-polymer interface showing: a. two distinct interfaces; b. achievement of intimate contact; c. collapse of the interface through interdiffusion [69].

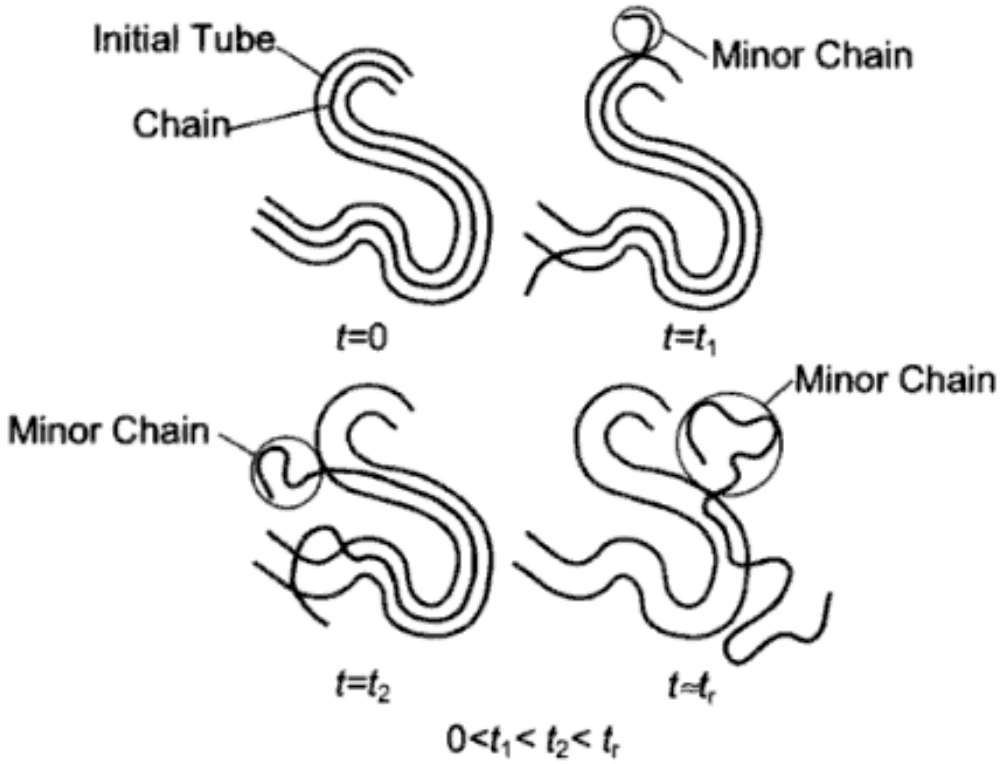

Figure 2.5 Polymer chain migration from its initial tube as described in the reptation theory [75]

According to the reptation theory, the reptation time, or tube renewal time, is defined as the time necessary for a polymer chain to exit totally the original tube in which it is confined. During the healing process, the development of mechanical strength is given by Wool and O'Connor [66, 67] as:

$$\frac{\sigma}{\sigma_\infty} \propto t^{1/4} M^{-3/4} \qquad \text{for } t<t_r \tag{2.1}$$

where σ is the mechanical strength at time t, σ_∞ the mechanical strength for infinite time, M the molecular weight and t_r the reptation time. The concept of degree of autohesion

was introduced to monitor the development of molecular diffusion as a function of time, and it is defined as [73]:

$$D_{au} = \frac{\sigma}{\sigma_\infty} = \left(\frac{t}{t_r} \right)^{1/4} \tag{2.2}$$

where the reptation time t_r is related to the temperature through an Arrhenius law,

$$t_r = B_r \exp\left(\frac{A_r}{T} \right) \tag{2.3}$$

where A_r and B_r are parameters determined experimentally.

2.2.2 Crystallization kinetics

The constituent and reinforcement phases have great influence on the bulk properties of composites [76, 77]. Processing conditions determine the morphology of the crystalline structures of a polymeric material [78, 79]. Different crystalline structure of a polymeric material affects the properties of the materials. By controlling the processing conditions, optimum properties can be obtained. Therefore, it is valuable to include crystallization kinetics in a general process model for fusion bonding.

The Avrami equation [80-82] is widely used for modeling the isothermal crystallization process, as follows,

$$1 - X(t) = \exp(-kt^n) \tag{2.4}$$

where $X(t)$ is the weight fraction of the crystalline material at time t, calculated from the following equation:

$$X(t) = \frac{\int_0^t \frac{dH}{dt} dt}{\int_0^\infty \frac{dH}{dt} dt} \tag{2.5}$$

where dH/dt is the rate of heat evolution, k the kinetic rate constant, and n the Avrami exponent. Values of n can be obtained from the slope of the double-logarithmic plot, log [-ln(1 - $X(t)$] versus log t.

The crystallization half-time ($t_{1/2}$) defined as the time taken for half of the crystallinity to develop is used for comparing the crystallization rate. The value of $t_{1/2}$ is easily obtained from the following relation:

$$t_{1/2} = \left(\ln 2 / k\right)^{1/n} \tag{2.6}$$

Different models have been developed for the evaluation of the crystallinity level in semi-crystalline polymers. According to the assumptions involved, these models exhibit different biases.

2.2.2.1 Ozawa's Crystallization kinetics model

Ozawa [83] has developed a model to describe the process of crystal nucleation and growth. It is derived from Avrami's equation and is only valid for isothermal processes. It has been extended to non-isothermal kinetics. The relative crystallinity c_r is expressed as a function of temperature and cooling rate:

$$\log[-\ln(1-c_r)] = \log\phi(T) + n\log\left(\frac{dT}{dt}\right) \tag{2.7}$$

The parameters $\phi(T)$ and n can be obtained from crystallinity measurements at different temperatures. This model does not account for the temperature of the melt [84]. It can't describe the non-isothermal crystallization kinetics very well, in which a large part of the crystallization is attributed to the secondary crystallization process. This model was applied in the simulation of compression molding [85] and tape laying and filament winding [86] of APC-2 composites.

2.2.2.2 The Velisaris and Seferis crystallization kinetics model

Velisaris and Seferis' crystallization model [87, 88] is a dual-mechanism crystallization kinetics model based on a linear combination of two Avrami's expressions. This model can account for the non-isothermal nature of the temperature history. The non-isothermal crystallization kinetics model is given by

$$c = \frac{w_1 F_{vc1} + w_2 F_{vc2}}{c_\infty} \tag{2.8}$$

where $w_1 + w_2 = 1$, w_1 and w_2 are the weight factors of the first and the second mechanisms respectively, c_∞ is the equilibrium volume fraction crystallinity, and

$$F_{vc1} = 1 - \exp\left[-C1_1 \int_0^t T \exp\left\{ -\left[\frac{C2_1}{(T - T_g + 51.6)} + \frac{C3_1}{\left(T\left(T_{m2} - T\right)^2\right)} \right] \right\} n_1 t^{n_1 - 1} dt \right] \tag{2.9}$$

and

$$F_{vc2} = 1 - \exp\left[-C1_2 \int_0^t T \exp\left\{ -\left[\frac{C2_2}{(T - T_g + 51.6)} + \frac{C3_2}{\left(T\left(T_{m2} - T\right)^2\right)} \right] \right\} n_2 t^{n_2 - 1} dt \right] \tag{2.10}$$

where $C1_1$, $C1_2$ are pre-exponential factors, $C2_1$ and $C2_2$ are empirical parameters associated with the temperature dependence of the viscosity, $C3_1$ and $C3_2$ are empirical parameters associated with the free enthalpy of nucleation, n_1 and n_2 are Avrami exponents, T_g is the glass transition temperature, and T_{m1} and T_{m2} the crystal melting temperatures.

2.2.2.3 The Choe and Lee crystallization kinetics model

Choe and Lee's crystallization model [89] is not based on the Avrami's equation. It is based on Tobin phase transformation kinetics [90-92] with growth site impingement.

This model includes the effect of the temperature of the melt, from which crystallization is performed [93]. This non-isothermal crystallization kinetics model is expressed as:

$$\frac{dc_r}{dt} = k_1 \exp\left(\frac{-3E_d}{RT}\right)\exp\left(\frac{-3\psi_1 T_m^0}{T(T_m^0 - T)}\right)t^2\left[1-c_r(t)\right]^2 + k_2 \exp\left(\frac{-4E_d}{RT}\right)\exp\left(\frac{-(3\psi_1+\psi_2)T_m^0}{T(T_m^0 - T)}\right)\left[1-c_r(t)\right]^2\int_0^t (t-w)^2\left[1-c_r(w)\right]dw \quad (2.11)$$

where k_1, k_2, ψ_1 and ψ_2 are kinetic parameters, E_d is the activation energy and T_m^0 is the equilibrium melting temperature.

2.2.2.4 Icenogle's crystallization kinetics model

Icenogle's crystallization model [94] based on Avrami's model describes the instantaneous heterogeneous nucleation followed by spherulitic growth. The non-isothermal expression of the model is given by:

$$c_r = 1 - \exp\left(-\frac{4}{3}\pi G^3 M t^3\right) \quad (2.12)$$

where M is the temperature-dependent nucleation density and G is the spherulitic growth rate.

2.2.2.5 The Maffezzoli et al. Crystal melting kinetics model

Maffezzoli et al. [95, 96] developed a crystal melting kinetics model which was applied to the resistance welding process. The model revealed the importance of insulation with metallic tooling leading to uncontrolled cooling rates and a low value for the final crystallinity content. The model defines a degree of melting X_f that is related to the crystal volume fraction and can be computed using

$$X_f = \frac{X_{vci} - X_{vc}}{X_{vci}} \quad (2.13)$$

$$\frac{dX_f}{dt} = K(1 - X_f)^n \tag{2.14}$$

where X_{vci} is the initial crystal volume fraction, X_{vc} the crystal volume fraction, n the kinetic order and K the kinetic constant given by an Arrhenius expression:

$$K = K_0 \exp\left(\frac{-E_a}{RT}\right) \tag{2.15}$$

where K_0 is the pre-exponential factor and E_a is the activation energy for the crystal melting process.

2.3 Etching and morphological study

2.3.1 Structure characterization using etching techniques

Chemical etching is a very prominent technique to reveal the microstructure in metal and polymers. Differential physical, chemical or structural inhomogeneities within a material have differential resistance to etchants. Often, etching is an effective means to reveal the material internal structure for microscopic observations. Unlike mechanical methods, such as sectioning and grinding, samples prepared in this method are left strain-free and undistorted [97]. Etching may be performed either by physical methods or by chemical methods. In physical methods, radiations including high energy beams such as plasmas and focused ion beams are typically used, while in chemical methods, an acid, a base or a specifically formulated liquid/vapor etchant is employed. Chemical etching is more widely used in the literature and, with a proper etchant, this method can provide an enhanced topographic contrast between structurally different regions.

There are two main types of chemical etching techniques: mild etching and severe etching, which is defined according to the proportion of the original material removed

during the process [98]. For mild etching, solvents or solvent vapors are applied to polymer to create a surface morphology representative of the underlying microstructure. The etching surface can be observed by optical or electron microscopy. In severe etching, an excessive amount of material is removed. Typically, mild etching, rather than severe etching, is desired in morphological studies.

2.3.1.1 Choice of etching agent

The chemical process involved in etching methods can be quite complex. Thus, choosing a suitable etching agent for a particular polymer is an important step. It is necessary to ensure that the structure produced by etching is indeed caused by the underlying inhomogeneities, rather than by a physical or chemical process involved. The reagent is thought to attack the polymer, cause chain scission, produce new molecular species and remove them from the site of reaction. Dissolution process is random; however, etching is selective. An etching agent should be able to distinguish between inhomogeneities such as crystalline and amorphous components. Due to different molecular packing, the etching degree and speed of amorphous and crystalline regions are different. Permanganic acid is a popular inorganic etchant which is used in this function. It involves an oxidation process, which preferentially attacks disordered regions of the polymer. This etchant is prepared using potassium permanganate with strong acids and was found suitable for polyethylene [99] and poly (aryl ether ether ketone) (PEEK) [100]. Sodium hydroxide solution was applied to PEN to investigate heavy ion tracks as a result of irradiation [101]. However, it is not a selective etchant. Organic hydrocarbons were used to etch nylon and polypropylene [102]. Sodium acetate can be used to etch polyethylene oxide [103].

The permanganic etching technique is frequently used to investigate the morphology of crystalline polymers such as PE and PP [104-106]. The permanganic etching technique is also efficient to characterize the amorphous regions in PET [107]. Some literature [108, 109] used a 40% aqueous solution of methylamine in selectively degrading PET. Methylamine principally attacks amorphous regions. It can react rapidly with PET at room temperature and minimize side effects of high temperatures. A more important advantage of choosing such an etchant is that its reactions with esters, aminolyses, are well known [110, 111]. Li et al. [111] studied the spherulitic structures of PET using a potassium hydroxide/methanol(5/95 w/w) solution as a chemical etchant. The spherulitic morphology was observed using high-magnification microscopy. In the literature [112, 113], pure water has also been used as an etchant for PET. By exposing the sample to pure water under elevated pressure at 180°C followed by extraction in ethanol, Miyagi and Wunderlich [112, 113] found that up to 40% of the material can be removed. Simultaneously, the molecular weight of the sample decreased considerably. Part of the material was hydrolyzed to ethylene glycol and terephthalic acid which was then dissolved by the ethanol. In the further evaluation, Miyagi and Wunderlich concluded that the amorphous material was removed from the sample completely.

2.3.1.2 Mechanism of Etching

The etching degree and speed is different inside of inhomogeneous polymers. Some researchers [114-116] have suggested that the etching process in all polymers containing lamellar crystals basically involves three different etching rates in decending order: attacking on amorphous, etching of side surfaces (prism faces), and etching of basal surfaces.

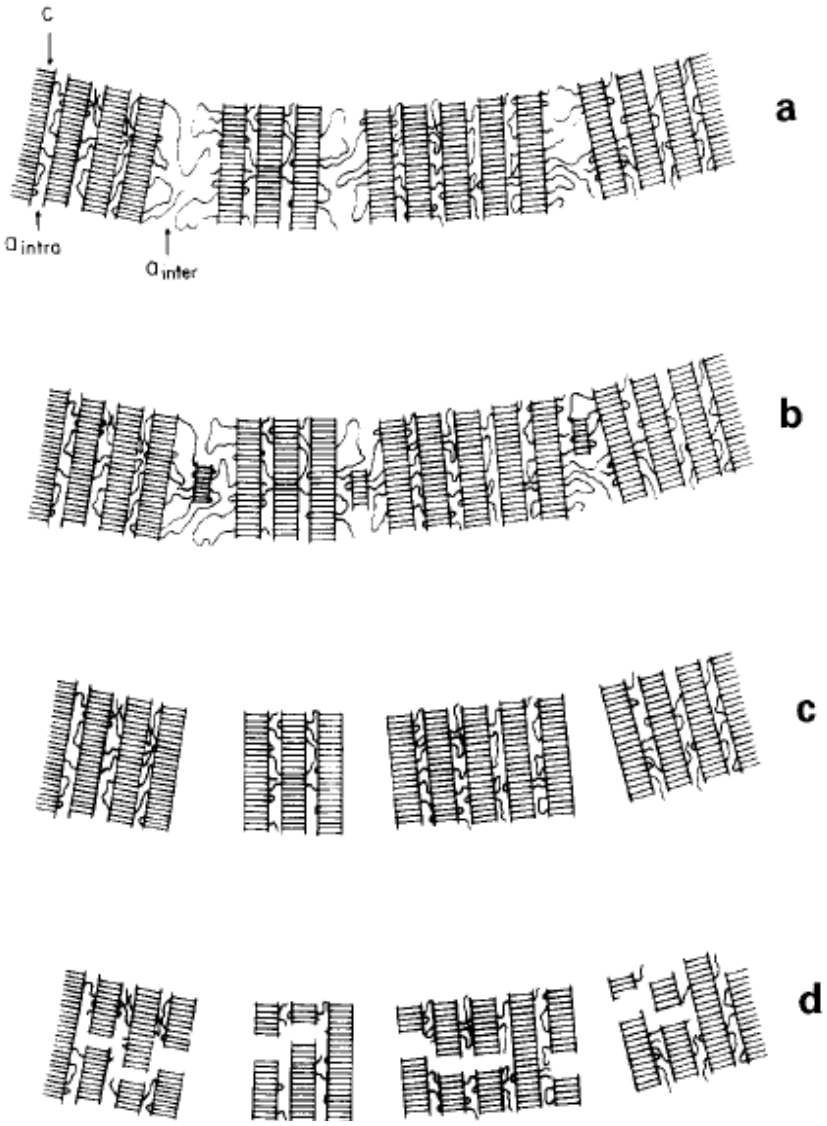

Figure 2.6 Schematic representation of the crystalline amorphous structure of PET at the different stages of etching: c, crystals; a_{intra}, intrastack amorphous regions; a_{inter}, interstack amorphous regions. For the sake of simplicity only a few chains have been indicated in the amorphous regions: (a) initial state; (b) end of the first stage ($t_H \approx 4$ h); (c) end of the second stage ($t_H \approx 16$ h); (d) third stage ($t_H > 62$ h). [115]

The etching rate of the amorphous phase is the fastest. The etchant attacks the side surfaces (prism faces) and the basal surfaces at a slightly slower rate. Figure 2.6 shows a schematic representation of the crystalline amorphous structure of PET at different stages of etching [115]. The intrastack amorphous regions are attacked first. These intrastack amorphous regions can be etched away completely. Then the materials, mostly crystalline regions, are etched away little by little at a relatively slower rate.

2.3.2 Characterization methods of etching morphology

2.3.2.1 Polarized optical microscopy (POM)

Chung et al. [117] observe the spherulitic morphology in the neat PET and PetLSNs using a polarized optical microscope equipped with a hot stage. After the samples are kept at 280°C for 1 min to eliminate the thermal history, it is cooled to the desired isothermal crystallization temperature at a rate of 20°C/min and maintained for different times. Figure 2.7 shows the POM images of neat PET, PetLSNeom, and PetLSNiom, which were crystallized at 230°C for 150 and 240 s.

Hwang et al. [118] studied the crystal growth mechanism of PET/clay nanocomposite materials. Figure 2.8 shows various spherulitic morphologies of PET and PET/clay nanocomposite materials. Pure PET shows a perfect spherulitic texture with a fibril pattern. There is a clean maltese cross at 200°C. With the increase of crystallization temperature, the maltese cross disappears. PET/Na^+-MMT and PET/A10-MMT exhibited typical crystalline morphologies at 200°C. It also indicates that clay effectively acts as a nucleating agent to increase the crystallization rate of PET. Relative to pure PET, the spherulites in the nanocomposites became smaller, with increasing nuclei density, at higher crystallization temperatures.

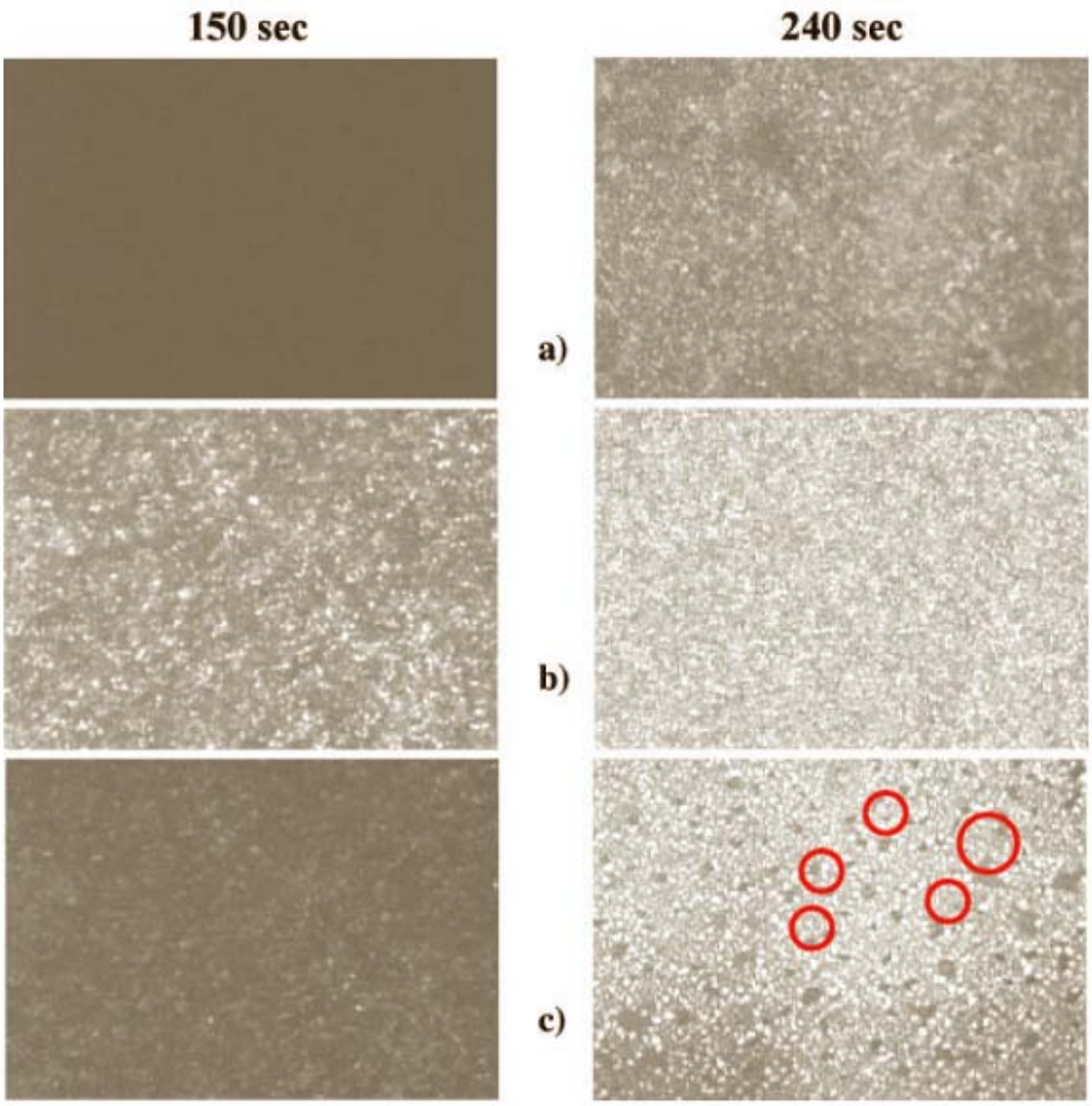

Figure 2.7 POM images of (a) neat PET, (b) $P_{et}LSN_{eom}$, and (c) $P_{et}LSN_{iom}$. [117]

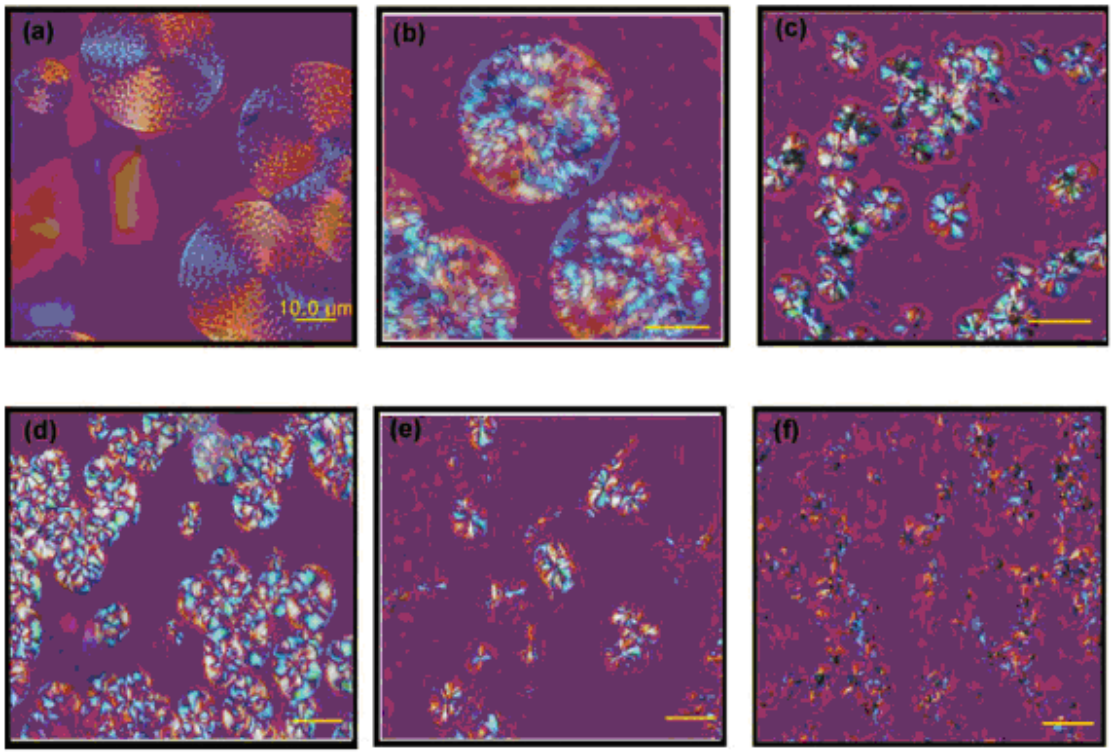

Figure 2.8 Micrographs showing spherulite growth from samples held at different crystallization temperatures for 5 min: (a) PET at 200°C, (b) PET at 220 °C, (c) PET/Na^+-MMT 0.5 wt % at 220 °C, (d) PET/Na^+-MMT 2.0 wt % at 220 °C, (e) PET/A10-MMT 2.0 wt % at 220 °C, and (f) PET/A10-MMT 5.0 wt % at 220 °C. [118]

2.3.2.2 Atomic force microscopy (AFM)

Gao et al. [119] used AFM to observe the phase images of pure PEN and PEN/1wt %LCP. The samples were crystallized at 210°C for 1 h. It shows that, for pure PEN, spherulitic morphology was obtained, while for PEN/1wt %LCP, the crystals were small and no spherulites were observed. Moreover, the lamellar of PEN became irregular in the presence of LCP. It may be due to the increase in the nucleation density and in the crystal linear growth rate of PEN blending with LCP which promoted the chain mobility of PEN.

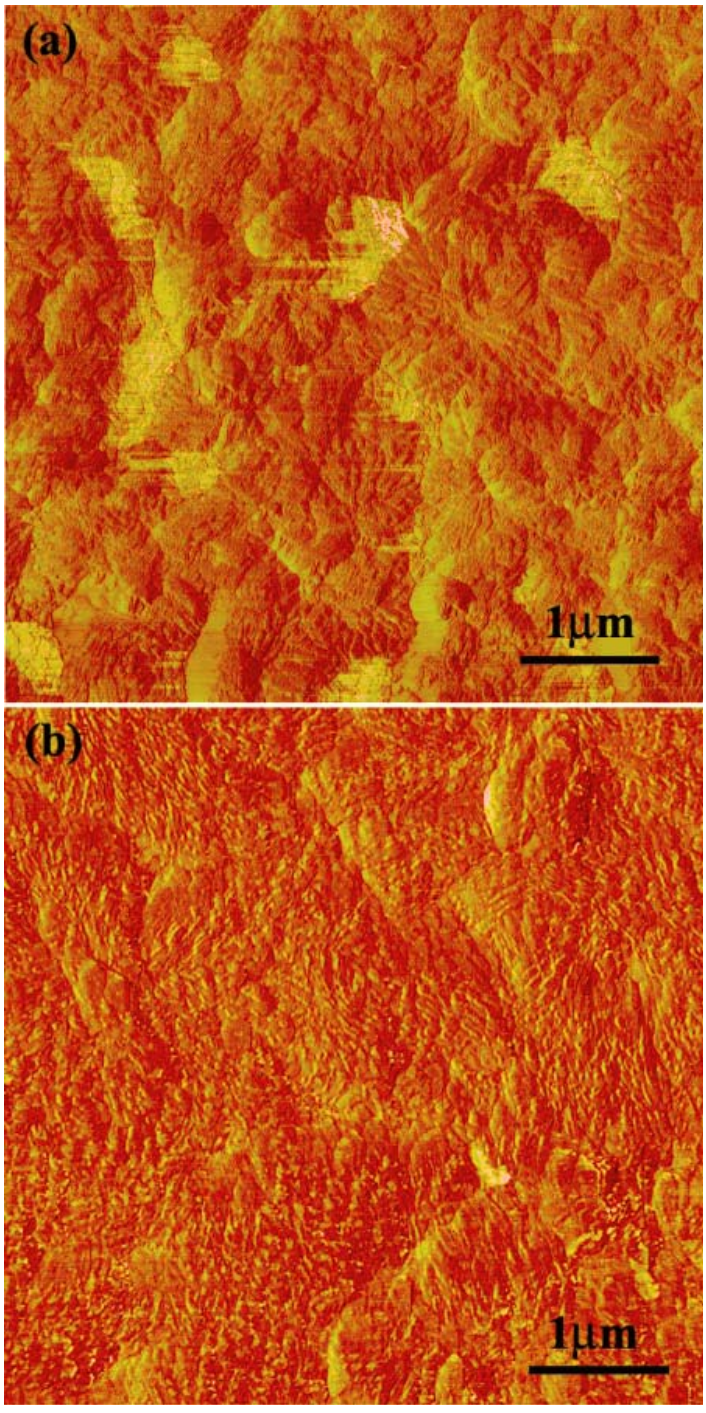

Figure 2.9 Typical AFM phase images of (a) pure PEN and (b) PEN/1 wt % LCP crystallized at 210°C for 1 h. [119]

2.3.2.3 Morphology as observed by scanning electron microscopy (SEM)

Li et al. [120] observed the spherulites of PET/CB and PET/GCB composites using SEM, after the materials surfaces were chemically etched by a potassium hydroxide/methanol (5/95 w/w) solution. For PET/CB (Figure 2.10 a and b), spherulitic morphology is observed. However, there are no clear boundaries between the spherulites; there are only voids between the spherulites. It indicates that those parts etched away were mostly amorphous zones. For PET/GCB (Figure 2.10 c and d), irregular texture was observed though spherulitic morphologies appeared in some locations. The boundaries between the spherulites are not clear, similar to PET/CB composites. The CB or GCB particles in the composites act as nucleating agents which results in the absence of clear boundaries between the spherulites. The added nuclei make the spherulites smaller. The shrinkage toward each nucleus is less, which induces less defined boundaries. The irregularly shaped amorphous zones have been etched away. Thus the etched surfaces are not very smooth.

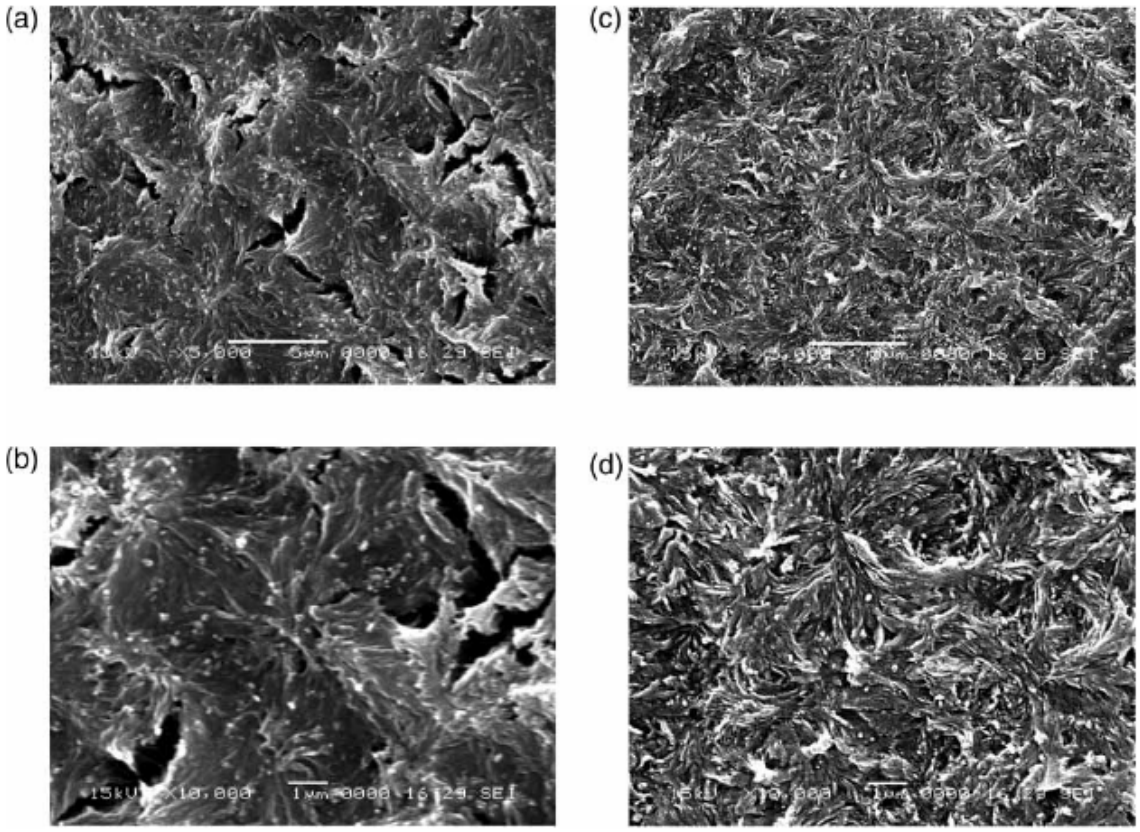

Figure 2.10 Micrographs of PET/CB and PET/GCB composites crystallized from 290°C to room temperature at 10°C/min (etched by potassium hydroxide/methanol (5/95 w/w) solution): (a) PET/CB (Magnification 5000x); (b) PET/CB (Magnification 10000x); (c) PET/GCB (Magnification 5000x); (d) PET/GCB (Magnification 10000x). [120]

2.3.2.4 Transmission electron microscopy (TEM)

Kawahara et al. [121] etched PET fiber using permanganic etching, and then the surface morphologies were investigated using TEM. In Figure 2.11, the TEM image of the two-stage surface replica of the etched HSS PET fibers is shown. Many projecting warts are observed, indicated by the arrows in the figure. Such unevenness is nearly observed in the TEM image of regular PET fiber (Figure 2.12). Comparing with the HSS ones, the regular PET fibers have well-oriented amorphous regions.

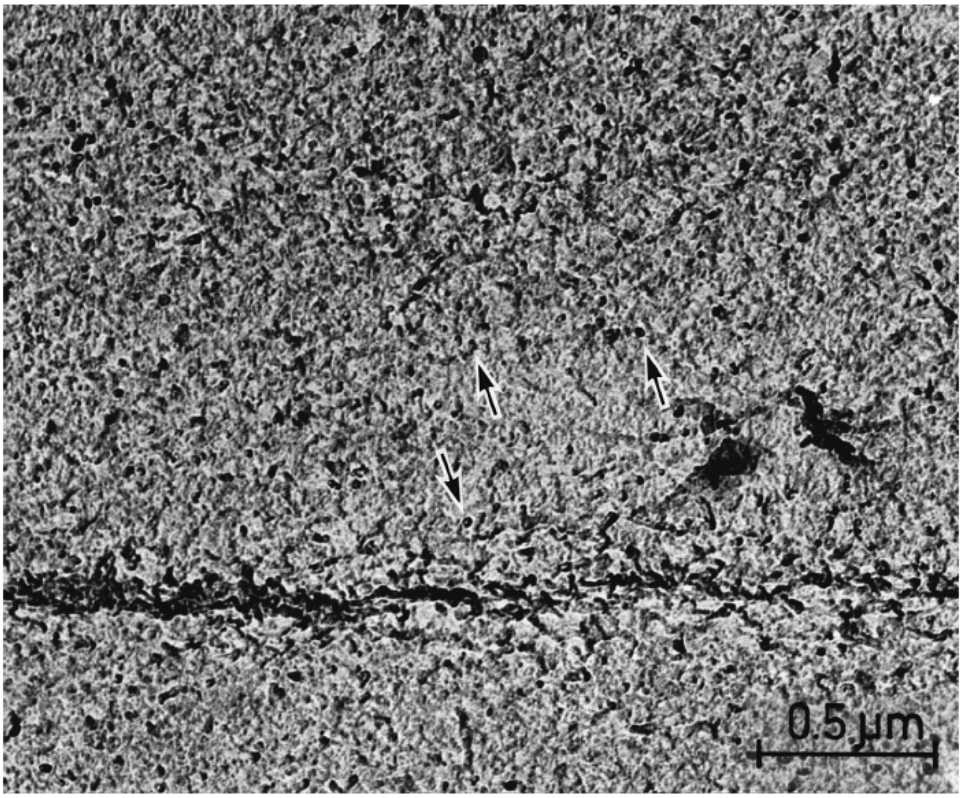

Figure 2.11 TEM image of the two-stage surface replica for the HSS PET fibers as etched in 1% $KMnO_4$ solution in 2:1 H_3PO_4:H_2SO_4 for 30 min at 30°C. The decrease in diameter by the etching was 13.2%. The fiber axis is horizontal. [121]

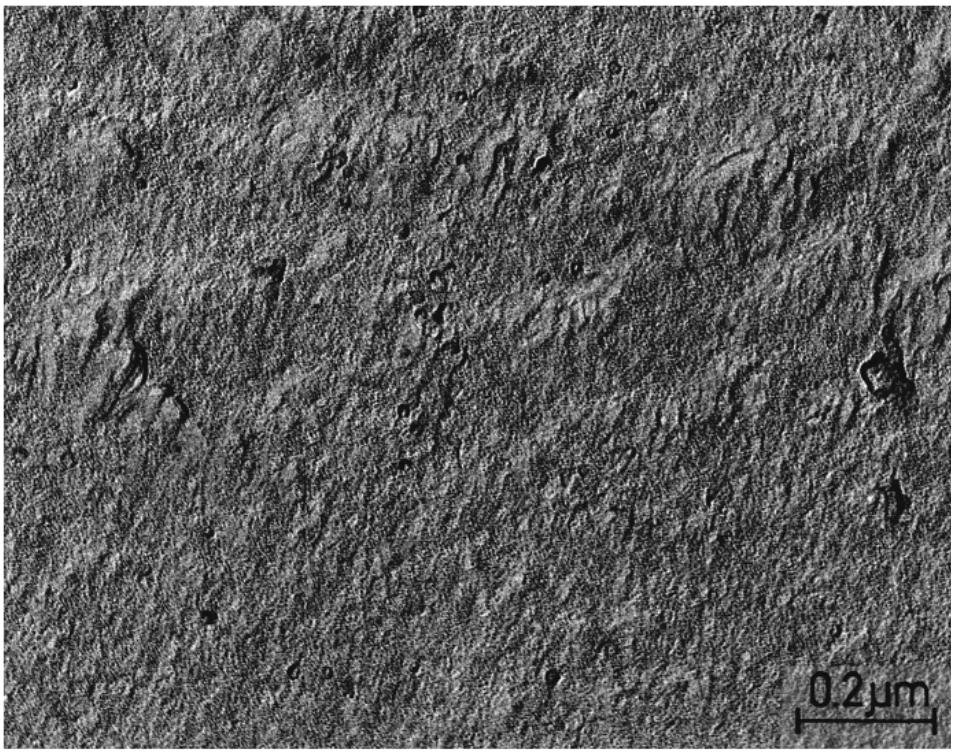

Figure 2.12 TEM image of the two-stage surface replica for the regular PET fibers as etched in 1% $KMnO_4$ solution in 2:1 H_3PO_4:H_2SO_4 for 30 min at 30°C. The decrease in diameter by the etching was 17.8%. The fiber axis is horizontal. [121]

CHAPTER 3

SINGLE POLYMER COMPOSITES BASED ON SLOWLY CRYSTALLIZING POLYMER

3.1 Introduction

The original concept of a single-polymer composites (SPCs), a composite with matrix and reinforcement from the same polymer, was presented by Capiati and Porter [122] three decades ago. The method utilized the noticeable difference in melting temperature between high-density polyethylene (HDPE) matrix and HDPE reinforcement to fabricate an HDPE homocomposites. Because the extent of adhesion between fibers and matrix is largely influenced by their physical and chemical compatibility, the polyethylene SPCs concept has been discussed in several studies [123-125] following Capiati and Porter's work. It has been shown that excellent bonding between fibers and matrix are achieved in HDPE SPCs, with the interfacial shear strength on the same order of that for glass fiber reinforced epoxy resins.

Despite the advantages of SPCs over heterogeneous composites in terms of chemical compatibility and recyclability, the small difference in melting temperature between the fiber and the matrix poses a great challenge during fabrication. For instance, the melting temperatures for HDPE matrix and fibers reported by Mead et al. [123] were 132°C and 139°C, respectively. In the case of ultrahigh molecular weight polyethylene (UHMWPE), the difference of melting temperature between the fiber and the matrix is in the range of 5-9°C [124]. With this small temperature window, it is difficult to process the SPCs under normal processing conditions without significantly annealing the fiber. It

is known that polyethylene fibers annealed at a temperature close to its melting temperature have a much reduced modulus toward that of bulk HDPE of about 1 GPa [123].

To enlarge the process window, the original SPCs concept was relaxed and extended to the incorporation of polymers with the same chemical composition but different chemical structures [126-128]. Examples are HDPE matrix reinforced by UHMWPE fibers [126, 127] and low-density polyethylene (LDPE) matrix reinforced by HDPE fibers [123]. In both cases, a process window of about 20°C results. When LDPE is reinforced by UHMWPE fibers, the process window can be further enlarged to about 40°C [128]. Although manufacturability is greatly enhanced in these composite systems, the interfacial adhesion was found to be lower than the original HDPE homocomposite [123, 128]. It should be noted that, except for different molecular weight, HDPE, LDPE and UHMWPE also bear different chain configurations. It is known that the difference in chain configurations, particularly the length of branched chains, significantly affects the compatibility and miscibility of different grades of polyethylene [129]. Another drawback of these composites arises from the increased difficulty in recycling. In a rigorous sense, they are not true single-polymer composites.

The SPCs concept has also been applied to polypropylene (PP) [50, 130-135] and poly(methyl methacrylate) (PMMA) [148]. Particularly, Ward and co-workers [131-135] developed a hot compaction method for manufacturing PP SPCs using highly oriented PP fibers and tapes. Being a fast-crystallizing polymer as polyethylene, PP faces the same processing difficulty because of a very narrow temperature window during processing. On the other hand, PMMA, as an amorphous polymer, is not a good choice in SPCs

applications because the system is now subjected to an additional drawback resulting from the low strength of amorphous PMMA fibers except for the narrow process window.

The previous work on SPCs mainly involved fast crystallizing polymers such as polyethylene and polypropylene. However, for these polymers, the proximity in the melting temperatures between the fiber and the matrix poses a considerable difficulty during SPCs processing. To solve these problems, a new approach to SPCs utilizing slowly crystallizing polymers is proposed, with poly(ethylene terephthalate) (PET) and poly(lactide acid) (PLA) as model systems. For this method, the fiber is the highly crystallizing polymer fibers. The matrix is an amorphous or low-crystallinity material made from the same grade of polymer as for the fibers. Upon heating above Tg but well below Tm, the fiber can keep its high orientation. The amorphous matrix can become rubbery and glue together at this processing temperature. The amorphous matrix can crystallize at the same time.

3.2 Concept and approach

The key issue in thermoplastic SPCs is how to melt-process the matrix without significantly annealing or even melting the fiber. It is well known that the melting temperature or the softening temperature of a polymer depend on its physical form, i.e., amorphous state, crystalline state and amount of crystallinity. Commonly used polymer fibers, such as PP, PE and nylon 6 or 6.6 fibers, are highly crystalline and have melting temperatures approaching those of single crystals. These polymers, however, have disadvantages in SPCs applications owing to their fast crystallization rate. Because of fast crystallization, the products derived from PE, PP and nylon are highly crystalline, resulting in closeness in melting temperature of these products. As a slowly crystallizing

polymer, PET stands out for SPCs applications. The typical half time of crystallization for PET is above 40 s [20]. Amorphous products will result if molten PET is rapidly cooled, e.g. a PET sheet produced by calendering and quenching. Amorphous PET is a rigid material at room temperature because its glass transition temperature is about 70°C. On the other hand, if PET is heated to above its crystallization temperature and kept for a few minutes or a shorter period under stretching, highly crystalline PET will be formed. Examples are PET fibers and heat-set PET films/sheets. The melting temperature of highly crystalline PET fibers is above 250°C. If a lamination of amorphous PET sheets and crystalline PET fibers is rapidly heated to significantly above the glass transition temperature of the amorphous phase, the amorphous PET will gain enough fluidity for encapsulating the PET reinforcement and form an integrated composite.

It should be noted that there are two competing processes occurring when an amorphous PET sheet is heated. First, the amorphous phase will experience a glass transition at its glass transition temperature, Tg, and the polymer will become rubbery and sticky at temperatures well above Tg (say 20ºC above Tg, depending on its molecular weight). Two such sticky pieces can be fused together through chain diffusion at the interface. The second competing process is crystallization. For a crystallizable amorphous phase, such as an amorphous PET phase, it will start to crystallize when its temperature is above Tg. Therefore, the just softened, rubbery and sticky amorphous phase will turn into a hardened crystalline phase at the same processing temperature.

Accordingly, the fusion quality of the matrix in SPCs manufacturing is subjected to the influences from two competing time scales; one is the characteristic fusion time, and the other is the characteristic crystallization time. Qualitatively, the reptation time of

a polymer chain, i.e. the time that the chain takes to escape from its original confined tube, can be considered to be the characteristic fusion time [136]. The characteristic fusion time is strongly dependent on the temperature and will decrease as temperature increases. Similarly, one can use the half time of crystallization as the characteristic crystallization time. The half time of crystallization is also a function of temperature and bears an inverse bell shape with Tg and Tm as its two limits. To achieve good fusion of the matrix, the characteristic fusion time should be smaller than the characteristic crystallization time. Figure 3.1 shows a feasible process window for fusion bonding crystallizable amorphous PET sheets. The promising process window is indicated as a hatched area. Within this process window, the characteristic fusion time is significantly smaller than the characteristic crystallization time, and thus the fusion process will dominate over the crystallization process. Associated with this process window is a minimum processing temperature, denoted as T_{min} in the figure. Note that, when the processing temperature is above the melting temperature, the problem will become a pure fusion problem. This higher processing temperature is used by standard welding of semicrystalline polymers, but cannot be used in SPCs manufacturing.

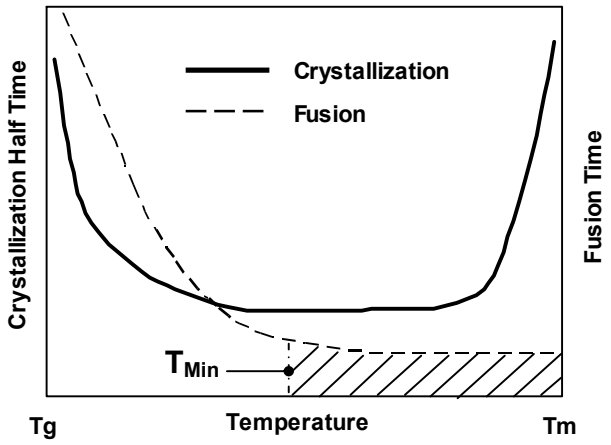

Figure 3.1 Feasible process window for fusion bonding amorphous sheets of a semicrystalline polymer.

3.3 Validation of the conceptual design

PET, a slowly crystallizing polymer, was used as a model system to demonstrate the concept of single-polymer composites of slowly crystallizing polymers. The main purpose of this initial study was driven toward the verification of the conceptual design presented in Section 3.2.

Three different physical forms of PET were used: PET fabrics, PET fibers and amorphous PET films, all obtained from commercial suppliers. The melting enthalpy, crystallizing enthalpy and melting temperatures of these PET derivatives were tested using DSC at the heating rate of 20°C/min using the 1st run curve. The crystallinity of PET is calculated using the following equation:

$$Crystallinity = \frac{\Delta H_m - \Delta H_c}{\Delta H_m^*} \times 100\% \qquad (3.1)$$

where ΔHm is melting enthalpy, ΔHc is crystallization enthalpy, and ΔH_m^* is the ideal melting enthalpy for a PET single crystal which is 140J/g.

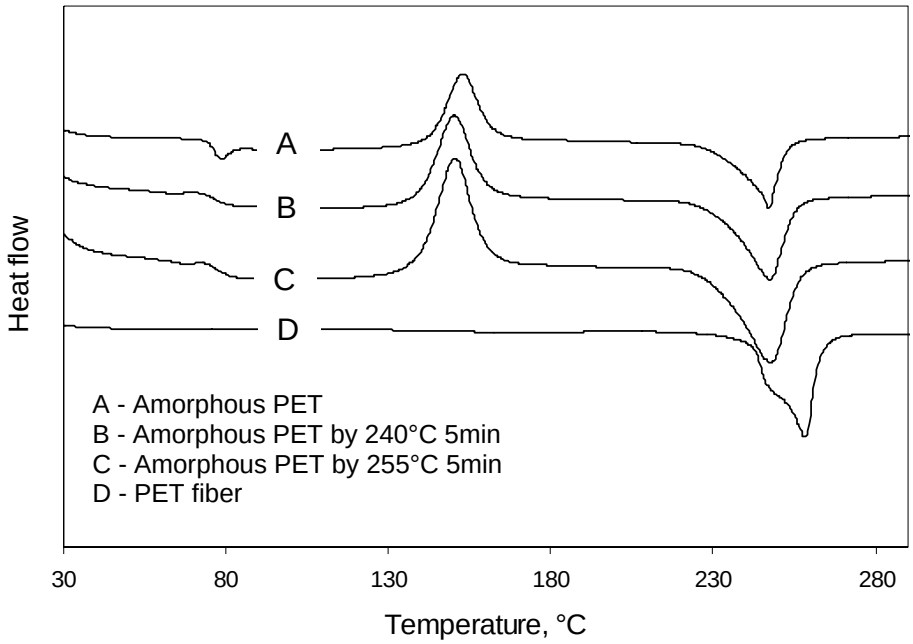

Figure 3.2 DSC curves of PET fibers and films

Table 3.1 Crystallinities and melting temperatures of PET fibers and films

		ΔHc, J/g	Tm, °C	ΔHm, J/g	Crystallinity, %
PET film	Amorphous film	-22.674	247.0	23.037	0.26%
	240°C, 5min hot plate, quenched	-24.567	247.1	26.375	1.30%
	255°C, 5min hot plate, quenched	-24.635	248.7	26.815	1.55%
	180°C, 15s hot plate, quenched	27.500	246.4	29.156	1.18%
PET fibers	PET fabrics	---	258.0	49.940	35.7%
	PET fibers	---	258.2	38.700	27.6%

Table 3.1 shows that the melting temperature difference between amorphous PET film and fibers is about 10°C. The crystallization rate for PET is expectedly slow. At high temperature, e.g. 240°C, when the heating time is more than 5 min, PET film is still nearly amorphous. At low heating temperature, e.g. 180°C, when the heating time is 15 s, PET film is still nearly amorphous. These experimental results demonstrate that it is promising to make PET SPCs with an extremely large processing temperature window.

To further explore these findings, PET SPCs were prepared using the following steps. First, an amorphous PET film was heated in the oven at the temperature of 254°C, which is lower than the melting temperature of PET fibers. At this temperature, the amorphous PET film becomes soft and liquid like. Then, PET fibers were imbedded into the heated resin by encapsulation and, after approximately 5 s, the composite was quenched into tap water. Polarized optical microscopy (POM) was used to observe the sample, and a POM micrograph is showed in Figure 3.3. The PET fiber under the polarized microscopy appeared much brighter than the surrounding material. This indicates that the PET fiber was able to retain its high orientation after undergoing the encapsulation process at such an elevated temperature. The PET resin coated on the PET fiber appeared dark, indicating a nearly amorphous state. DSC results also show that the crystallinity of the encapsulating resin in the composite prepared at this elevated temperature was very low and nearly amorphous. The PET processed under a much lower encapsulation temperature 180°C and the encapsulation time 15 s is nearly amorphous too. Under the polarized optical microscope, the fiber in this composite showed a similar bright appearance as that in Figure 3.3. DSC tests also confirmed that the PET resin encapsulating at 180°C for 15 s remain nearly amorphous. SEM was conducted to

investigate the fracture interface of these composites. Even at the lower encapsulating temperature, i.e., 180°C, no fiber pull-out was observed (Figure 3.4). All these results demonstrate that, with a slowly crystallizing polymer, SPCs may be produced with an extremely large processing window.

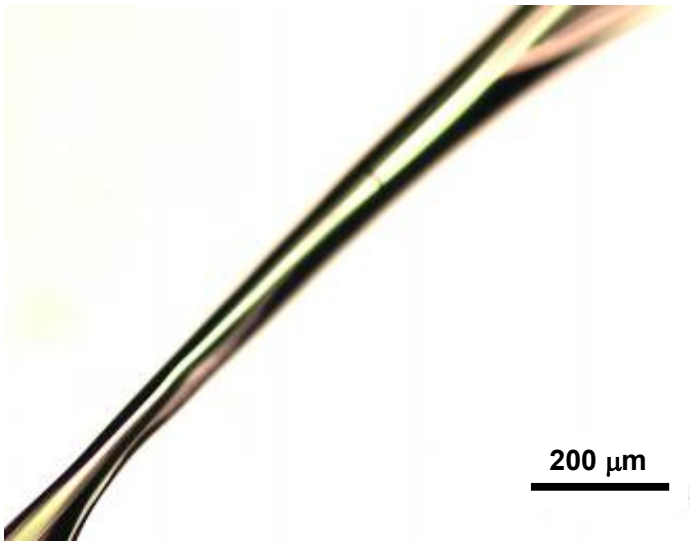

Figure 3.3 PET fiber imbedding in 254°C resin

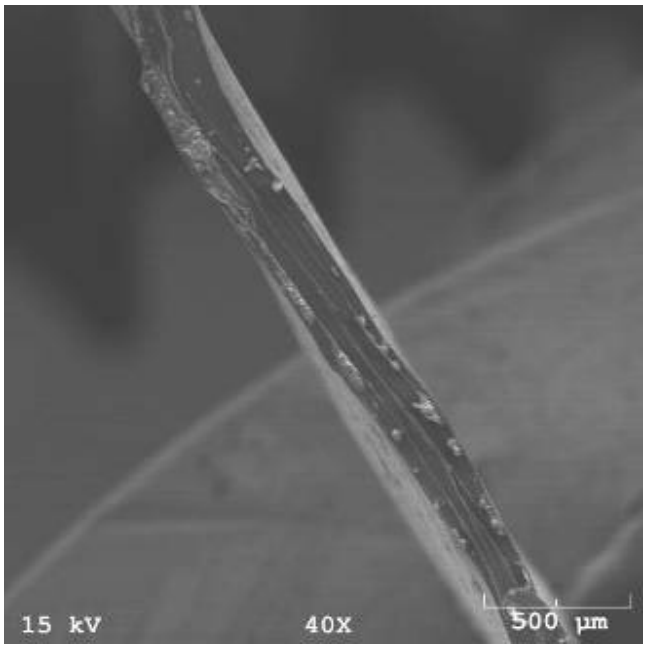

Figure 3.4 Broken surface of PET SPCs reinforced by single PET fibers at the processing condition of 180°C and 15 s

3.4 Effect of heating time on crystallinity

For better understanding of the working mechanism of the proposed SPCs manufacturing process, isothermal crystallization experiments of amorphous PET films were conducted at 180°C using a hot press. The holding time was varied. The results were showed in Figure 3.5. The "0 s" sample corresponds to the original PET sheet. From the DSC curve of the original PET sheet, Tg and Tm for this grade of PET can be determined to be 70ºC and 250ºC, respectively. For all compression molded samples with different holding times, the amount of crystallinity was calculated using the DSC data. Relative crystallinity, ξ , was comparatively determined based on the melting and crystallization enthalpies using the following formula:

$$\xi = \frac{\Delta H_m - \Delta H_c}{\Delta H_m} \times 100\%. \tag{3.2}$$

With this definition, $\xi = 100\%$ means that the compression molded sample's crystallinity is comparable to that of a fully crystallized one after prolonged isothermal crystallization. The ξ data are summarized in Figure 3.6. It can be seen that the relative crystallinity of the original PET sheet is almost zero, indicating a nearly amorphous polymer. As the holding time increases, the crystallinity keeps increasing until reaching a plateau region at a holding time about 40 s. As the holding time increased, the compression molded and quenched samples were transparent for short holding times (e.g. 10 s), then became translucent for medium holding times (e.g. 25 s), and final turned opaque for long holding times (e.g. 60 s). This change in appearance signifies the increase in crystallinity, agreeing with the data in Figure 3.6. It is interesting to point out that, when compression molding amorphous PET, there exist two solidification mechanisms. For short holding times and a followed quenching step, the verification of the amorphous phase is the main solidification mechanism, and therefore the samples turns into a transparent amorphous glass. For long holding times, the polymer will experience sequential fluidization (or rubbery softening) and solidification (crystallization induced) under an isothermal molding condition. Fluidization occurs almost instantaneously (within 1 s) when the sample contacts with the two heated platens. On the contrary, the crystallization occurs over a relatively long period (40 s or above). For long holding times (e.g. 60 s), the sample is substantially crystallized and becomes a solid between the two heated platens. Prolonged holding times above 2 min were found to be detrimental to the mechanical properties of the composite because the sample becomes brittle. The embrittlement is believably caused by thermal degradation.

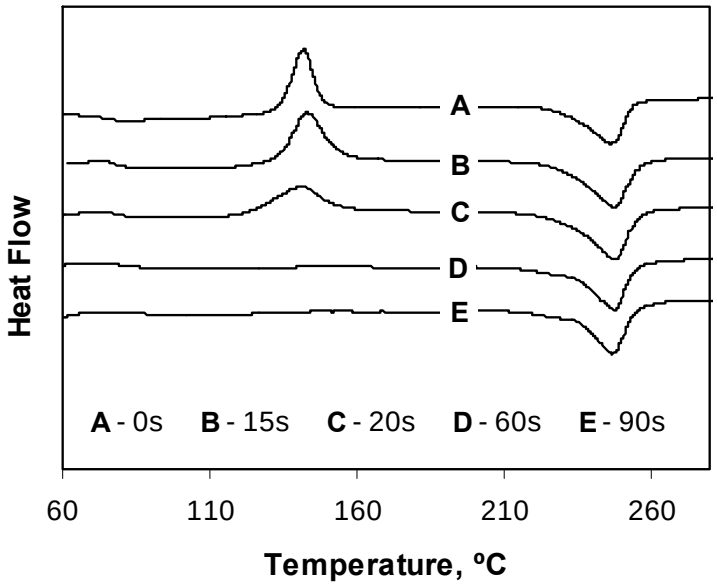

Figure 3.5 DSC curves of PET prepared by compression molding two amorphous PET sheets at 180°C but using different holding time. A heating rate around 10ºC/min was used for the DSC experiments.

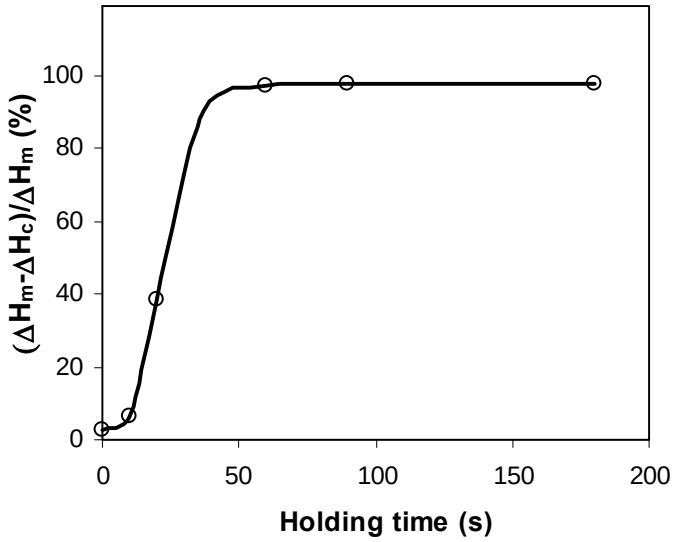

Figure 3.6 Relative crystallinity for samples prepared by compression molding two amorphous PET sheets at 180°C using varied holding time. The relative crystallinity is represented by $\frac{\Delta H_m - \Delta H_C}{\Delta H_m} \times 100\%$, where ΔH_m and ΔH_c are the melting and crystallization enthalpies, respectively.

CHAPTER 4

PET SINGLE POLYMER COMPOSITES

4.1 Introduction

PET has found usage in a wide variety of industrial and commercial applications, such as packaging and reinforcement materials [137]. PET is one of the most versatile polymers used in films and synthetic fibers due to its high-glass transition temperature and slow crystallization rate, which offers various methods of controlling its final morphology. PET has a very high melting point close to 260°C, and its crystallization takes place mainly at a temperature between 100 and 240°C. PET in its natural state is a crystalline resin. Clear products can be produced by rapidly cooling molten polymer to form an amorphous solid. PET tends to produce many small crystallites when crystallized from an amorphous solid, rather than forming one large single crystal.

The crystalline structure of PET is triclinic [138, 139]. The crystalline c axis of PET is very close to the direction parallel to the fiber axes. It does not present (hkl) planes normal to the c axis with observable intensity [140]. However, the planes with Miller indices (-1 0 5) give a very strong X-ray diffraction intensity and their normal makes an angle of 9.778° with the c axis, calculated with the PET lattice parameters given by Daubney et al. [139] The (-1 0 5) reflection is used to evaluate crystalline orientation factor (fc). Often it does not overlap with other (hkl) reflections [140]. Dumbleton and Bowles [141] used the azimuthal scan of X-ray diffraction intensity distribution from (-1 0 5) planes to calculate fc.

Amorphous PET can transform to a semicrystalline state by both thermal annealing [142, 143] and solvent treatment [144, 145]. The crystallization processes are caused by thermal annealing and solvent induction, respectively. As a slowly crystallizing polymer, PET stands out for SPCs applications. The typical half-crystallization time for PET is above 40 s. Amorphous products will result if molten PET is rapidly cooled, e.g. a PET sheet produced by calendering and quenching. On the other hand, if PET is heated to above its crystallization temperature and kept for a few minutes or a shorter period under elongational stress, highly crystalline PET will be formed. Examples are PET fibers and heat-set PET sheets. If a lamination of amorphous PET sheets and crystalline PET fibers is rapidly heated to above the softening temperature of the amorphous phase, the amorphous PET will gain enough fluidity for encapsulating the PET reinforcement.

4.2 Experimental

4.2.1 Materials

PET woven fabrics, amorphous PET sheets and undrawed PET fibers were obtained from Goodfellow Co. Highly orientated crystalline PET fibers were acquired from High Performance Fibers Co. The PET fabric is plain weaved, 0.15 mm thick, with 33% open area, and have 55 threads per cm. The monofilament diameter is around 21 μm. The nominal aperture size of the fabric is 100 μm. The amorphous PET sheet is 0.25 mm thick. The tensile strengths for the fabric and the amorphous sheet are 160 and 65 MPa, respectively. The tensile modulus for the fabric and the amorphous sheet are 3300 and 2080MPa

4.2.2 PET SPCs manufacturing

4.2.2.1 Compression molding of PET fabrics and amorphous PET sheets

PET fabrics and amorphous PET sheets can be compression molded to form single polymer composites. After heating between Tg and Tm under compression, the amorphous sheets can bond together while the fibers still keep their high orientations. In this case, PET fabrics are the reinforcement and amorphous PET sheets are the matrix. The experimental setup for making such composites is schematically shown in Figure 4.1. PET fabrics were placed between two amorphous PET sheets. Laminations of two amorphous PET sheets with a PET woven fabric in between were compressed between two heated platens on a Carver hydraulic press. It is important that the lamination is heated rapidly so that crystallization during the heating stage can be suppressed. The shim springs made of thin brass shims (0.05 mm in thickness) help to achieve uniform and quick contact of the lamination with the heated platens when the top platen moves downward. Thin Teflon® films (0.07 mm in thickness) on both sides were used for easy mold separation. An additional Teflon film in the middle of the lamination was employed to create an unbonded region for peeling testing. Spacers were inserted between the heated platens to control the thickness of the fabricated composite sheet. The adhesion properties of the matrix and the fiber were studied by varying the platen temperature, the compression force and holding time. The PET SPCs obtained were rapidly quenched into tap water. The molded PET SPCs had a thickness around 0.5 mm. Uni-axially reinforced PET SPCs were made by compression molding two amorphous PET sheets with uni-axial PET fibers fixed onto a metal frame in a similar setup as shown in Figure 4.1.

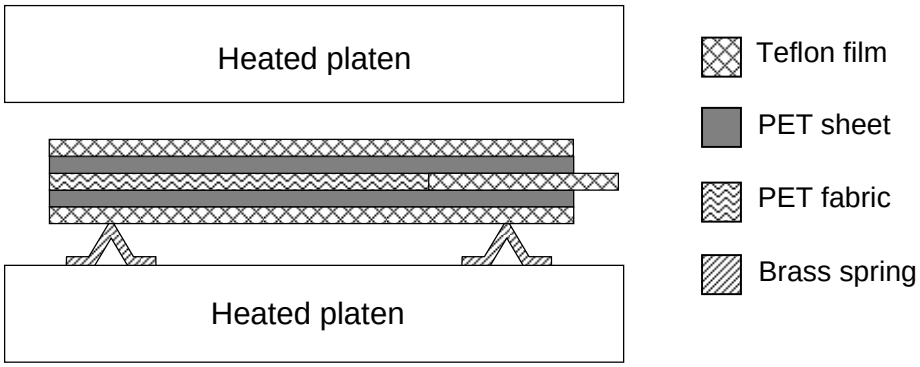

Figure 4.1 Experimental setup for PET SPCs manufacturing

4.2.2.2 Compression molding of mixed PET fibers and undrawn PET fibers

Another processing method was used to manufacture slowly crystallizing PET SPCs. In this method, highly crystallizing PET fibers were premixed with undrawn amorphous PET fibers and then compression molded. Upon heating to an appropriate temperature between Tg and Tm, the amorphous fibers can be softened and bonded together while the high crystalline fibers are nearly attacked by the heat. In this case, the highly crystalline fibers serve as reinforcement and the fused amorphous fibers serve as matrix.

4.2.3 Characterizations

The compression molded laminations, both fabric reinforced and non-reinforced, were subjected to interfacial peeling and the peeled interfaces were investigated using optical stereomicroscopy and scanning electron microscopy (SEM) to determine the quality of the fusion bond and the adhesion between the matrix and the fabric. Scanning

electron microscopy (SEM) analyses were performed using a Hitachi S-800 (FEG) with surfaces coated with a thin gold layer to ensure surface conductivity.

Tensile tests were conducted using an Instron universal testing machine (type 4206) with a crosshead speed of 0.05 mm/s. Tensile specimens of standard dimensions were punched from molded samples. The mold standard is DIN-53504-S2. The ends of the tensile specimen were glued using an epoxy adhesive between two nylon stubs to avoid premature failure at the clamping points.

The ISO 6603 method was chosen to test the impact strength of PET SPCs. This method is applicable to rigid plastic specimens of thickness between 1 and 4 mm. The instrumented impact testing equipment used in this study was an ITR-2000 impact tester. The general features of the testing apparatus are shown in Figure 4.2. The material specimen is a flat plate, approximately 5" × 5", which is securely clamped over a 4" diameter annular anvil. The test consists of complete penetration of the specimen by a 0.5" diameter hemisphere probe which is guided through the center of the annulus under conditions of near constant velocity. The probe is equipped with transducers for measuring velocity and the load interaction between the probe and specimen. With this instrumented method, the total absorbed energy is calculated from the measured force history.

The thermal properties, particularly Tg and Tm, of the PET sheets were examined using differential scanning calorimetry (DSC Q200 from TA instruments). The heating rate is 20°C/min. The heating temperature range was from 20°C to 300°C. The first-run curves were used to calculate the crystallinities.

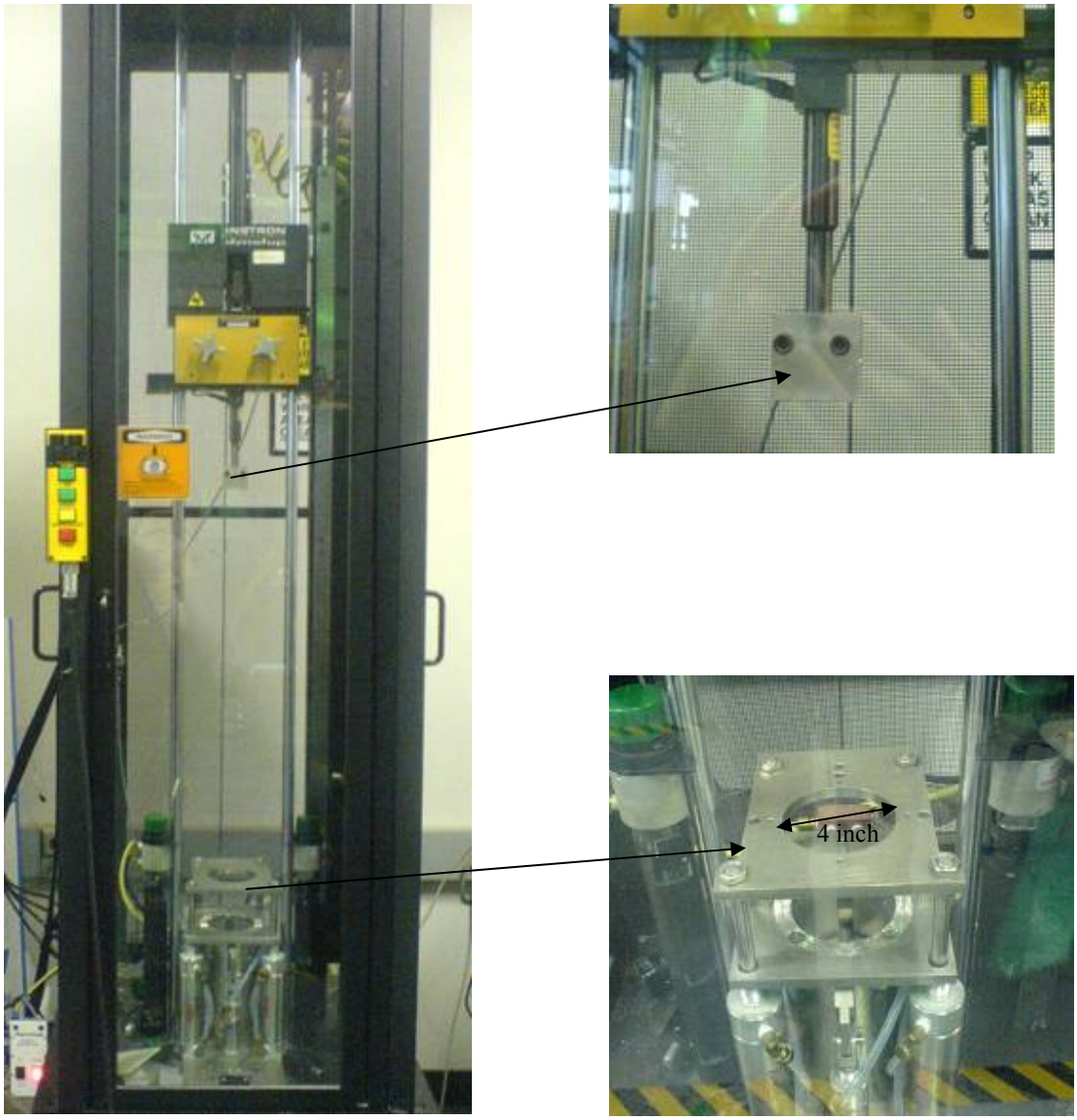

Figure 4.2 Instrumented falling weight impact tester

The primary thermograms of amorphous PET fibers and film, PET fibers and PET fibers after heat treatment were recorded using a Perkin-Elmer TGA-7 instrument in nitrogen atmosphere at a heating rate of 10°C/min in the temperature range 25-500°C in nitrogen atmosphere.

X-ray diffraction patterns were taken on PET fibers using a Philips X-ray diffractometer, model Xpert MPD with symmetrical reflection geometry. The Cu Ka radiation generated at 45 KV and 40 mA was used. The scattering intensities were recorded every 0.058" over the range of 10–60°. Time per step was 10 s. Samples were prepared in two different forms. In the first form, the filaments were horizontal and used for equatorial scan. The parallel bundles of filaments with length of 10 mm were mounted horizontally in the sample holder of the wide-angle X-ray scattering (WAXS) instrument, and the direction of incident beam was perpendicular to the fibers axis. In the second form, the filaments were vertical and used for meridional scan. The filaments were paralleled and then the ends were glued. The bundle of filaments was mounted vertically in the sample holder and the superfluous fibers were cut. In both cases, care has been taken to have a flat surface with suitable thickness. The WAXS patterns are analyzed by curve-fitting procedures to separate crystalline reflections from amorphous scattering to obtain crystallinity and crystallite sizes. Commercial software MDI Jade 8.5 was used to analyze the data.

The molecular weights of PET film, PET fibers and undrawn amorphous PET fibers were measured using Ubbelohde Type I viscometers. The solvent is 60/40 phenol-1,1,2,2-tetrachloroethane. The PET solutions have been prepared with different concentrations: 0.17, 0.2, 0.24, 0.3 g/dL. The experimental procedure is described in detail in Appendix A. The viscometer was rinsed thoroughly with solvent to remove dirt and dust and then conditioned in constant temperature water bath for 10-15 minutes at 25°C. Additionally 15 ml solution was added into the viscometer and equilibrated in the viscometer a few minutes before testing. The efflux time of the solution was tested 10

times in viscometer. The measurements were consistent to within ±1 s. The characterization began with the least concentrated system. The relative, specific, reduced and inherent viscosities were calculated for all concentrations using the efflux time. The reduced viscosity and inherent viscosity as a function of concentration was drawn in the same plot to find the intrinsic viscosity. Then the molecular weight was calculated.

4.3 Results and discussion

The crystallinities and melting temperatures of amorphous PET films, high-performance PET fibers, and amorphous PET fibers were tested using DSC at a heating rate of 20°C/min with testing temperature range from 0 to 300°C. The 1st run DSC curve was used to evaluate the crystallizing enthalpy and melting enthalpy of these different material forms of PET. Equation 3.1 was used to calculate the crystallinity. The results are summarized in Table 4.1. The DSC curves are shown in Figure 4.3.

As seen in Table 4.1, the crystallinities of amorphous PET film and amorphous PET fibers are similar, both close to zero. This indicates that both amorphous PET film and amorphous PET fibers were nearly amorphous before the DSC experiment. Upon heating from 30°C to 300°C, both of them started to crystallize. However, the crystallization peak of the amorphous PET fiber is wider than that of the amorphous PET film. The melting temperature of the highly crystalline fiber is about 10°C higher than the amorphous film and the undrawn fibers. There was no recrystallization peak observed for the highly crystalline PET fibers when they were heated from 30°C to 300°C.

Table 4.1 Crystallinities and melting temperatures of PET fibers

	ΔHc J/g	Tm °C	ΔHm J/g	Crystallinity %
Amorphous film	-22.674	247	23.037	0.26%
Amorphous PET fibers	-23.13	251.2	26.15	2.1%
PET fibers	---	258.2	38.7	27.6%

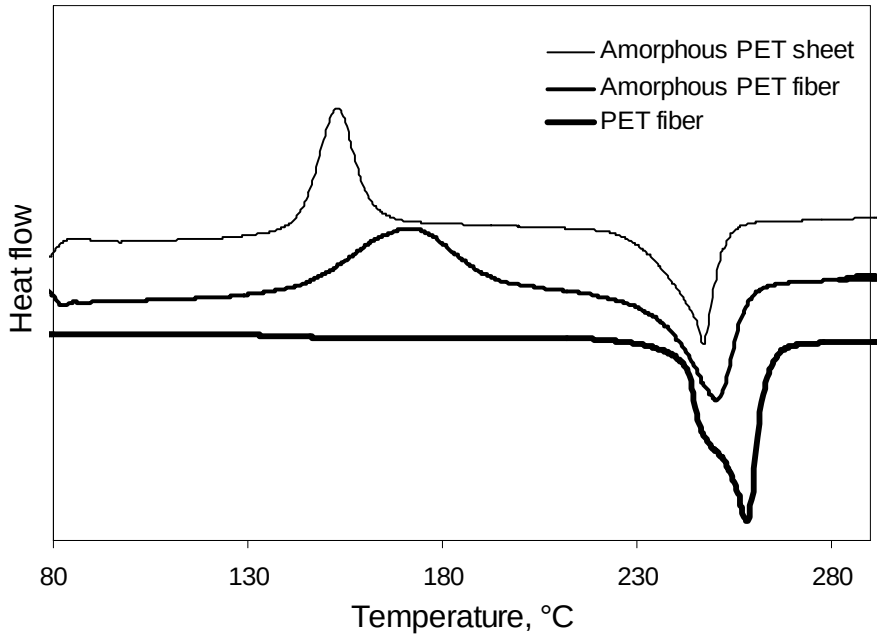

Figure 4.3 DSC curves of PET fibers and film

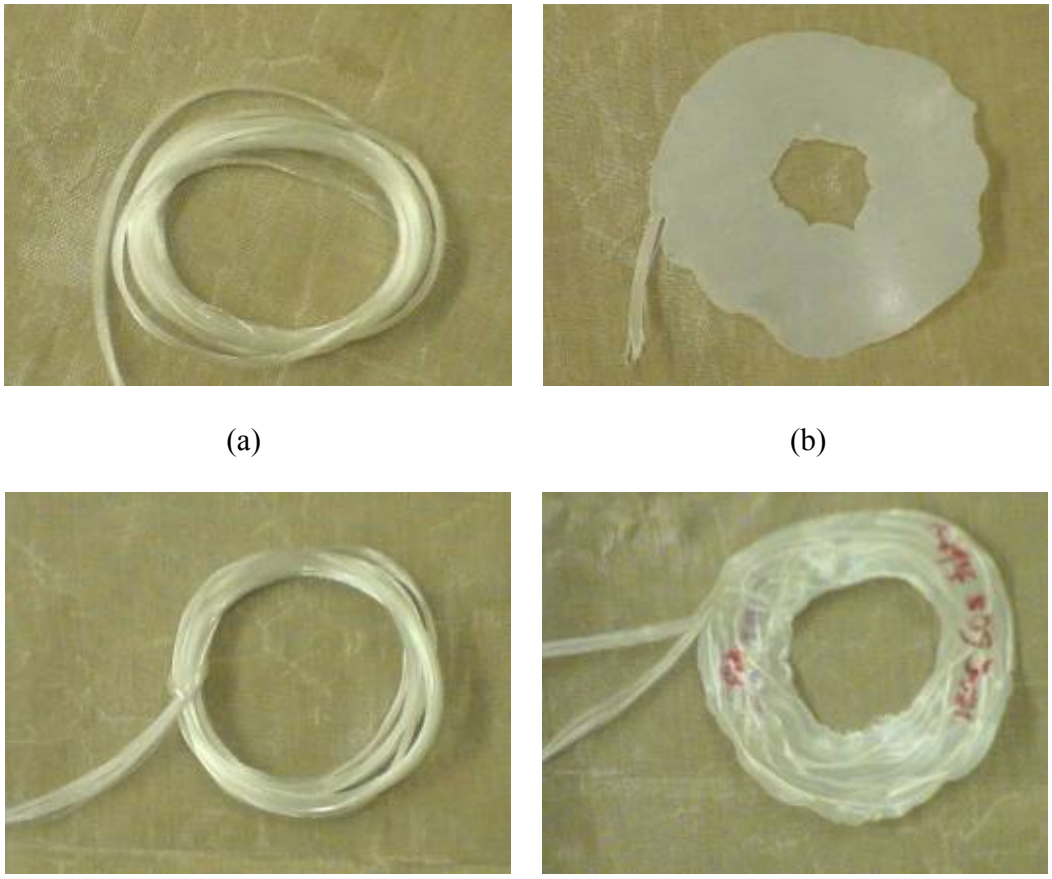

(a) (b)

(c) (d)

Figure 4.4 Highly crystallizing PET filament fibers and amorphous PET filament fibers. (a) Amorphous PET fiber bundle, (b) 180°C 60 s A-PET fiber bundle, (c) Amorphous PET and PET fiber bundle, (d) 180°C 60 s mixed A-PET and PET fiber bundle

The specimens obtained from compression molding of amorphous PET (A-PET) sheets and highly crystalline PET fabrics were in a sheet form, with a thickness around 1 mm. Characterizations were mainly conducted on these SPCs sheets. Samples were also prepared using the fiber mixing and compression molding method. Different fiber mixing schemes were used in sample preparation, including mixing highly crystallizing filament fibers with undrawn amorphous filament fibers, mixing highly crystalline staple fibers

with amorphous staple fibers, and mixing highly crystalline filament fibers with amorphous staple fibers. Figure 4.4 shows a couple of samples prepared using this fiber mixing and compression molding method.

4.3.1 Effect of thermoprocessing conditions

The crystallinities and melting temperatures of the amorphous PET film and the undrawn PET fibers are similar, both with a crystallinity close to zero and a melting temperature around 250°C. Thus, effects of the thermoprocessing conditions are expected to be similar when either of these two amorphous material forms is used as a matrix material. Thus, the PET film was used as a model matrix to investigate the effects of thermoprocessing conditions on the properties of PET SPCs. Two major parameters, platen temperature and heating time, were studied.

4.3.1.1 Effect of platen temperature on adhesion

The uni-axial fiber reinforced PET SPCs were made by compressing two amorphous PET sheets with separated uni-axial PET fibers fixed on the metal frame. While the heating time kept at 30 s, platen temperatures were changed among 160, 170, 180 and 210ºC. Then the uni-axial fiber reinforced PET SPCs was fractured using the Instron machine. SEM was used to observe the broken surfaces.

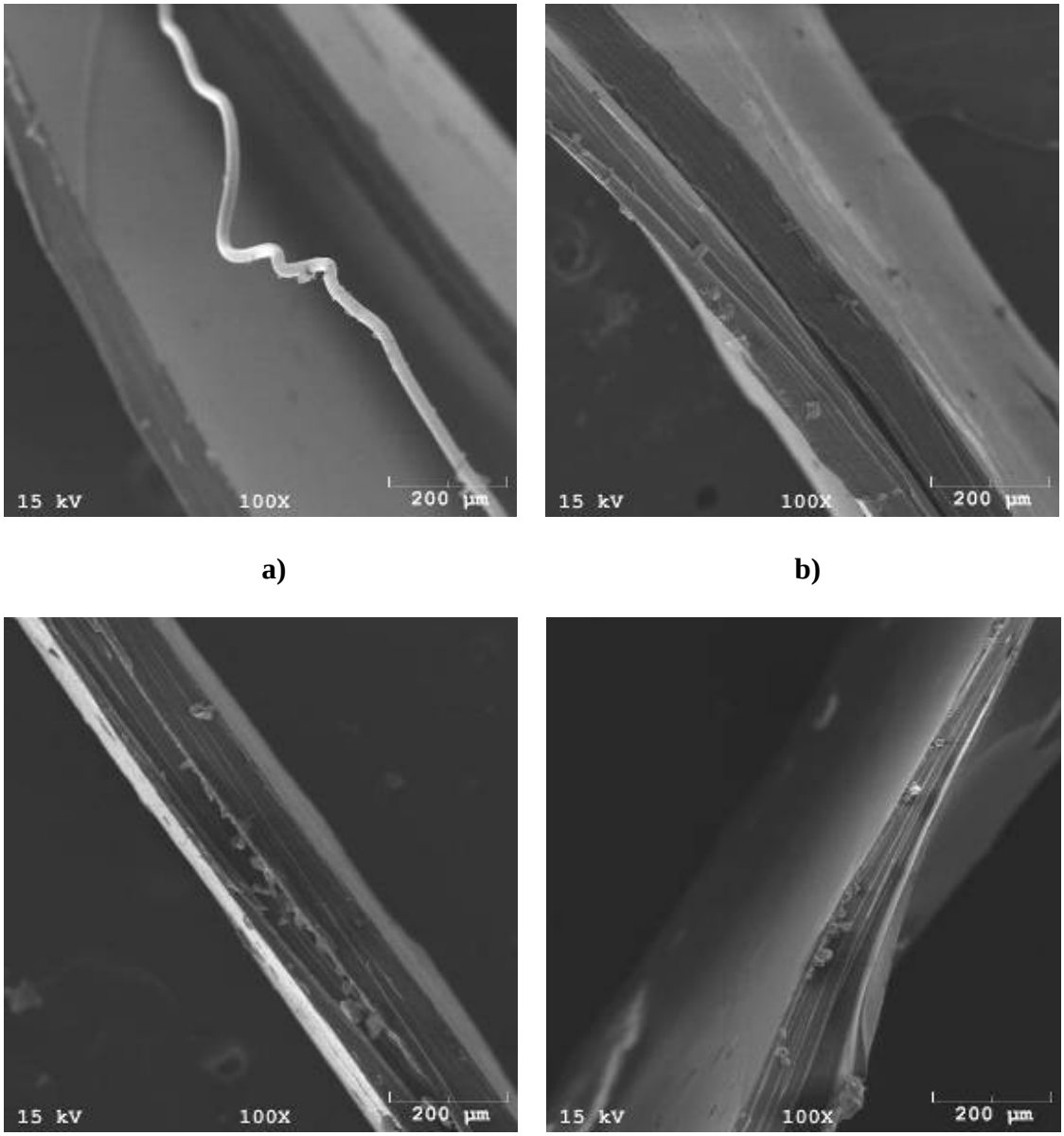

a) **b)**

c) **d)**

Figure 4.5 Appearance of fractured PET SPCs compression molded with a constant heating time of 30 s but varied platen temperatures of a) 160 ºC, b) 170 ºC, c) 180 ºC, and d) 210 ºC.

With the increase of platen temperature, the bonding between PET sheets and the bonding between fiber and matrix were both improved. With the increase of platen temperature, the pulled out length of PET fiber decreased, indicating improved bonding quality. When the platen temperature was 180ºC or above, the pulled out length was minimal. Based on this finding, a platen temperature at 180ºC was used for focused studies. A compression pressure around 0.7 MPa was found to be appropriate for laminating the films and the fabrics into composites. At this pressure, the compression molded samples were free from air bubbles and the molded thickness was well controlled.

4.3.1.2 Effect of holding time on adhesion

The effect of heating time on the interfacial adhesion between the matrix and the reinforcement was studied by examining the broken surfaces of uni-axial fiber reinforced PET SPCs, as shown in Figure 4.6. The state of matrix-fiber adhesion can be qualitatively evaluated by checking the pulled out length of fibers. The results show that after 15 s at platen temperature 180ºC, the pulled out fiber lengths were almost the same. For a heating temperature of 180ºC, excellent adhesion was achieved after the heating time 15 s. Based on the PET SPCs bonding test, heating time longer than 15 s was found to give excellent fusion bonding and thus used for focused studies.

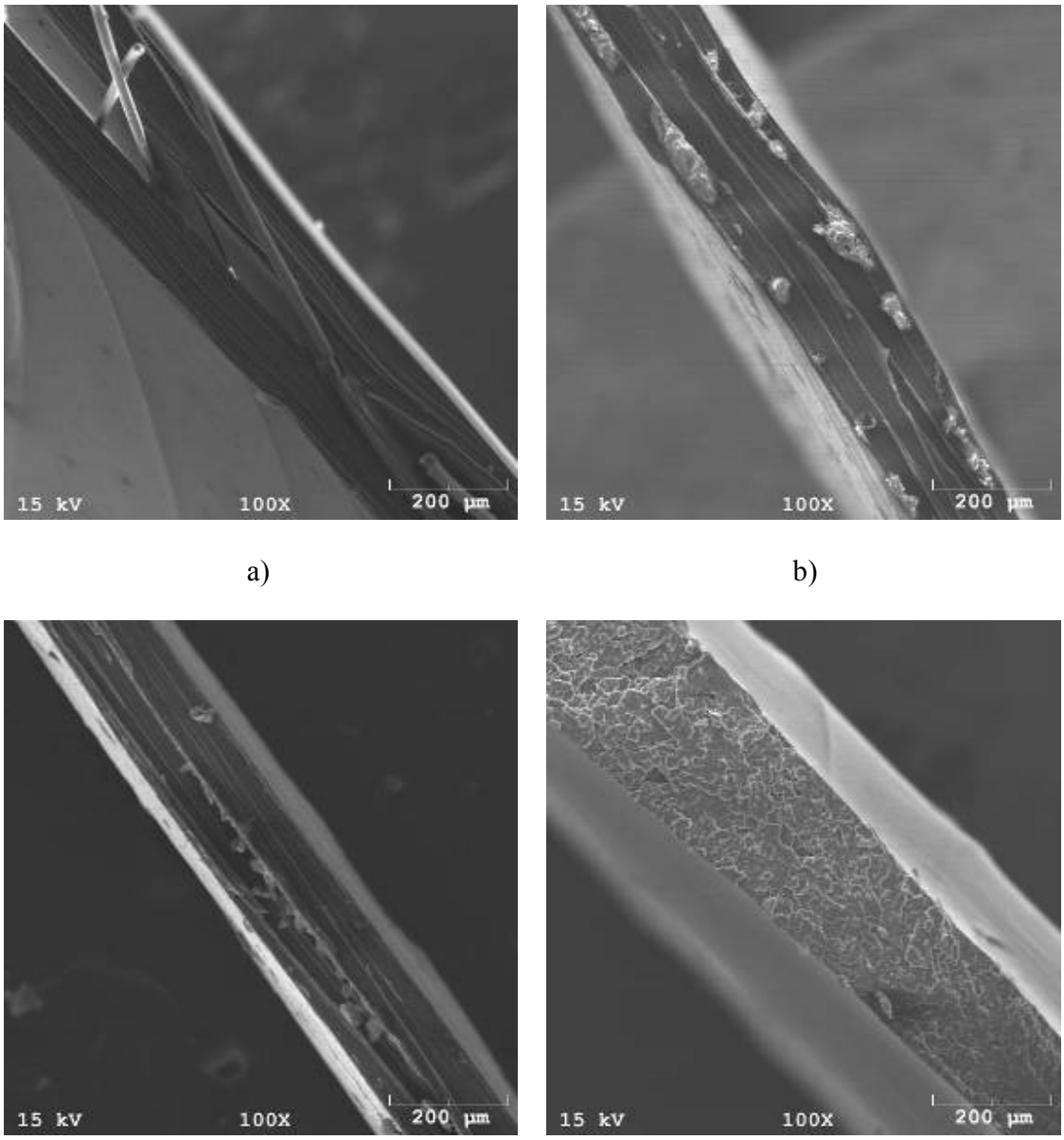

Figure 4.6 Broken surface of PET SPCs reinforced by uni-axial PET fibers at a constant platen temperature of 180 ºC but varied holding time: a) 5 s, b) 15 s, c) 30 s, and d) 60 s

4.3.2 Mechanical properties of PET SPCs

4.3.2.1 Tensile properties of PET SPCs

Figure 4.7 shows the load versus displacement curves of the PET SPCs and the non-reinforced PET, both fabricated under the same processing condition with platen temperature of 180ºC and holding time of 90 s. Shims were used to control the reinforced PET SPCs and the non-reinforced PET into the same thickness. The strength of the 25% PET SPCs is 94 MPa, significantly higher than that of the non-reinforced PET, 50 MPa. The initial linear elastic region also shows a higher yielding strength for the PET SPCs than the non-reinforced PET. Figure 4.8 compares the different failure mechanisms of the PET SPCs and the non-reinforced PET. Necking is suppressed in the SPCs, while the non-reinforced PET is subjected to a large degree of flow under a constant load. The fracture of the PET homocomposite was initiated by the failure of the fiber mesh. Because the ductile sheath (from the original PET sheet) and the brittle core (i.e. the fabric) break at the same instant, it can be deduced that reasonably good interfacial bonding and interlocking between the matrix and the reinforcement are achieved in the PET SPCs.

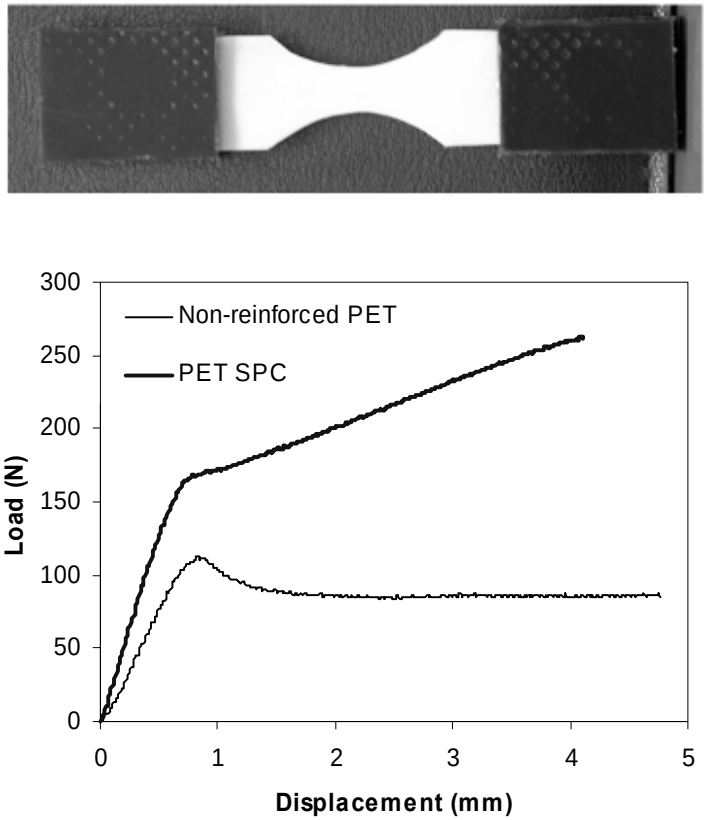

Figure 4.7 Load displacement curves for the PET single-polymer composite and the non-reinforced PET. Both reinforced and non-reinforced PET samples were compression molded at 180ºC with a holding time around 90 s.

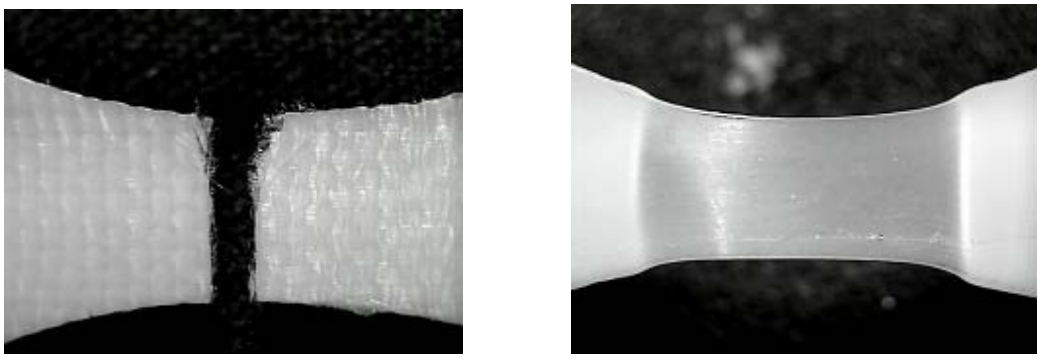

(a) (b)

Figure 4.8 Comparison of the failure mode between (a) PET single-polymer composite and (b) non-reinforced PET. Necking is suppressed in the composite while the non-reinforced PET is subjected to a large amount of flow during tensile testing.

4.3.2.2 Tensile testing results of PET SPCs from commingled fibers

Highly crystalline unidirectional PET filament fibers were commingled with undrawn amorphous PET filament fibers in a mixing ratio of 45/55 by weight to make PET SPCs. The processing conditions are similar to those used for compression molding of PET sheets and fabrics. The tensile strengths of amorphous PET film, undrawn amorphous PET fibers and PET SPCs were tested on an Instron universal testing machine at a displacement speed of 5 mm/min with gap distance of 4 cm. The tensile curves in Figure 4.9 show that the tensile strength of amorphous PET film and undrawn amorphous PET fibers are similar. The DSC curves discussed earlier also show that their crystallinities are very close. Thus, their processing conditions are expected to be alike. With a platen temperature of 180ºC and a holding time of 60 s, after reinforced, the tensile strength of PET SPCs is almost five folds of that of amorphous PET.

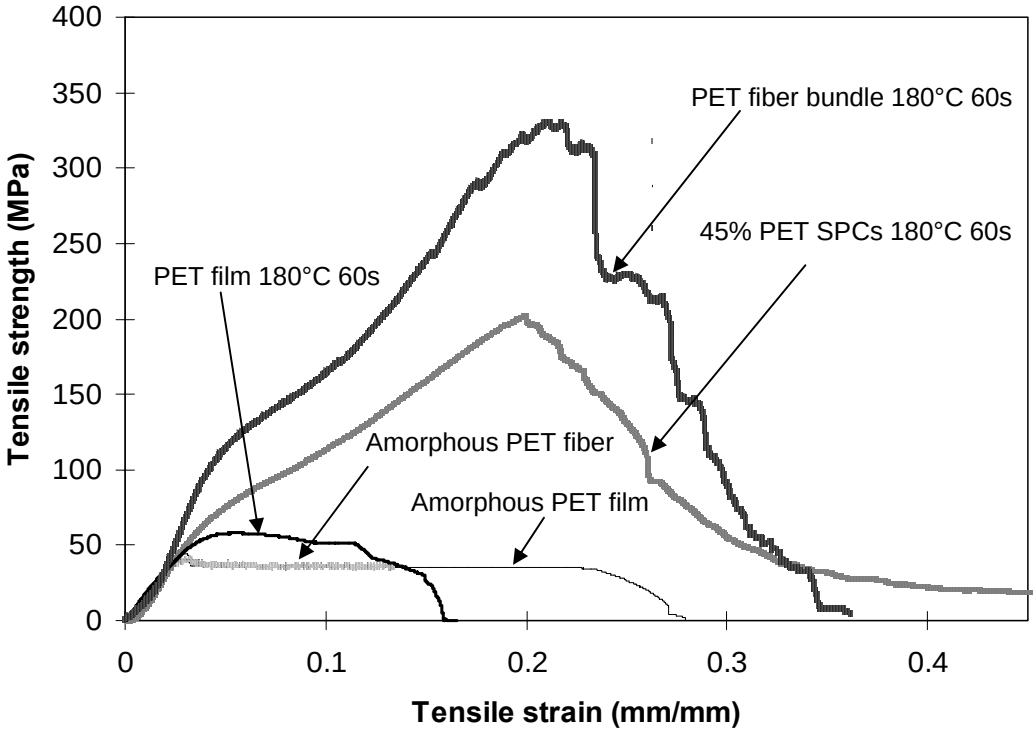

Figure 4.9 Tensile curves for the PET SPCs, amorphous PET film and undrawn PET fibers.

Table 4.2 Average tensile strength and modulus of PET

	Average tensile strength, MPa	Average tensile modulus, MPa
Amorphous PET film/fiber	46	2079.6
180°C 60 s PET fiber bundle	348	3378.4
180°C 60 s 45% PET SPCs	183	2435.3
Model predict	182	2664.0

4.3.2.3 Rule of mixtures model and prediction

Using rule of mixtures, the composites properties can be approximately estimated based on the assumption that the properties of composites are the volume weighed average of the phases (matrix and dispersed phase) properties [146]. The long-fiber reinforced composites in longitudinal direction can be demonstrated in Figure 4.10. Equation (4.1) and Equation (4.2) can be used to predict the tensile strength and modulus of the aligned continuous fiber composites. According to Rule of mixtures properties of composite materials of Aligned continuous fibers are estimated as follows:

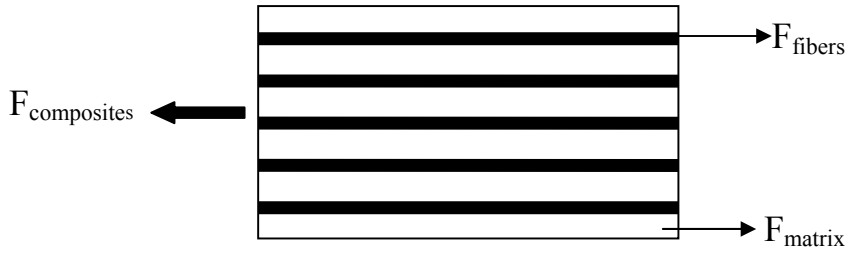

.

Figure 4.10 Tensile strength of long-fiber reinforced composite in longitudinal direction.

$$F = F_m + F_f$$

$$\sigma A = \sigma_m (1-f) A + \sigma_f f A$$

$$\sigma = \sigma_m (1-f) + \sigma_f f \tag{4.1}$$

F, force applied to the composite as a whole

F_m, force in the matrix

F_f, force in the fiber

A, cross-sectional area of the composite

σ, tensile strength of the composites

σ_m, tensile strength of the matrix

σ_f, tensile strength of the fibers

f, volume fraction of fibers

$$E = E_m(1-f) + E_f f \tag{4.2}$$

E, modulus of elasticity of the composites

E_m, modulus of elasticity of matrix material

E_f, modulus of elasticity of fiber material

f, volume fraction of fibers

The tensile strength and modulus of amorphous PET, highly crystallizing PET fibers processed by 180°C 60 s and PET SPCs processed by 180°C 60 s have been tested using the Instron machine. The results are showed in Table 4.2. The average tensile strength and modulus of the amorphous PET are 46MPa and 2079.6MPa. The average tensile strength and modulus of the highly crystallizing PET fibers bundle processed by 180°C 60s are 348MPa and 3378.4MPa. According to the rule of mixing (Equation (4.1) and Equation (4.2)), the predicted tensile strength and modulus of 45% PET single polymer composites should be 182MPa and 2664MPa. The tested tensile strength and modulus of 45% PET single polymer composites are 183MPa and 2435.3MPa. Thus the rule of mixing works very well for PET single polymer composites.

4.3.2.4 Impact testing results

Impact properties of two PET sheets processed under 180°C 60s and PET single polymer composites processed under 180°C 60s have been tested. Impacts were inflicted on the laminates using an instrumented impact tester. The diameter of the impact tip was 12.7 mm while the 100×100 mm size specimens were clamped by an aluminum fixture by a pneumatic pressure of 600 kPa. The impact velocity was around 11.45 ft/sec. The impact loads were showed in Table 4.3 and Figure 4.11. The photographs of the impacted specimens were shown in Figure 4.12.

Table 4.3 and Figure 4.11 showed that the impact strength of PET SPCs was higher than the crystallized PET sheets. The photographs of the impacted specimens showed that the failure mode was different for two PET sheets processed under 180°C 60s and PET single polymer composites processed under 180°C 60s. PET sheet processed under 180°C 60s was very brittle. The sample was broken completely after impacting. Little deformation and failure appeared on the reinforced PET single polymer composites after being impacted. The impact strength was also higher than crystallized PET.

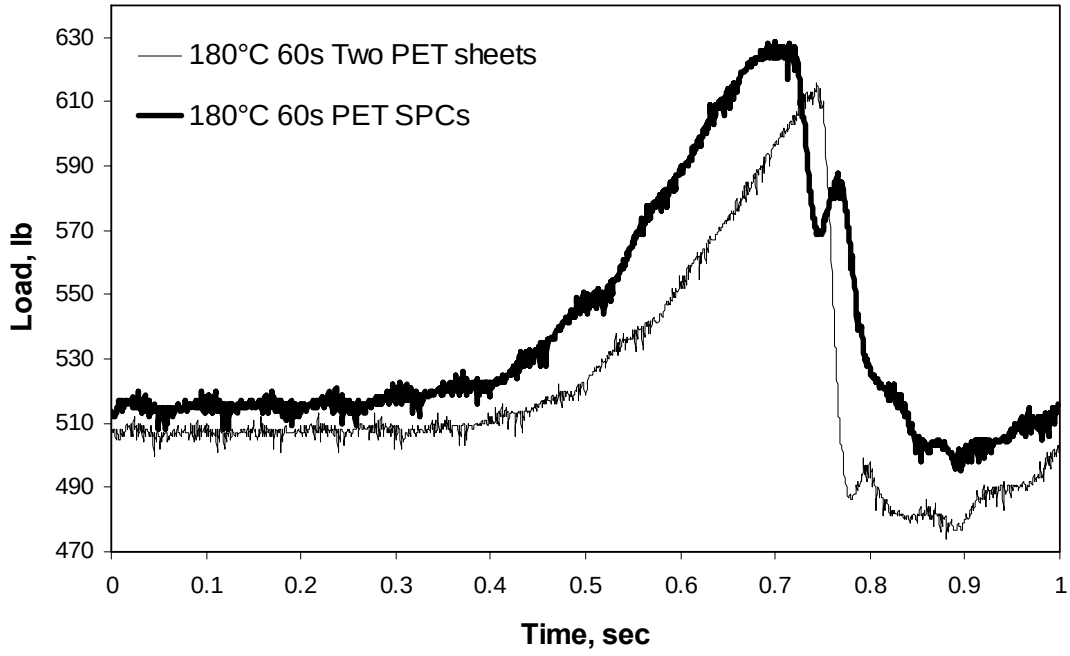

Figure 4.11 Impact properties of two PET sheets processed under 180°C 60 s and PET single polymer composites processed under 180°C 60 s.

Table 4.3 Impact testing results

	Impact velocity (ft/sec)	Maximum load (lb)
Two PET sheets processed at 180°C 60 s	11.45	96.22
PET SPCs processed at 180°C 60 s	11.45	99.78

a) b)

Figure 4.12 Photographs of the impacted specimens. a) Two PET sheets processed under 180°C and 60 s, b) PET SPCs processed under 180°C and 60 s.

4.3.3 Changes of PET fibers before and after 180°C 60 s heat treatment

4.3.3.1 XRD results

Amorphous PET sheet, amorphous PET fibers, PET fibers and PET fibers processed under 180°C 60 s were investigated using X-ray diffraction. The equatorial slices was derived to examine the appearance of the equatorial peak as shown in Figure 4.13, from which the crystal sizes were determined for the (010), (110), and (100) planes, as listed in Table 4.4. XRD results show that there is no sharp peak for the amorphous PET film and fibers, which prove that the crystallinity is very low in them and is in accord with the DSC results. The crystallinity reflection peaks of PET fibers and PET fibers processed under 180°C 60 s are in the same position. However, the crystal size

increased when the heat treatment was applied. Dae Hwan Cho et al. [147] mentioned that the short heat treatment results in the series arrangement of the crystalline and amorphous regions. Dae Hwan Cho et al. [147] used Figure 4.14 to demonstrate the morphological change of PET fibers by heat treatment. The crystal size increased when the short heat treatment was applied.

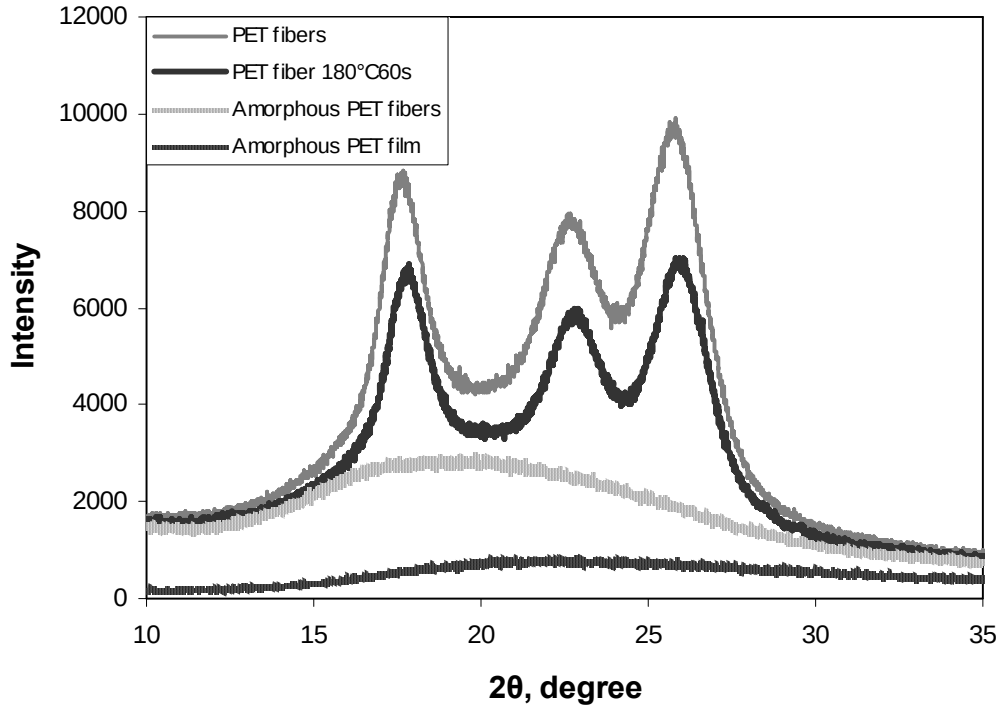

Figure 4.13 X-ray diffraction results

Table 4.4 XRD results

	Crystal size (Å)			
	Equatorial			Meridional
	(010)	(110)	(100)	(-105)
PET fiber	61(1)	39(1)	38(1)	40(2)
PET fiber processed under 180°C 60 s	64(1)	43(1)	40(1)	54(2)

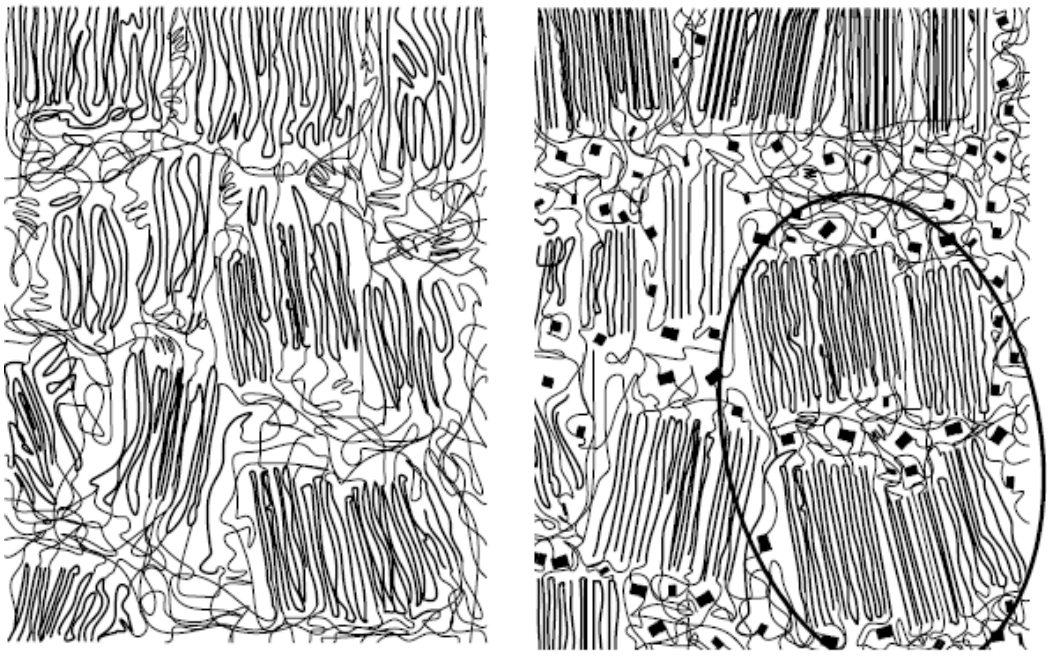

a) Untreated b) Heat treated*

Figure 4.14 Morphological change of PET fibers by heat treatment [147].

4.3.3.2 DSC results

The crystallinities of PET fibers and PET fibers processed under 180°C 60s have been tested using DSC. The heating rate is 20°C/min. The DSC curves are showed in Figure 4.15. The melting temperature and crystallinity are summarized in Table 4.5. The DSC curves of PET fibers and PET fibers processed under 180°C 60 s are very similar. There is not recrystallizing peak when the PET fibers and PET fibers processed under 180°C 60 s are heated from 30°C to 300°C. The crystallinity is nearly the same. But after heat treatment of 180°C 60 s, the crystallinity of PET fiber is increased a little. XRD results showed that after heating, the crystal size is increased a little. The crystallinity increase may be caused by the increase of the crystal size.

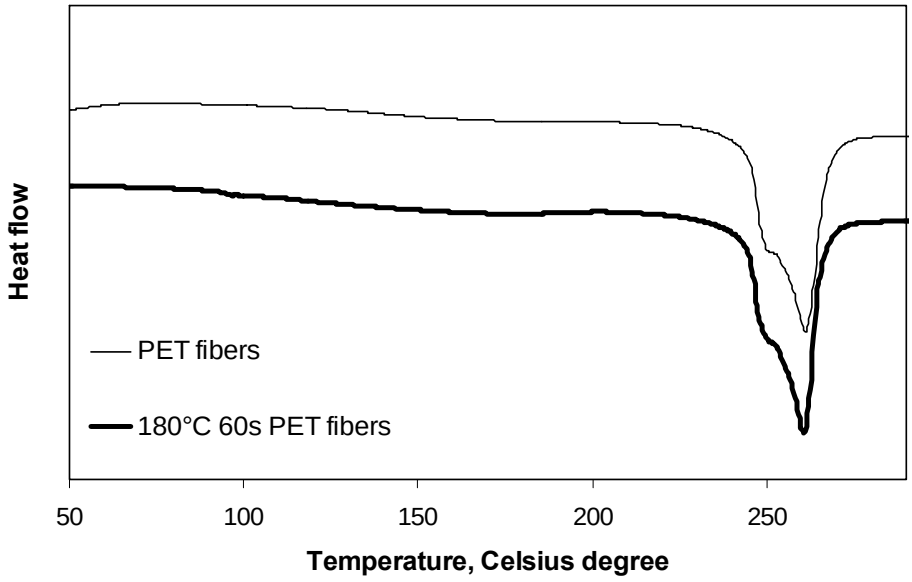

Figure 4.15 DSC curve of PET fibers and PET fibers processed under 180°C 60 s

Table 4.5 DSC results of PET fibers and PET fibers processed under 180°C 60 s

	Tm, °C	ΔHm, J/g	Crystallinity, %
PET fibers	261.3	43.1	30.81
PET fibers under 180°C and 60 s	260.3	43.2	30.83

4.3.3.3 Thermogravimetric analysis (TGA)

Amorphous PET sheet, amorphous PET fibers, PET fibers and PET fibers processed under 180°C 60 s were investigated using TGA. The results were showed in Figure 4.16. Figure 4.16 showed that the heat degradation curves of PET fibers, and amorphous PET fibers were very similar. Stability of PET fibers processed under 180°C 60 s was slightly decreased, but the curve was almost the same with untreated fibers. After heat treatment, the tensile strength was decreased a little, because after hot compression treatment, some of the molecular chains in the fibers were broken. Fiber spinning can break the molecular chain too. Thus the stability of the PET film was a little higher than the PET fibers.

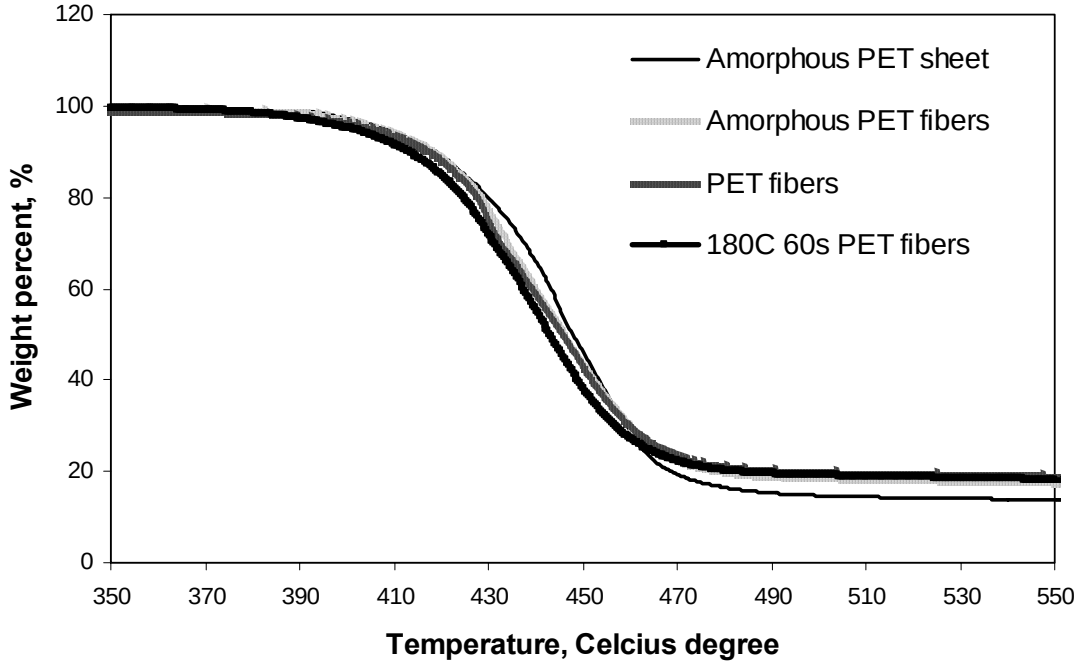

Figure 4.16 TGA results of PET film, PET fibers and PET fibers processed under 180° C and 60 s

4.3.3.4 Molecular weight

The molecular weights of PET film, PET fibers and undrawn amorphous PET fibers were measured using Ubbelohde Type I viscometers. The solvent is 60/40 phenol-1,1,2,2-tetrachloroethane. The PET solutions have been prepared with different concentrations: 0.17, 0.2, 0.24, 0.3 g/dL. The efflux time of the solution was tested 10 times in viscometer. The measurements were consistent to within ±1 s. The relative, specific, reduced and inherent viscosities were calculated for all concentrations using the efflux time. The reduced viscosity and inherent viscosity as a function of concentration was drawn in the same plot to find the intrinsic viscosity in Figure 4.17.

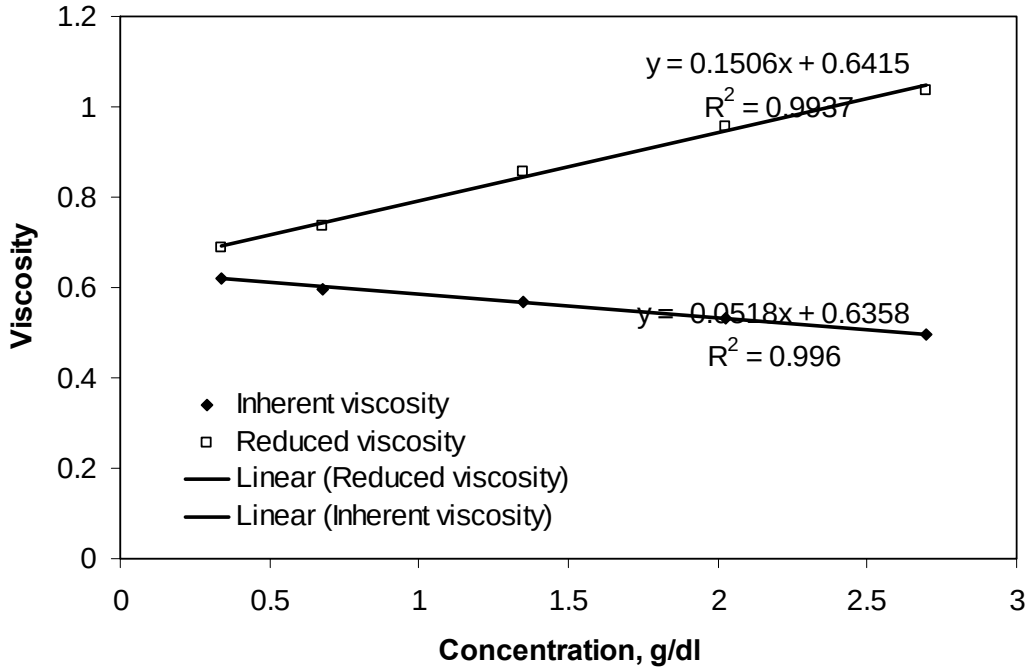
y = 0.1506x + 0.6415
R2 = 0.9937
y = -0.0518x + 0.6358
R2 = 0.996
Inherent viscosity
Reduced viscosity
Linear (Reduced viscosity)
Linear (Inherent viscosity)
Viscosity
Concentration, g/dl
0
0.2
0.4
0.6
0.8
1
1.2
0.5
1.5
2
2.5
3

a)

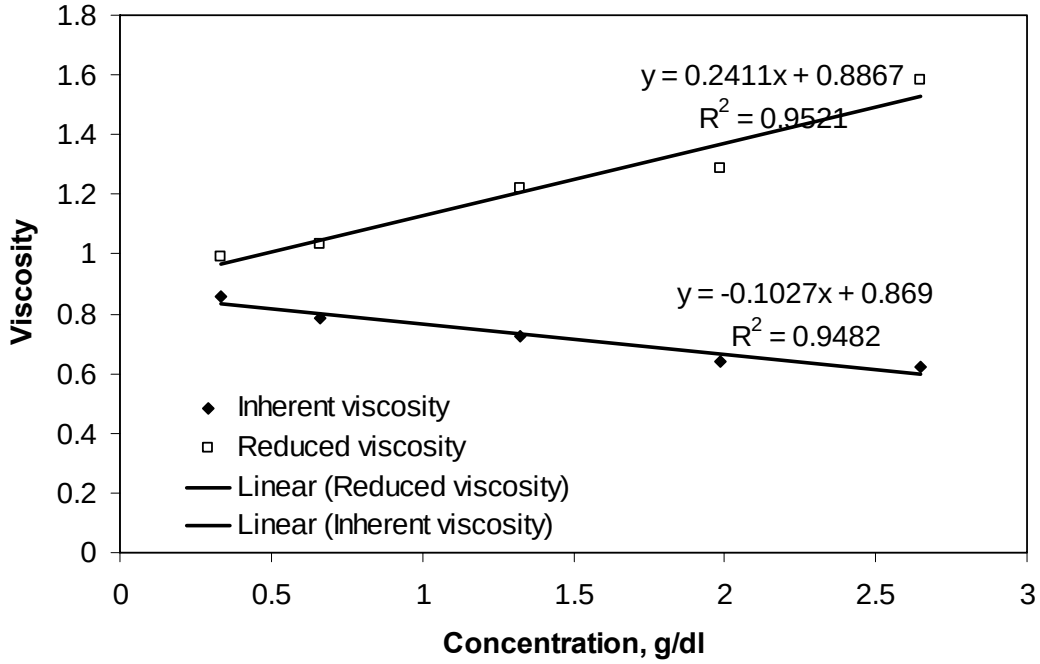
y = 0.2411x + 0.8867
R2 = 0.9521
y = -0.1027x + 0.869
R2 = 0.9482
Inherent viscosity
Reduced viscosity
Linear (Reduced viscosity)
Linear (Inherent viscosity)
Viscosity
Concentration, g/dl
0
0.2
0.4
0.6
0.8
1
1.2
1.4
1.6
1.8
0.5
1.5
2
2.5
3

b)

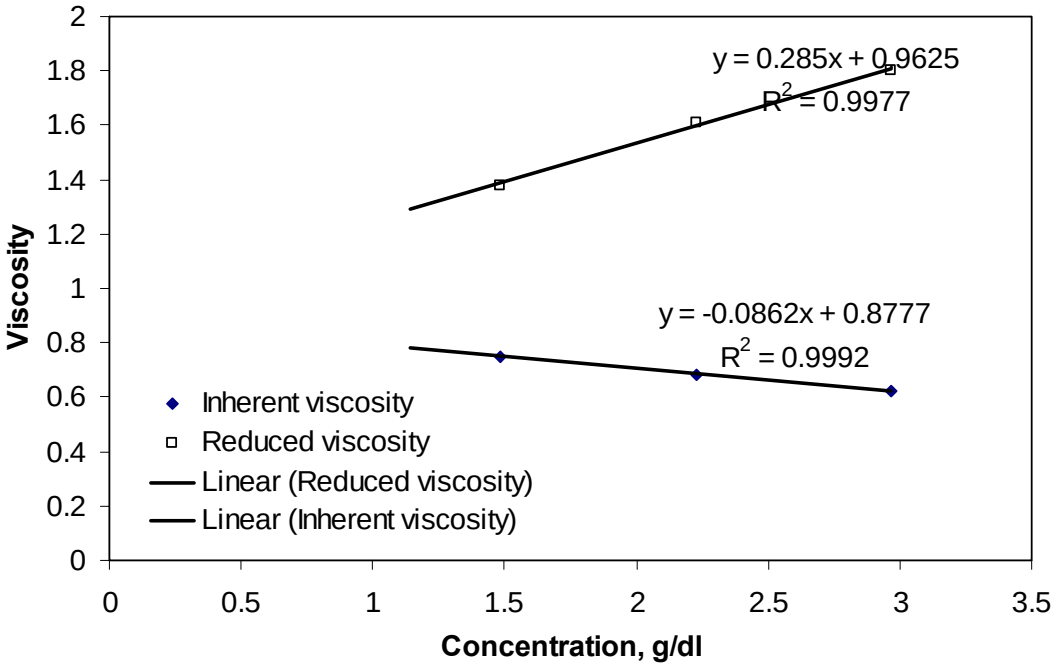

c)

Figure 4.17 Plot of viscosity versus concentration for amorphous PET film, amorphous PET fiber and PET fiber at 25°C: a) amorphous PET film, b) amorphous PET fibers, and c) PET fibers.

For the condition as used for PET/60/40 phenol-1,1,2,2-tetrachloroethane/25° C, the following relations can be found in the literature [148, 149]:

$$\eta = 3.72 \times 10^{-4} (\overline{Mn})^{0.73} \tag{4.3}$$

$$\eta = 4.68 \times 10^{-4} (\overline{Mn})^{0.68} \tag{4.4}$$

Thus, after the determination of the intrinsic viscosity of all PET samples by using the solvent mixture 60/40 phenol/1,1,2,2-tetrachloroethane at 25°C, Equations 4.3 and 4.4 were used to calculate Mn and Mw of the samples by the Mark–Houwink method.

The molecular weight and intrinsic viscosity of PET fiber, amorphous PET fiber and amorphous PET film are given in Table 4.6. The data showed that the molecular weight of PET fiber and amorphous PET fibers are on the same molecular weight level. The molecular weight of amorphous PET film is lower.

Table 4.6 The molecular weight and intrinsic viscosity of PET

	Mn g/mol	Mw g/mol	Intrinsic viscosity at 25° C dl/g
PET fiber	44499	69745	0.9201
Amorphous PET fiber	41723	65086.4	0.869
Amorphous PET film	26820	40768	0.6358

4.3.4 Formability test

To test the formability of the PET SPCs sheets, 3-D dome shape molds were designed and fabricated. The mold and the experimental setup are showed in Figure 4.18. The molds are one step hot embossing molds. Laminations of two amorphous PET sheets with a PET woven fabric in between were compressed between two molds on a Carver hydraulic press. It is important that the lamination is heated rapidly so that crystallization during the heating stage can be suppressed. The springs (Figure 4.18 (b)) inside the mold made of thin brass shims help to achieve uniform and quick contact of the lamination with the molds when the top platen moves downward. After hot embossing, the molds are quenched using cold water input to acquire the PET SPCs.

a)

b)

Figure 4.18 Experimental equipment and molds for 3-D SPCs,

a) Experimental equipment, b) 3-D dome molds

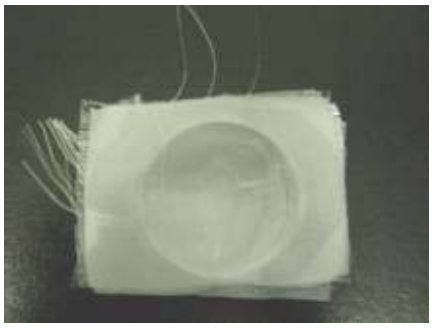

a)

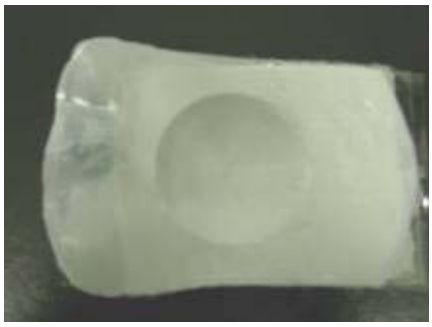

b)

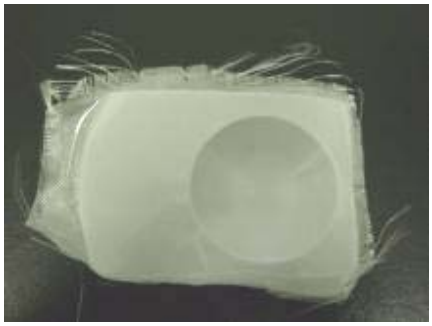

c)

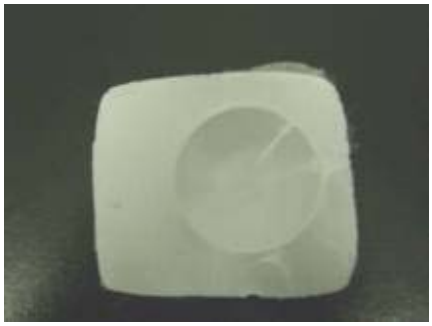

d)

Figure 4.19 3-D dome shape PET SPCs under different processing temperatures,

a)130°C, b)150°C, c) 180°C, c) 210°C

Using the above experimental equipment and molds, 3-D dome shape PET SPCs were manufacturing under different temperatures. The pictures are shown in Figure 4.19. Figure 4.19 shows that when the processing temperature was lower than 180°C, the 3-D dome shape of PET SPCs was not well replicated. When the processing temperature is 180°C or above, there was good bonding between fabrics and matrix and the dome shape was well replicated.

4.3.5 Comparative studies with other composite materials

The uni-axial fiber reinforced PET SPCs was made by compressing two amorphous PET sheets with uni-axial separated single PET fibers fixed on the metal frame. The uni-axial glass fiber reinforced PET matrix composites was made by compressing two amorphous PET sheets with uni-axial separated single glass fibers. The processing condition is platen temperatures 180ºC and heating time 30 s. Then the composites were broken using Instron machine. SEM and microscopy were used to observe the broken surfaces.

Figure 4.20 show that the pull out length of glass fibers for the glass fiber/PET matrix composites are much longer than that of PET fibers for PET SPCs, which show that the bonding of PET fibers to PET matrix is better than the bonding of glass fibers to PET matrix. It gives another advantage for PET SPCs -- the adhesion between fibers and matrix is better.

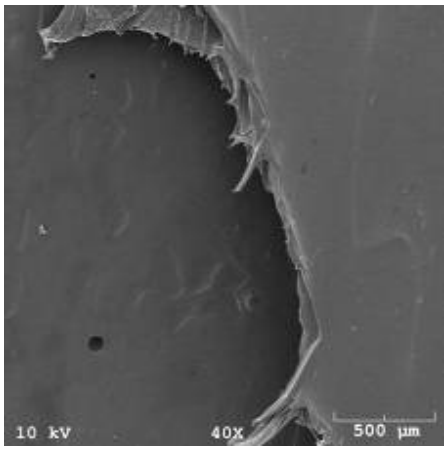

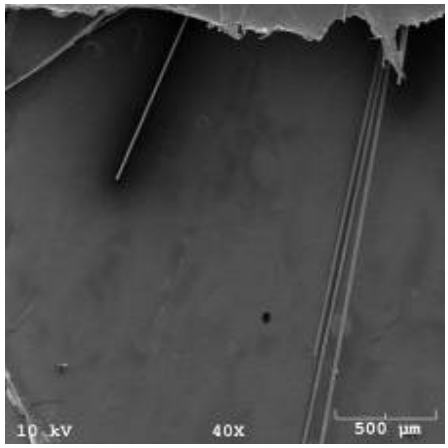

a) b)

Figure 4.20 Broken surface of PET SPCs and glass fiber/PET matrix composites, a) PET single polymer composites at 180°C and 30 s, b) Glass fiber composites at 180°C and 30s

Table 4.7 Comparisons with commercialized SPCs

	Tensile strength, MPa	Processing window
Curve®	120	around 1-2° C
Pure®	200	around 40° C
PET SPCs	230	around 70° C

.The tensile strength and the processing window of PET single polymer composites, Curve® single polymer composites and Pure® single polymer composites have been listed in Table 4.7. The processing window of PET single polymer composites is almost two times wider than that of the existing commercialized Curve® single polymer composites and Pure® single polymer composites. The tensile strength of PET SPCs is much higher than Curve® single polymer composites and Pure® single polymer

composites. The fiber orientation of PET fiber, PET fiber processed under 180°C 60s, and PET single polymer composites using hot compaction method has been evaluated using XRD.

The crystalline system of PET is known to be triclinic [150, 151]; the crystalline c axis is very close to the direction parallel to the fiber axes. However, the planes with Miller indices(-1 0 5) give a very strong X-ray diffraction intensity and their normal makes an angle of 9.778 with the c axis. The (-1 0 5) reflection is used for the evaluation of crystalline orientation factor fc. Often it does not overlap with other (hkl) reflections. [152]

Figure 4.21 showed that the orientation of PET fiber processed under 180°C and 60 s nearly change comparing with that of untreated PET fiber. However, the fiber orientation has been decreased tremendously for PET fibers processed using hot compaction method. This showed single polymer composites manufactured using slow crystallizing polymer has lots of advantages over the tradition method. After processing, there is no change of fiber crystallinity. The processing window is much higher than the other methods.

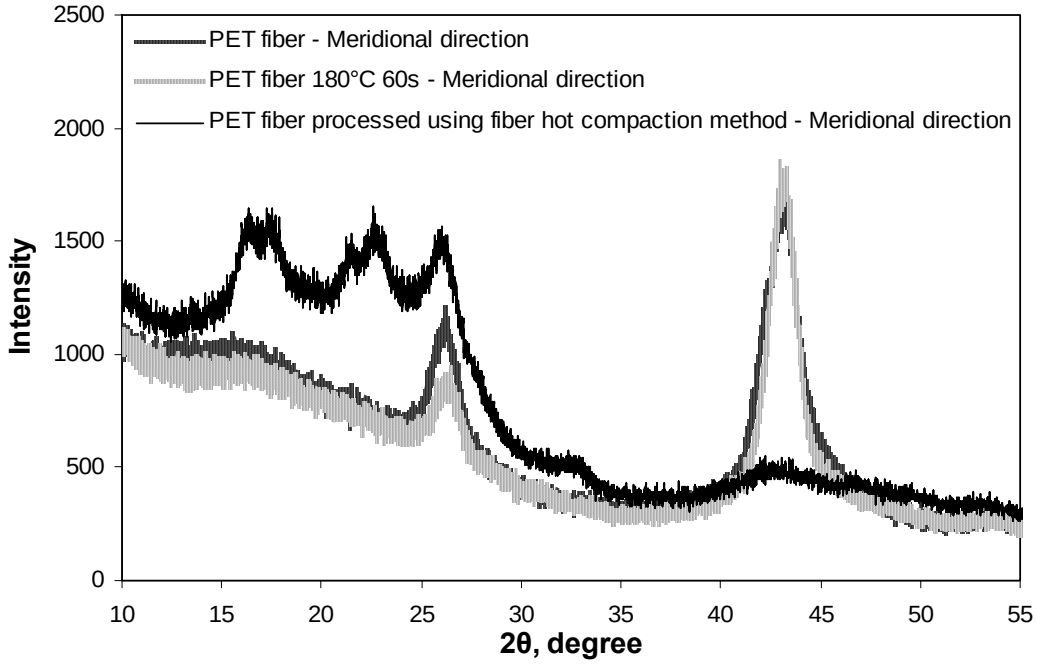

Figure 4.21 XRD results of PET fiber, PET fiber processed under 180°C and 60s, PET fibers using hot compaction method

4.4 Conclusions

PET single-polymer composites were prepared by compression molding laminations of thin amorphous PET sheets/fibers and thin crystalline PET fabrics/fibers. Because amorphous PET experiences softening at a much lower temperature than the melting temperature of its crystalline counterpart, a large processing temperature window can be used to manufacture PET SPCs. The PET SPCs were found to have significant improvement in mechanical properties over non-reinforced PET. The impact properties of PET SPCs had been improved a lot. After reinforced, the tensile strength of PET SPCs was almost five folds of that of amorphous PET. The tensile strength and modulus of amorphous PET, highly crystallizing PET fibers and PET SPCs have been tested using

the Instron machine. Rule of mixing has been used to predict the tensile strength and modulus of PET SPCs. The experimental results showed that the rule of mixing works very well for PET single polymer composites The heating temperature and holding time were found to play a profound role in influencing the properties of the SPCs. Excellent fiber-matrix interfacial adhesion was obtained at a low consolidation temperature of 180ºC, more than 70°C below PET's normal melting temperature, and a holding time of 30 s. After heat treatment, PET fibers didn't change a lot. Unwanted annealing effect was minimized. The fibers were able to maintain their highly orientated crystalline structure. To process slowly crystallizing PET SPCs at the temperature much lower than the melting temperature of the polymer is feasible. The method is equally applicable to other slowly crystallizing polymer, such as poly (lactic acid) (PLA), poly (ether ether ketone), poly (arylene ether ketone), poly (trimethylene terephthalate), poly (phenylene sulfide), syndiotactic polystyrene, to name a few.

CHAPTER 5

FUSION BONDING OF TWO CRYSTALLIZABLE AMORPHOUS PET SHEETS

5.1 Introduction

The previous chapters have shown that different material forms from a slowly crystallizing polymer can be used for effective fabrication of single polymer composites. This method has considerable advantages over traditional single polymer composites manufacturing methods. First, the processing temperature window is much wider than in processes where fast crystallizing polymers are used. Second, no chemical inhomogeneities (e.g., due to the involvement of copolymers, due to the variation of chain configuration and chirality, or due to the variation in molecular weight) are introduced into the system. When PET is used in this method, the reinforcement can be highly crystalline PET fibers/fabrics, and the matrix can be formed from nearly amorphous PET films or fibers. Upon heating between Tg and Tm, the nearly amorphous PET becomes rubbery and can work as a binding material for the reinforcements. Since the mechanical properties of the composite are largely dependent on the fusion quality of the matrix material, it is important to study the fusion bonding behavior of the crystallizable amorphous PET matrix.

Fusion bonding, or welding, is a well-established technology in the thermoplastics industry where the efficiency of the welded joint can approach the bulk properties of the adherents [153, 154]. Fusion bonding plays a major role in many aspects of processing of thermoplastics and thermoplastic composites, including inter-ply consolidation, repair

and new manufacturing techniques such as integrated processing [155]. Fusion bonding is to heat the polymer at the interface to a viscous state, physically causing polymer chains to inter-diffuse, and cooling the polymer for join consolidation [156, 157]. The polymer chains are mixed across the interface during welding, resulting in the fusion of the joint surfaces and development of the ability to transfer loads through the welded area [158]. During fusion bonding, both heat and pressure are applied to the two thermoplastic surfaces in contact. The applied heat causes the material to soften, while the simultaneous application of pressure causes the softened asperities to spread at the interface between the thermoplastic surfaces. The high temperature at the interface leads to interdiffusion of polymer chains across the area. The main goal of fusion bonding is to produce a monolithic structure by intimate contact, molecular interdiffusion healing, and interlaminar void reduction. In particular, the coupled processes of intimate contact and healing contribute to interfacial bond [159]. Processing conditions have great influence on the efficiency of the bonding process. Strong bonding between identical or miscible amorphous polymers can be promoted by elevated contact pressures and temperatures well above the glass transition temperature [160-167]. Fusion bonding of semicrystalline polymers generally requires interface temperatures above the melting temperature.

Fusion bonding of amorphous polymers above the glass transition temperature and fusion bonding of semicrystalline polymers above the melting temperature have been well studied in the literature. However, little knowledge is available on fusion bonding of crystallizable amorphous polymers. The fusion bonding behavior of crystallizable amorphous polymer is expected to be more complex because of the crystallization at the time of heat sealing. For single-polymer composites made of slowly crystallizing

polymers, the unique fusion bonding behavior of these polymers should have a great influence on the properties of the composite. Thus, to study the fusion bonding behavior of such polymers is not only fundamentally interesting but also highly desired in end applications.

In this study, the fusion bonding behavior of PET was investigated. There are two competing processes occurring when an amorphous PET sheet is heated. First, the amorphous phase will experience a glass transition at its glass transition temperature, Tg, and the polymer will become rubbery and sticky at temperatures well above Tg (say 20ºC above Tg). Two such sticky pieces can be fused together through chain diffusion at the interface. The second competing process is crystallization. For a crystallizable amorphous phase, such as an amorphous PET phase, it will start to crystallize when its temperature is above Tg. Therefore, the just softened, rubbery and sticky amorphous phase will turn into a hardened crystalline phase at the same processing temperature. Note that, when the processing temperature is above the melting temperature, the problem will become a pure fusion problem.

5.2 Experimental

Amorphous PET sheets with a thickness of 0.25 mm were used in the experiments. Two PET sheets were compressed between two heated platens on a Carver hydraulic press. Then the compressed sheet was rapidly quenched into tap water. Thin Teflon® films (0.07 mm in thickness) were used on both sides for easy mold separation. Additional Teflon film was employed in the middle of the lamination to create an unbonded region for peeling testing. Spacers were inserted between the heated platens to control the thickness of the sheet. The major process parameters including the platen

temperature, the compression force and the heating time were varied to study their effects on the interfacial bonding. The compressed PET sheet had a thickness around 0.5 mm. The bonding developed after compaction was evaluated using a T-peel test (according to ASTM D1876). The width of the peeling samples is 10 mm. The peel tests were carried out at a displacement rate of 20 mm/min on an Instron tensile testing machine.

The failure surfaces on broken samples from peeling tests were examined using SEM (Hitachi S-800 SEM). SEM samples were sputter coated with gold for a period of 2 minutes with current at 20 mA under vacuum of 0.7 torr. The actual thermal responses at the middle of the laminations with Teflon sheets of varied thickness inserted were measured using a K-type thermocouple.

DSC was conducted on a TA Instruments DSC Q-100. All samples were exposed to consecutive heating and cooling programs: first heating (30 to 300ºC), cooling (300 to 30ºC) and second heating (30 to 300ºC), cooling (300 to 30ºC). The DSC data were taken from the first heating cycle. The heating and cooling rates were 20ºC/min. All scans were run under N_2 atmosphere.

5.3 Results and discussion

5.3.1 Effect of heating rate on the adhesion of two PET sheets

Generally, the heating rate greatly affects the fusion bonding quality of two sheets. In order to study the effect of the heating rate on the fusion bonding quality, Teflon sheets with different thickness (from 0.05 mm to 1.5 mm) were inserted between the two PET sheets and the two platens. The platen temperature was kept at 180ºC. With Teflon sheets inserted, the temperature at the fusion bonding interface will rise at a slower rate. The actual thermal responses at the middle of the lamination, with Teflon sheets of varied

thickness inserted, were measured using a K-type thermocouple; the results are shown in Figure 5.1. With 1.23 mm thick Teflon sheets inserted on each side of the sample, the interface temperature took more than 15 s to reach about 150ºC and much longer to reach close to 180 ºC . The slow cooling rates resulted in the coupling of the fusion process and the crystallization process, thus deteriorating the fusion bonding quality. When heat conduction was used as a means for heating, slow heating was an inherent problem for thick laminations. In this case, other heating methods with which energy can penetrate directly into the sample would be desirable. One possible method is high-frequency dielectric heating. Using this method or alike, the thick sample may be rapidly heated throughout the entire thickness.

For small thickness of the Teflon sheet, e.g. 0.25 mm and 0.5 mm, good fusion of the two PET sheets was obtained and a similar topography as in Figure 5.2 (b) was observed on the broken surface of peeled samples. When the thickness of the inserted Teflon sheet increased to above 1 mm, good fusion did not form, and the samples can be peeled apart with hands and the failure propagated along the original interface with a failure surface topography similar to that of Figure 5.2 (a).

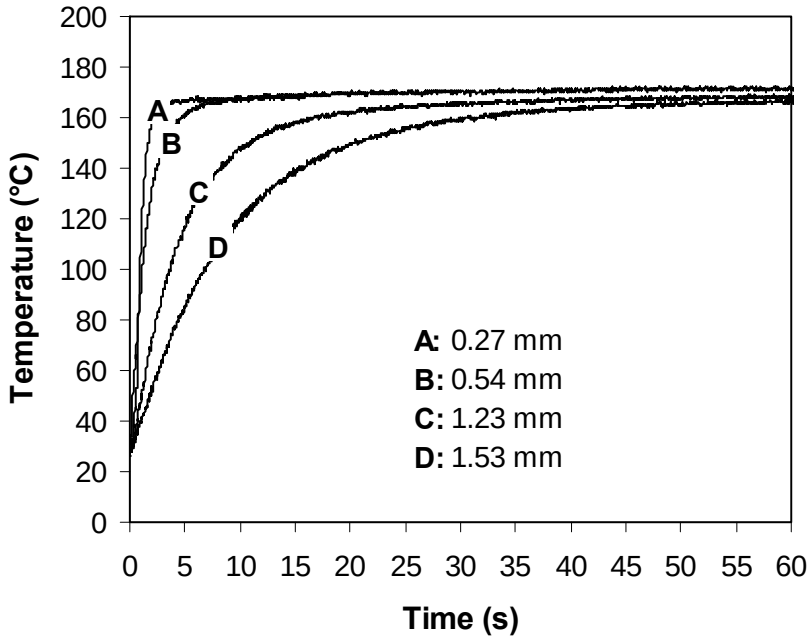

Figure 5.1 Temperature responses measured at the interface between two Teflon sheets under compression by two heated platens set at 180ºC. The thickness of the two Teflon sheet is the same for a given experiments, but varied in different experiments. The four levels of thickness used in the experiments are: A – 0.27 mm, B – 0.54 mm, C – 1.23 mm, and D – 1.53 mm.

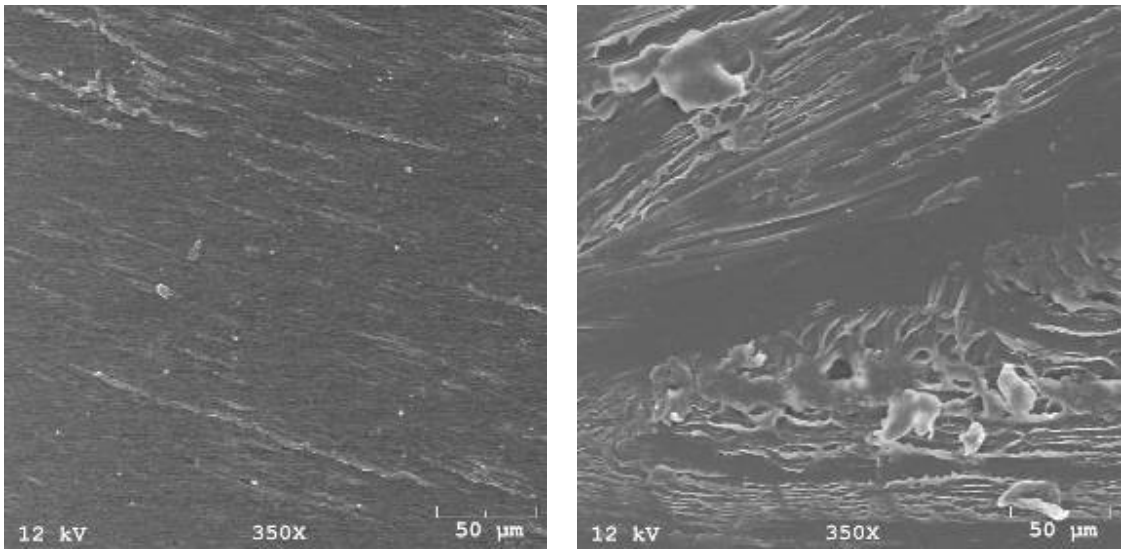

(a) (b)

Figure 5.2 Peeling failure surfaces of samples prepared by compression molding two amorphous PET sheets with different heating rate a) poor fusion bonding and b) good fusion bonding.

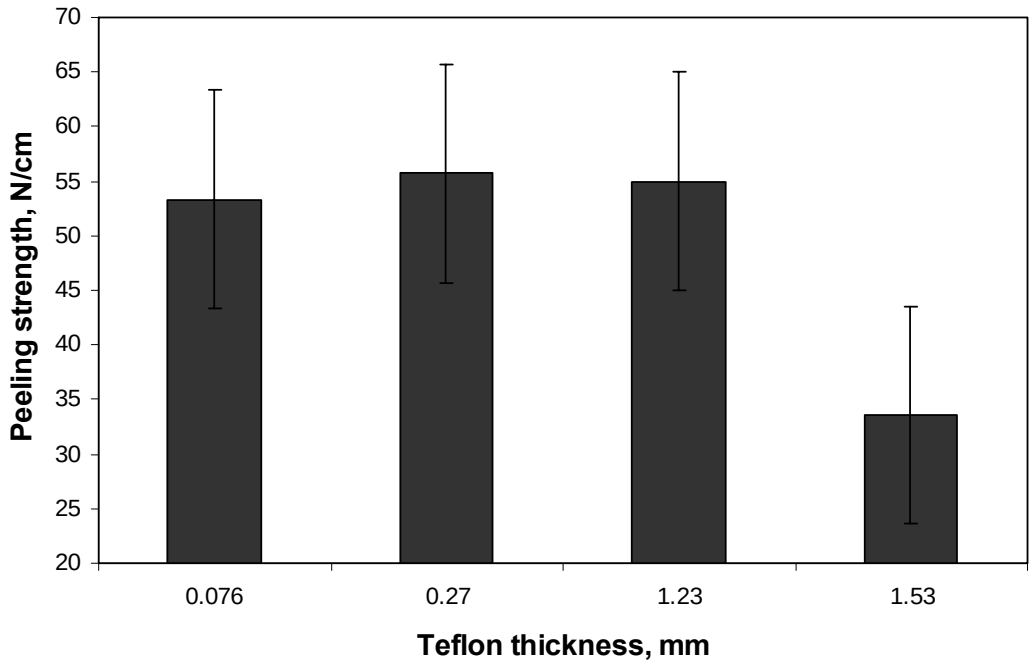

Figure 5.3 Effect of Teflon thickness on the peeling strength at 180°C and 20 s.

By changing the thickness of Teflon sheets, the heating rate can be changed. The effect of Teflon thickness on the peeling strength at 180°C and 20 s is given in Figure 5.3. When the thickness of Teflon sheet increased, the peeling strength was stable first and then decreased. When the lamination was thick, e.g. several millimeters, the heating process would significantly slow down and the rubbery softening process would be coupled with the crystallization process. In this case, the polymer would have a large dwell time in the temperature range lower than the desired minimum processing temperature.

The PET lamination can be heated rapidly upon contact with the two heated platens. The temperature response, $T(t)$, in the middle of the lamination may be predicted using the analytical solution available in the literature [169-170]:

$$\widetilde{T}(t) = \frac{T_0 - T(t)}{T_0 - T_i} = 2\sum_{n=0}^{\infty} \frac{(-1)^n}{(n+1/2)\pi} e^{-4(n+1/2)^2 \pi^2 \alpha t / H^2} \tag{5.1}$$

where α is the thermal diffusivity, T_i is the initial temperature of the lamination, T_0 is the heated platen temperature, H is the lamination thickness, and $\widetilde{T}$ is dimensionless temperature. The density, thermal conductivity, and specific heat for the amorphous PET film are 1400 Kg/m^3, 1350 J/Kg-K, and 0.3 W/m-K, respectively, giving $\alpha = 1.6 \times 10^7$ m^2/s. Simple calculation showed, for a 0.5 mm thick lamination, $\widetilde{T}$ was equal to 0.9 at $t = 0.4$ s. This heating time was about 2 orders of magnitude faster than the typical half time of crystallization of PET. It can thus be assumed that the lamination was instantaneously heated.

Therefore, the Teflon laminations used in the following experiments were very thin, on the order of 0.5 mm. The samples were rapidly heated to the target temperature

within a very short period. This short period of heating, about 1 s or less, was considerably smaller than the crystallization time scale. Thus rubber softening dominated during the heating stage. The resulting polymer after the short period of heating was sticky and a fusion bond was rapidly formed before significant crystallization occurred.

5.3.2 Comparision of fusion bonding behavior of amorphous polymer and crystallizable amorphous polymer

The fusion bonding behavior of amorphous polymer heated above its glass transition temperature was similar with that of semicrystallizing polymer heated above its melting temperature. The polymer becomes viscous first. Then the polymer chains at the interface interdiffuse with each other until the polymer is cooled and consolidated.

Two sheets of amorphous polymer ABS were heated at 160°C with different heating times of 5 s, 15 s, 30 s, and 60 s. Two sheets of crystallizable amorphous PET had been fused at the same conditions. The results are provided in Figure 5.4 and Figure 5.5. The fusion bonding of the two polymer sheets were evaluated using peeling test. Figure 5.4 shows that the peeling strength of amorphous polymer ABS remained nearly unchanged with the increase of the heating time at 160°C. For amorphous polymer, the bond strength generally increased with the welding time, but the increase is typically not very obvious [171]. However, the fusion bonding behavior of crystallizable amorphous PET sheets was quite different. With the increase of the heating time, the peeling strength was decreased considerably. An explanation to this difference is given below. The heating temperature 160°C was between the glass transition temperature and the melting temperature of PET. At the beginning, the polymer became rubbery and sticky at 160°C and chain diffusion started at the interface. At the same time, the crystallizable

amorphous phase began to crystallize when the temperature was above Tg. The crystallization could cause a decrease in fusion bonding, because a relatively brittle interface could be formed. Thus, lower seal strength would be obtained.

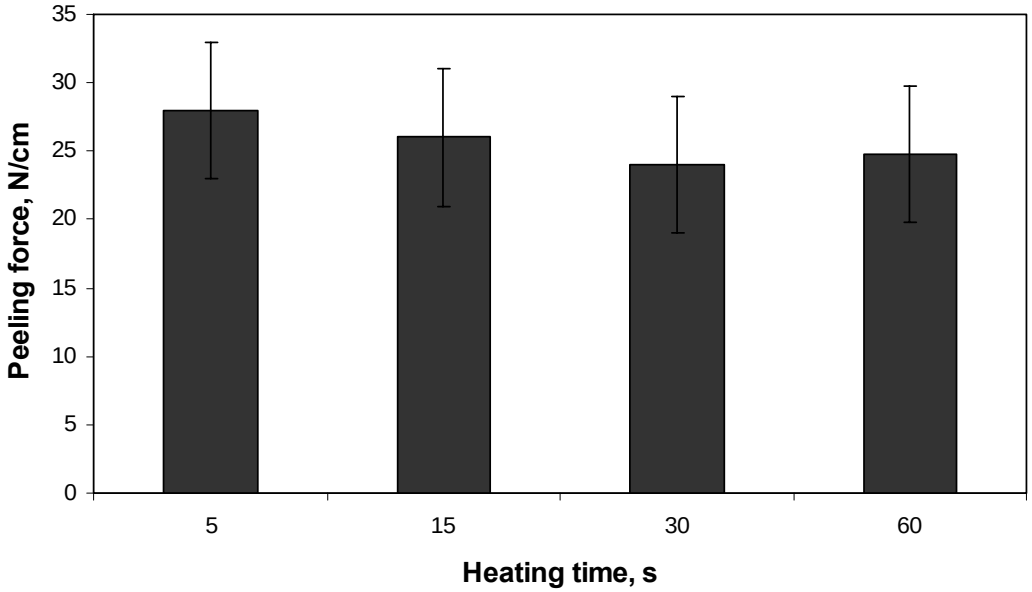

Figure 5.4 Fusion bonding of amorphous polymer (ABS) at 160°C.

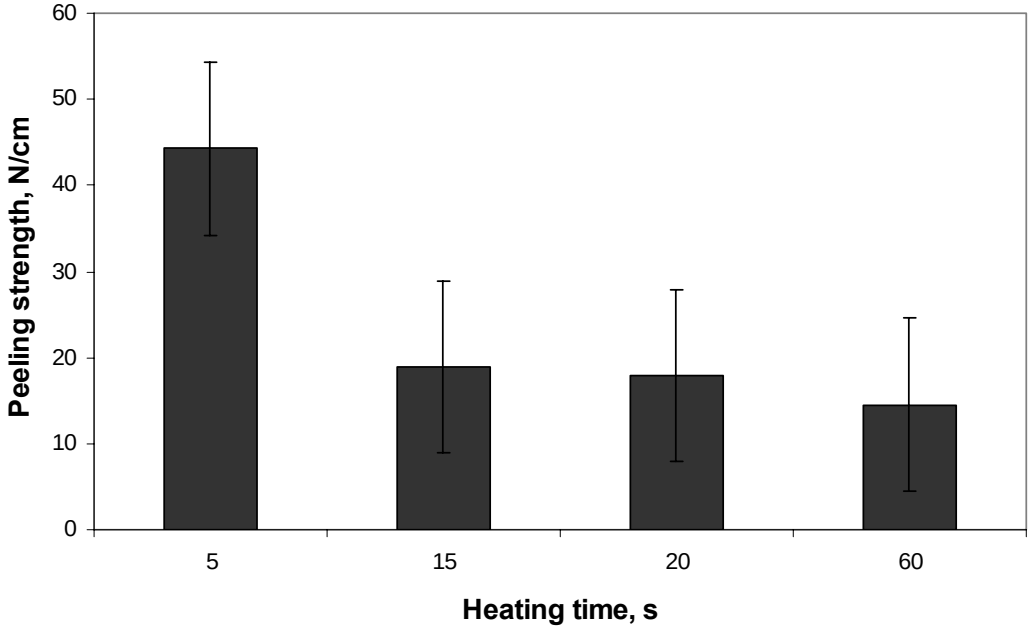

Figure 5.5 Fusion bonding of crystallizable amorphous polymer (PET) at 160°C.

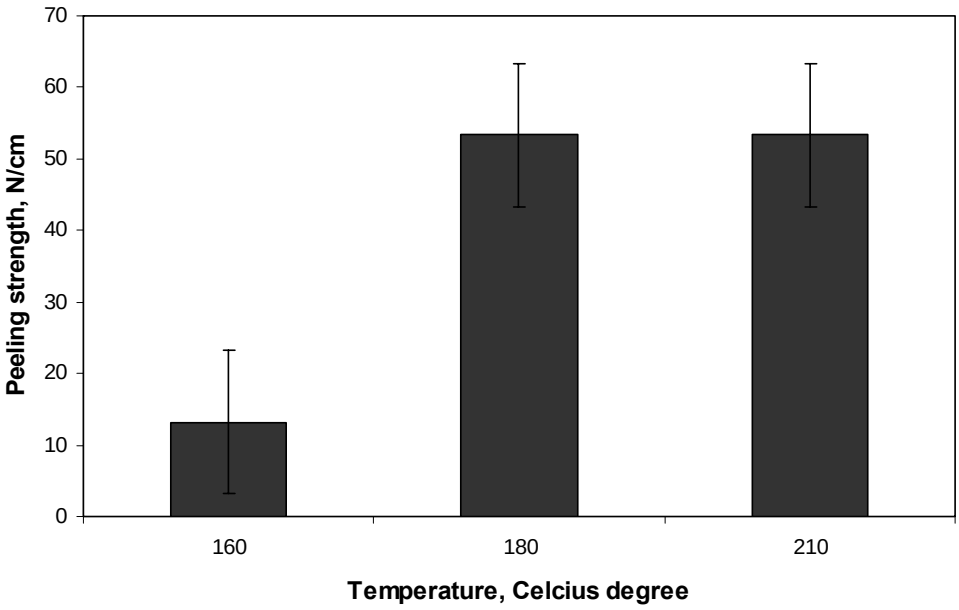

Figure 5.6 Effect of platen temperature on the peeling force of two PET sheets with heating time 20 s.

5.3.3 Effect of platen temperatures on the adhesion

For prescreening purpose, different levels of platen temperatures were used during direct compression of two amorphous PET sheets. Experiments were performed to study the fusion mechanism of amorphous PET sheets. These amorphous sheets were produced using rapid quenching but they will start to recrystallize when reheated. The compressed PET sheet was peeled apart from the unbonded region. The plot of platen temperature vs. peeling strength is shown in Figure 5.6. For temperatures at 130ºC or below, good fusion bonding was hard to form and the compressed sample can be peeled apart at the interface with hands. With the increase of the heating temperature, the peeling force was increased. When the heating temperature was above 180ºC, the peeling force changed little with increase of heating time. The peeling force at 210ºC was a little

lower than that at 180ºC, which may be caused by the difference of crystallinity and bubbles.

5.3.4 Fusion bonding behavior of crystallizable amorphous polymer at different temperature

The fusion bonding behavior of crystallizable amorphous polymer is expected to be more complex than that of purely amorphous polymer. Based on the unique behavior of crystallizable amorphous polymer, a mechanism for fusion bonding is proposed below. When the amorphous sheets are heated above the glass transition temperature, the molecular chains become mobile and the interface becomes rubbery and viscous. With the increase of the heating temperature, the viscosity of the interface decreases, so the interdiffusion speed of polymer chain increased. However, at the same time, crystallization takes place between Tg and Tm; this can cause the softened, rubbery and sticky amorphous phase to turn into a hardened crystalline phase. If crystallization should be much faster than fusion bonding, the molecular chains would have already been frozen by crystallization before significant interdiffusion should occur. In this case, no fusion bonding would be formed between the two polymer sheets. It is well known that, for most polymers, the quiescent crystallization rate at a temperature near the melting temperature is low, while the chain diffusion process is fast at the same temperature. Therefore, at such elevated temperature, the polymer chains at the interface would have enough time to interdiffuse with each other before the crystallization could stopped the interdiffusion and convert the viscous interface into a crystallized solid. The size and distribution of the crystalline structure may also affect the bonding strength [172]. When two crystallizable amorphous sheets are heated above Tg, the molecular chains will

diffuse into each other at the beginning. At the same time, the interface begins to crystallize, and the bulk away from the interface crystallizes too. However, the crystallization speed and the morphology and size of the crystal can be substantially different between the interface and and the bulk. Thus, the difference between interface and bulk could increase with the increase of the heating time, resulting in decreased bonding strength.

For purely amorphous polymers, previous investigations have showed that the bonding strength increases with the increase of temperature [173-176]. The bonding strength can also slightly increase with the increase of heating time.

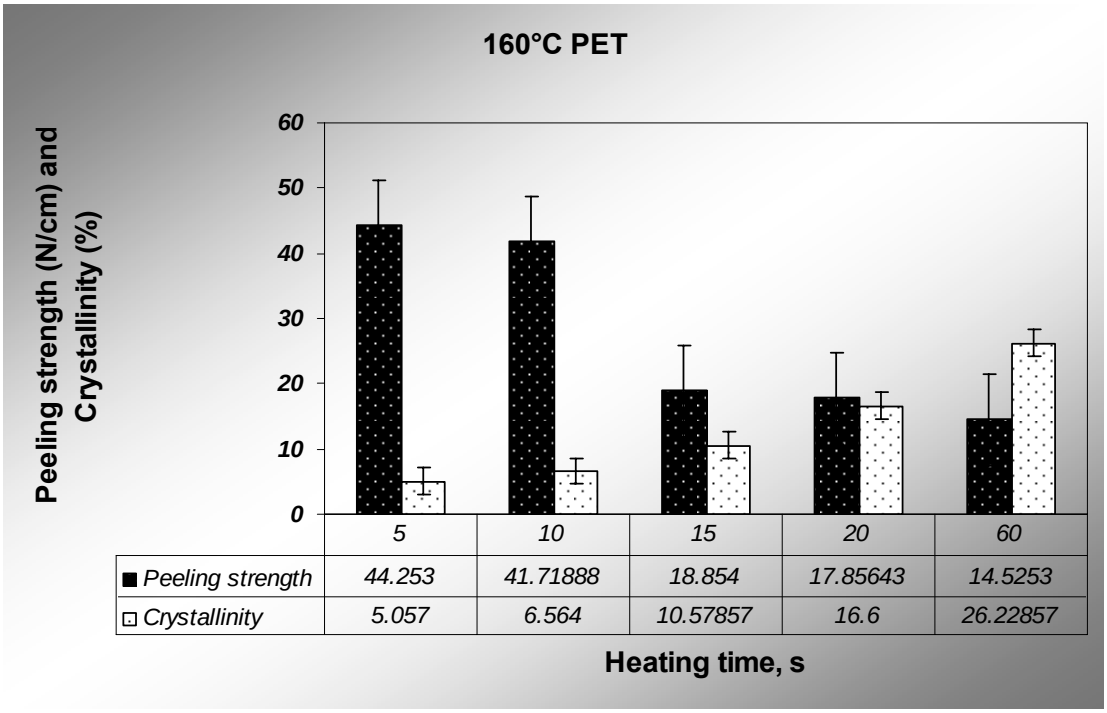

Figure 5.7 Effect of heating time on the bonding strength at 160°C.

The fusion bonding behavior of crystallizable amorphous PET under different platen temperature was studied. Three different temperatures were used: 160°C, 180°C

and 210°C. Of these temperatures, 160°C was far below the melting temperature of PET, while 210°C was far above the glass transition temperature; 180°C was the intermediate temperature. The effects of the heating times on the peeling strength and the crystallinity under 160°C, 180°C and 210°C are presented in Figure 5.7, Figure 5.8 and Figure 5.9.

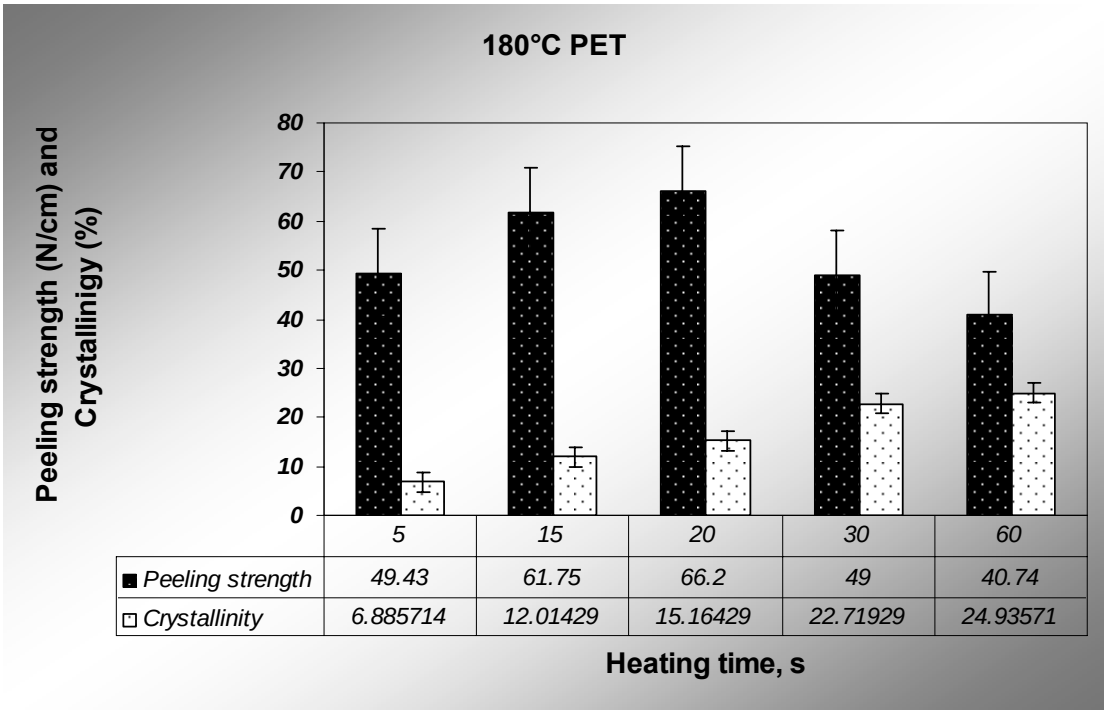

Figure 5.8 Effect of heating time on the bonding strength at 180°C.

At 160°C, with the increase of the crystallinity, the interfacial bonding strength was decreased. With the increase of the heating time, the crystallinity of PET sheets was increased. These results are explained below. Crystallinity may affect the fusion bonding between the two PET sheets. At shorter heating time, the polymer sheets is nearly amorphous, the polymer chain can interdiffuse with each other at the interface. Thus the peeling strength was higher. However, with the increase of the heating time, crystallinity

is increased. Crystallization is the (natural or artificial) process of formation of solid crystals precipitating from an identical solution or melt, or more rarely deposited directly from a gas. After crystallization, the rubbery state of the polymer becomes solid crystals. Crystallization may freeze the movement of polymer chains. After the polymer chain is frozen by the crystallization, the interdiffusion of the polymer chain at the interface may be stopped by the crystals. There may be a great difference between the interface and the bulk, which may decrease the fusion bonding strength between the two PET sheets. At this temperature, the difference between interface and bulk may increase with the increase of heating time. Thus, the peeling strength at 160°C was decreased with the increase of the heating time.

Peeling strength was higher at 180°C than at 160°C. Figure 5.8 shows that, with the increase of the heating time, the fusion bonding strength of the crystallizable amorphous PET was increased and then decreased. This behavior is explained below. At 180°C, the fusion bonding speed is expected to be faster than at 160°C, but the crystallization speed may remain unchanged (known from the typical bell shape for the half time of crystallization). At the beginning, diffusion was predominant. With the increase of the heating time, the amount of diffusion increased, and the interface and bulk became more uniform, resulting in the increase of the bonding strength. Thus with the increase of the heating time, the fusion bonding strength was increased at the beginning. When interdiffusion and the crystallization were in balance, the interfacial bonding strength reached the highest. Later crystallization became predominant. With the increase of the heating time, crystallization may cause a brittle interface, resulting in decreased bonding strength.

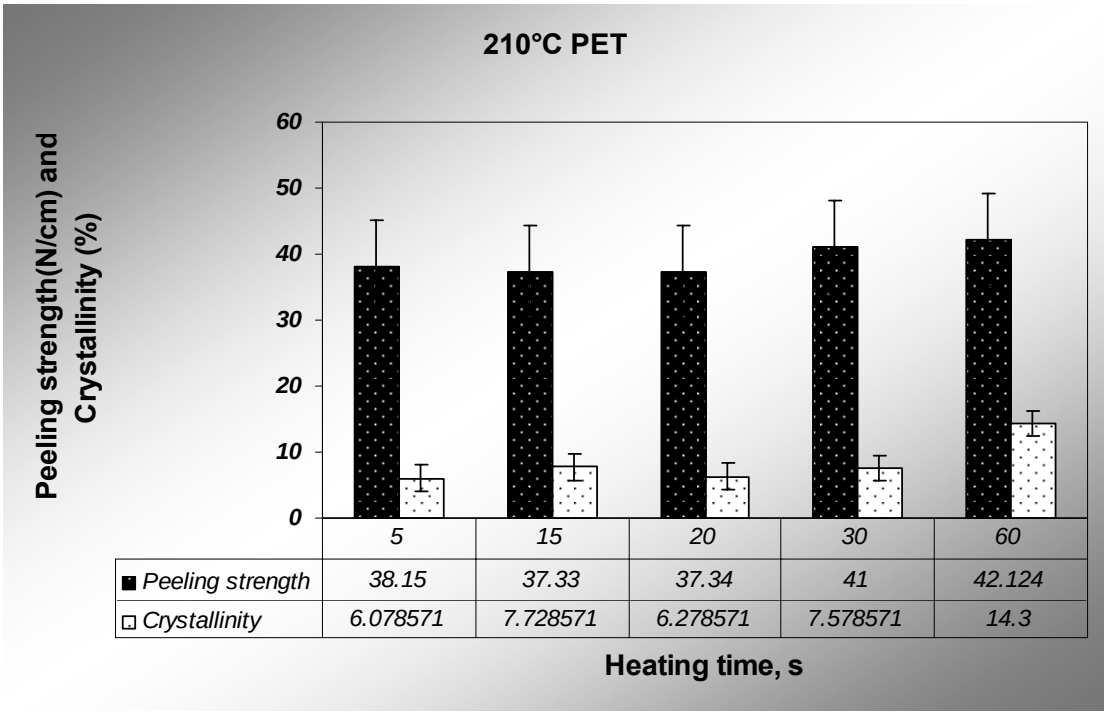

Figure 5.9 Effect of heating time on the bonding strength at 210°C.

The heating temperature of 210°C is much closer to the melting temperature of PET than the other two temperatures. At this temperature, the fusion bonding speed was faster. However, the crystallization speed was slower (known from the bell shape for the half time of crystallization). Thus molecular chains interdiffusion was predominant. With the increase of the heating time, the peeling strength was increased then became stabilized. At this temperature, the fusion bonding behavior of the two crystallizable amorphous PET was somewhat similar to that of purely amorphous polymer with heating temperature above Tg.

5.4 Conclusions

In this chapter, the fusion bonding behavior of crystallizable amorphous polymer was investigated. Peeling tests were used to evaluate the interfacial bonding strength between the polymer sheets. The effects of heating rate, heating temperature and heating time on the fusion bonding of the crystallizable amorphous polymer were studied. The results showed that faster heating rate and higher temperature resulted in stronger bonding between two crystallizable amorphous PET sheets. The fusion bonding behavior of crystallizable amorphous polymer was found to be vastly different from that of purely amorphous polymer. For a non-crystallizable amorphous polymer, with the increase of heating time, the bonding strength was known to increase. For crystallizable amorphous polymer, the bonding behavior appeared to be more complex. It was found that the interfacial bonding quality was significantly affected by the state of crystallization and the morphological development at the bonding interface. It was also found that, at different processing temperature, the fusion bonding behavior was different. At low temperature, with the increase of heating time, the bonding strength decreased monotonically. At higher temperature, the bonding strength increased first and then decreased. At the temperature near the melting temperature, the fusion bonding behavior was similar to that of purely amorphous polymer.

CHAPTER 6

MORPHOLOGY OF FUSION BONDING ZONE OF CRYSTALLIZABLE AMORPHOUS PET SHEETS

6.1 Introduction

The concept of single polymer composites was originally proposed by Mead and Porter [1]. Single polymer composites are the composites with fiber and matrix made from the same polymer. They are environmentally benign materials and can be recycled following the standard single polymer recycling practice. The previous work on SPCs mainly involved fast crystallizing polymers such as polyethylene and polypropylene [8-24]. These polymers, however, have disadvantages in SPCs applications owing to their fast crystallization rate. Because of fast crystallization, the products derived from PE, PP and nylon were highly crystalline, resulting in closeness in melting temperature of these products. The proximity in the melting temperatures between the fiber and the matrix poses a considerable difficulty during SPCs processing. To overcome these problems, a new approach to SPCs utilizing slowly crystallizing polymers has been investigated with PET and PLA as model systems [177, 178]. Due to slow crystallizing nature, slowly crystallizing polymer can be prepared as amorphous polymer by rapid quenching. On the other hand, if PET is heated to above its crystallization temperature and kept for a shorter period under stretching, highly crystalline PET will be formed. Upon reheating between Tg and Tm, the amorphous PET will become rubbery and sticky. Two such sticky pieces can be fused together through chain diffusion at the interface [62]. When the amorphous PET should be used to encapsulate the highly crystalline PET fibers in the said temperature range, the reinforcement would still keep its high mechanical performance.

However, upon heating between Tg and Tm, the amorphous PET film would also be subjected to influences from crystallization. Fusion bonding and crystallization are two competitive processes. Thus the fusion bonding behavior of the crystallizable amorphous polymer is expected to be more complex than that of a non-crystallizable amorphous polymer.

Crystallization occurs when polymer chains fold up on themselves in a repeating, symmetrical pattern. Crystallization is a kind of basic phase transitions in polymers and polymer blends. Nucleation can be classified into: homogeneous nucleation, heterogeneous nucleation and self-nucleation. Heterogeneous nucleation is usually initiating polymer crystallization. Heterogeneous nucleation is often triggered by interfaces provided, e.g., by foreign species, surface and impurities such as catalysts, dust particles, and additives [179]. Ma et al. [180] have studied the interface induced heterogeneous crystal nucleation in an immiscible polymer blend. The interface of the immiscible polymers can induce heterogeneous crystal nucleation in the polymer [180]. In fiber-reinforced semicrystalline polymer composites, fibers have high nucleating ability toward the matrix [181]. The enhanced interfacial crystallization is caused by preferential nucleation on the surface of the fibers compared to the nucleation in the bulk matrix [182]. The nucleation ability of certain fibers is extremely high so that subsequent crystal growth is normal to the fiber until the growing front is impeded by the growth of spherulites nucleated in the bulk [183]. Such crystallization is often referred to as transcrystallization. A number of papers have reported transcrystallinity whether the substrate was a film [184, 185] or a fiber [186, 187]. Thermodynamic conditions, such as crystallization temperature and cooling rate, play an important role on transcrystallization.

Several other factors [181] also affect the appearance of transcrystallinity: (1) lattice matching and chemical similarity between fiber and matrix; (2) flow field near the interface, which can create a high degree of chain orientation and promote nucleation; (3) high surface free energy substrate, which can induce hererogeneous crystallization; (4) lower temperature at the fiber surface which increases the probability of nucleation; (5) stresses at the fiber/matrix interface; (6) molecular weight [188]. The Young's modulus of a transcrystalline region is typically larger than that in the bulk [189-192]. It is often believed that transcrystallinity has a positive effect on the interfacial bond strength.

The interface and interfacial nucleation in polymer-fiber composites, the interface and interfacial nucleation in immiscible polymer blends, and the interface and interfacial nucleation of fast crystallizing polymer under nonisothermal bonding conditions have been studied extensively in the literature. However, the knowledge is rather little on the interface and interfacial nucleation of crystallizable amorphous polymer (made of slowly crystallizing polymer) under an isothermal bonding condition. For fast crystallizing polymer, the crystal and interfacial morphology can typically be observed using polarized microscopy. However, for slowly crystallizing polymer, the crystallization rate is slow, and the crystal formed under normal polymer processing conditions is typically small. Thus, morphological studies of such an interface bring in additional difficulties.

In this study, the interfacial morphology of crystallizable amorphous polymer under the isothermal bonding condition was investigated. PET, a common slowly crystallizing polymer, was chosen in the experiments. The fusion bonding morphology of this polymer was characterized using SEM, TEM, and polarized optical microscopy either on etched or non-etched sample slices. A double-zone morphology was observed in

the vicinity of the interface. Right at the interface, a transcrystalline region was observed. A secondary transitional zone was also observed. With the increase of the holding time, the overall width of the interfacial region decreased.

6.2 Experimental

6.2.1 Sample preparation

The amorphous PET sheet is 0.25 mm thick. Two amorphous PET sheets were compressed between two heated platens on a Carver hydraulic press. Then the PET sheet obtained was rapidly quenched into tap water. Thin Teflon® films (0.07 mm in thickness) were used on both sides for easy mold separation. Additional Teflon film was employed in the middle of the lamination to create an unbonded region for peeling testing. Spacers were inserted between the heated platens to control the thickness of the sheet. The major process parameters including the platen temperature, the compression force and the heating time were varied to study their effects on the interfacial bonding. The experimental setup is showed in Figure 6.1.

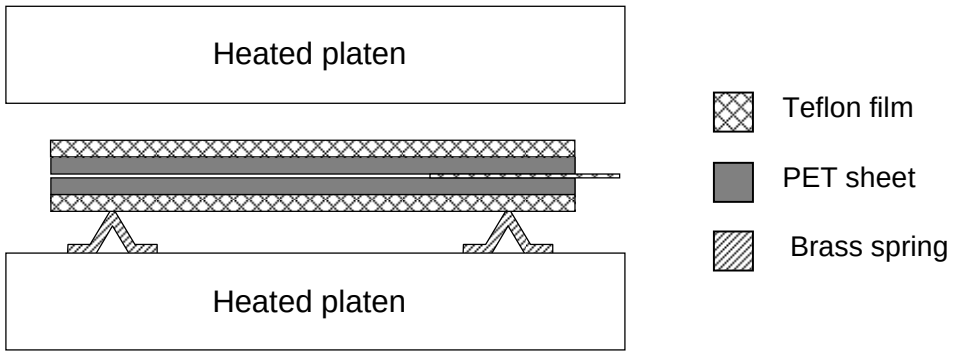

Figure 6.1 Experimental setup for two sheets bonding.

6.2.2 Etching and morphological characterization

After fusion bonding, the bonded sheets were cut into 1 cm × 4 cm rectangles. These rectangles were then sliced into stripes with 500 μm thickness. The surfaces of the resulting samples were etched with a 2 wt% potassium hydroxide/isopropanol solution for 30 min, 1 h, 2 h, 3 h, 4 h, 5 h and 6 h at room temperature. Then these samples were washed by isopropanol, extracted in ethylene glycol for 24 h, and afterwards washed by acetone and water in sequence. The etched and washed specimens were dried at room temperature and then coated with a fine gold layer by ion-sputtering for examination on a S-800 SEM system (low resolution) and a LEO 1530 SEM system (high resolution).

The bonded sheets were also sliced by microtome for transmission electron microscopy (TEM) and polarized optical microscopy. TEM was performed on a Hitachi HF2000 TEM system. For optical microscopy, an Olympus BH-2 optical microscope was used. All optical micrographs presented in this chapter were taken under crossed polarizers.

6.3 Results and discussions

6.3.1 Morphology of interface at different heating temperature

PET has a relatively high melting point of 258°C, and its crystallization takes place mainly at a temperature between 100 and 240°C. The two crystallizable amorphous PET sheets were fused together under different heating temperatures and heating times. The bonded PET sheets were etched using 2 wt% potassium hydroxide/isopropanol solution for 4 h. Then the interfacial morphology of the fusion bonding region were observed using SEM. The interfacial morphologies of the fused sheets under different

heating times at 180°C are showed in Figure 6.2. Two distinct zones were observed in the vicinity of the interface. Figure 6.3 shows the inner zone right at the interface with a larger magnification. After etching, the remaining crystalline material at the interface formed many tiny bridges which connect the two sides of the interface. Note that this transcrystalline region was formed at a very short heating time (cf. Figure 6.3 (a)). With the increase of the heating time, the transcrystalline region appeared to grow tighter (comparing Figure 6.3 (a) with Figure 6.3 (c)). The growth of this transcrystalline region over time is understandable from basic crystal growth kinetics. However, the rapid formation of the transcrystalline region at a very short heating time, e.g., less than 10 s, indicated the presence of nucleation effects at the interface.

Heterogeneous nucleation is often triggered by interfaces provided, e.g., by foreign species, surface and impurities such as catalysts, dust particles, and additives [179]. Particularly, the surface of a specimen can serve as a heterogeneous nucleus [193]. Thus, the contact interface between two polymer film can trigger crystal nucleation. Due to the geometric nature of the polymer molecule the surface-nucleated crystal growth should have its chain axis parallel to the surface for maximum reduction of free energy of nucleation. The fastest crystal growth direction should be normal to the surface [193]. Figure 6.4 is a schematic illustration of the transcrystal microstructure model. The lamellae grew outward from the contact interface, which was perpendicular to the contact interface. This heterogeneous nucleation and transcrystal growth theory can be used to explain the unique morphology at the PET-PET interface observed in this study. It can be seen from Figure 6.3 the growth direction of crystals at the interface was perpendicular to the interface. The transcrystalline region was formed at a very short time scale, e.g. 5 s.

This time scale is much shorter than the quiescent crystallization time scale of PET. However, at the initial stage, the transcrystallinity appeared to be low, with relatively thin transcrystals at the contact interface (cf. Figure 6.3 (a)). With the increase of the heating time, the.transcrystalline region became denser and the visible void space (corresponding to the etched amorphous polymer) at the interface were smaller.

Figure 6.2 also reveals that, besides the transcrystalline zone, there existed a second interfacial region. Different reasons may be used to explain the formation of this second zone. However, it is highly likely that the transcrystals at the interface may cause nucleation in the surrounding material. Note that the nucleation of this type would be anisotropic and directional, different from the homogeneous nucleation in the bulk far away from the interface. Thus, the crystalline region in the neighborhood of the interface may bear a distinct morphology compared with that in the bulk, resulting in the formation of the second interfacial zone. The crystals in the inner interfacial region may keep growing until the growing front is impeded by the crystal growth in the second interfacial zone. For the PET-PET interface, in fact, a distinct boundary was observed between the two zones after a long period of growth, as shown in Figure 6.3 (c). Likewise, the growth of the crystals in the second interfacial zone may be hindered by the homogeneous crystal growth in the bulk. This causes the formation of the other boundary of the second interfacial zone. In additional to anisotropic nucleation effects, heat transfer may provide a driving force for formation of the second interfacial region. When the samples were heated, the heat was transferred from outside to the interface. There could be a temperature gradient in the thickness direction, particularly when relatively large

interfacial thermal resistance should be involved. However, such nonisothermal effects are expected to be low due to the small thickness of the films used in the experiments.

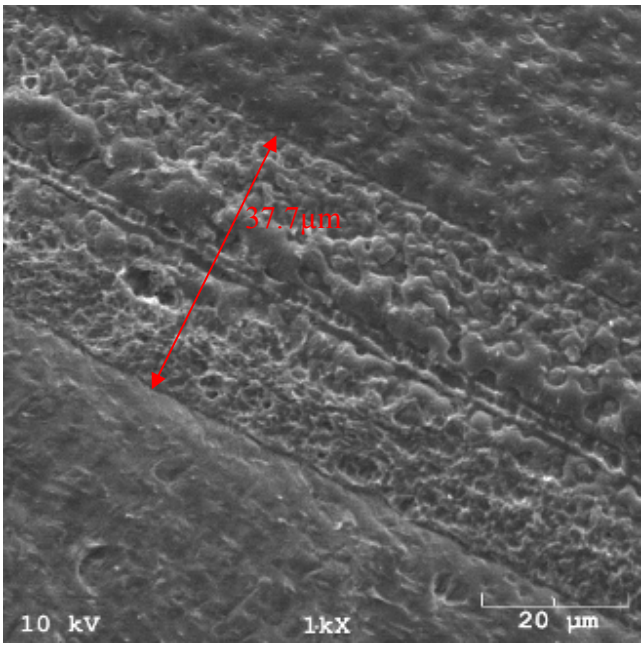

a)

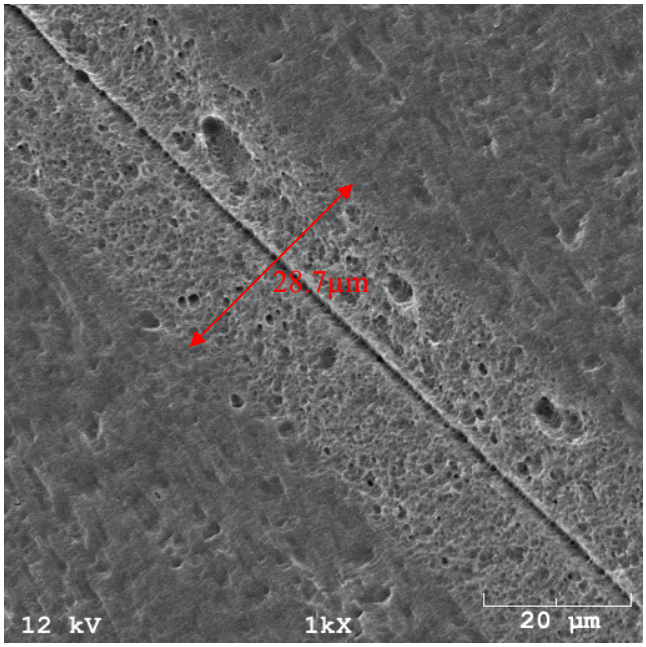

b)

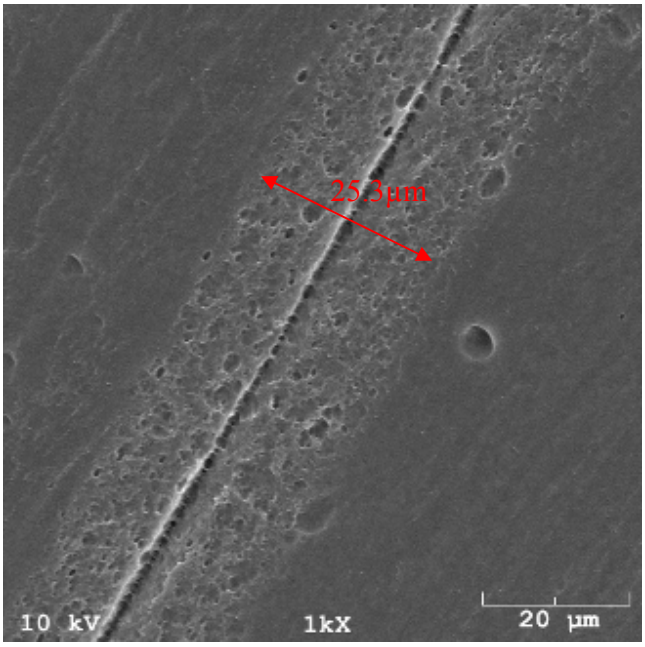

c)

Figure 6.2 Interfacial bonding morphology of two crystallizable amorphous PET sheets etched by 2 wt% potassium hydroxide/isopropanol solution for 4 h. The PET sheet was fused at heating temperature 180°C with different heating times: a) 10 s, b) 30 s, and c) 60 s.

Figure 6.2 also shows that with the increase of the heating time, the total width of the double interfacial zone decreased. The reduction in width was rapid at the beginning but slowed down in the later stage. The crystallinty and the properties of the second interfacial zone are expected to be more similar with the bulk than with the transcrystalline region at the interface. This is supported by the relatively lower contrast in morphology between the second zone and the bulk, as observed on the etched sample. With the increase of the heating time, the molecular chains and crystals may rearrange themselves in the second zone. Thus, healing effects may be presented at the boundary

between the second zone and the bulk, resulting in reduction of the width of the second interfacial zone.

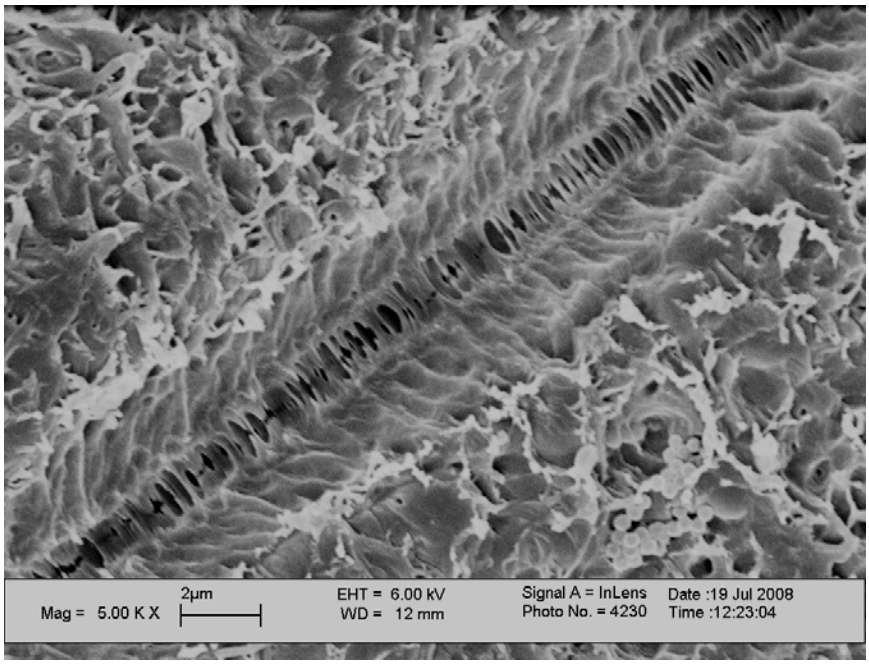

a)

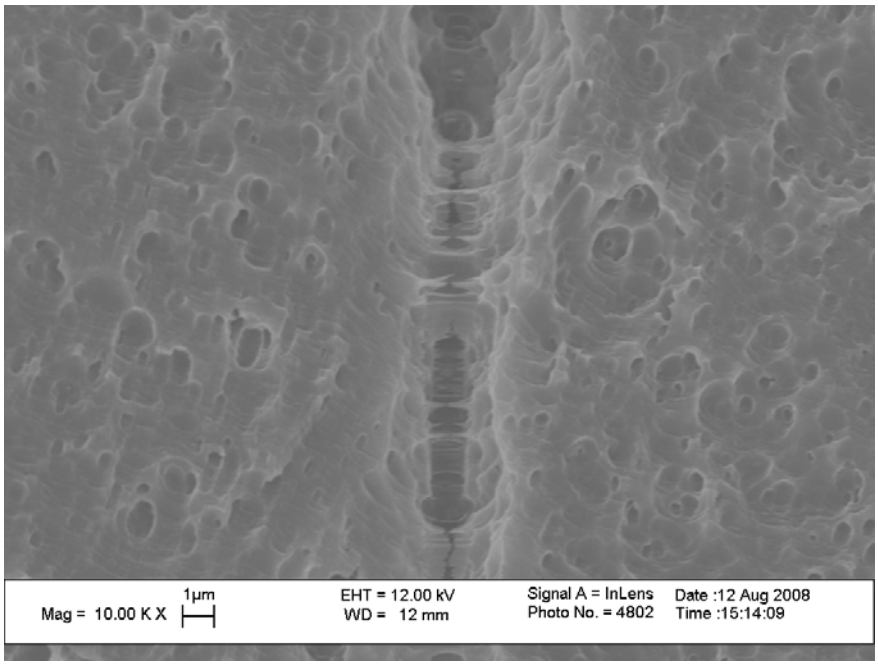

b)

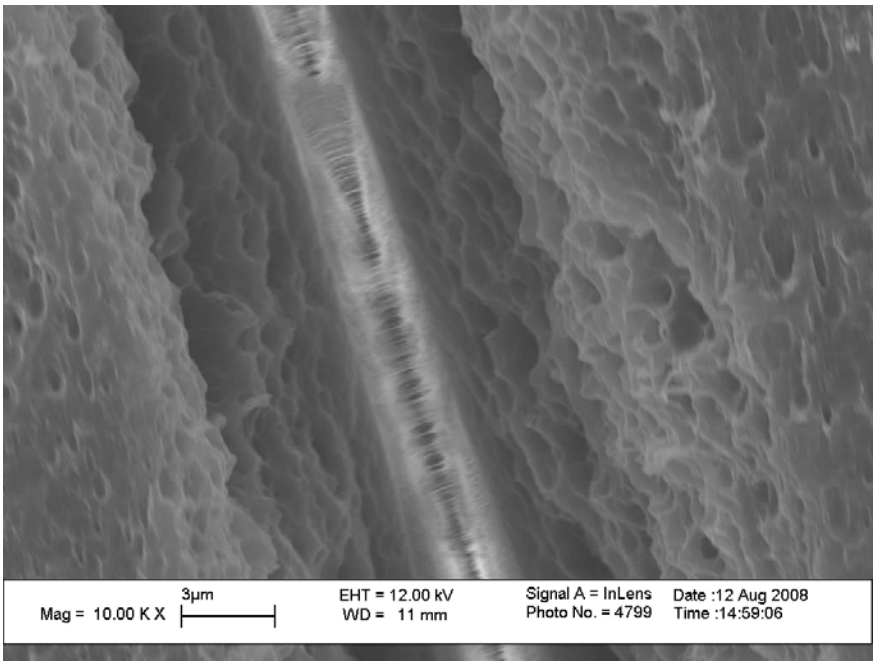

c)

Figure 6.3 Transcrystallinity morphology of two crystallizable amorphous PET sheets etched by 2 wt% potassium hydroxide/isopropanol solution for 4 h. The PET sheet was fused at heating temperature 180°C with different heating times: a) 10 s, b) 30 s, and c) 60 s.

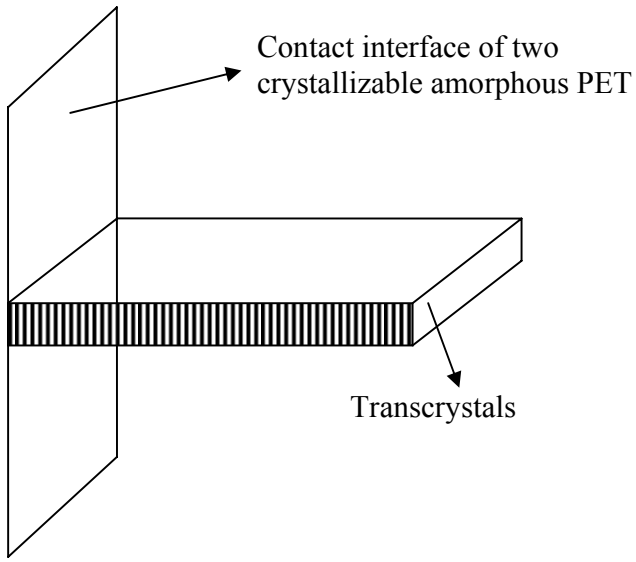

Figure 6.4 Schematic illustration of transcrystals microstructure model

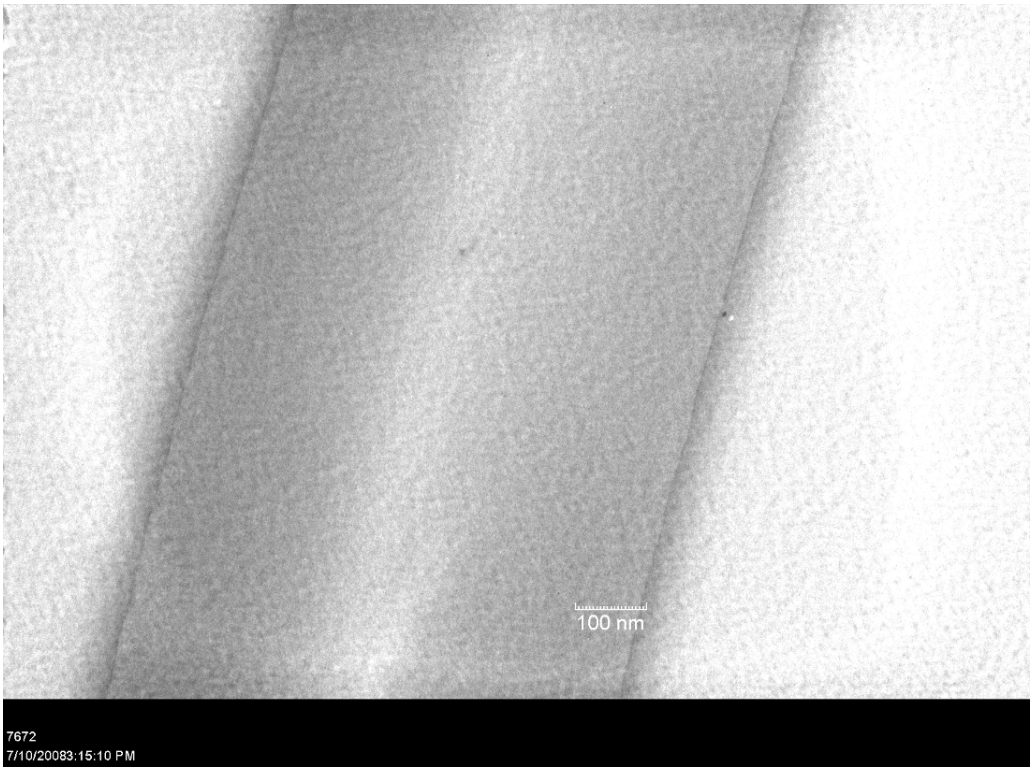

a)

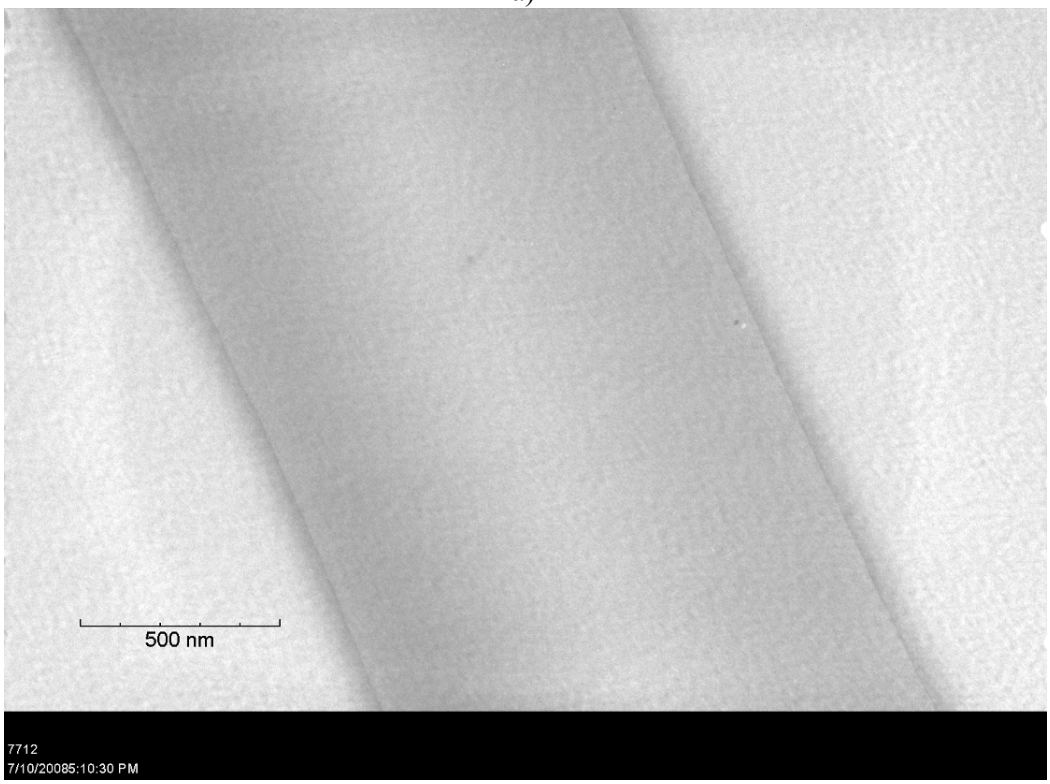

b)

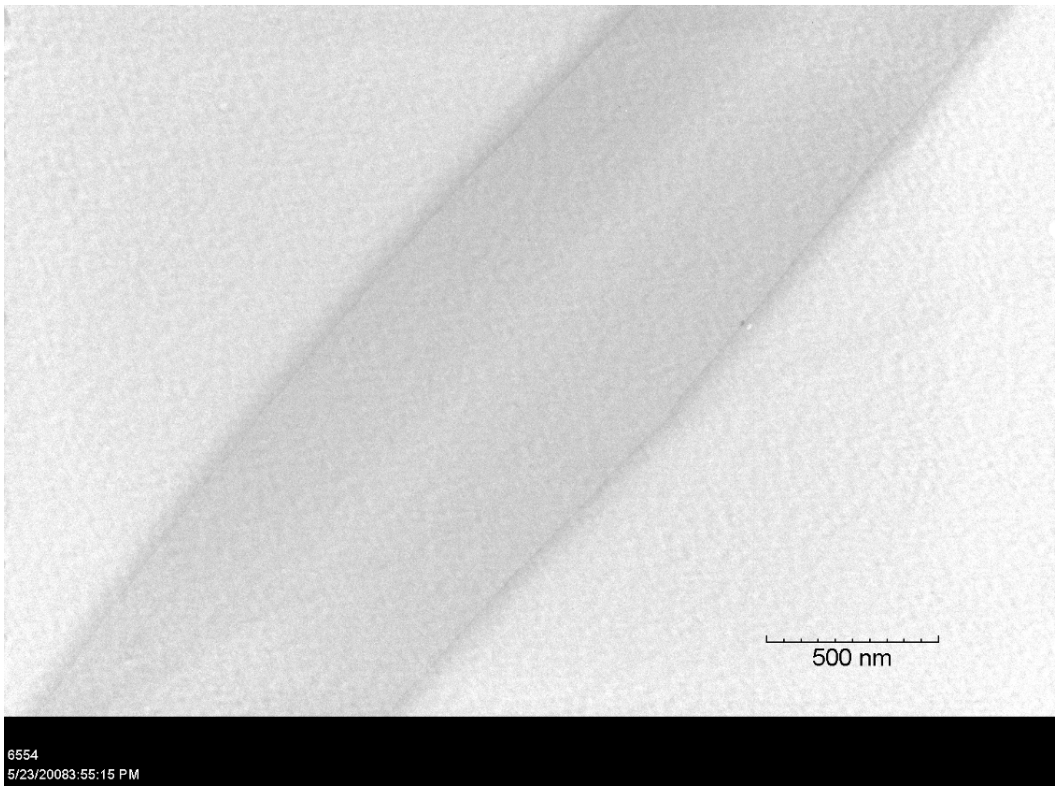

c)

Figure 6.5 TEM images of the interfacial zone of two crystallizable amorphous PET sheets fused at heating temperature 180°C with different heating times: a) 5 s, b) 20 s, and c) 60 s.

The interfacial bonding region of two crystallizable amorphous PET sheets was also observed using TEM, as shown in Figure 6.5. From this figure, it is seen that the shades of the interfacial region and the bulk were different; the interfacial region was darker. The width of the interfacial region was similar to the first interfacial zone observed by SEM. Thus the darker interfacial region in the TEM pictures was the transcrystalline region in the interfacial zone. Typically, higher crystallinity and density gives a darker appearance in TEM. The darker appearance of the transcrystalline region,

therefore, indicated relatively higher crystallinity in this region. When the heating time was shorter, the center of the interfacial region was a little brighter. With the increase of the heating time, the bright center gradually reduced in its size. The bright center was the contact interface of the crystallizable amorphous PET. This relatively low crystalline region agreed with the relatively amorphous center (with spaces left after etching) at the contact interface observed in the SEM micrographs (Figure 6.3). An attempt for explaining the formation of this relatively amorphous center and its subsequent reduction in size is give below. At the beginning, when the two amorphous PET were heated, the interface was in a rubbery state, serving as a nucleation center. Transcrystals started to grow on it at a relatively faster growth rate comparing with the bulk. This faster growth rate resulted in thin crystals rapidly formed at the original interface. It appeared that the growth rate in the lateral direction was much slower than in the perpendicular direction. Away from the original contact interface, the lateral growth rate was higher. Later, with the increase of the heating time, the transcrystals may keep growing in the perpendicular direction but at the same time thickening at a slow rate in the center region. Thus more transcrystallinity gained at the contact interface. Therefore, a relatively brighter center was observed in TEM for shorter heating times, and this center became darker with increase in contact time. The TEM image also clearly shows the impingement boundary between the transcrystalline region and the bulk.

Polarized optical microscopy in Figure 6.6 also indicates the existence of the distinct interfacial zone at the PET-PET joint, particularly for samples bonded with short heating times. The width of the interfacial zone observed by polarized optical microscopy is comparable to that of the second interfacial region in the SEM. The colorful zones on

samples with short heating times, e.g. 10 s, were caused by the uneven scratches of knife on the cutting surface. These scratches gave rise to birefringence, and therefore colorful fringes, when the sample was observed with polarized light. The center zones in Figure 6.6 (a) or (b), corresponding to the interfacial zones, had a more uniform surface appearance on the cutting surface; therefore, with polarized light, it showed a small amount of birefringence and appeared dark. The reason for this difference in appearance is attempted below. When the heating time was shorter, the crystallinity of the bulk was low. Thus the modulus of the bulk would be lower that that of the interfacial zone. In fact, for fast crystallizing polymers, several previous papers [189-192] have already reported that the modulus of the transcrystalline region is higher than that of the bulk phase. The bulk material would thus be easier to be scratched during slicing, while the hard interfacial transcrystalline region would be more resistant to scratches. Figure 6.6 also illustrates the effect of heating time on the interfacial appearance. As the heating time increased, the difference in appearance diminished. For example, the sample prepared with a long heating time of 60 s showed a uniform appearance under the polarized optical microscope (Figure 6.6 (e)). This change in cross-sectional appearance with heating time can again be attributed to crystallization; with increased crystallinity at longer heating times, the crystallinity of the bulk material increased and thus provide improved resistance to scratches.

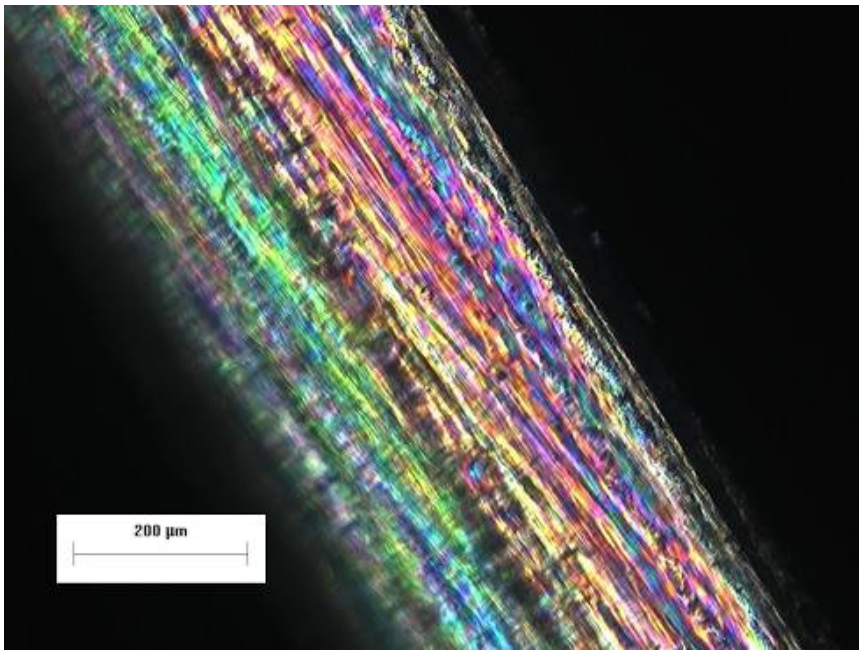

a)

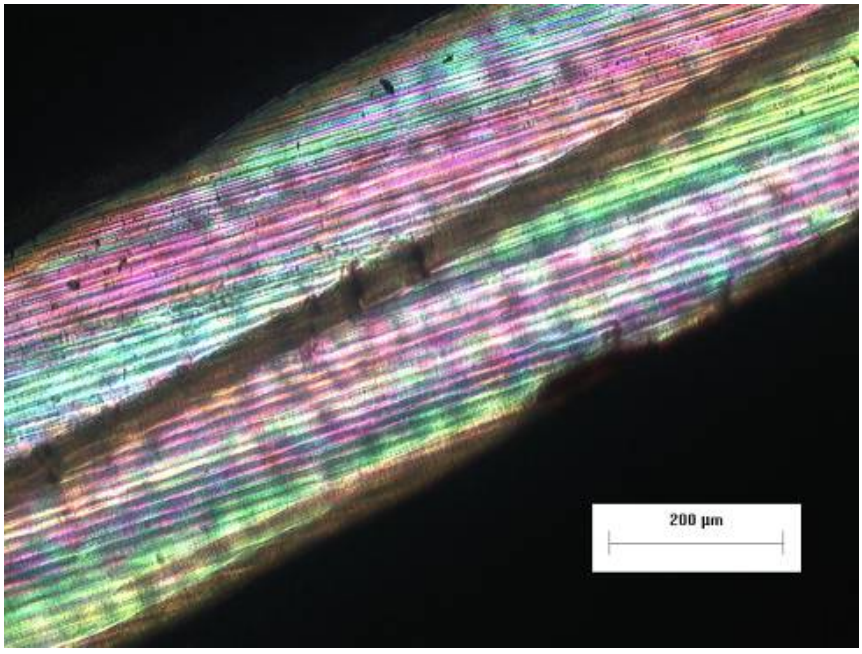

b)

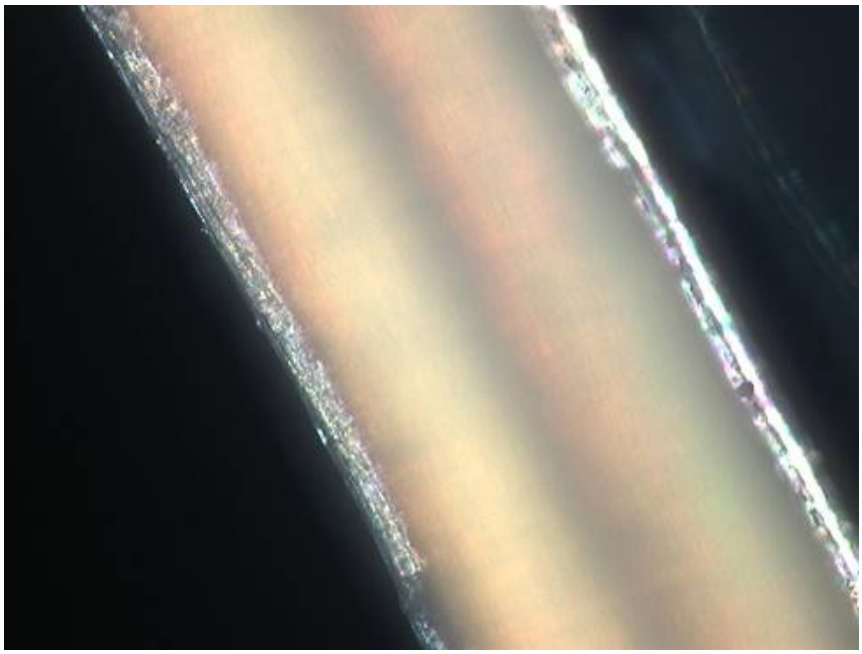

c)

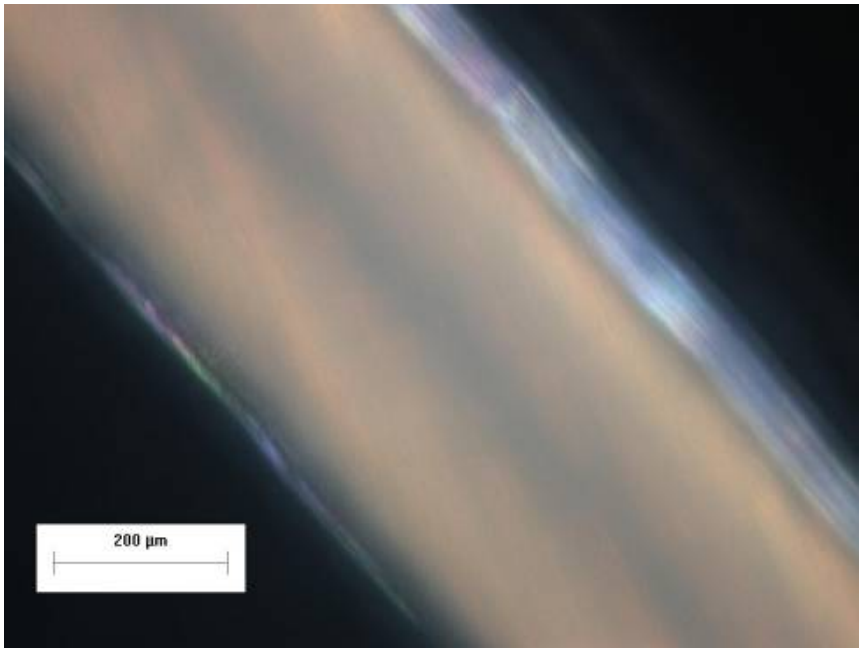

d)

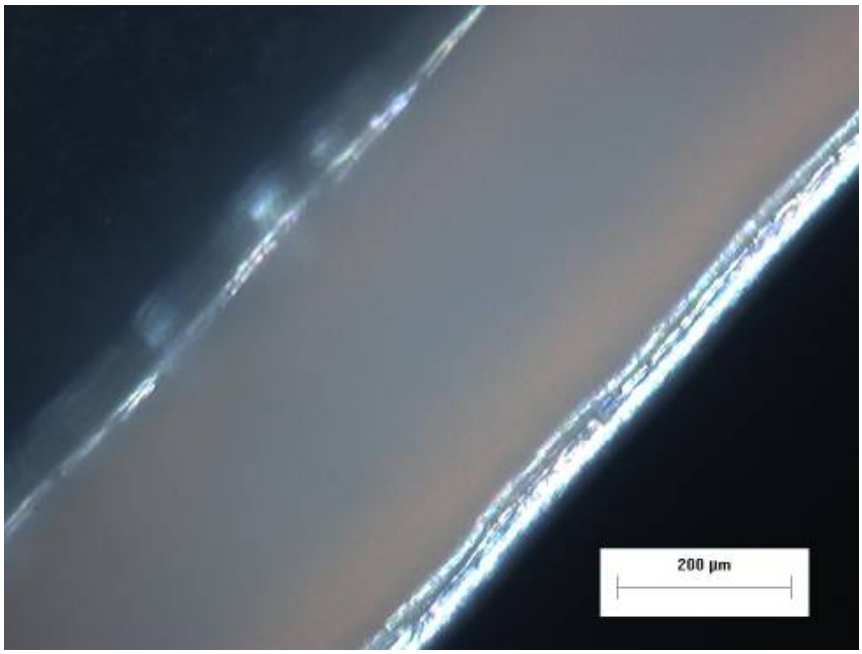

e)

Figure 6.6 Polarized micrographs of the interfacial zone of two crystallizable amorphous PET sheets bonded at heating temperature 180°C with different heating times: a) 5 s, b) 10 s, c) 20 s, d) 30 s, and e) 60 s.

The double interfacial region was also observed on samples prepared at different heating temperatures of 160°C and 210°C, as showed in Figure 6.7 and Figure 6.8. However, with the increase of the heating time, the interfacial morphology changed in different way at different temperature. The width of the interfacial region decreased more slowly with the increase of the heating time at 160°C. At 210°C, the width of the interfacial region decreased more rapidly with the increase of the heating time. An explanation for the different responses to the change in heating time is given below. Upon heating above Tg, the amorphous PET becomes a rubbery material. However, at this same temperature, the amorphous PET also crystallizes. When the heating

temperature was low, e.g. 160°C, the mobility of the molecular chain in amorphous region was relatively low; yet, crystallization was still as comparably fast as with a higher heating temperature, as inferred from the bell shape of half-time of crystallization. As a result, the change in morphology due to rearrangement of inter-crystal chains would be slow at this low heating temperature. At a higher heating temperature, e.g. 210°C, the mobility of the molecular chains would be much higher. Therefore, more annealing would be expected at higher temperature, resulting in homogenization of morphology between dissimilar crystalline regions. It is thus understandable that, the higher the heating temperature, the faster the width of the interfacial region decreased.

The interfacial morphology of samples prepared at 160°C and 210°C was also studied using TEM and polarized microscopy. The results are shown in Figures 6.9-6.12. These results were similar to those observed on the sample fused at heating temperature 180°C. Again, the interfacial zone in TEM corresponded to the transcrystalline region in SEM, while in polarized microscopy it was correlated with the second bonding zone in SEM.

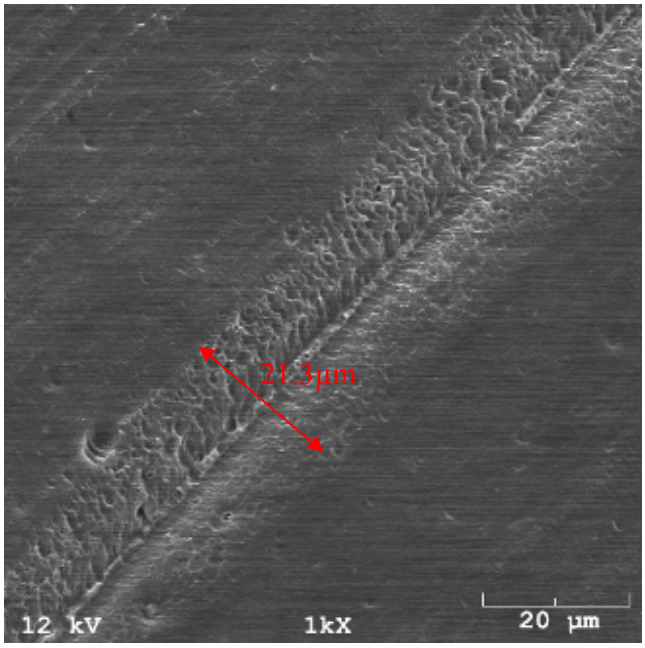

a)

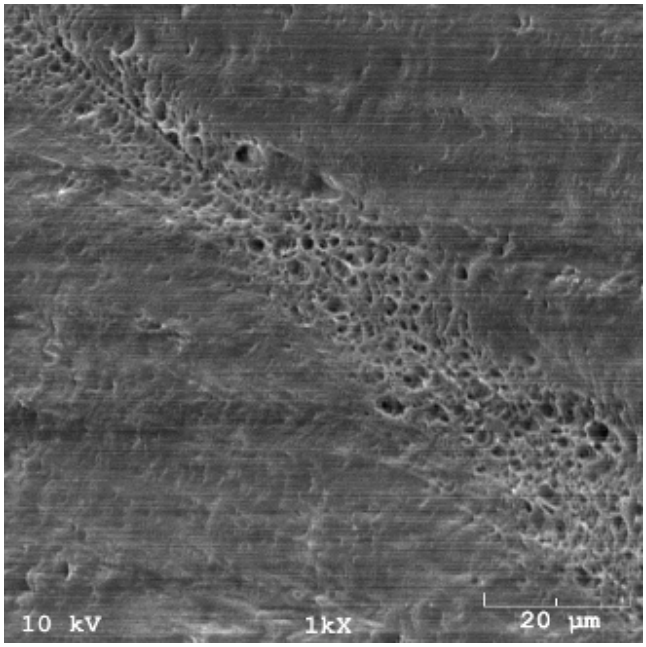

b)

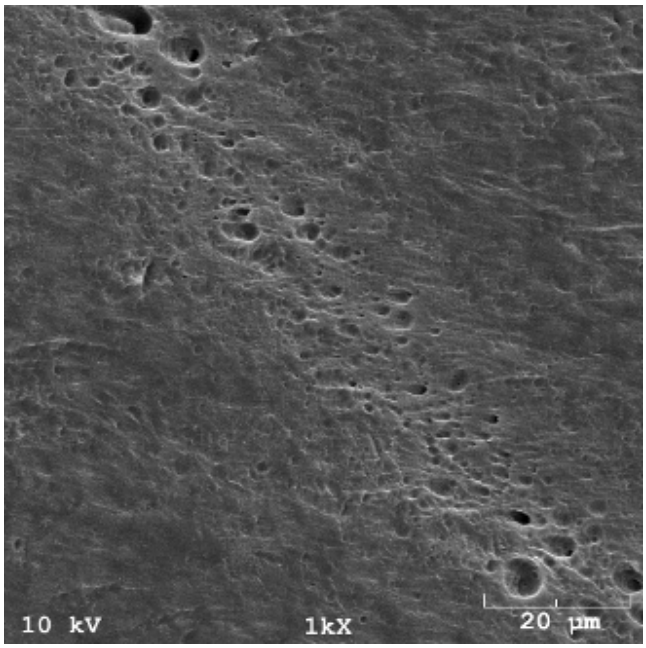

c)

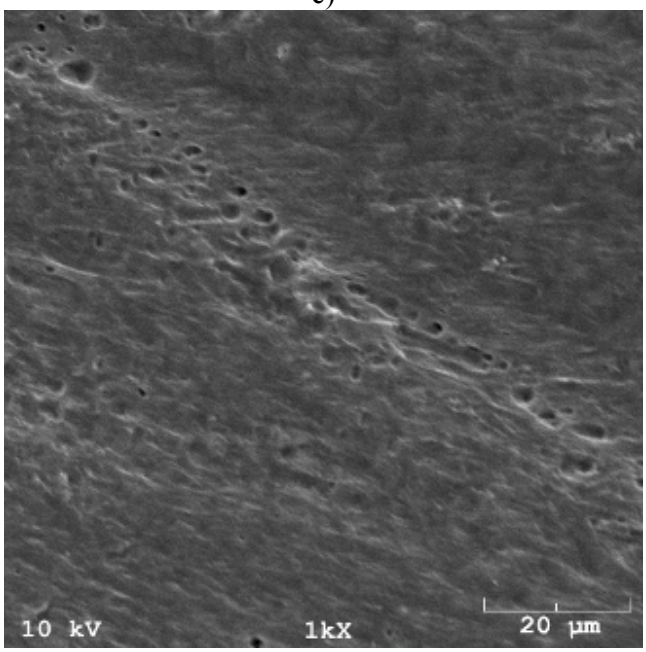

d)

Figure 6.7 Interfacial bonding morphology of two crystallizable amorphous PET sheets etched by 2 wt% potassium hydroxide/isopropanol solution for 4 h. The PET sheet was fused at heating temperature 210°C with different heating times: a) 10 s, b) 30 s, c) 60 s, and d) 90 s.

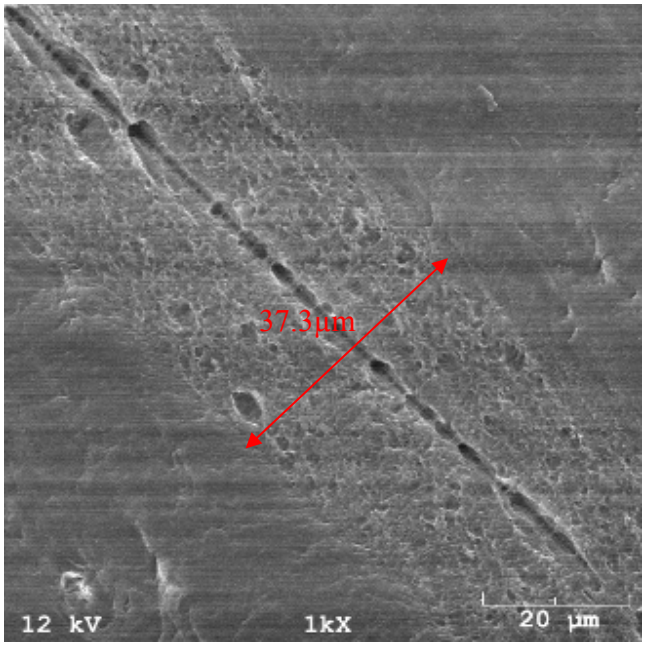

a)

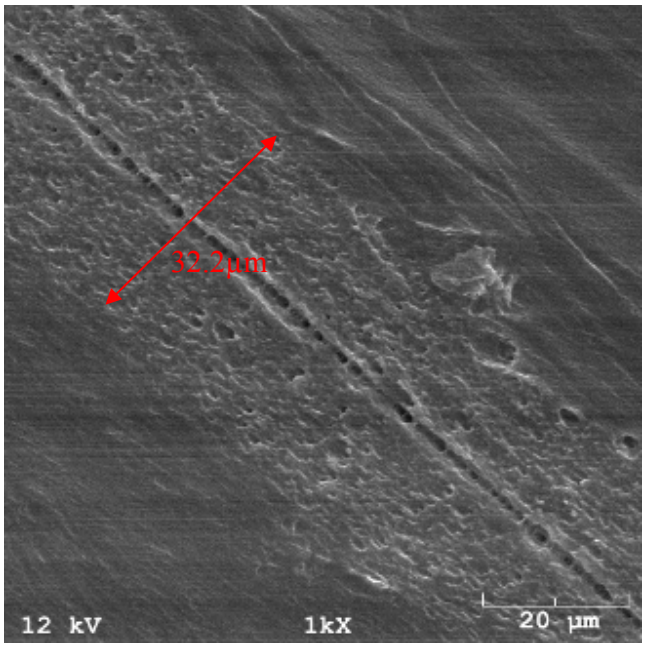

b)

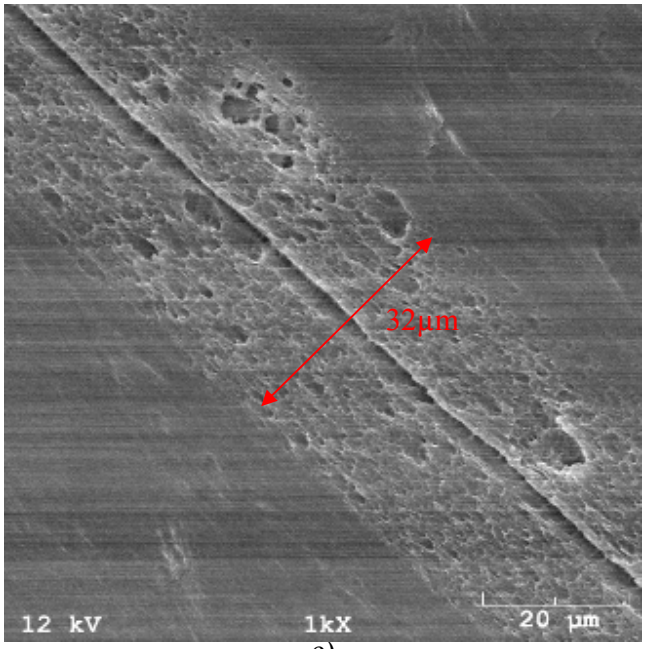

c)

Figure 6.8 Interfacial bonding morphology of two crystallizable amorphous PET sheets etched by 2 wt% potassium hydroxide/isopropanol solution for 4 h. The PET sheet was fused at heating temperature 160°C with different heating times: a) 10 s, b) 30 s, c) heating time 60 s.

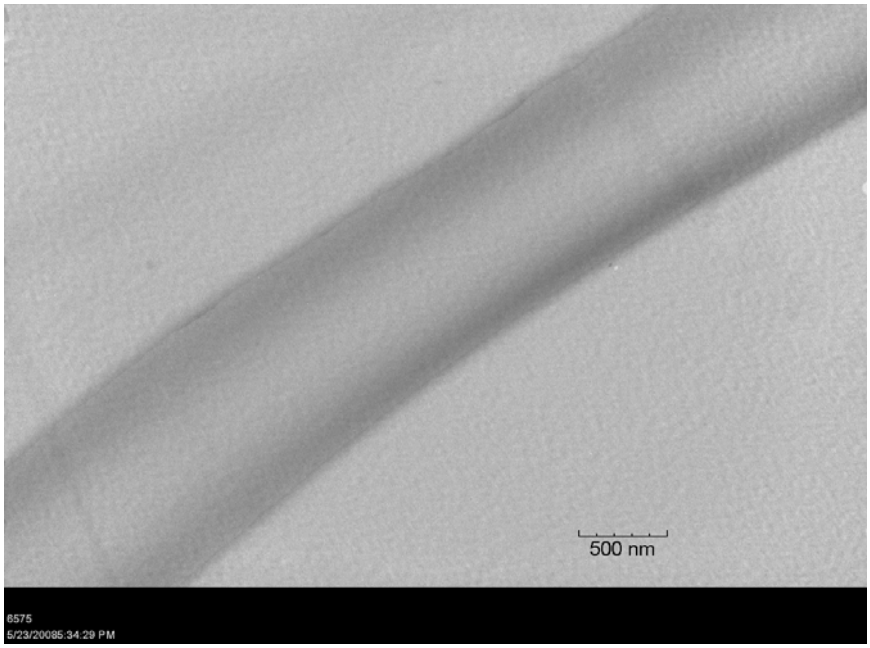

Figure 6.9 TEM images of the interfacial zone of two crystallizable amorphous PET sheets fused at heating temperature 210°C and heating time 60 s.

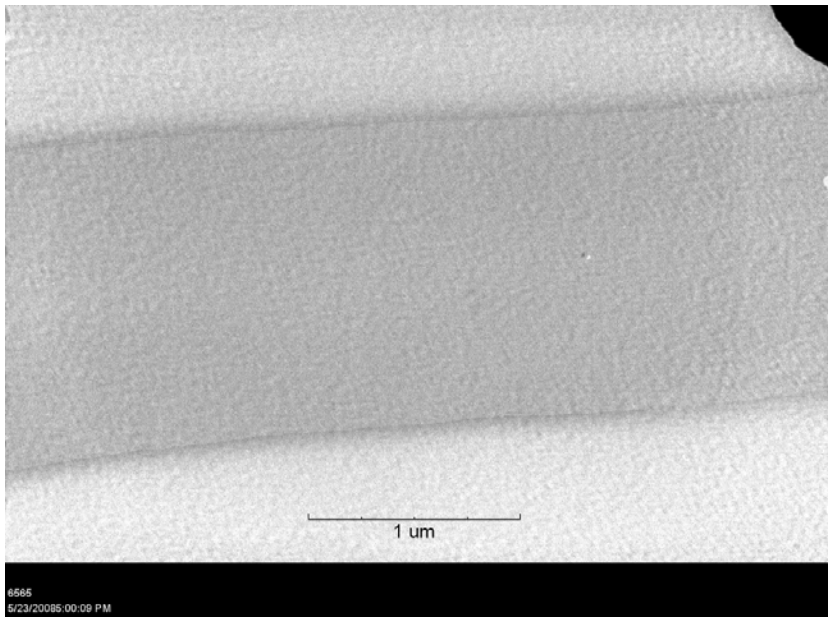

a)

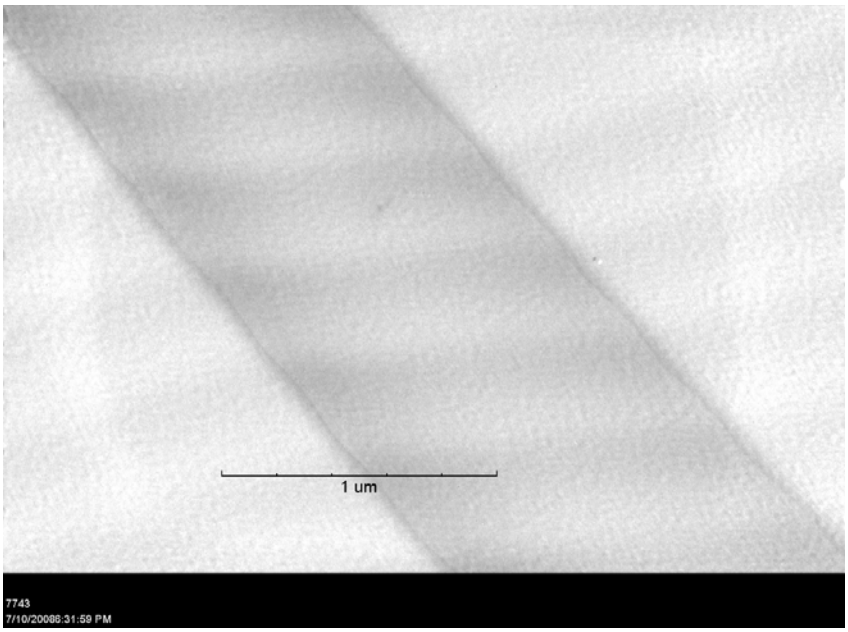

b)

Figure 6.10 TEM images of the interfacial zone of two crystallizable amorphous PET sheets fused at heating temperature 160°C with varied heating time: a) 30 s and b) 60 s.

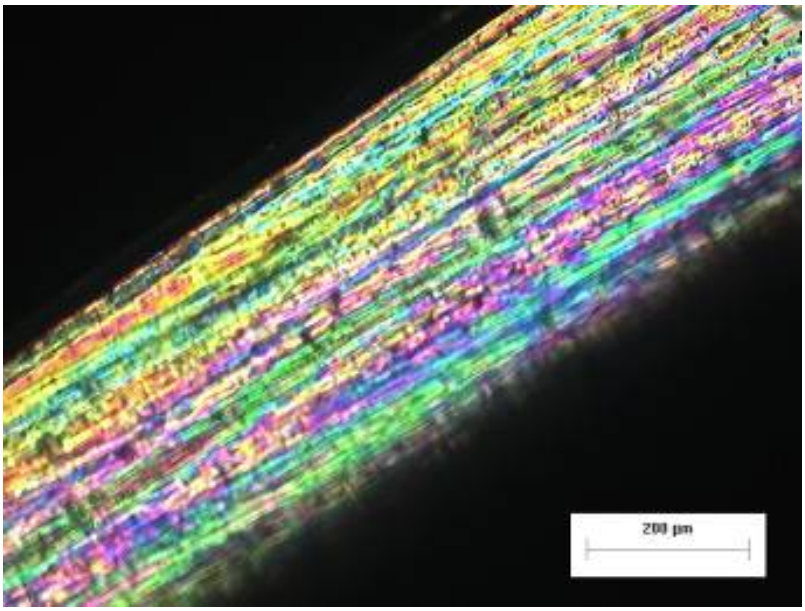

a)

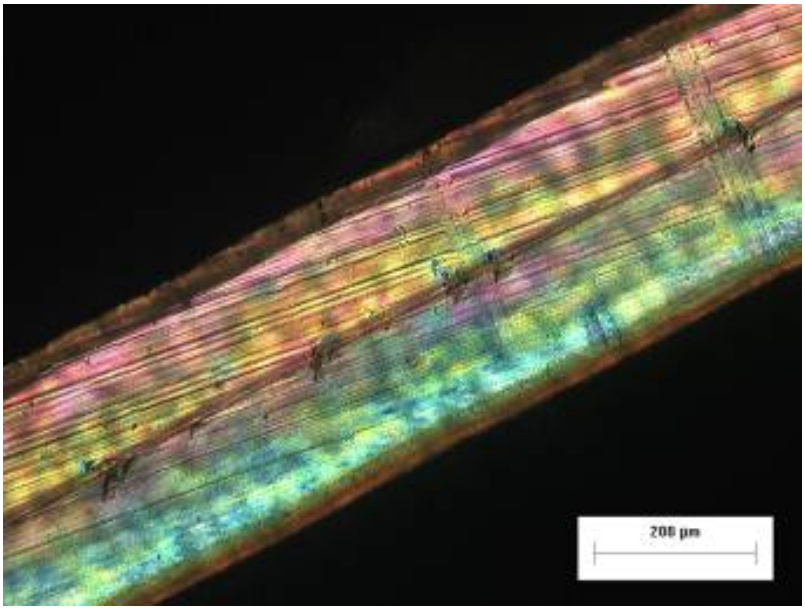

b)

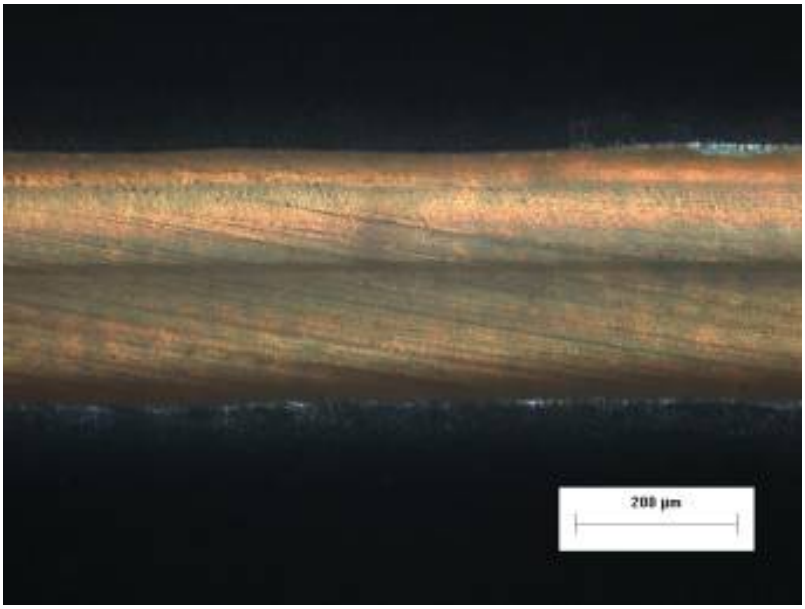

c)

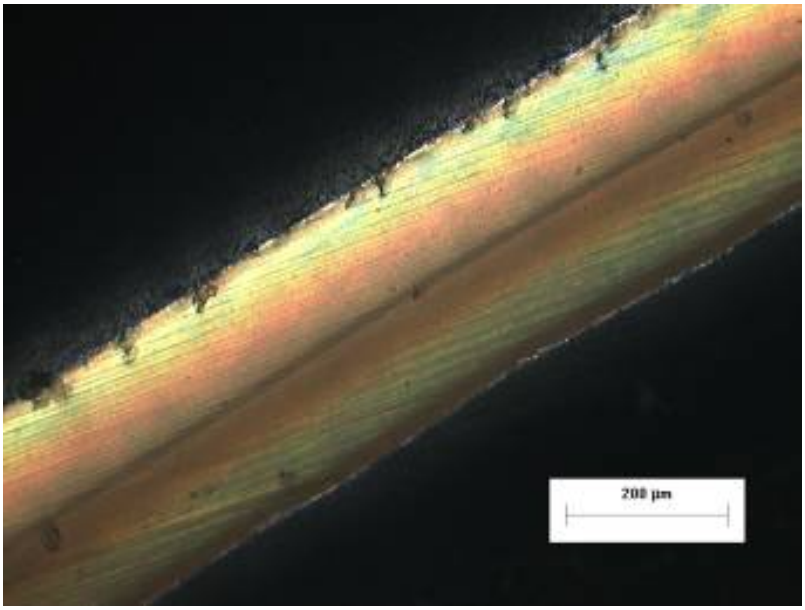

d)

Figure 6.11 Optical micrographs of the interfacial zone of two crystallizable amorphous PET sheets fused at heating temperature 210°C with varied heating time: a) 5 s, b) 30 s, c) 60 s, and d) 90 s.

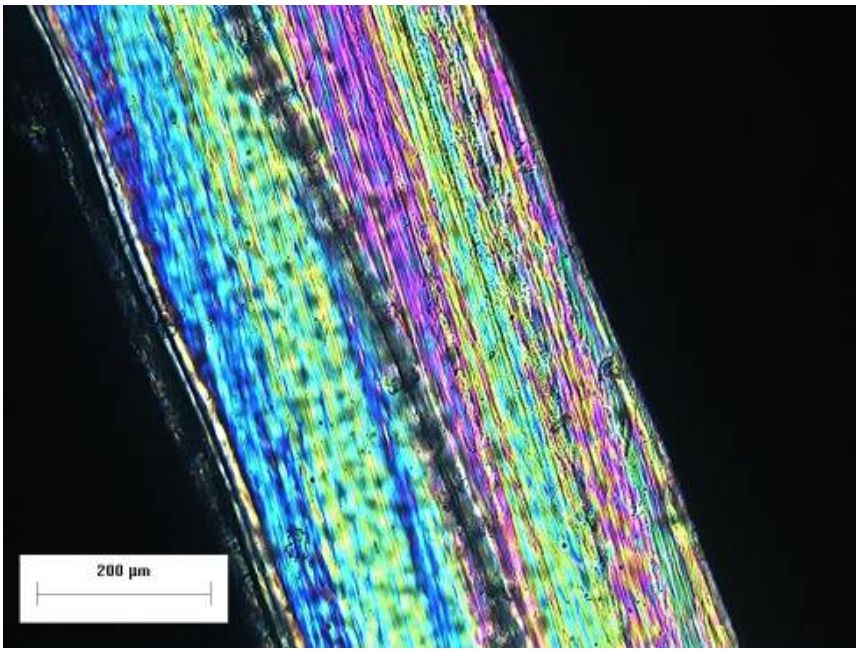

a)

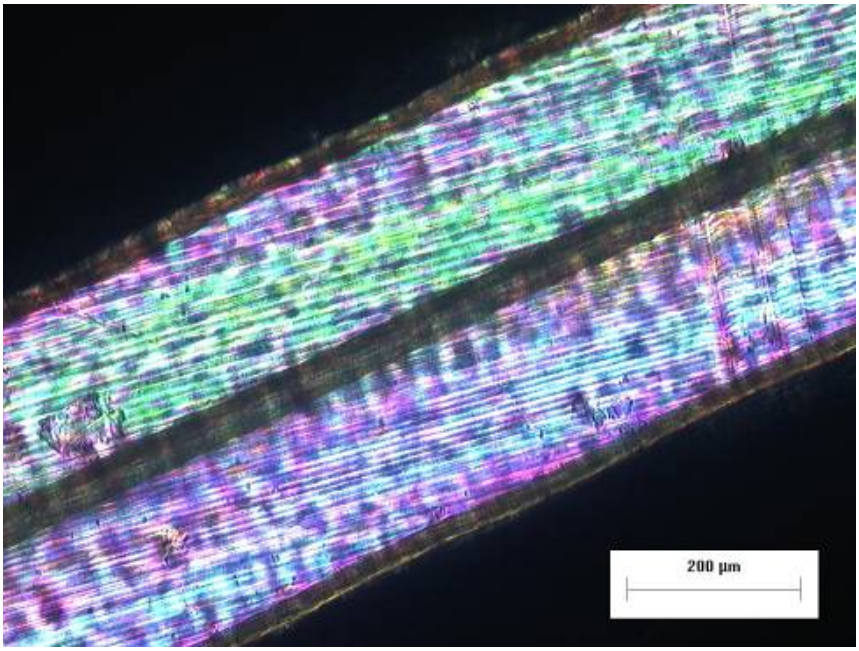

b)

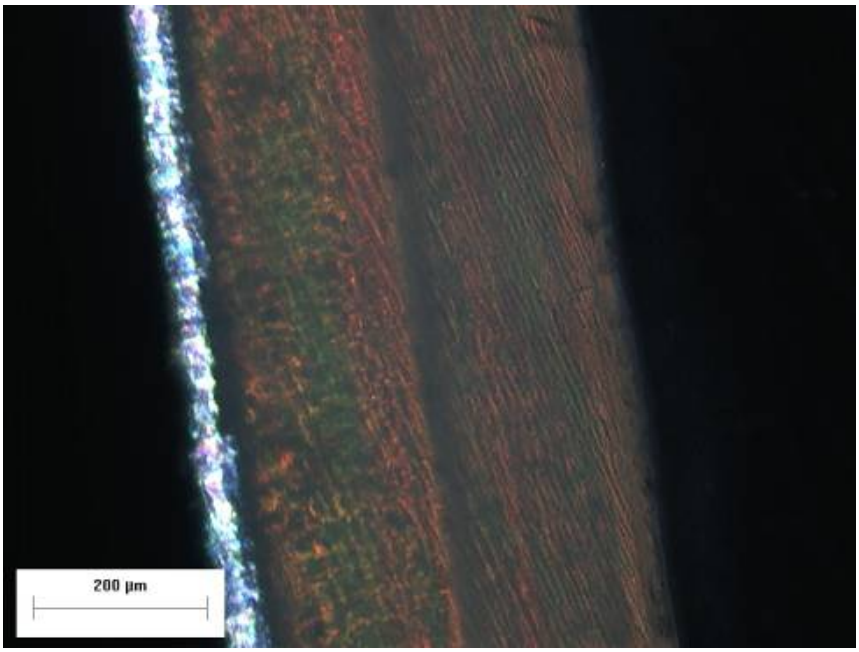

c)

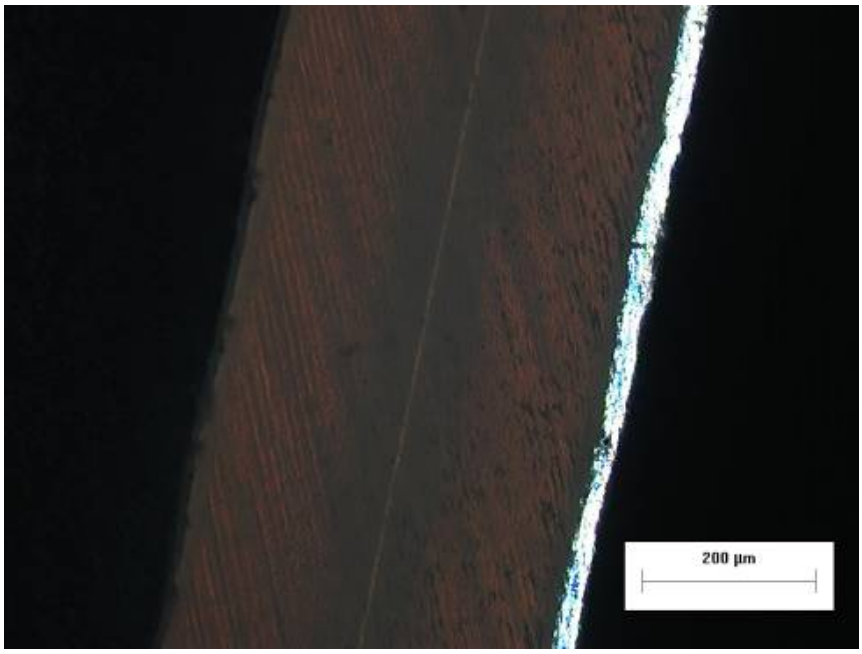

d)

Figure 6.12 Optical micrographs of the interfacial zone of two crystallizable amorphous PET sheets fused at heating temperature 160°C with varied heating time: a) 5 s, b) 15 s, c) 30 s, and d) 60 s.

6.3.2 Model of two crystallizable amorphous polymer sheets bonding

Fusion bonding is the principal phenomenon that takes place during the manufacture of thermoplastic composites. When heat and pressure are applied to two thermoplastic surfaces in contact, the materials are softened by the applied heat. The pressure causes the softened surface to spread, resulting in an intimate contact interface between the thermoplastic surfaces. Then the high temperatures at the interface can make polymer chains across the interface interdiffuse until the materials are cooled down or solidified. Fundamental studies of the thermally induced bonding of themoplastics have focused on amorphous polymer with bonding temperatures above Tg [194-196] and semicrystalline polymer with fusion bonding temperature above Tm. Studies on the fusion bonding behavior of crystallizable amorphous polymers with fusion bonding temperature between Tg and Tm are rare.

The fusion bonding mechanism for amorphous polymer with bonding temperatures above Tg and semicrystalline polymer with fusion bonding temperature above Tm have been studied very well. Squeeze flow and intermolecular diffusion model [197] can be used to explain fusion bonding mechanism for amorphous polymer with bonding temperatures above Tg and semicrystalline polymer with fusion bonding temperature above Tm. When two polymer interfaces are brought together into intimate contact, healing of the interfaces occurs. When amorphous polymer is heated above Tg or semicrystalline polymer is heated above Tm, polymer chains diffuse across the interface and entangle with other polymer chains. With the increase of the heating time, the degree of healing increases. When healing is completed, polymer chains from each side migrate

across the interface. The interface becomes indistinguishable from the bulk material. This is demonstrated in Figure 6.13.

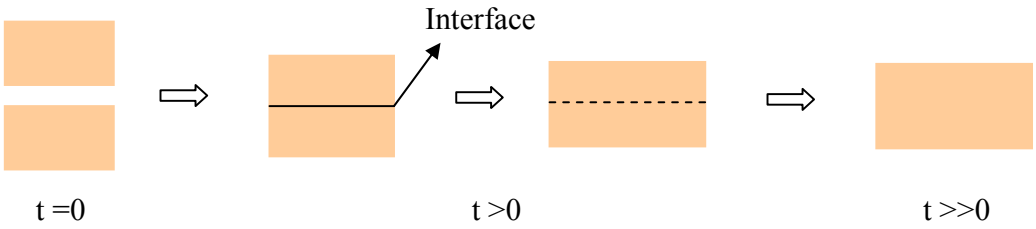

Figure 6.13 Schematic representation of bonding of two amorphous polymer sheets above Tg [198] or bonding of two crystallized polymer sheets above Tm.

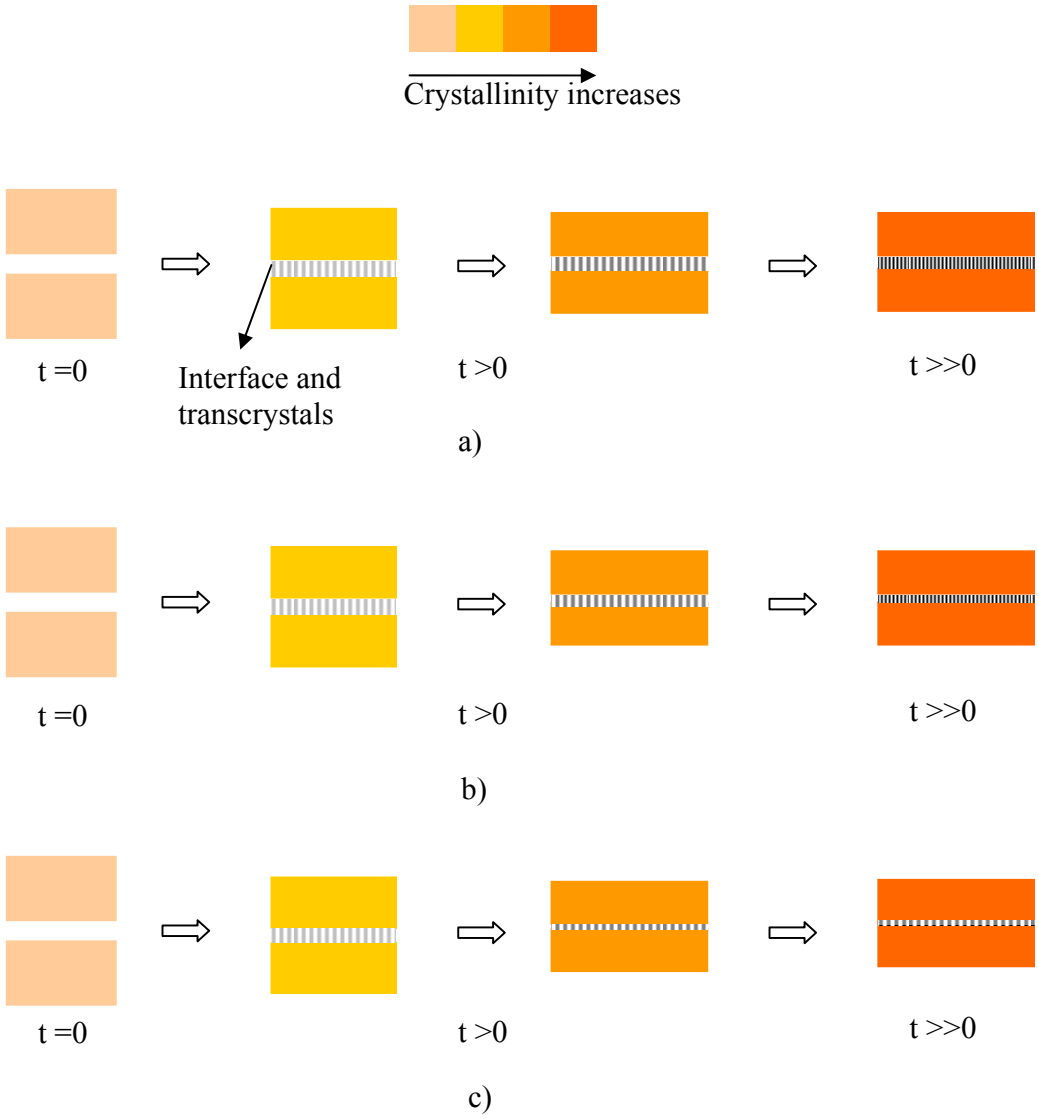

Figure 6.14 Schematic representation of bonding of two crystallizable amorphous polymer sheets between Tg and Tm when fusion bonding rate is faster than crystallizing rate: a) low temperature, b) intermediate temperature, and c) high temperature (near the melting temperature).

For crystallizable amorphous polymer bonded at temperatures between Tg and Tm, the fusion bonding mechanism was different. Originally, the thermoplastic polymer

was amorphous. When the polymer was heated between Tg and Tm, the polymer will be softened and interdiffuse with each other. At the same time, with the increase of the heating time, the crystallizable amorphous polymer can crystallize. Crystallization can make the polymer become hard and hinder the interdiffusion.

By using the experimental results from etching, SEM, TEM and polarized microscopy shown above, a fusion bonding model of crystallizable amorphous polymer with bonding temperature between Tg and Tm, was proposed, as shown in Figure 6.14. When two crystallizable amorphous sheets are heated between Tg and Tm and brought into a contact, molecular chains on each side of the interface will diffuse into each other. At the same time, the interface can induce nucleation. Then crystals grow on the interface. These crystals in the vicinity of the interface can induce nucleation in the bulk to form a second interfacial region. Simultaneously, homogeneous crystal nucleation and growth happens in the bulk. Later, with the increase of the heating time, the width of the interfacial region will decrease due to the annealing effects. Therfore, at a higher heating temperature, the width of the interface becomes smaller.

6.4 Conclusions

The fusion bonding morphology of crystallizing amorphous PET was studied using etching techniques, TEM and polarized optical microscopy. Double interfacial regions were observed at the bonding interface when two crystallizable amorphous PET films were bonded together at a temperature between Tg and Tm. The appearance of the interfacial morphology was found to be significantly affected by the processing conditions, particularly by the heating temperature and the holding time. The contact interface of the two PET sheets appeared to impose strong nucleating effects on the

crystallization of PET. Crystals were nucleated right at the interface. The crystals on the interface may induce self-nucleation in the PET bulk to form the second interfacial region. Temperature gradient across the thickness may also contribute to the formation of the double interface region. With the increase of the heating time, the width of the interfacial region decreased.

CHAPTER 7

POLY(LACTIC ACID) (PLA) SINGLE POLYMER COMPOSITES (SPCS)

7.1 Introduction

Poly(lactic acid)(PLA) belongs to the family of aliphatic polyesters commonly made from α-hydroxy acids, which include polyglycolic acid or polymandelic acid, and are considered biodegradable and compostable. PLA is a thermoplastic, high-strength, high-modulus polymer that can be made from annually renewable resources to yield articles for use in either the industrial packaging field or the biocompatible/bioabsorbable medical device market. PLA is degraded by simple hydrolysis of the ester bond and does not require the presence of enzymes to catalyze this hydrolysis. The rate of degradation is dependent on the size and shape of the article, the isomer ratio, and the temperature of hydrolysis [199]. High-molecular-weight poly(lactic acid) is a colorless, glossy, stiff thermoplastic polymer with properties similar to polystyrene. Poly (lactic acid) homopolymers have a glass-transition and melt temperature of about 55°C and 175°C, respectively. They require processing temperatures in excess of 185-190°C [200].

Three stereoisomers exist for lactide, cyclic dimer of lactic acid: (L,L)-lactide, (D,D)- lactide and meso (D,L)-lactide. Without racemization reactions, polymerization of (L,L)-lactide (LLA) and its enantiomer (D,D)-lactide (D-LA) give isotactic semi-crystalline polymers. The polymerization of meso (D,L)-lactide, or racemic mixture of 50% of D-LA and 50% of L-LA gives an amorphous polymer while the polymerization

of optically pure monomers (L-LA or D-LA) gives a semi-crystalline polymeric material [201]. The mixture (50/50) of preformed chains of P(L,L)LA and P(D,D)LA gives a stereocomplex with physicochemical and structural properties quite different from those of the correspondent homopolymers. In particular, the melting temperature of the stereocomplex is 230 °C, i.e. 50 to 60 °C higher than that of the corresponding homopolymers [202, 203]. P(L,L)LA crystallizes with an orthorhombic unit cell with crystallographic parameters a = 1.060 nm, b = 0.610 nm and c (chain axis) = 2.88 nm. The chain configuration is a 10_7 helix. The unit cell contains two chains.

It has been reported that PLA fibers have two crystal modifications depending on the spinning and drawing conditions. De Santis and Kovacs [6] reported that the crystal structure of the R modification for solution-spun fibers can be defined as a pseudo-orthorhombic with parameters *a*) 1.07 nm, *b*) 0.645 nm, and *c* (fiber axis)) 2.78 nm, where the molecules were assumed to have a left-handed 10_3 helical conformation. On the other hand, Eling et al. [204] found that the X-ray diffraction diagrams for the solution-spun fibers were different from those for the melt-extruded fibers, and they revealed the *â* structure. The unit cell of the *â* structure was proposed to be orthorhombic with dimensions *a*) 1.031nm, *b*) 1.821 nm, and *c* (fiber axis)) 0.900 nm, and the chain conformation of the *â* structure was left-handed 3_1 helices.

The production of PLA presents numerous advantages: (1) it can be obtained from a renewable agricultural source (corn); [205-207] (2) its production consumes quantities of carbon dioxide; [208] (3) it provides significant energy savings; [209] (4) it is recyclable and compostable;[210, 211] (5) it can help improve farm economies and (6)

the physical and mechanical properties can be manipulated through the polymer architecture.[212-219]

The crystallization rates of PLA are extremely slow in comparison with those of commodity thermoplastics such as PE. PLA SPCs were prepared by utilizing its slow crystallizing characteristics. As compared with PET, PLA's half time of crystallization does not follow a typical bell shape. Rather, PLA crystallizes extremely fast around 110ºC. Further, the difference between Tg and Tm is much smaller than that of PET (about 90ºC smaller). Therefore, it is expected that it would be more difficult to implement the slowly crystallizing method in PLA SPCs preparation. Accordingly, additional processing strategies may be needed in processing PLA SPCs. Since PLA is also a biodegradable polymer, PLA SPCs would be environmentally friendly and safe to dispose after a product life cycle. These were the main incentives for the present study.

7.2 Experimental

7.2.1 Materials

PLA in different physical forms was used in the experiments, including amorphous sheets and highly crystalline fibers, yarns and fabrics. The sheet was extrusion grade (made of PLA from Natureworks LLC, Grade 4032D), 0.1 mm thick, provided by Plastic Suppliers, Inc. The PLA fabric, about 0.3 mm thick, made of Natureworks LLC Ingeo® fibers, was supplied by Copland Industries. It has a cross-ply woven structure, made of textured continuous filament yarns. Each yarn consists of 135 bulked continuous filaments, with a filament diameter of about 20 μm. The filaments were melt spun, with tensile strength approximately 150 MPa, actually measured on an

Instron tensile testing machine. The porosity of the fabric is about 50%, measured based on the volume and weigh of the fabric and the density of the fiber. Some fabrics were de-woven, and recovered yarns and fibers were also used as reinforcing materials. All these materials were made of PLA supplied by Natureworks, LLC. As disclosed by the resin supplier, the Natureworks extrusion and fiber grade PLA is mainly poly(L-lactic acid), with a small portion of D-lactic acid existing as copolymer. The crystallinity of the PLA sheet and fiber used in the experiments were about 5% and 40%, respectively, measured by differential scanning calorimetry (DSC). The Tg and Tm of the PLAs used for the sheet and the fabric were approximately 60°C and 167°C, respectively, as measured by DSC.

7.2.2 Fabrication

A similar experimental setup as in a previous study was used in this study. Summarizing that approach, a lamination of two amorphous PLA sheets and a layer of PLA fabric or yarns in between was compressed between two heated platens on a Carver hydraulic press. It is important that the lamination is heated rapidly so that crystallization during the heating stage can be suppressed. Thin Teflon® films (0.07 mm in thickness) were used on both sides for easy mold separation. Additional Teflon film was employed in the middle of the lamination to create an unbonded region for peeling testing. Spacers were inserted between the heated platens to control the thickness of the molded composite sheet. The major process parameters including the platen temperature, the compression force and the heating time were varied to study their effects on the fiber-matrix adhesion properties. The PLA SPCs obtained were rapidly quenched into ice

water. Non-reinforced PLA was fabricated using the same setup by compressing two amorphous PLA sheets without insertion of the PLA fabric.

7.2.3 Characterization

DSC was conducted on a TA Instruments DSC Q-100. All samples were exposed to consecutive heating and cooling programs: first heating (30 to 200ºC), cooling (200 to 30ºC) and second heating (30 to 200ºC). The DSC data were taken from the first heating cycle. The heating and cooling rates were 20ºC/min. All scans were run under N2 atmosphere. Mechanical tests, including peeling, tearing and tensile tests were carried out at room temperature and a humidity of 63% on an Instron 5566 universal machine with a crosshead speed of 5 mm/min. Compression molded PLA and its SPCs were cut into tensile samples with a narrowed middle section in a width of 5 mm, using a cutting die (supplied by Qualitest, Inc.) according to DIN-53504-S2. For yarn reinforced SPCs, the tensile force direction was along the yarn direction. For fabric reinforced SPCs, 50% of fibers were aligned along the test direction, and the remaining 50% were along the vertical direction. For tearing test, an SPCs sheet was cut to an 80x20 mm2 rectangular shape. Then, an edge cut was made in the middle of the sample to form two arms, and the 40 mm arms were torn apart using the Instron machine. The failure surfaces on broken samples from mechanical tests were examined using stereo optical microscopy and scanning electron microscopy (SEM) (Hitachi S-800 SEM). SEM samples were sputter coated with gold for a period of 5 minutes with current at 20 mA under vacuum of 0.7 torr.

7.3 Results and discussion

In order to form a PLA SPC by compression molding a lamination of amorphous sheets and crystalline fibers, it is needed that the amorphous PLA fuses together into a matrix material at a temperature much lower than PLA's crystalline melting temperature. Otherwise, the fiber may be significantly annealed or even melted during processing, thus deteriorating its mechanical performance. It should be noted that there are two competing processes occurring when amorphous PLA is heated. First, the amorphous phase will experience a glass transition at its Tg, and the polymer will become rubbery and sticky at temperatures well above Tg (e.g., 50ºC above Tg). Two such sticky pieces can be fused together through chain diffusion at the interface. The second competing process is crystallization. The amorphous PLA will start to crystallize when its temperature is above Tg. Therefore, the just softened, rubbery and sticky amorphous phase will be transformed into a hardened crystalline phase at the same processing temperature. When preparing PLA SPCs, one needs to promote the first mechanism while restraining the second one. To promote fusion, the amorphous PLA should be rapidly heated to well above Tg, preferably above the rubbery plateau termination temperature, within a short period of time during which no significant crystallization occurs.

7.3.1 Peeling of thermally bonded PLA sheets

Given the small thickness of the amorphous PLA sheets used in this study, the lamination is expected to be heated rapidly. With typical thermal properties of PLA, analytical calculation showed that the time needed for the center of the 0.5 mm thick PLA lamination to undertake 90% of the imposed heating temperature difference is less than 0.5 s, about 2 orders faster than the typical half time of crystallization of PLA. Therefore,

rapid heating is not a problem. However, an appropriate heating temperature for enhancing fusion bonding needs to be determined. For prescreening purpose, different levels of platen temperature were used during hot compression of two-sheet laminations. The effects of platen temperature and holding time on the peeling force between two PLA sheets are shown in Figure 7.1. The compression pressure was set to about 1.5 MPa.

For a temperature at 120°C or below, good fusion bonding was not formed. The compressed sample could be peeled apart at the interface with hands. Increase of the holding time from 5 s and change of the compression pressure did not significantly affect the bonding quality. A drastic increase in peeling force was observed at a platen temperature of 130°C. Compared with 120°C, the peeling force at 130°C was several orders higher. Such a significant improvement at 130°C deserves an explanation, as attempted below. From previous studies [220, 221], it has been shown that PLA crystallizes at the fastest rate at temperatures around 110°C. To greatly restrain the crystallization process, a higher temperature is desired. At a higher temperature, the characteristic fusion time is also reduced, allowing the two films to fuse together rapidly. When the lamination was compressed at 130°C, a significant amount of squeezing flow was observed; that is, liquid squeezed out in the lateral directions. The fluidity of the material suggested that the rubbery plateau termination temperature of amorphous PLA should be in the vicinity of 130°C. This rapid liquefaction near 130°C is believed to be the main cause for the drastic increase of the fusion quality.

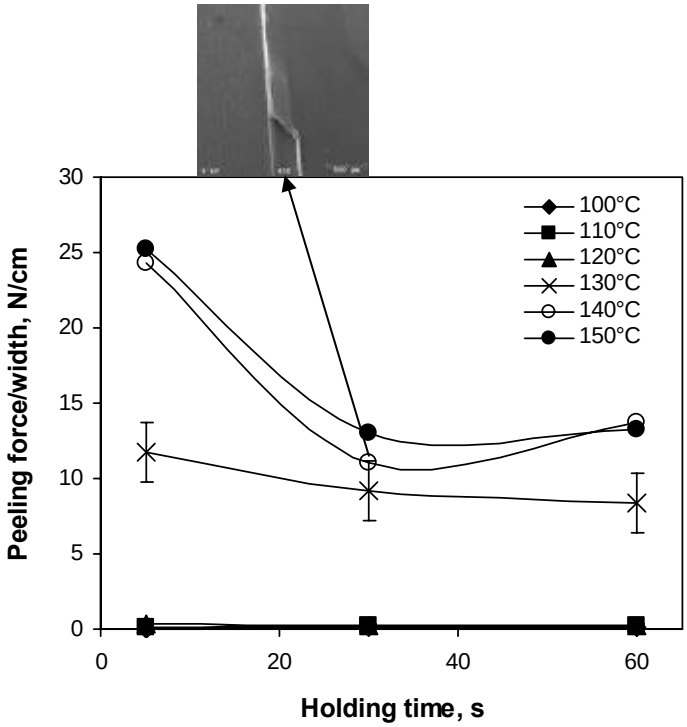

Figure 7.1 Effect of the platen temperature and the holding time on the peeling failure force for samples prepared by compression molding two PLA sheets at a compression pressure of 1.5 MPa.

Based on the prescreening findings, the platen temperature for the focused study on SPC formation was set to 130°C or above. If successful, this would result in a processing temperature window about 40°C. A compression pressure around 1.5 MPa was found to be appropriate for laminating PLA films and the composites. At this pressure, the compression molded samples are free from air bubbles, and the molded thickness can be well controlled.

7.3.2 Crystallinity development during hot compression

Figure 7.2 shows DSC thermograms at a heating rate of 20°C/min for samples prepared by compression molding two laminated amorphous PLA sheets at

140ºC with varied holding time. The "0 s" sample corresponds to the original PLA sheet. From the DSC thermograms, the amount of crystallinity for samples with different holding times can be compared. The enthalpy of melting for a pure PLA crystal (i.e., 100% crystallinity) calculated through extrapolation of experimental results was reported to be 93.7 J/g. [222] The crystallinity of the molded sample was determined by taking the ratio of the difference between the DSC melting and crystallization enthalpies to the single-crystal melting enthalpy. The results are summarized in Figure 7.3. For comparison purposes, the crystallinity of the PLA fibers used in this study is also shown in the figure. It is observed that the crystallinity of the original PLA sheet was less than 5%, indicating a nearly amorphous polymer. As the holding time increased, the compression molded and quenched samples were transparent for short holding times (e.g. 10 s), but became translucent for longer holding times (e.g. 50 s). This change in appearance signifies the increase in crystallinity, agreeing with the data in Figure 7.3. It is interesting to point out that, when compression molding amorphous PLA, two solidification mechanisms exist. With short holding time before quenching, vitrification of the amorphous phase is the main solidification mechanism, and therefore the samples turn into a transparent amorphous glass. For longer holding times, the polymer experiences sequential fluidization (i.e., softening and liquefaction of the amorphous phase) and solidification (crystallization induced) under an isothermal molding condition. For the lamination of two thin PLA sheets, fluidization occurs almost instantaneously (within 1 s) when the sample comes into contact with the two heated platens. On the contrary, crystallization occurs over a much longer period. For longer holding times

(above 60 s), the sample was substantially crystallized and became a solid between the two heated platens.

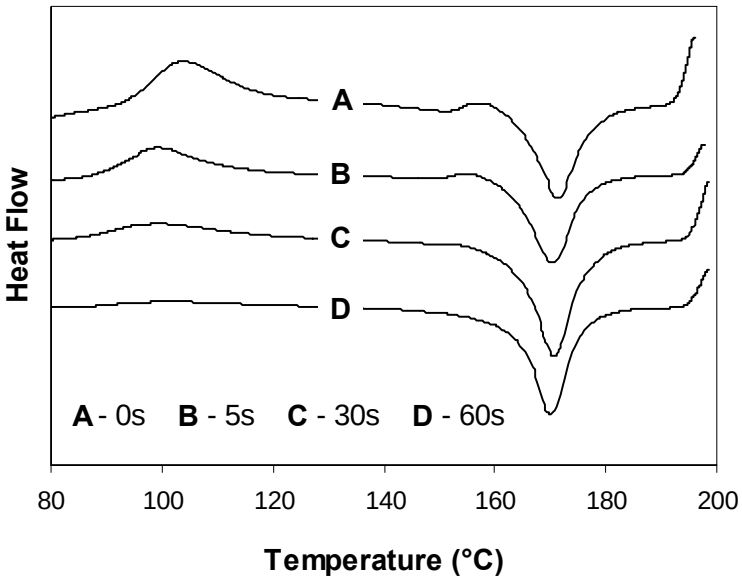

Figure 7.2 DSC thermograms of PLA prepared by compression molding two PLA sheets at 140°C with different holding time. The four levels of holding time are labeled as A, B, C, and D in the figure. A heating rate around 20ºC/min was used in the DSC experiments.

7.3.3 Fiber-matrix bonding

PLA SPCs were prepared by compression molding a layer of PLA fabric sandwiched between two amorphous PLA sheets. Tensile specimens were cut from the molded SPC sheet and tested using an Instron machine. The surface topology of the broken samples were examined using SEM. Representatively, two different types of broken surface topology from samples prepared using different platen temperatures are shown in Figure 7.4. The holding time was set to 30 s. For SPCs specimens molded at 130°C, very long pull-out fibers were observed at the broken surface, indicated by arrows

in Figure 7.4 a and Figure 7.4 c; the pull-out length is several times larger than the thickness of the SPCs sheet. As the platen temperature increased to 140°C, the fibers pulled out at the broken surface were short; most fibers were broken at the same broken surface of the matrix. This indicated that a strong bonding between the fiber and the matrix occurred. Since an abrupt change in the bonding quality occurred during manufacture of the SPCs in a small temperature window of 10°C, one may define a bonding transition temperature using the median temperature, i.e., 135°C. This transition temperature specifies the low boundary of the processing temperature window for successful PLA SPCs manufacturing.

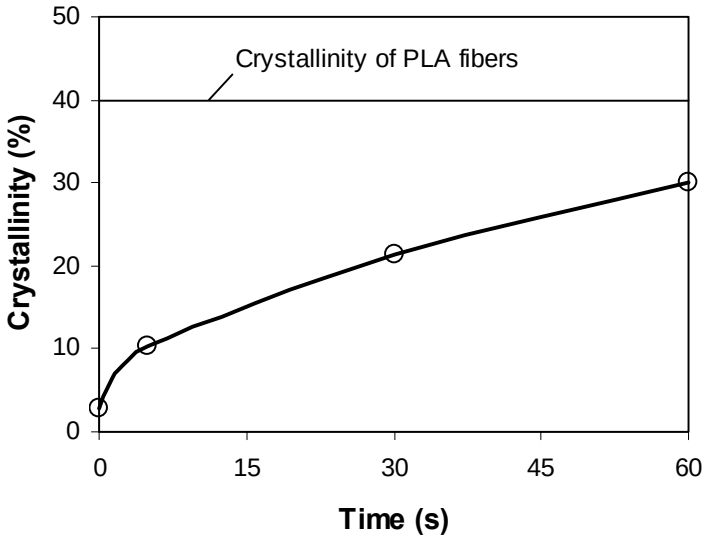

Figure 7.3 Crystallinity for PLA samples prepared by compression molding two as-received PLA sheets at 140°C using varied holding time. For comparison, the crystallinity of as-received PLA fibers is given in the figure.

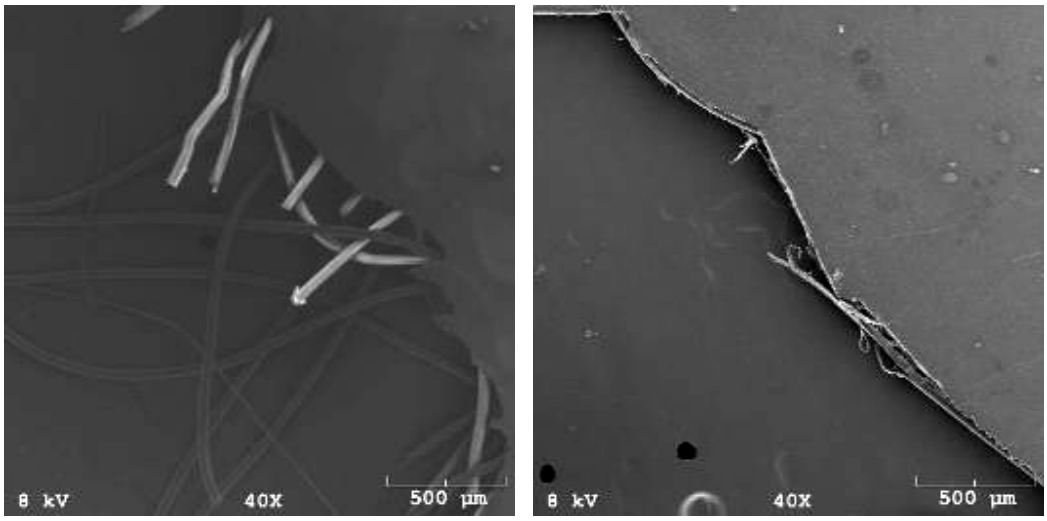

a) b)

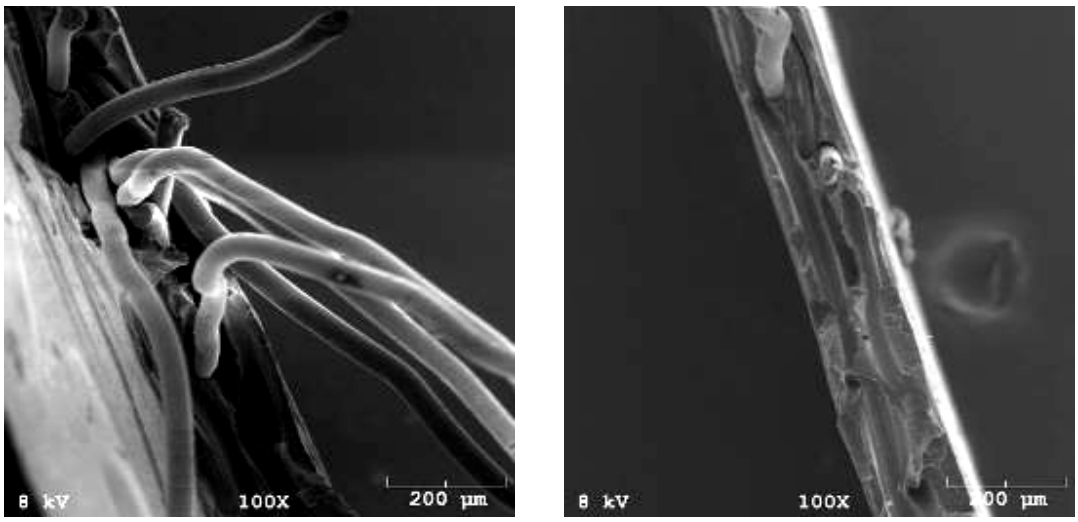

c) d)

Figure 7.4 Topography at the tensile failure surface of compression molded PLA SPCs : a) side view, platen temperature at 130°C, b) side view, platen temperature at 140°C, c) front view, platen temperature at 130°C, and d) front view, platen temperature at 140°C. The holding time was 30 s.

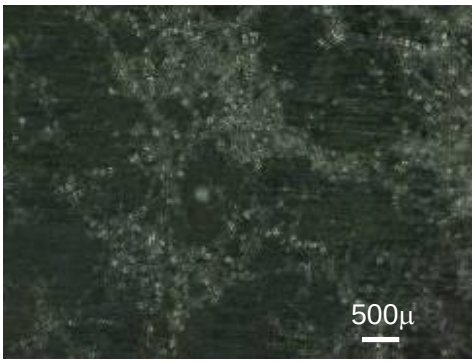

a)

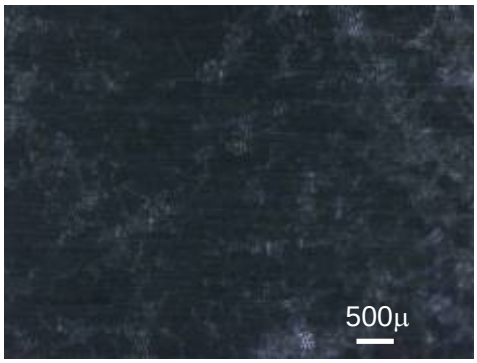

b)

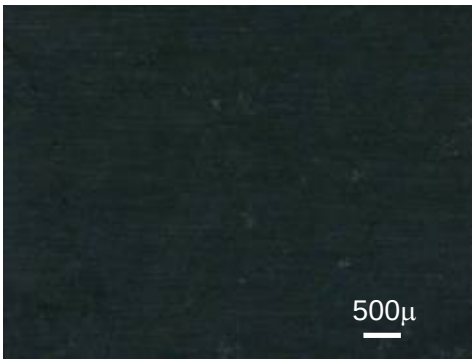

c)

Figure 7.5 Effect of heating time on the appearance of compression molded PLA SPCs at platen temperature 130°C with varied holding time: a) 5 s, b) 30 s, and c) 60 s.

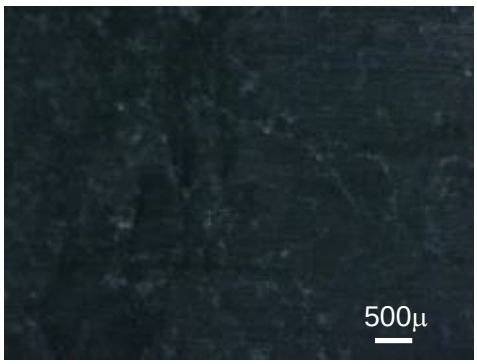

a)

b)

c)

Figure 7.6 Effect of heating time on the appearance of compression molded PLA SPCs at platen temperature 140°C with varied holding time: a) 5 s, b) 30 s, and c) 60 s.

Fiber-matrix bonding could also be evaluated by observing the degree of transparency of the molded SPCs. As an example, Figure 7.5 compares the microscopic appearance of different samples molded under different conditions. The platen temperature was set to the same at 130°C, but the holding time was varied from 5 s to 60 s. With the increase in holding time, the transparency of the SPCs was increased. The higher transparency at a holding time of 60 s indicated that the fiber and the matrix in the SPCs were highly affine to each other. The microscopic appearance of different samples molded at 140°C with different holding times is shown in Figure 7.6 When the holding time is 30 s, there is higher transparency indicated that the fiber and matrix were highly affine to each other.

7.3.4 SPCs with PLA fabric as reinforcement

The as-received PLA fabric was used as a reinforcing material in the SPCs. Figure 7.7 compares the tensile behavior of three SPC sheets compression molded under different conditions. The weight fraction of the fabric in the SPC was 50%. The SPCs

molded at platen temperature 140°C and holding time 50 s exhibited a considerably higher strength (almost twice higher) than the SPCs molded at platen temperature 130°C and holding time 20 s. In the former case, the fiber and the matrix broke simultaneously, with a composite failure strain about 0.03. In the latter case, the matrix and the reinforcement broke at different strains, about 0.03 and 0.5, respectively; after the matrix broke, the fabric was pulled out and continued to elongate until failure occurred. The difference in the tensile behavior can be correlated with the different fiber-matrix bonding conditions in the two different samples. Since the fabric is more ductile than the matrix, the concurrent failure of the matrix and the fabric signifies a strong adhesion between them. An intermediate case with a platen temperature of 130°C and a holding time of 50 s was also given in Figure 7.7. Some intermediate tensile behavior was shown in this case.

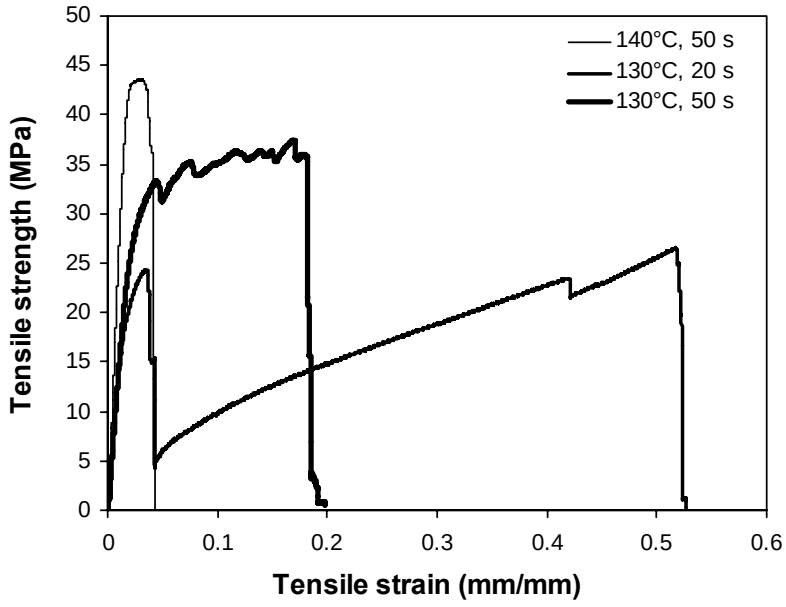

Figure 7.7 Tensile behavior of PLA SPCs prepared by compression molding a lamination of two PLA sheets and one layer of PLA fabric.

For better understanding of the composite behavior, the tensile behavior of the matrix and the reinforcement were obtained, as shown in Figure 7.8. The matrix PLA had a failure strain around 0.03. The fabric appeared to be much more ductile, with a failure strain about 0.5. This ductile behavior is attributed to the fabric's textured structures and porosity. For poor interfacial bonding, the fabric will slip in the matrix and deform freely. When the bonding is strong, the matrix and the fabric will assume the same strain during deformation. In this case, the structural elasticity of the fabric will be suppressed, and the composite exhibits a single point of failure.

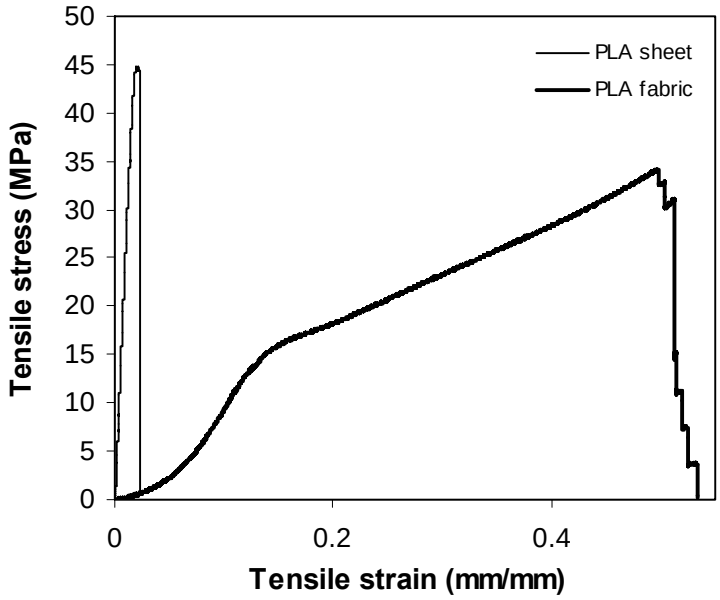

Figure 7.8 Tensile behavior of PLA sheet and PLA textile fabric. The PLA sheet was prepared by compression molding two as-received PLA sheets at 140°C with a holding time of 50 s.

The tearing behavior of the SPCs sheet and the original PLA sheet were also tested and compared. An edge cut was made in the middle of the sample to form two arms, and the arms were then torn apart using the Instron machine. Figure 7.9 shows that the tearing strength of the SPCs sheet is about 8 times higher than that of the non-reinforced PLA sheet. Both samples were molded with a platen temperature of 140°C and a holding time of 50 s. The non-reinforced PLA appeared to be a notch sensitive material. The propagation of the crack was greatly suppressed by the fabric in the SPCs. This substantial increase in tearing strength would be desired in many membrane and packaging applications. [223] Figure 7.10 shows the formability of the fabric-reinforced PLA SPCs sheet. A dome shape with a 50-mm diameter was successfully molded on a 0.5-mm thick PLA SPCs sheet.

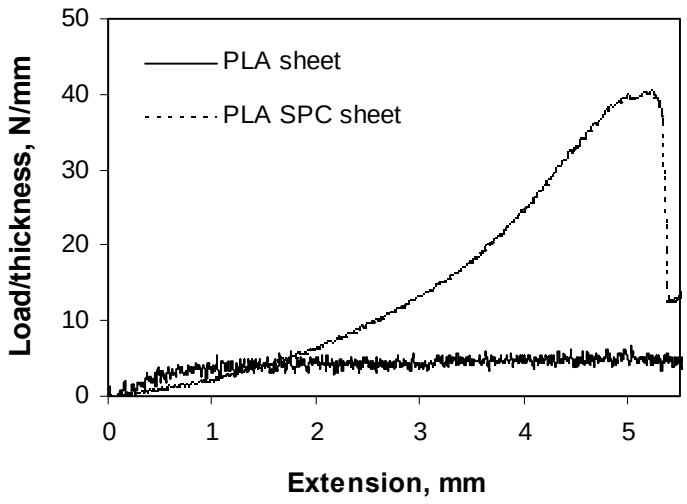

Figure 7.9 Tearing tests of non-reinforced PLA sheet and PLA SPCs sheet, both molded at a platen temperature of 140°C and a holding time of 50 s.

7.3.5 SPCs with PLA yarns as reinforcement

Although the tearing strength was significantly improved, the tensile strength of is in a cross-ply configuration, only 50% yarns were involved in load transfer. The remaining yarns orientated in the transverse direction to the loading direction contributed little to the strength of the SPCs, although they accounted for about 25% by weight of the SPCs. To create stronger PLA SPCs, yarns were separated from the fabric and used to make uniaxially reinforced SPCs. The resulting yarn was made of 135 textured continuous filaments in a diameter of about 20 μm. Figure 7.11 shows the tensile stress-strain curve of the yarn. Because of the texturing structure, the yarn showed structurally elastic behavior, exhibited by a low modulus, at the beginning of the stress-strain curve. During this initial period, the curled yarn was uncurled. The ultimate tensile strength of the yarn was about 130 MPa, which is considerably lower than was reported by Natureworks, [224] above 300 MPa. The reduced strength might have resulted from damage during yarn post processing, as well as during fabric knitting and weaving steps, since PLA's properties are sensitive to thermal and mechanical influences. Figure 7.12 compares the tensile behavior of the yarn-reinforced SPCs with that of the non-reinforced PLA. The percentage of yarns by weight in the SPCs was 25%. Both samples were compression molded at platen temperature 140°C and holding time 50 s. Again, the structurally elastic behavior of the yarn (due to texturing) was suppressed in the SPCs, indicating strong bonding between the fiber and the matrix. About 30% improvement in tensile strength was observed for the SPCs. It is expected that, with the employment of stronger PLA fibers and increased fiber percentage, the tensile strength can be further

improved. The tensile properties for PLA SPCs described above are summarized in Table 7.1.

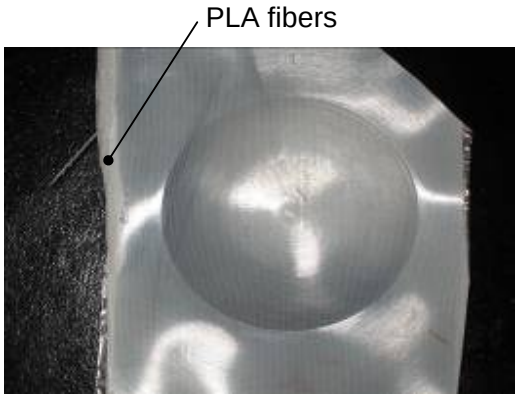

Figure 7.10 A dome-shaped sample (with a 50-mm diameter dome) made of PLA SPCs and compression molded at platen temperature 140°C.

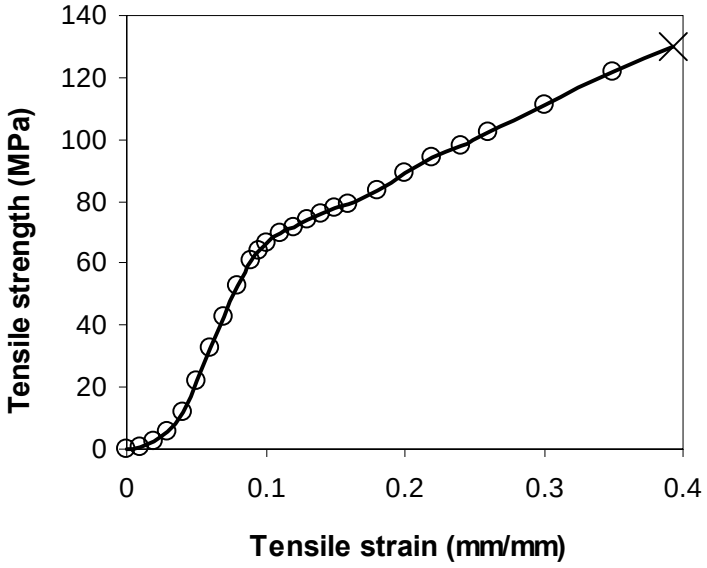

Figure 7.11 Tensile behavior of PLA yarns. Each yarn is made of about 135 textured continuous filaments in a diameter of about 20 μm.

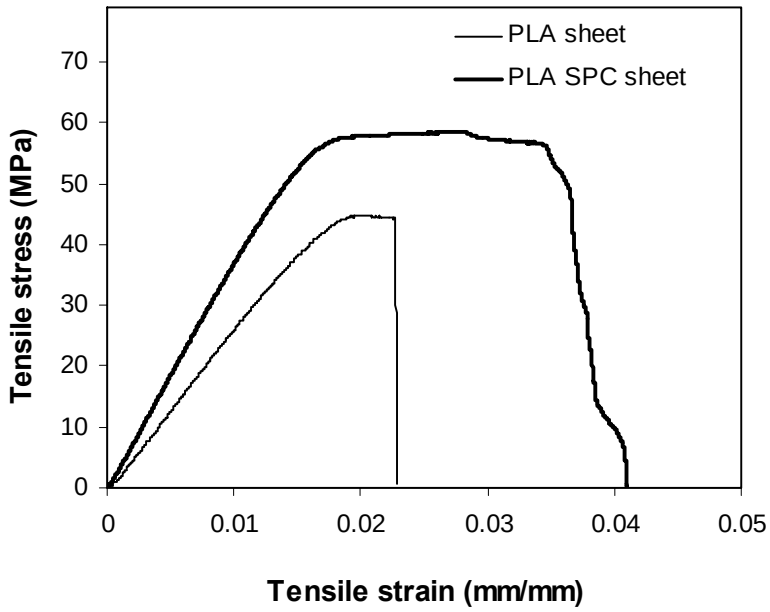

Figure 7.12 Comparison of tensile properties of non-reinforced PLA sheet and PLA SPCs sheet reinforced by 25%-wt. unidirectional PLA yarns. Both samples were compression molded at platen temperature 140°C and holding time 50 s.

Table 7.1 Tensile properties of PLA materials with different physical forms.

Type of PLA Materials	Young's modulus (GPa)	Tensile strength (MPa)	Failure strain (%)
*Non-reinforced sheet	2.5	44.8	2.3
Textile fabric	<0.1	34.2	50
Yarn	~1.1	133	40
*SPC with 50%-wt fabric	2.3	43.6	5
*SPC with 25%-wt yarns	3.7	58.6	4

*Compression molded at platen temperature 140°C and holding time 50 s.

7.4 Conclusions

Single PLA composites were prepared by compression molding a lamination of PLA fibers in yarns or fabrics sandwiched between thin amorphous PLA sheets. Utilizing the slowly crystallizing characteristics of PLA, a processing temperature window greater than 30°C was obtained. The fusion quality of the matrix and the bonding between the matrix and the fiber were evaluated by peeling test and microscopic examination of the failure surface and the optical appearance of the SPCs. An abrupt improvement in matrix-fiber bonding quality was observed at 135°C, signifying the low boundary of the processing temperature window. With strong interfacial bonding, the PLA SPCs showed a single point of failure during tensile test, and the original texturing-induced structural elasticity of the reinforcement was restrained. The SPCs exhibited a significant improvement in mechanical properties. Particularly, with 50%-wt fabric as reinforcement, the tearing strength was improved by almost an order. Increases in tensile strength and modulus were also obtained for uniaxially reinforced PLA SPCs. The improved mechanical properties, together with the formability of the resulting SPCs sheet, indicated its potential applications in the packaging industry.

CHAPTER 8

SUMMARY, CONCLUSIONS AND FUTURE WORK

8.1 Summary of work done

A novel approach for formulating and processing SPCs utilizing the distinct physical forms of slowly crystallizing polymers to enlarge the processing temperature window was investigated in this thesis research. PET and PLA were used as two model systems. Focused studies, including SPCs manufacturing, composites characterizations, interfacial bonding investigations, and interfacial morphological characterizations, were carried out on PET SPCs. PLA was used in a second case study of the proposed new method. The major experimental studies performed in this research are summarized as follows:

- The feasibility of the new SPCs manufacturing method was investigated. The crystallinities of PET under different processing conditions were measured using DSC. PET fibers coated with nearly amorphous PET were observed under polarized microscopy. Bonding between fiber and matrix was evaluated by SEM. Effect of heating time on the crystallinities was studied by DSC.
- The effects of heating temperature and heating time on the properties of PET SPCs were studied. The tensile strength and modulus of amorphous PET, highly crystallizing PET fibers and PET SPCs were measured using the Instron tensile machine. Rule of mixing was used to predict the mechanical properties of PET SPCs. The impact properties of PET SPCs and crystalline PET sheets were evaluated using an impact testing machine. The properties of PET SPCs prepared

by the new method were compared with those of existing single-polymer composites. The PET fibers before and after heat treatment were studied using XRD, TGA, DSC and so on.

- The fusion bonding behavior of crystallizable amorphous PET was investigated. Peeling test was used to evaluate the fusion bonding strength. The failure surfaces on broken samples from peeling tests were examined using SEM. The fusion bonding behavior of crystallizable amorphous polymer was compared with that of the non-crystallizable amorphous polymer. The effects of heating temperature and heating time on the bonding strength were studied. The relation between crystallization and fusion bonding was explored.
- The interfacial morphology of crystallizable amorphous PET was observed using different methods, including SEM, TEM, and polarized optical microscopy either on etched or non-etched sample slices. Effects of heating temperature and heating time on the interfacial morphology were studied.
- Another slowly crystallizing polymer, PLA, has also been used in SPCs preparation. The interfacial bonding strength was evaluated by peeling testing. The bonding between fiber and matrix was evaluated by SEM and optical microscopy. The crystallinities of PLA were measured using DSC. The effects of heating temperature and heating time on the PLA SPCs were investigated. The mechanical properties of the PLA SPCs were evaluated.

8.2 Conclusions

The major conclusions derived from the thesis study are summarized in the following:

- The experimental results showed that, with slowly crystallizing polymers, SPCs having enhanced mechanical performance can be produced using a large processing temperature window spanning from a lower temperature not far above Tg to a higher temperature close to Tm. Compared with the currently most popular fiber hot compaction method, the processing temperature window for this method is many times wider. On the other hand, unlike co-polymer approaches or other molecular approaches, the SPCs made from this method are true single-polymer composites, with both matrix and reinforcement made from the same polymer with the same chemical structure.
- The PET SPCs were found to have significant improvement in mechanical properties over non-reinforced PET. After reinforcement, the tensile strength of PET SPCs was almost five folds of that of amorphous PET. Rule of mixing was used to predict the tensile strength and modulus of PET SPCs. The experimental results showed that the rule of mixing works well for PET single polymer composites. The heating temperature and holding time were found to play a profound role in influencing the properties of the SPCs. Excellent fiber-matrix interfacial adhesion was obtained at a low consolidation temperature of 180ºC, more than 70°C below PET's normal melting temperature, and a holding time of 30 s. It was found that, under these processing conditions, the crystallinity and orientation of PET fibers were nearly affected, judged by DSC and XRD; unwanted annealing effect was minimized, and the fibers were able to maintain their highly orientated crystalline structure. All these results demonstrated the

technical feasibility of processing slowly crystallizing PET SPCs at a temperature much lower than the melting temperature.

- The results from the fusion bonding study showed that faster heating rate and higher temperature resulted in stronger bonding between two crystallizable amorphous PET sheets. It was found that the interfacial bonding quality was significantly affected by the state of crystallization and the morphological development at the bonding interface. It was also found that, at different processing temperature, the fusion bonding behavior was different. At low temperature, with the increase of heating time, the bonding strength decreased monotonically. At intermediate temperature, the bonding strength increased first and then decreased. At high temperature near the melting temperature, the fusion bonding strength increased with the increase of heating time. This fusion bonding behavior is vastly different from that of non-crystallizable amorphous polymer. For a non-crystallizable amorphous polymer, with the increase of heating time, the bonding strength was known to increase, disregarding the heating temperature. For crystallizable amorphous polymer, the bonding behavior appeared to be more complex.
- The fusion bonding morphology of crystallizable amorphous PET sheets was studied using etching techniques, SEM, TEM and polarized optical microscopy. Double interfacial regions were observed when two crystallizable amorphous PET were bonded together between Tg and Tm. The contact interface of the two PET sheets appeared to serve as a strong nucleating site for the crystallization of PET in the vicinity. Transcrystals were nucleated at the interface. The transcrystals on

the interface appeared to induce nucleation in the PET bulk to form the second interfacial region. With the increase of the heating time, the width of the interfacial region decreased. Based on the experimental observations, a fusion bonding model of crystallizable amorphous polymer was proposed.

- For PLA SPCs, a processing temperature window greater than 30°C was obtained. An abrupt improvement in matrix-fiber bonding quality was observed at 135°C, signifying the low boundary of the processing temperature window. With strong interfacial bonding, the PLA SPCs showed a single point of failure during tensile test, and the original texturing-induced structural elasticity of the reinforcement was restrained. The SPCs exhibited a significant improvement in mechanical properties. Particularly, with 50%-wt fabric as reinforcement, the tearing strength was improved by almost an order of magnitude. Increases in tensile strength and modulus were also obtained for uniaxially reinforced PLA SPCs. The improved mechanical properties, together with the formability of the resulting SPCs sheet, indicated its potential applications in the packaging industry.

8.3 Recommendations for further work

Besides PET and PLA, the new method for SPCs manufacturing is equally applicable to other slowly crystallizing polymer, such as poly (ether ether ketone), poly (arylene ether ketone), poly (trimethylene terephthalate), poly (phenylene sulfide), syndiotactic polystyrene, to name a few. Therefore, aside from testing the commercial scalability of PET SPCs and PLA SPCs, one future endeavor is to investigate and develop SPCs made of other slowly crystallizing polymers.

From the literature survey provided in this thesis, it can be seen that the major issue in SPCs manufacturing is on how to process the matrix material in its liquid state without significantly degrading the useful engineering properties of the reinforcement. Compared with the single-component method, the two-component method has more flexibility in composites design and manufacture. The small process window problem in single-component processing is inherent, but becomes less stringent in two-component processing because of the employment of two distinct material forms. Therefore, it would be interesting to see any new developments of physical processes for two-component SPCs manufacturing.

Looking at SPCs manufacturing in terms of two elementary steps are useful. The first step is to create two distinct physical phases from a same polymer and the second is to consolidate the two phases. The steps may be considered independently in the development of new processes. Particularly, new SPCs manufacturing processes could result if new practical approaches for creating distinct physical forms of the same polymer should be uncovered. Likewise, new processes could be created if new consolidation method should be found.

It would also be interesting to use the two-component approach to develop amorphous layer coated crystalline fibers, because the resulting fiber will offer a great flexibility in manufacturing. This may be achieved using the rapid coagulation method to precipitate a thin layer on the highly crystalline fiber. Similarly, it would also be interesting to see other new processes which could result in differentiation of the fiber structure from the skin to the core.

APPENDIX A

MOLECULAR WEIGHT DETERMINATION OF PET USING DILUTE SOLUTION VISCOMETER

1 Equipment

Constant temperature water bath, Ubbelohde Type I viscometers, Volumetric flasks, Stop watches

2 Materials

1) Poly(ethylene terephthalate) – PET fibers, amorphous, PET fibers and amorphous PET sheet of unknown molecular weight
2) 60/40 phenol-1,1,2,2-tetrachloroethane/25 °C

3 Procedure

1) Make up four solutions of polymer in Co-solvent, 0.17, 0.2, 0.24 and 0.3 g/dL (wt %).
2) Rinse viscometer thoroughly with solvent to remove dirt and dust.
3) Condition viscometer in bath for 10-15 minutes.
4) Pipette the appropriate amount of solvent into the viscometer. Allow the solution to equilibrate in the viscometer a few minutes before you start measuring efflux times.
5) Determine efflux time of solvent 4 times in viscometer. Measurements should be consistent to within ±1 second.

6) Repeat steps 5 and 6 for the polymer solutions starting with the least concentrated system.

APPENDIX B

ETCHING AND MORPHOLOGY

B.1 Interfacial bonding morphology of two crystallizable amorphous PET sheets at heating temperature 160 °C

B.1.1 Interfacial bonding morphology of two crystallizable amorphous PET sheets at heating temperature 160°C and heating time 10 s

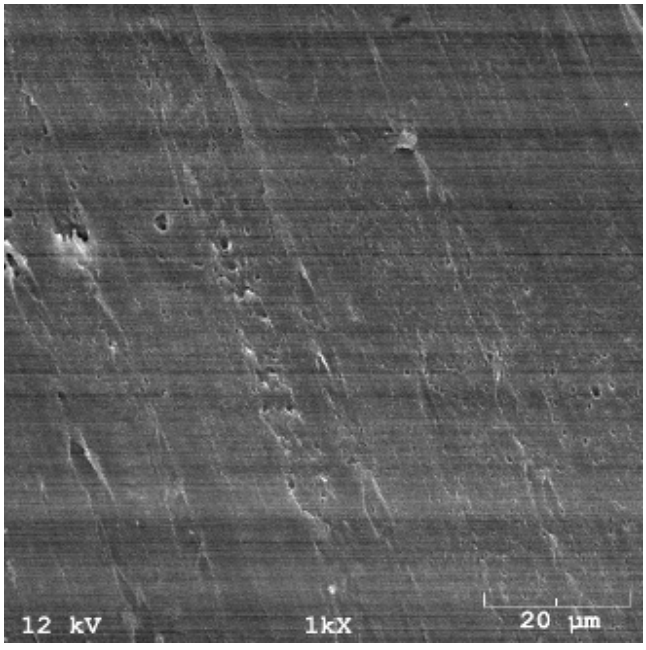

a) etching 30 min

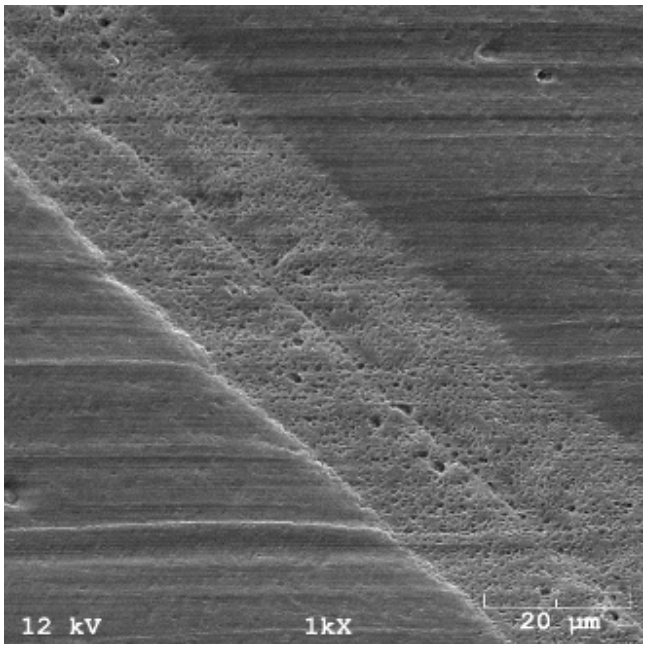

b) etching 1 h

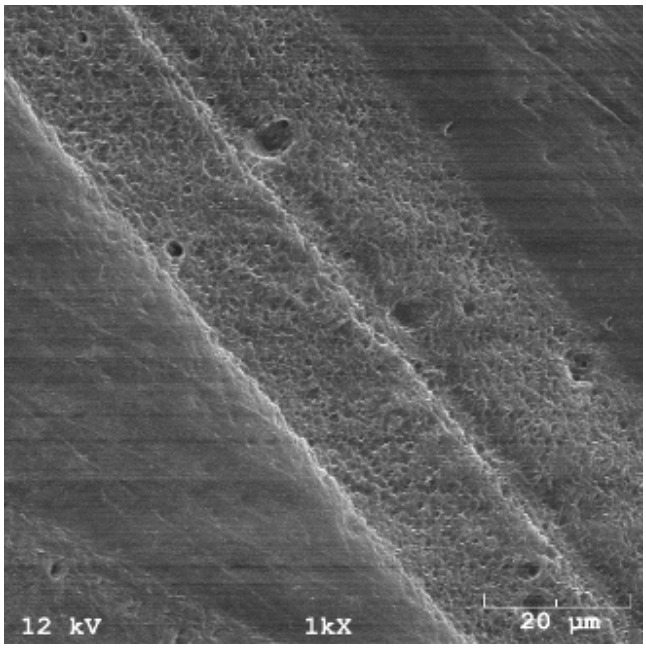

c) etching 2 h

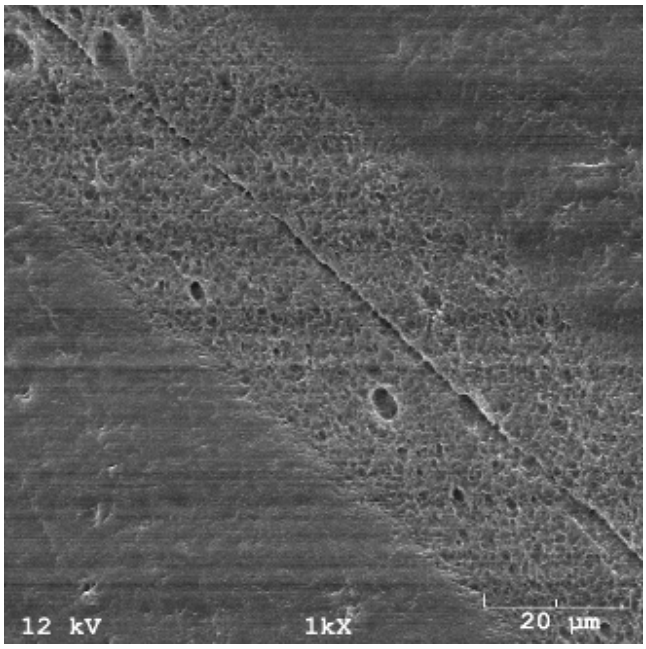

d) etching 3 h

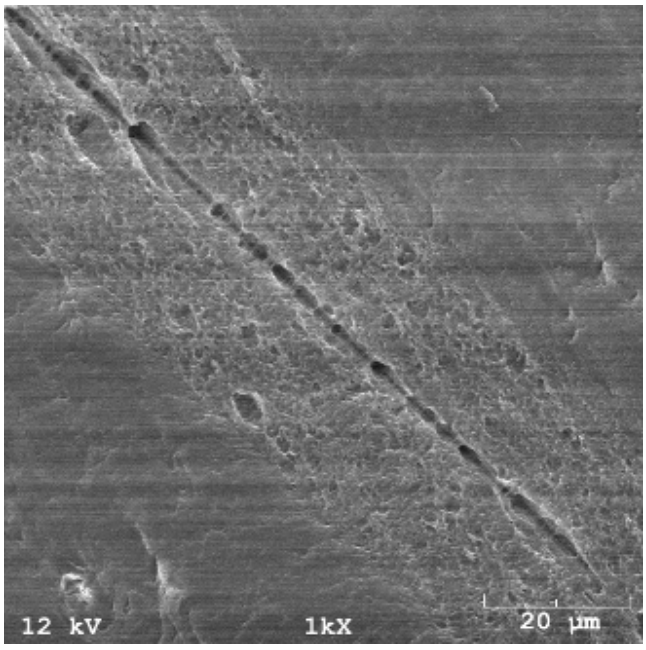

e) etching 4 h

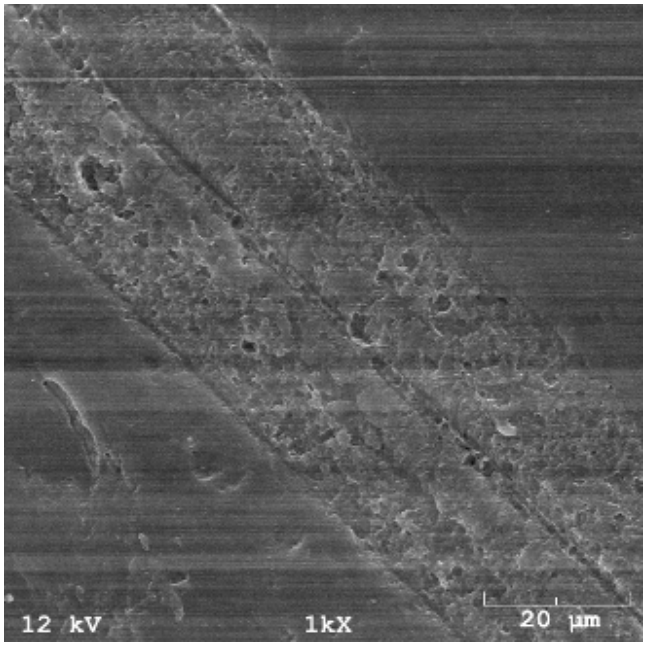

f) etching 5 h

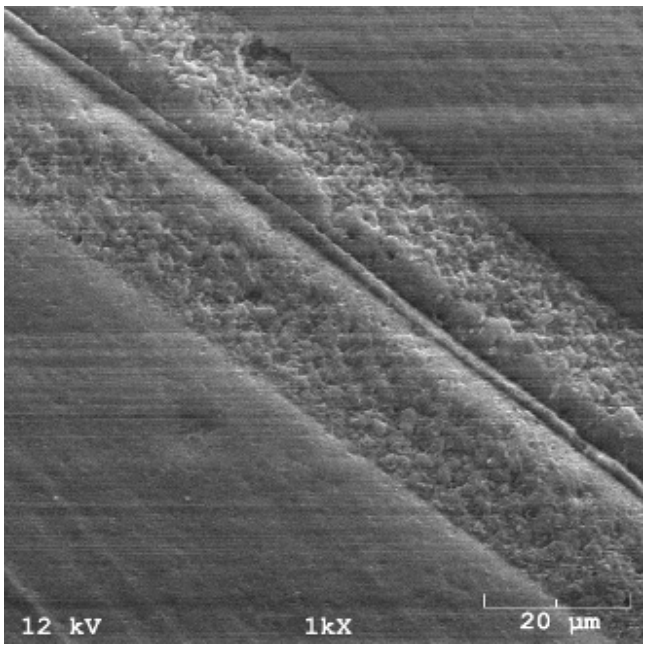

g) etching 6 h

Figure B.1 Interfacial bonding morphology of two crystallizable amorphous PET sheets etched by 2 wt% potassium hydroxide/isopropanol solution at heating temperature 160°C and heating time 10 s, a) etching time 30 min, b) etching time 1 h, c) etching time 2 h, d) etching time 3 h, e) etching time 4 h, f) etching time 5 h, g) etching time 6 h.

B.1.2 Interfacial bonding morphology of two crystallizable amorphous PET sheets at heating temperature 160°C and heating time 30 s

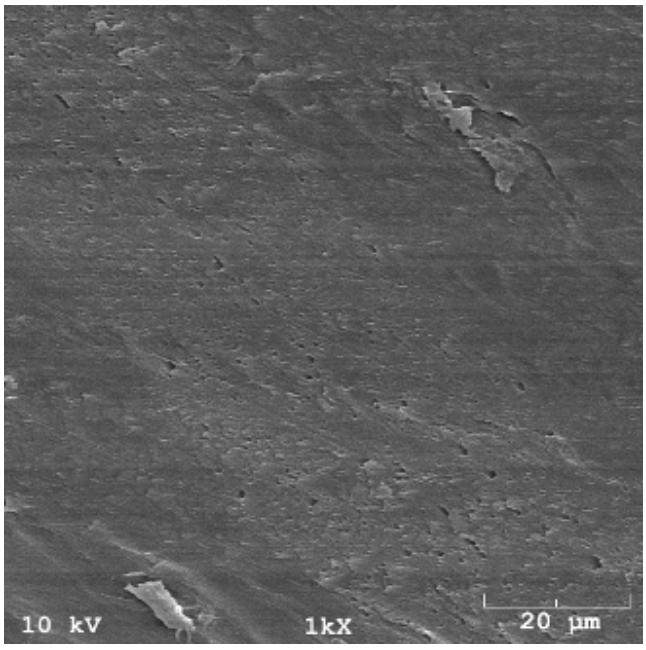

a) etching 30 min

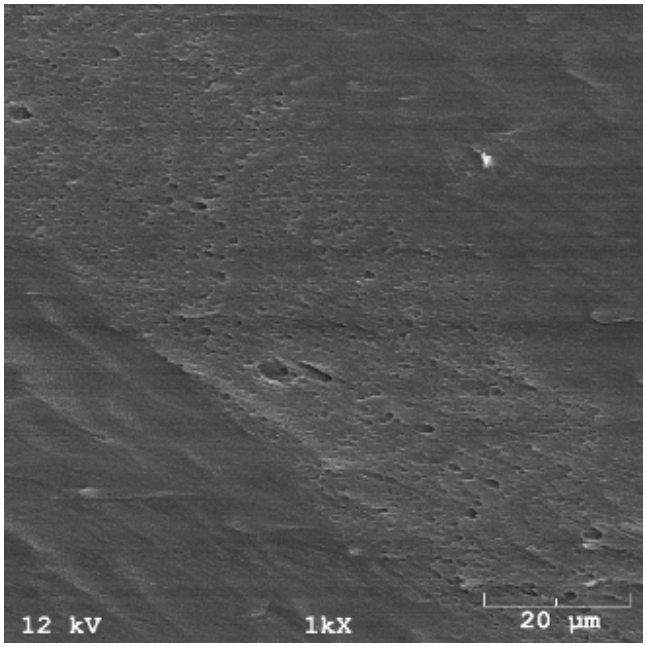

b) etching 1 h

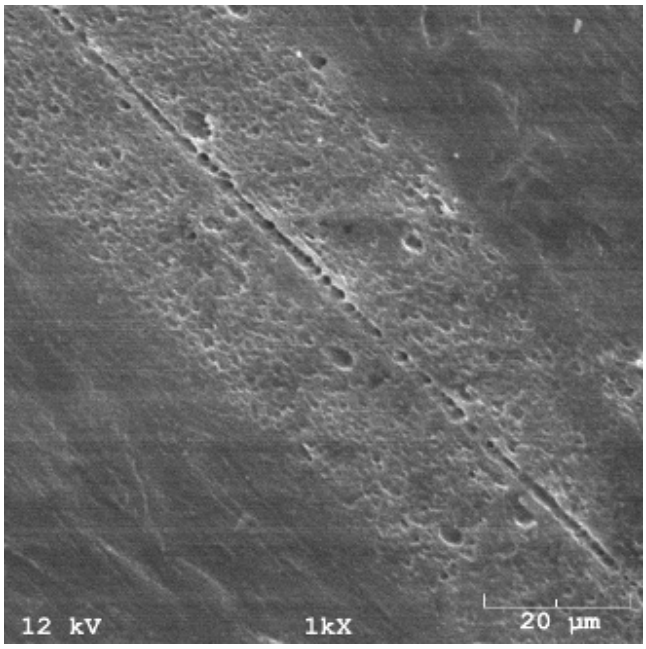

c) etching 2 h

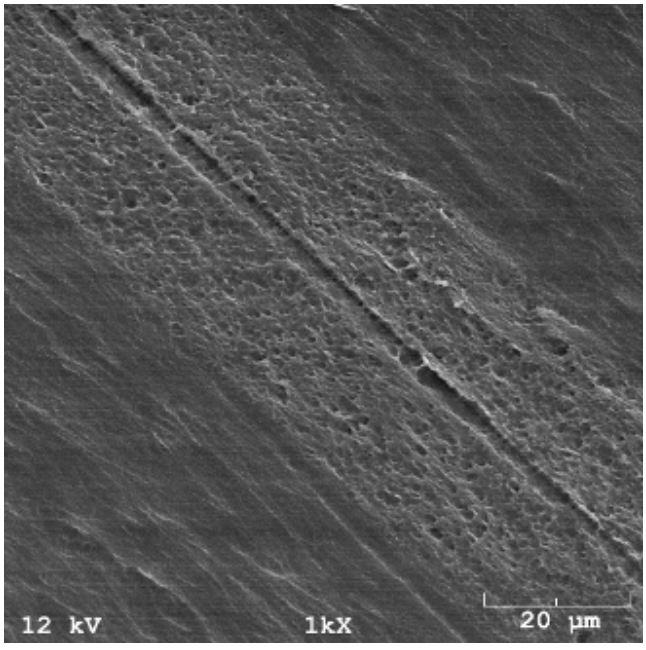

d) etching 3 h

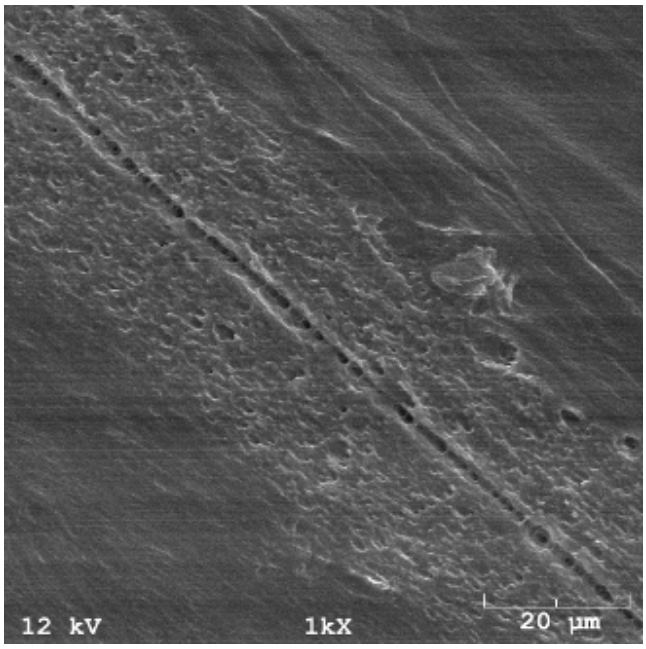

e) etching 4 h

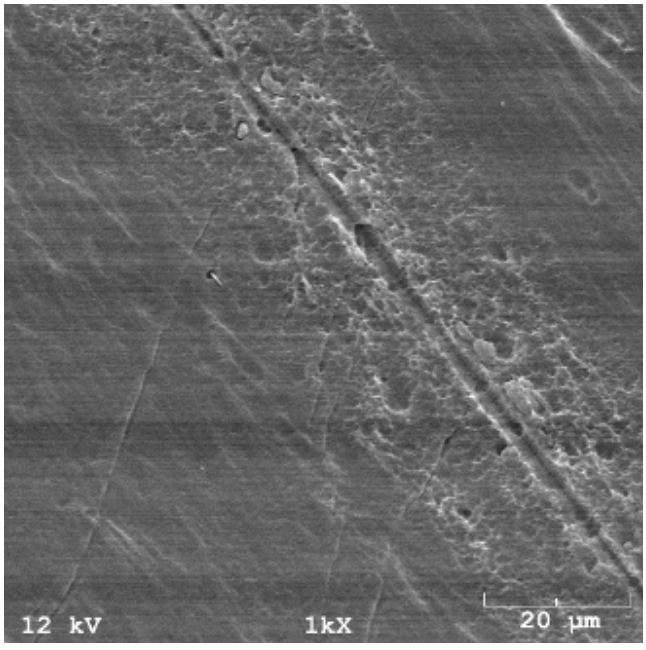

g) etching 5 h

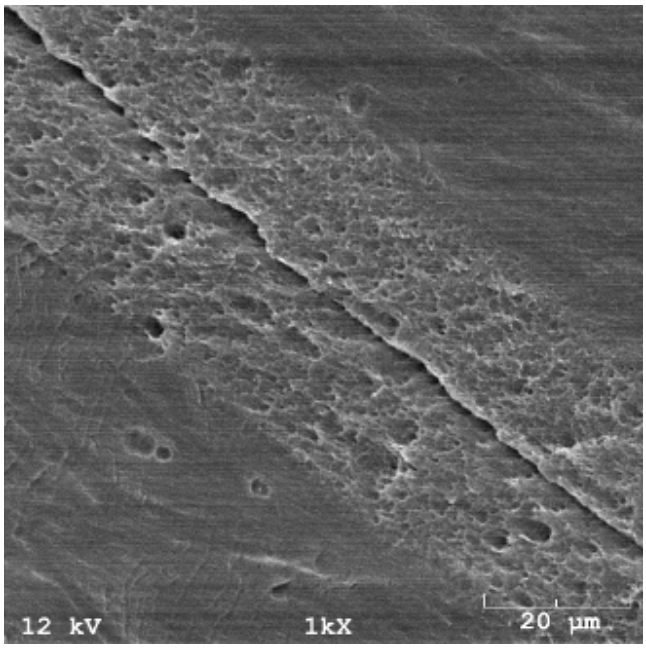

g) etching 6 h

Figure B.2 Interfacial bonding morphology of two crystallizable amorphous PET sheets etched by 2 wt% potassium hydroxide/isopropanol solution at heating temperature 160°C and heating time 30 s, a) etching time 30 min, b) etching time 1 h, c) etching time 2 h, d) etching time 3 h, e) etching time 4 h, f) etching time 5 h, g) etching time 6 h.

B.1.3 Interfacial bonding morphology of two crystallizable amorphous PET sheets at heating temperature 160°C and heating time 60 s

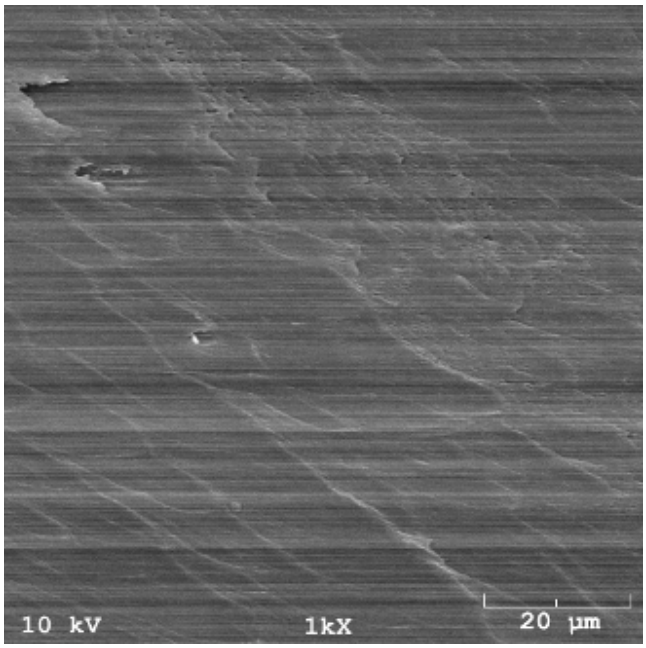

a) etching 30 min

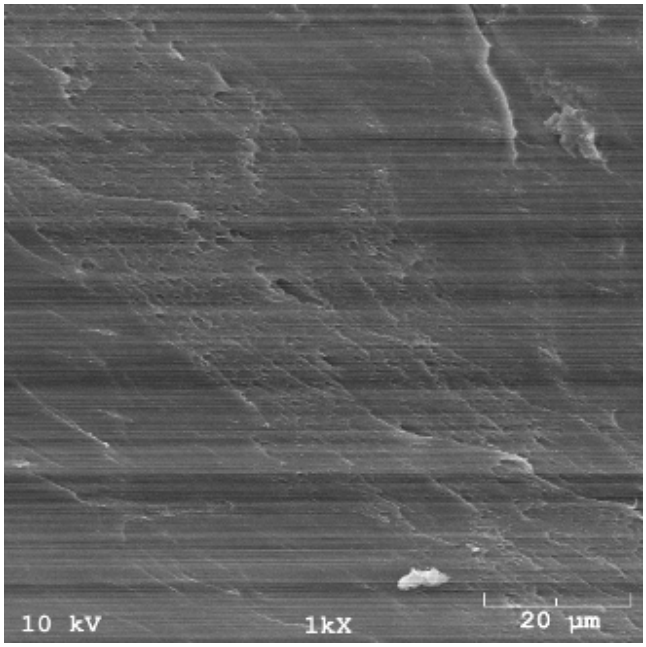

b) etching 1 h

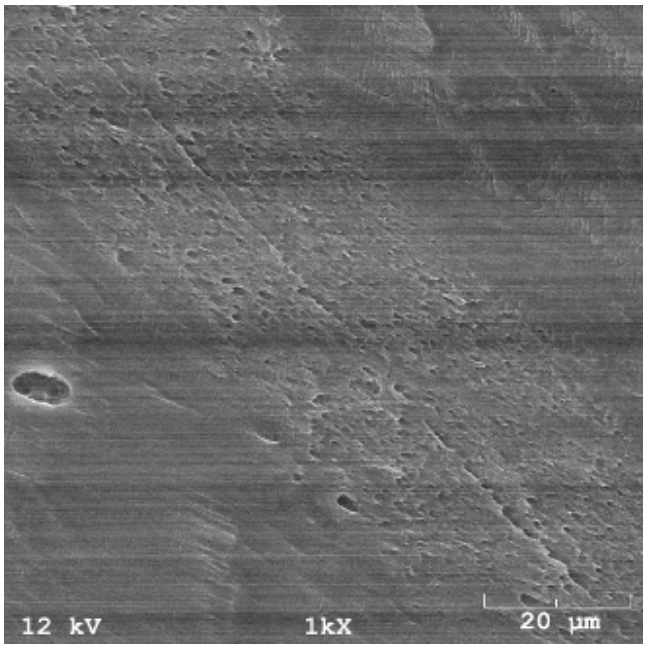

c) etching 2 h

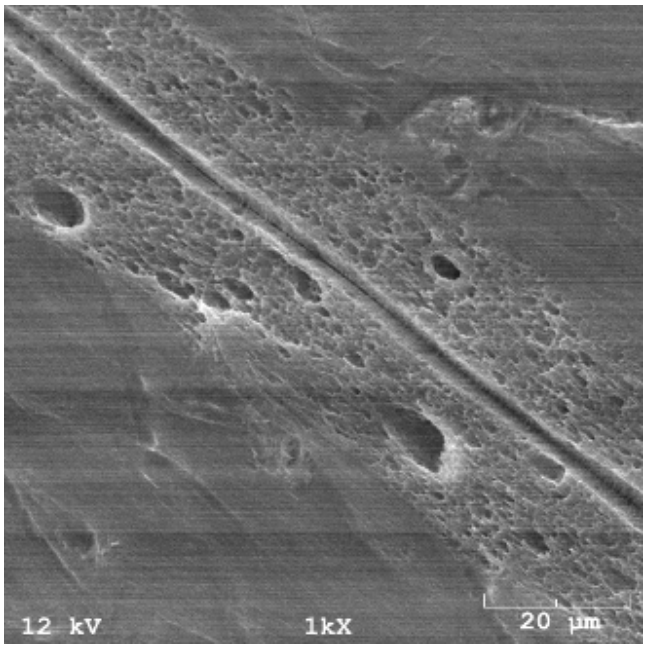

d) etching 3 h

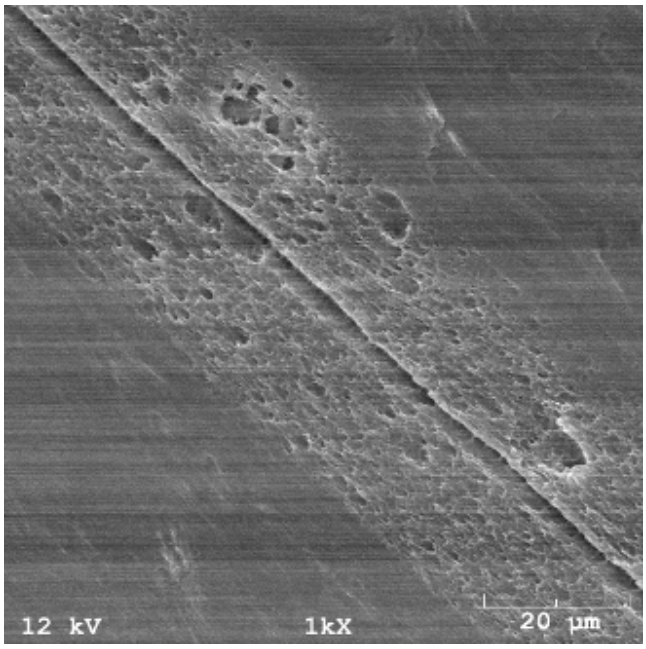

e) etching 4 h

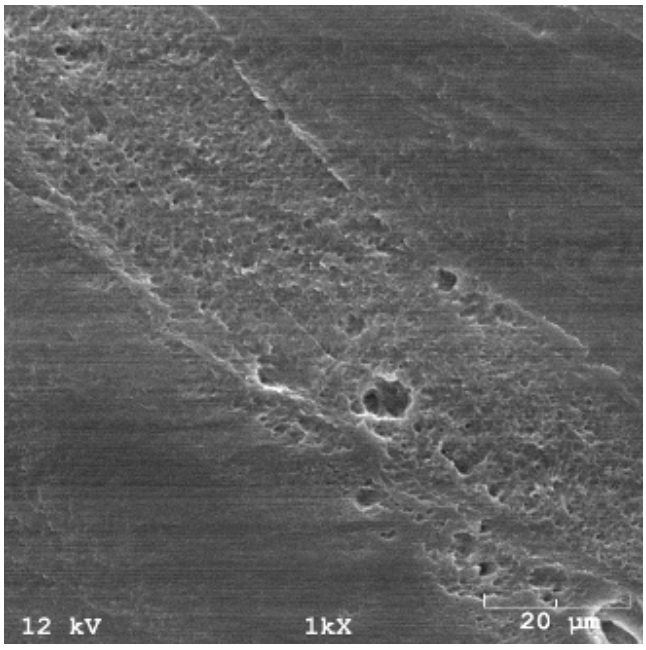

f) etching 5 h

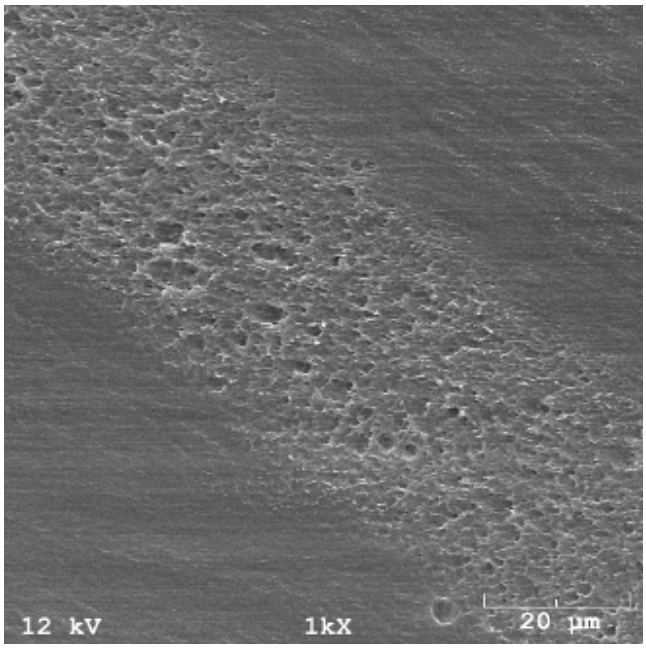

g) etching 6 h

Figure B.3 Interfacial bonding morphology of two crystallizable amorphous PET sheets etched by 2 wt% potassium hydroxide/isopropanol solution at heating temperature 160°C and heating time 60 s, a) etching time 30 min, b) etching time 1 h, c) etching time 2 h, d) etching time 3h, e) etching time 4 h, f) etching time 5 h, g) etching time 6 h.

B.2 Interfacial bonding morphology of two crystallizable amorphous PET sheets at heating temperature 180°C

B.2.1 Interfacial bonding morphology of two crystallizable amorphous PET sheets at heating temperature 180°C and heating time 10 s

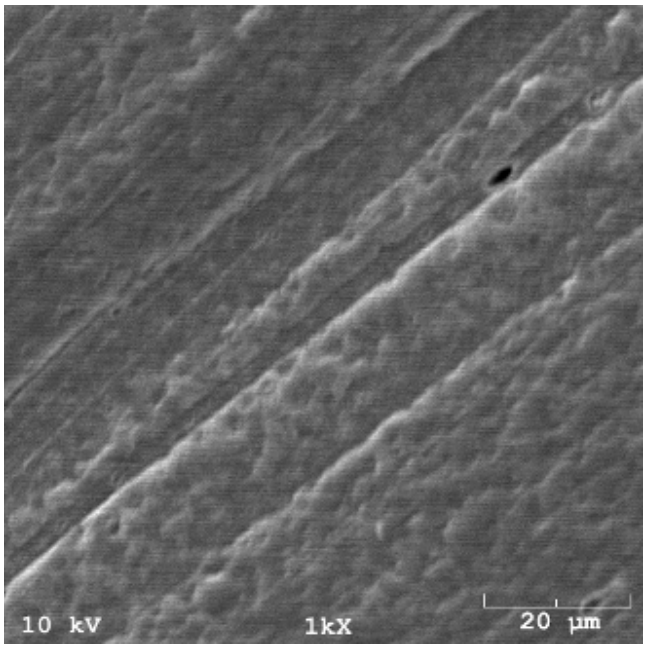

a) etching 30 min

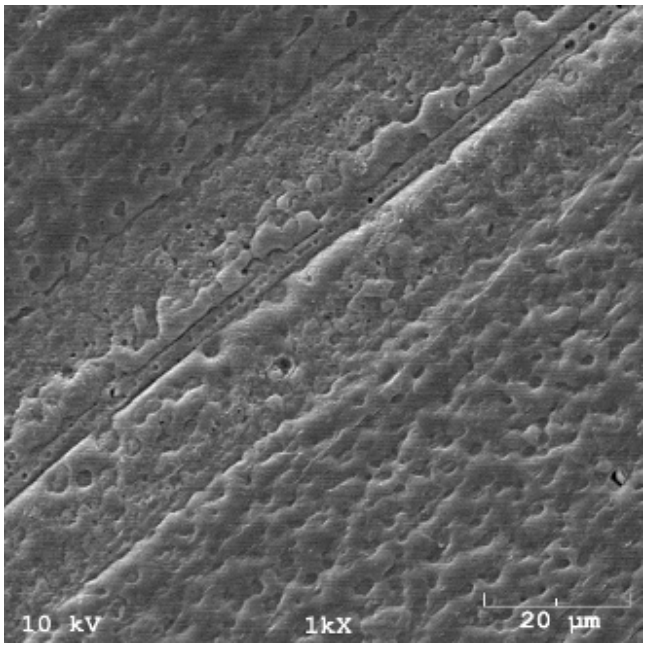

b) etching 1 h

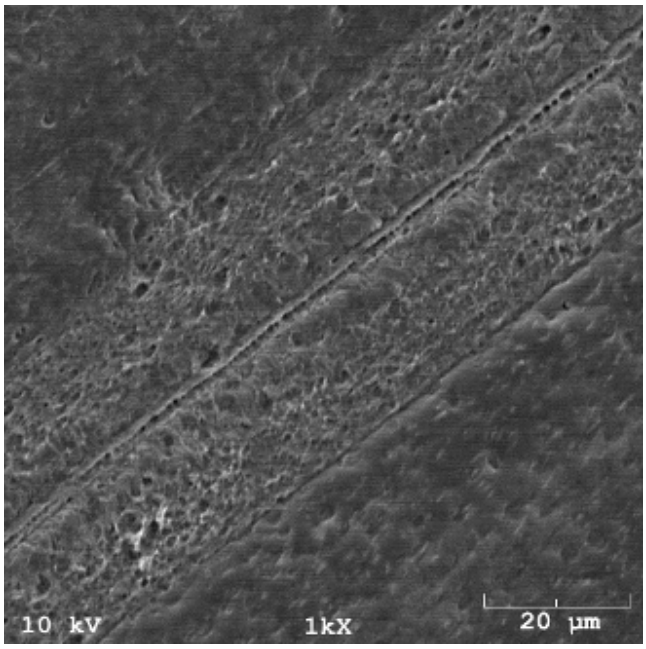

c) etching 2 h

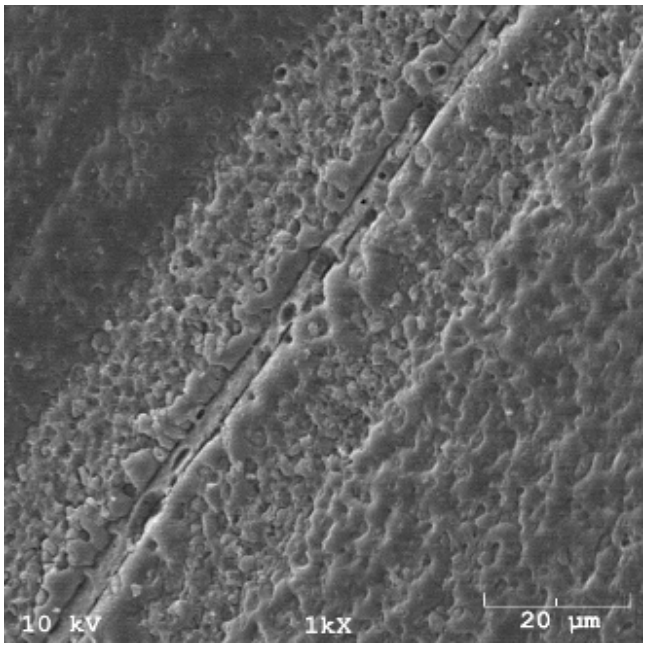

d) etching 3 h

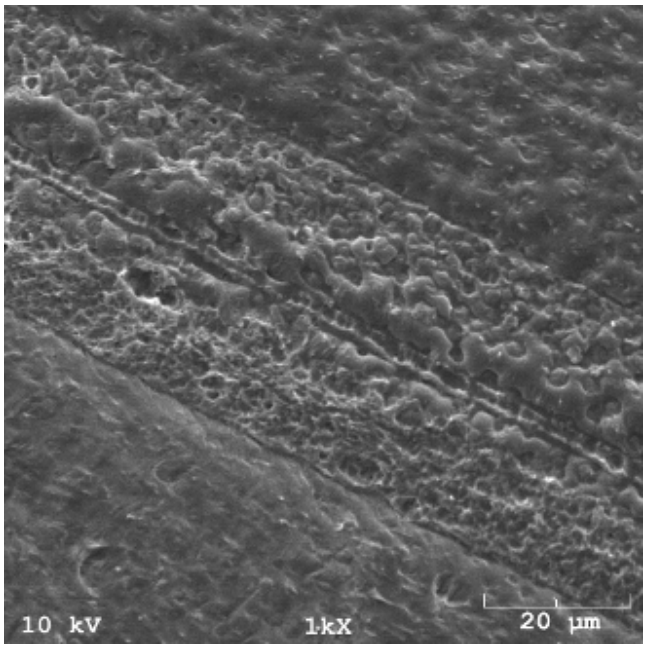

e) etching 4 h

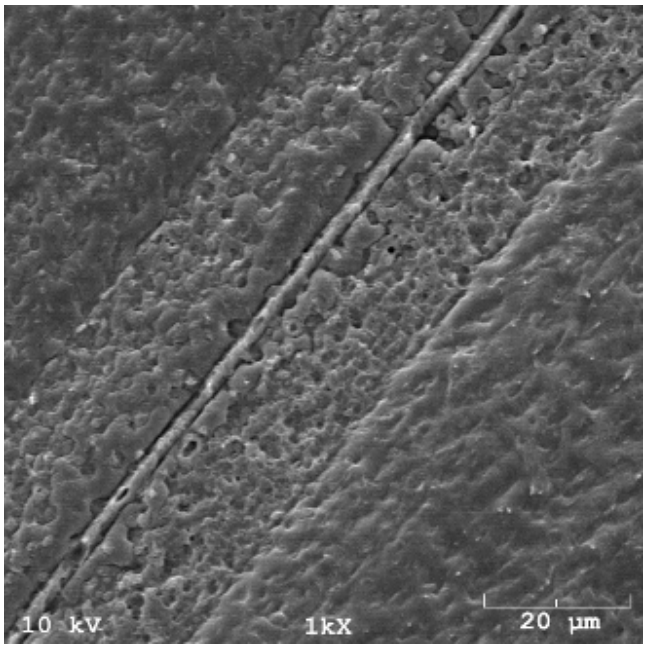

f) etching 5 h

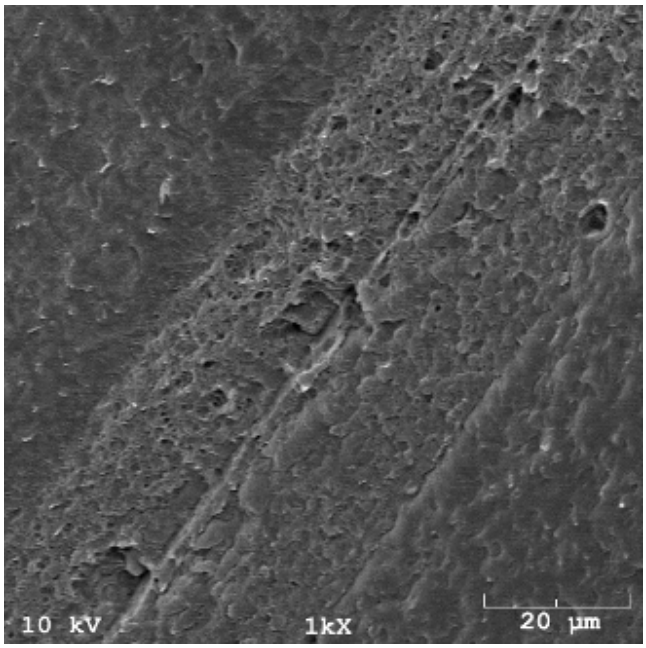

g) etching 6 h

Figure B.4 Interfacial bonding morphology of two crystallizable amorphous PET sheets etched by 2 wt% potassium hydroxide/isopropanol solution at heating temperature 180°C and heating time 10 s, a) etching time 30 min, b) etching time 1 h, c) etching time 2 h, d) etching time 3 h, e) etching time 4 h, f) etching time 5 h, g) etching time 6 h.

B.2.2 Interfacial bonding morphology of two crystallizable amorphous PET sheets at 180 °C and 30 s

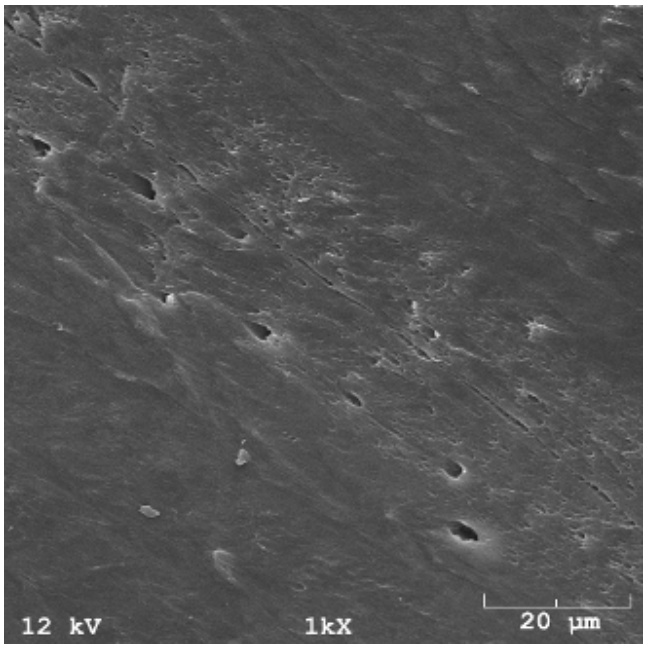

a) etching 30 min

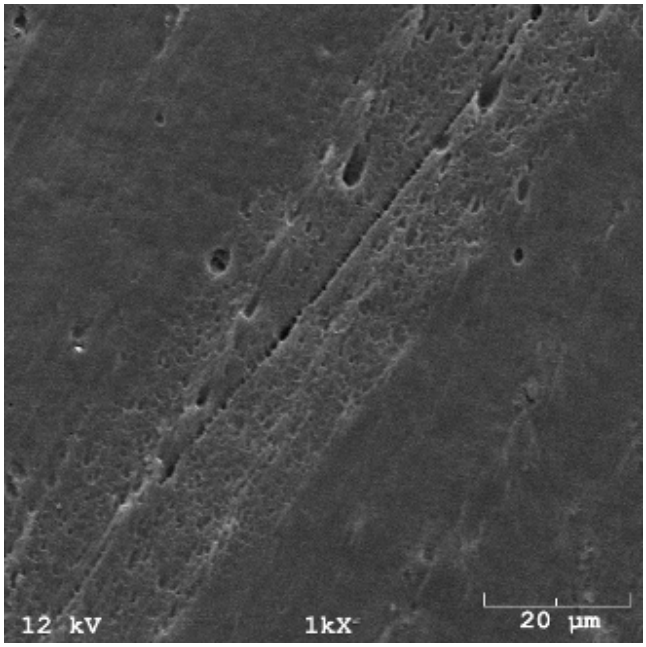

b) etching 1 h

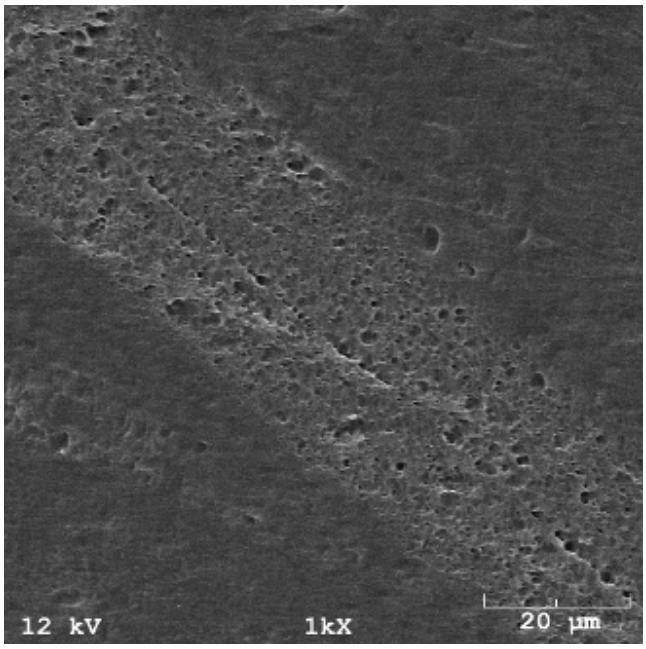

c) etching 2 h

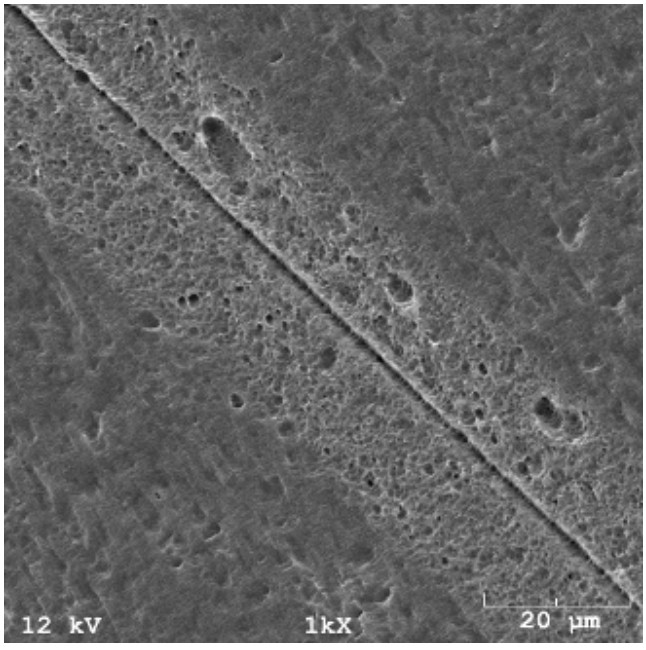

d) etching 3 h

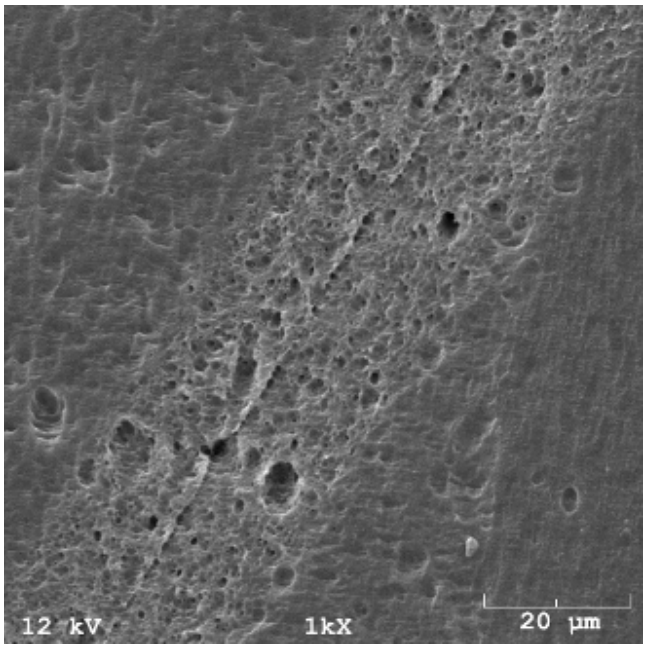

e) etching 4 h

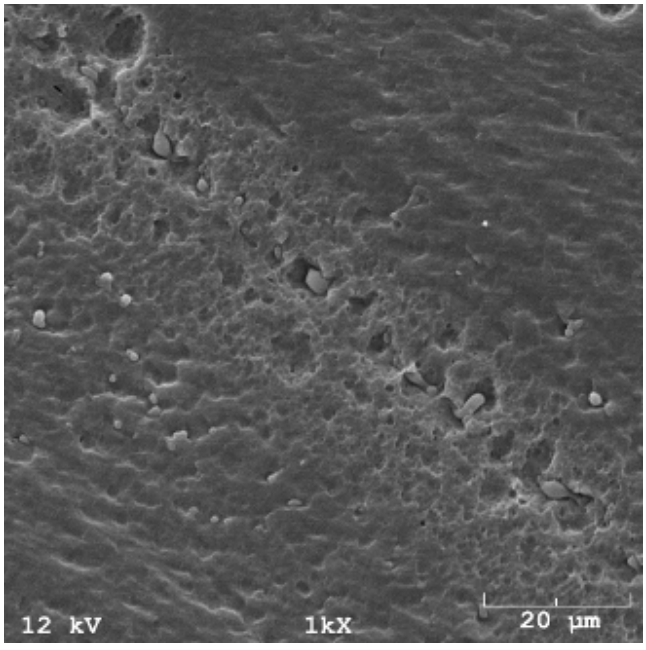

f) etching 5 h

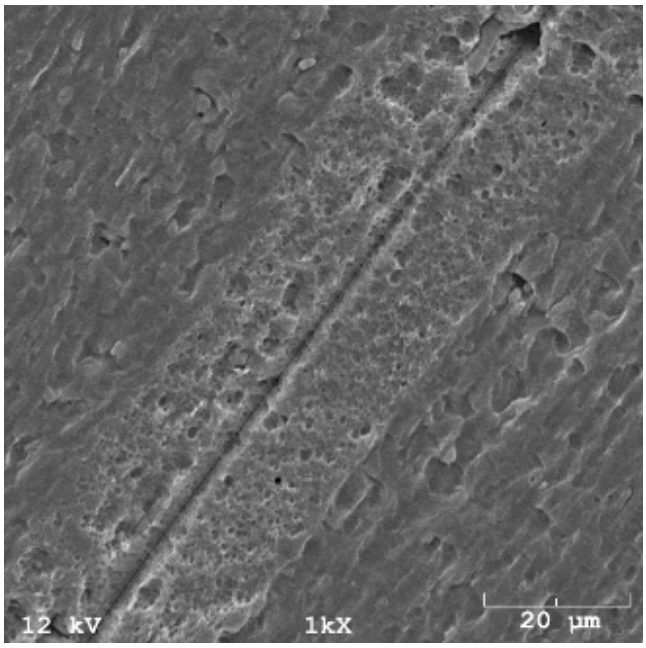

g) etching 6 h

Figure B.5 Interfacial bonding morphology of two crystallizable amorphous PET sheets etched by 2 wt% potassium hydroxide/isopropanol solution at heating temperature 180°C and heating time 30 s, a) etching time 30 min, b) etching time 1 h, c) etching time 2 h, d) etching time 3 h, e) etching time 4 h, f) etching time 5 h, g) etching time 6 h.

B.2.3 Interfacial bonding morphology of two crystallizable amorphous PET sheets at 180°C and 60 s

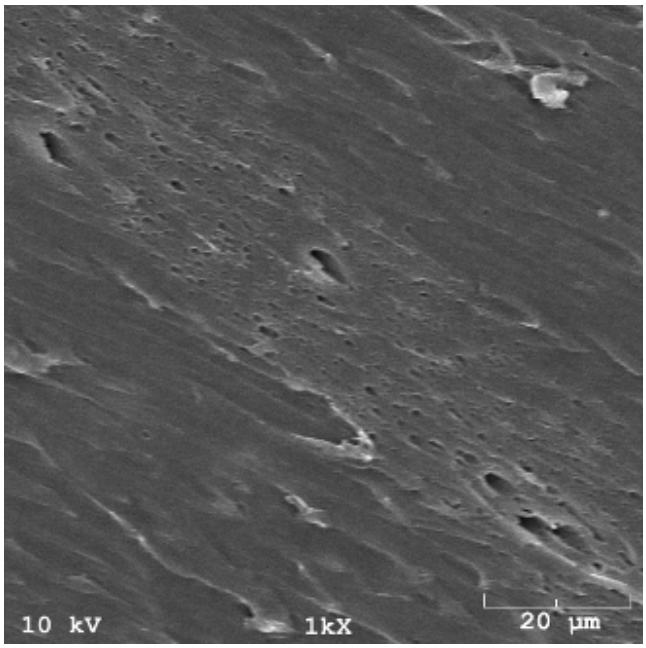

a) etching 30 min

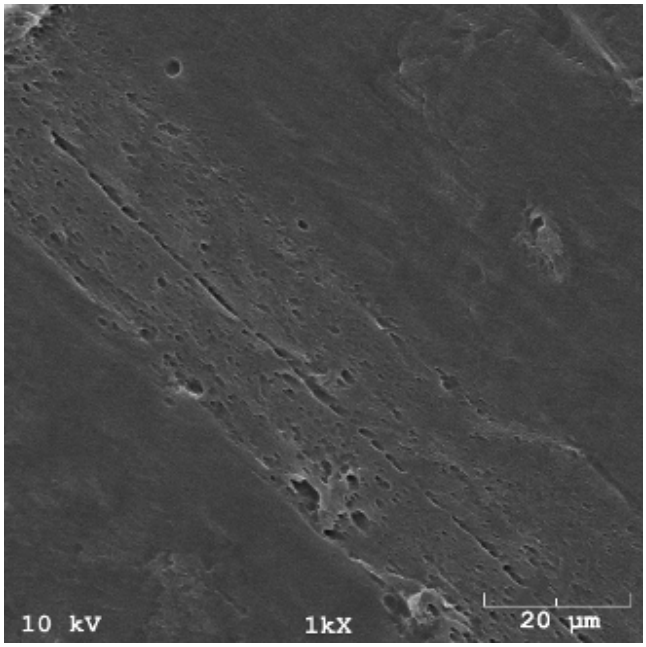

b) etching 1 h

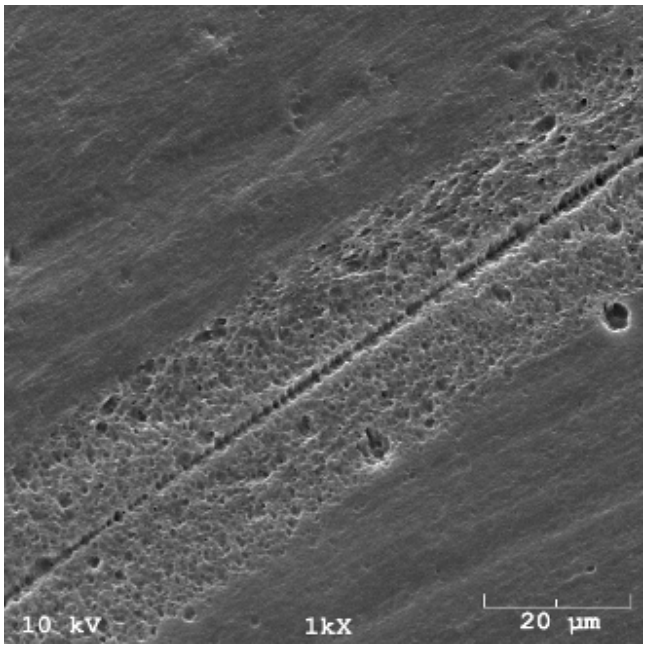

c) etching 2 h

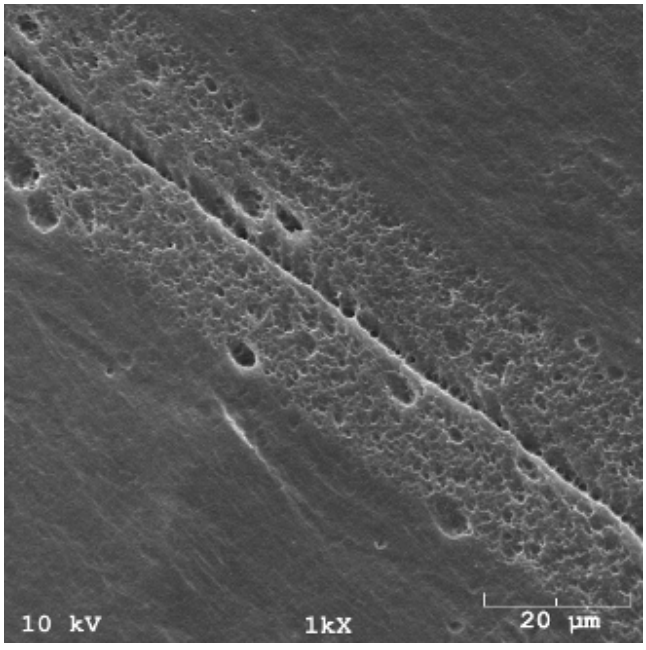

d) etching 3 h

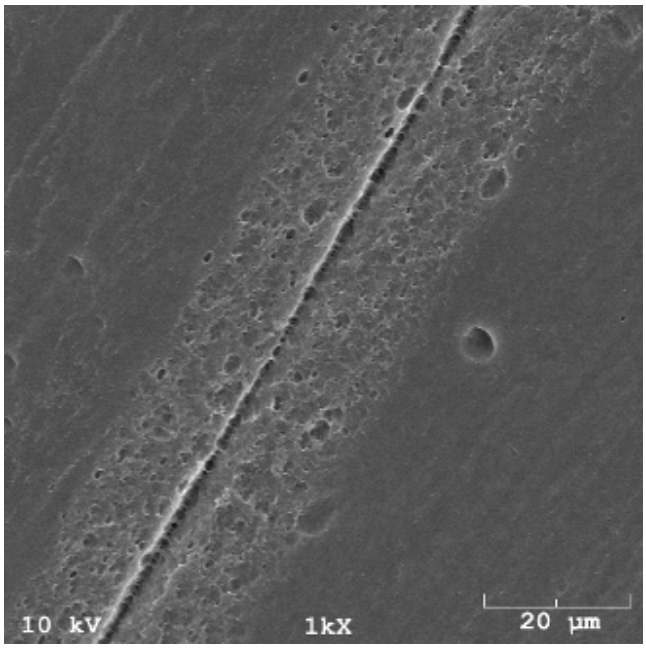

e) etching 4 h

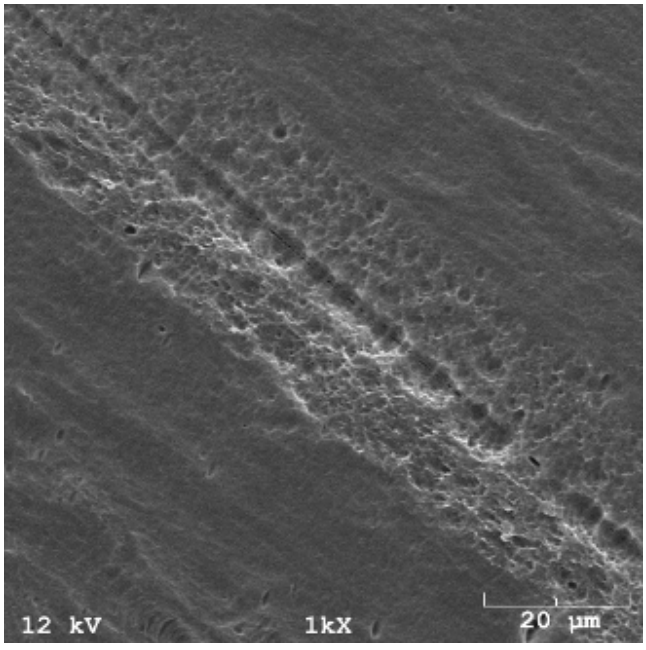

f) etching 5 h

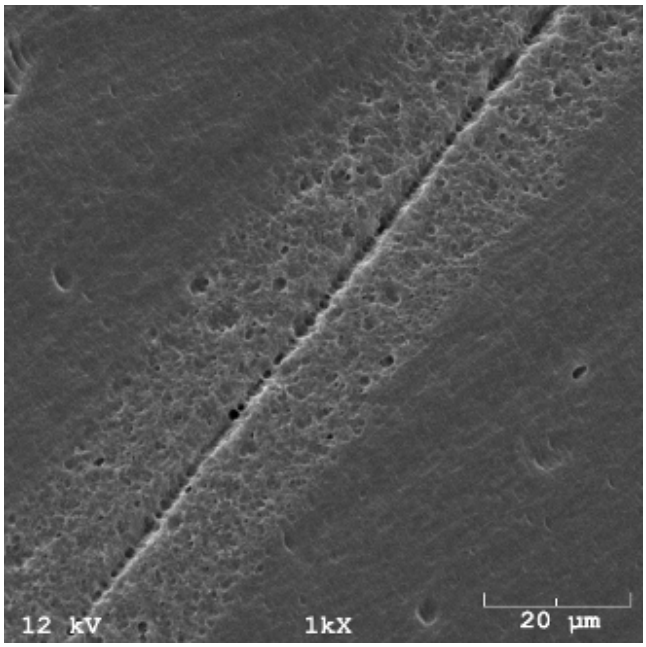

g) etching 6 h

Figure B.6 Interfacial bonding morphology of two crystallizable amorphous PET sheets etched by 2 wt% potassium hydroxide/isopropanol solution at heating temperature 180°C and heating time 60 s, a) etching time 30 min, b) etching time 1 h, c) etching time 2 h, d) etching time 3 h, e) etching time 4 h, f) etching time 5 h, g) etching time 6 h.

B.3 Interfacial bonding morphology of two crystallizable amorphous PET sheets at heating temperature 210°C

B.3.1 Interfacial bonding morphology of two crystallizable amorphous PET sheets at heating temperature 210°C and heating time 10 s

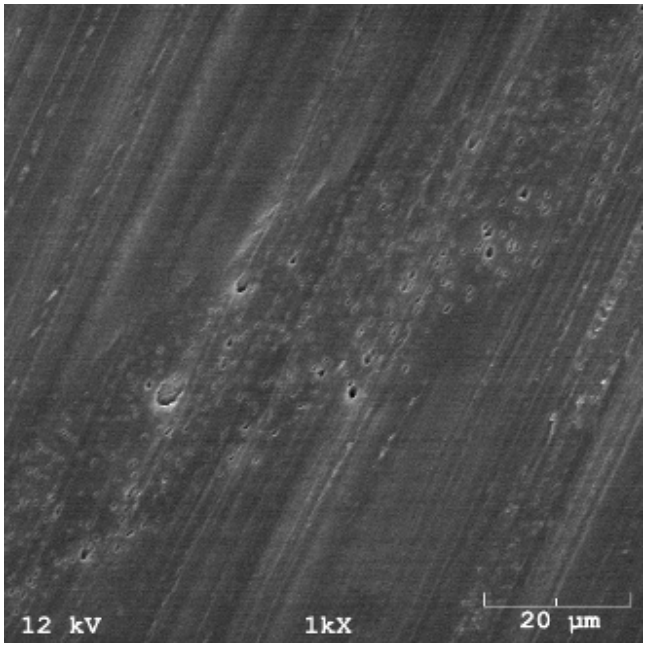

a) etching 30 min

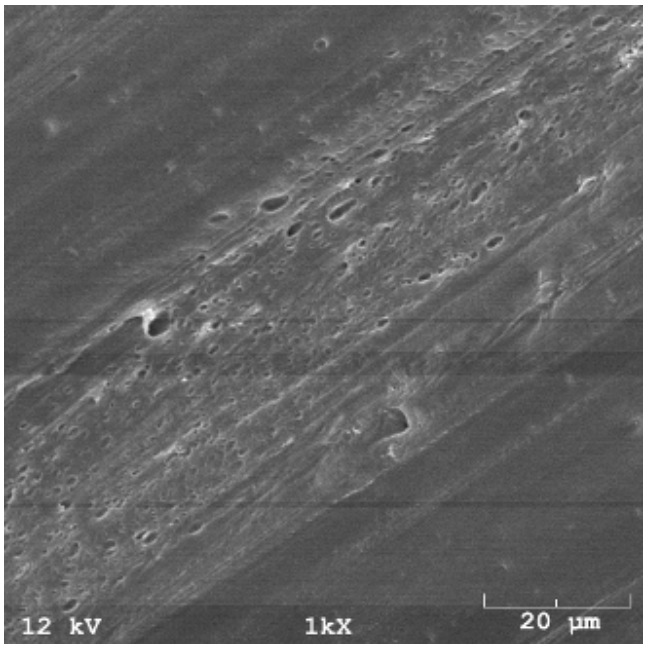

b) etching 1 h

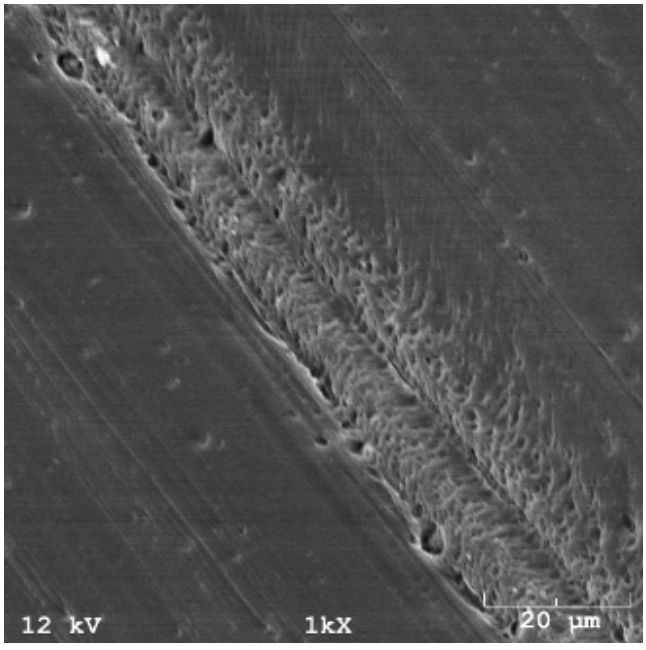

c) etching 2 h

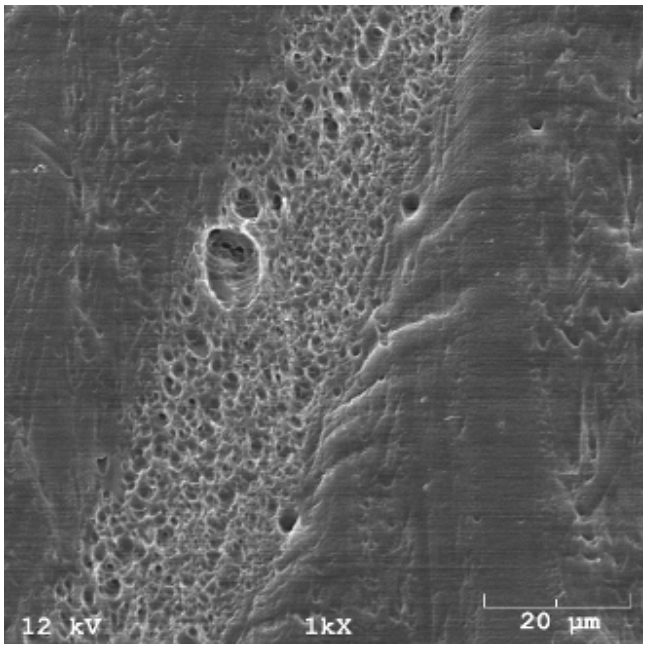

d) etching 3 h

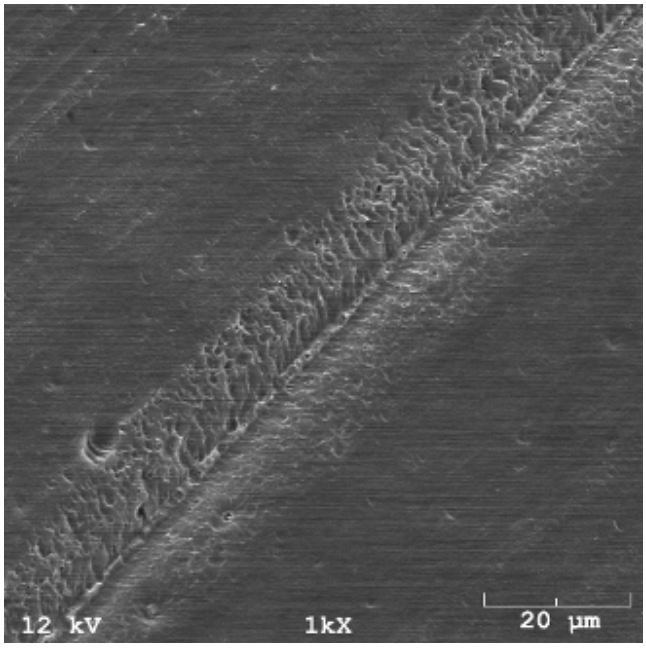

e) etching 4 h

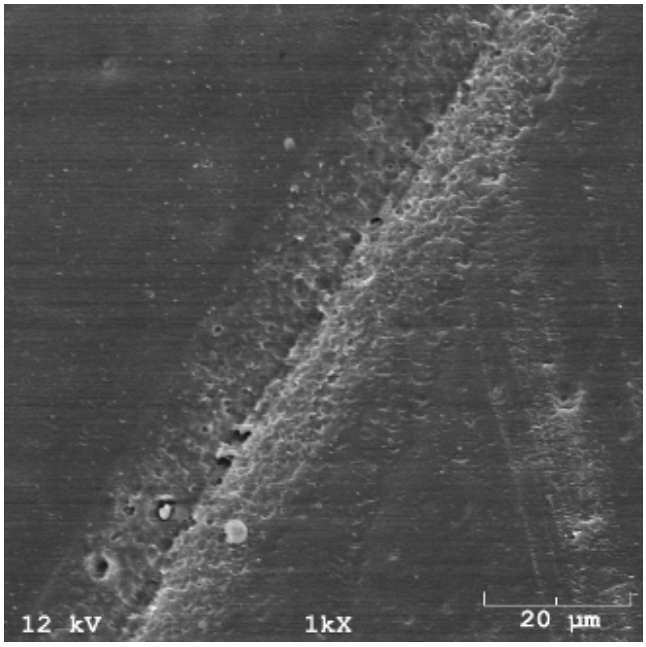

f) etching 5 h

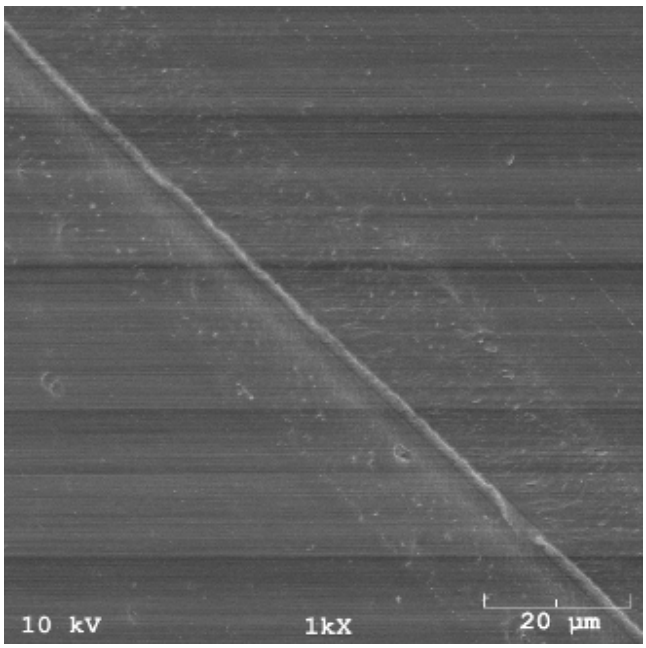

g) etching 6 h

Figure B.7 Interfacial bonding morphology of two crystallizable amorphous PET sheets etched by 2 wt% potassium hydroxide/isopropanol solution at heating temperature 210°C and heating time 10 s, a) etching time 30 min, b) etching time 1 h, c) etching time 2 h, d) etching time 3 h, e) etching time 4 h, f) etching time 5 h, g) etching time 6 h.

B.3.2 Interfacial bonding morphology of two crystallizable amorphous PET sheets at heating temperature 210°C and heating time 30 s

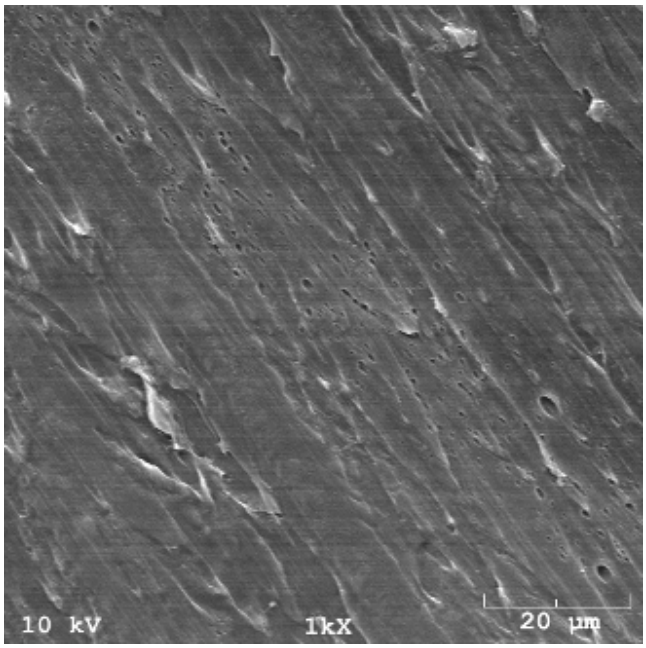

a) etching 30 min

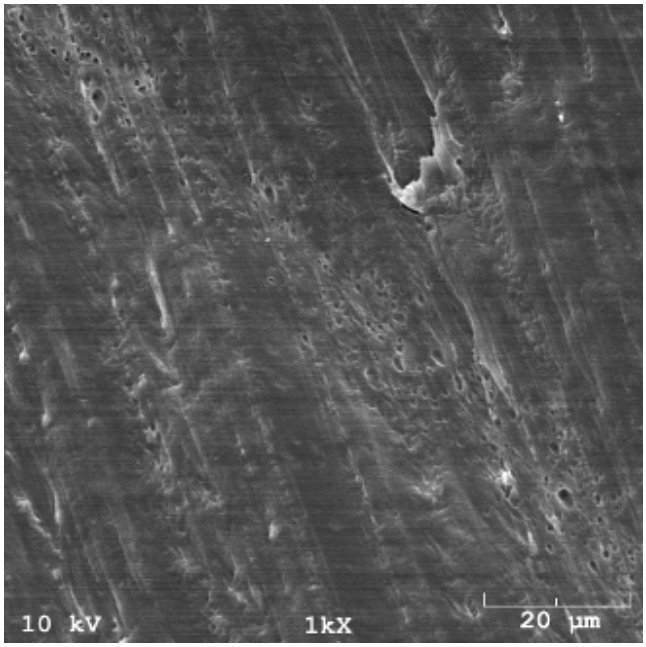

b) etching 1 h

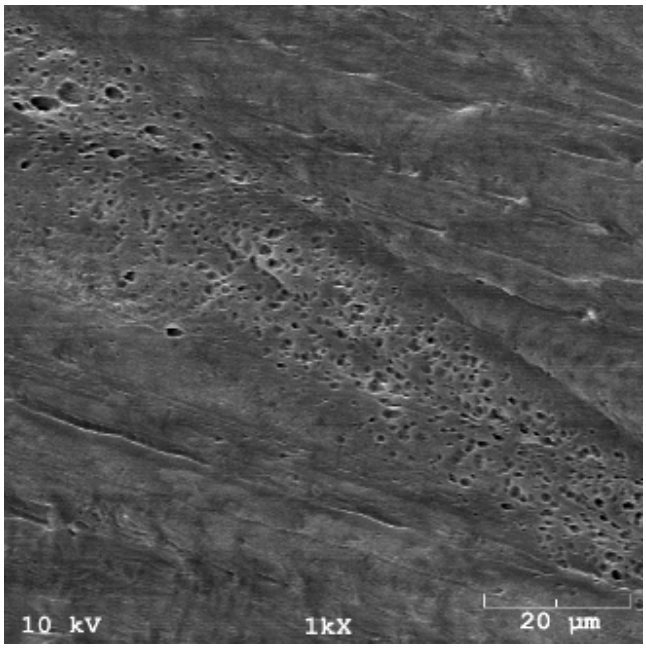

c) etching 2 h

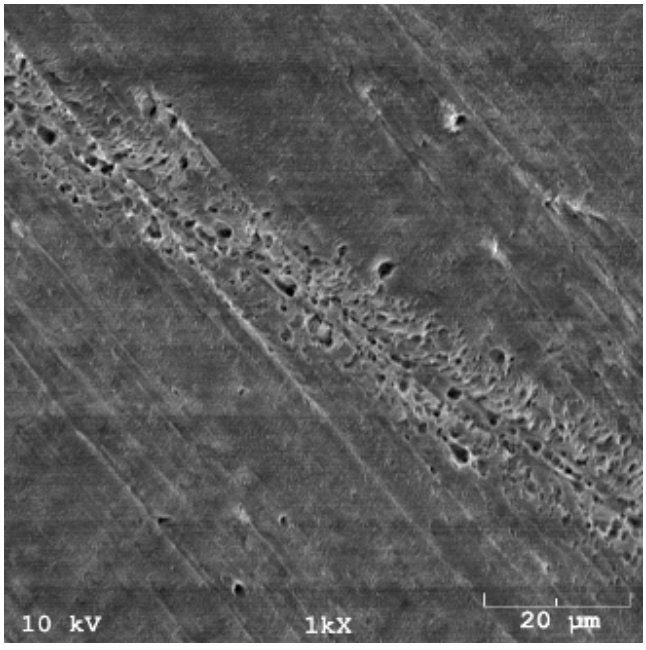

d) etching 3 h

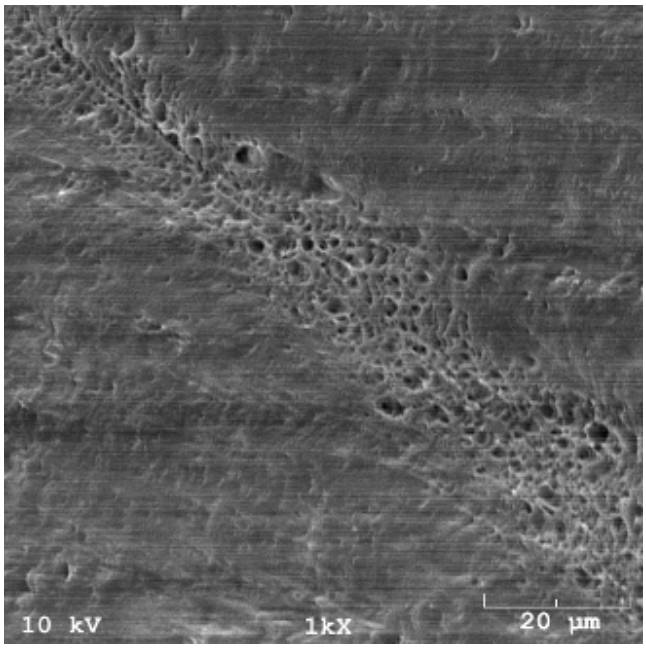

e) etching 4 h

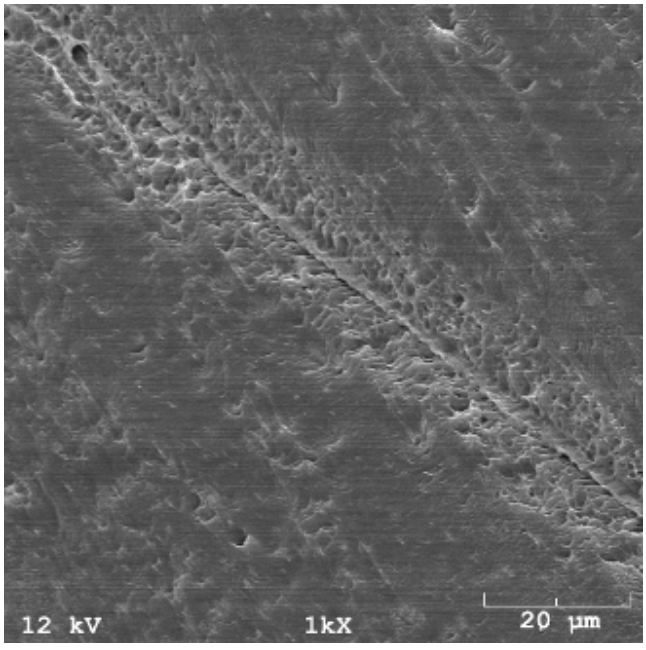

f) etching 5 h

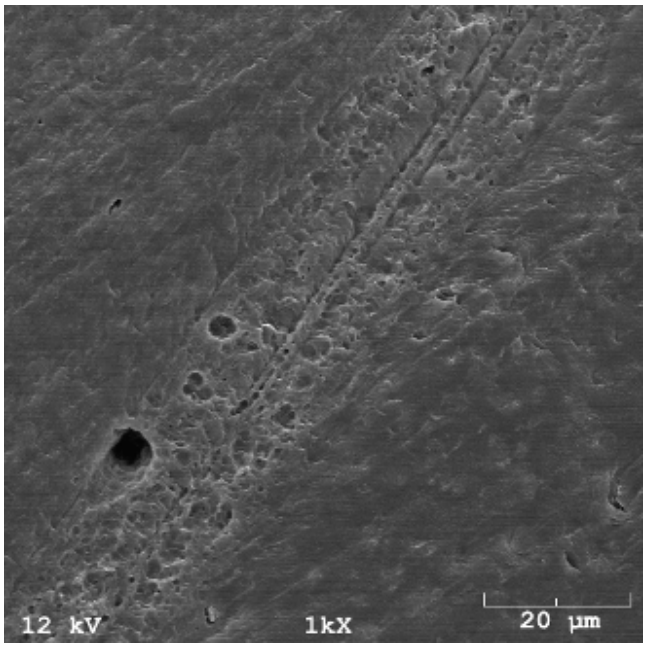

g) etching 6 h

Figure B.8 Interfacial bonding morphology of two crystallizable amorphous PET sheets etched by 2 wt% potassium hydroxide/isopropanol solution at heating temperature 210°C and heating time 30 s, a) etching time 30 min, b) etching time 1 h, c) etching time 2 h, d) etching time 3 h, e) etching time 4 h, f) etching time 5 h, g) etching time 6 h.

B.3.3 Interfacial bonding morphology of two crystallizable amorphous PET sheets at heating temperature 210°C and heating time 60 s

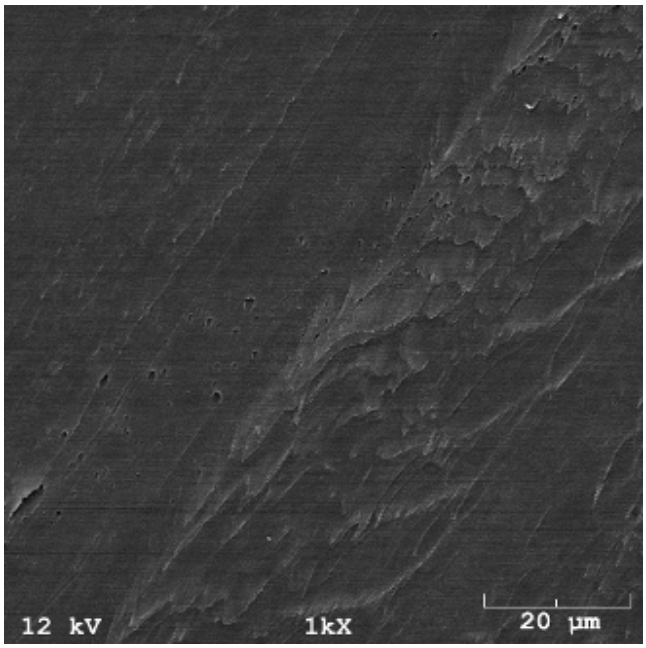

a) etching 30 min

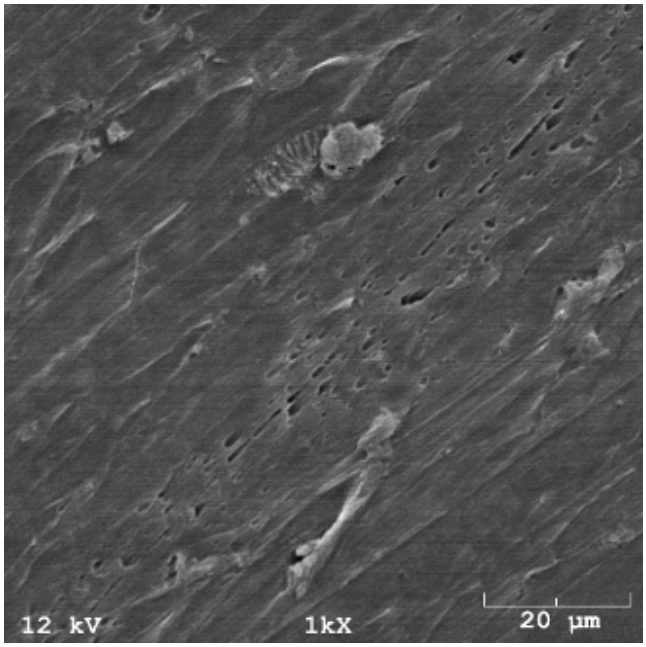

b) etching 1 h

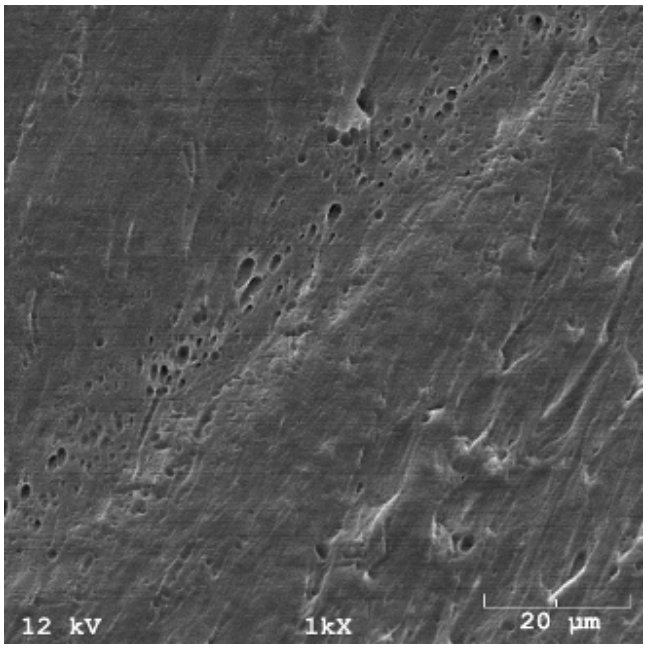

c) etching 2 h

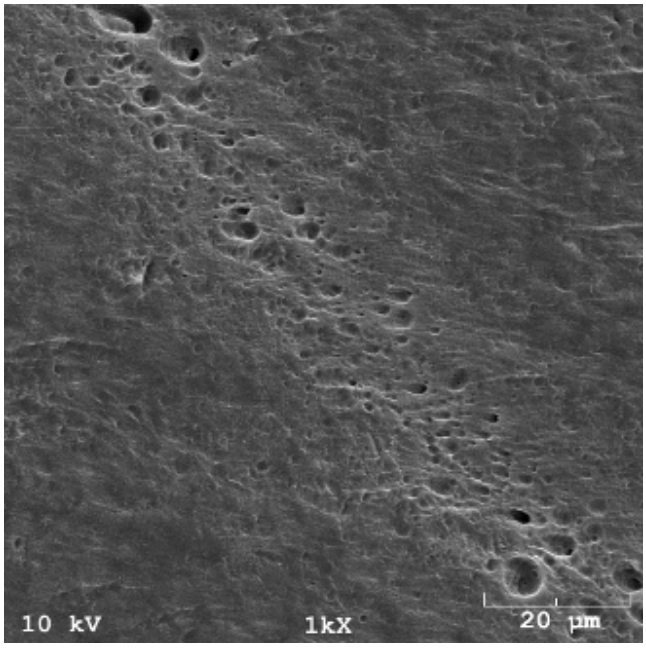

d) etching 4 h

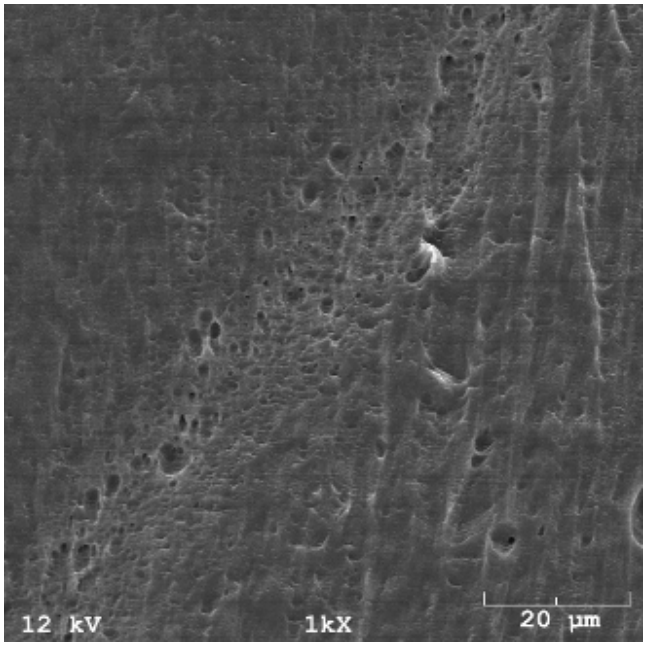

e) etching 5 h

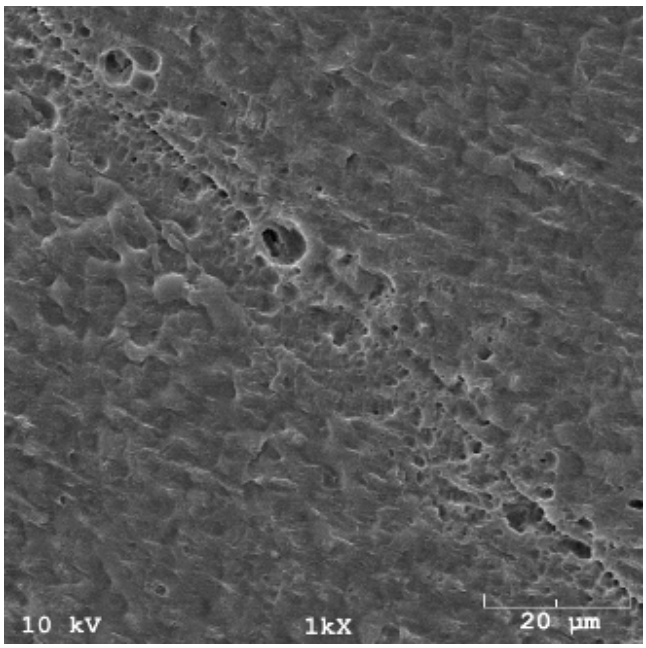

f) etching 6 h

Figure B.9 Interfacial bonding morphology of two crystallizable amorphous PET sheets etched by 2 wt% potassium hydroxide/isopropanol solution at heating temperature 210°C and heating time 60 s, a) etching time 30 min, b) etching time 1 h, c) etching time 2 h, d) etching time 4 h, e) etching time 5 h, f) etching time 6 h.

B.3.4 Interfacial bonding morphology of two crystallizable amorphous PET sheets at heating temperature 210 °C and heating time 90 s

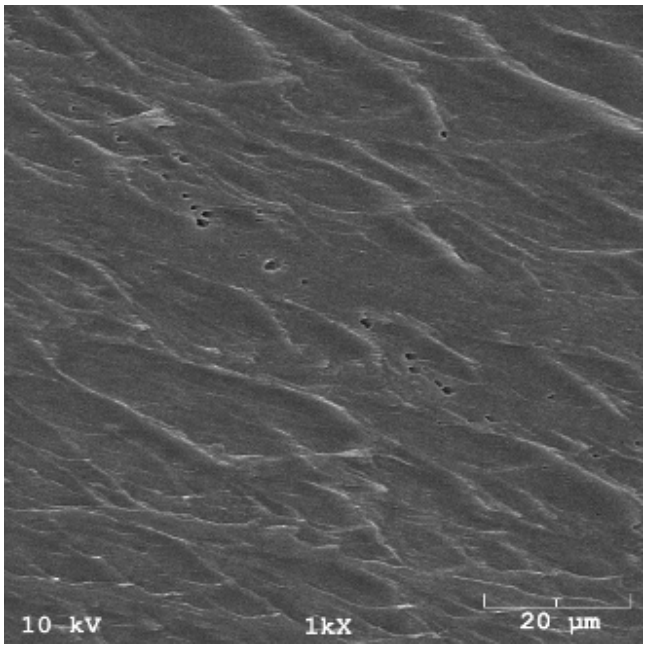

a) etching 30 min

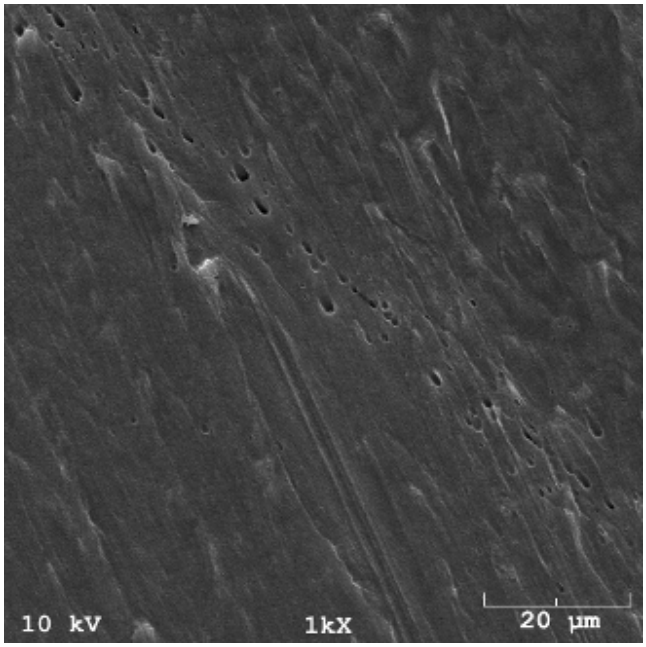

b) etching 1 h

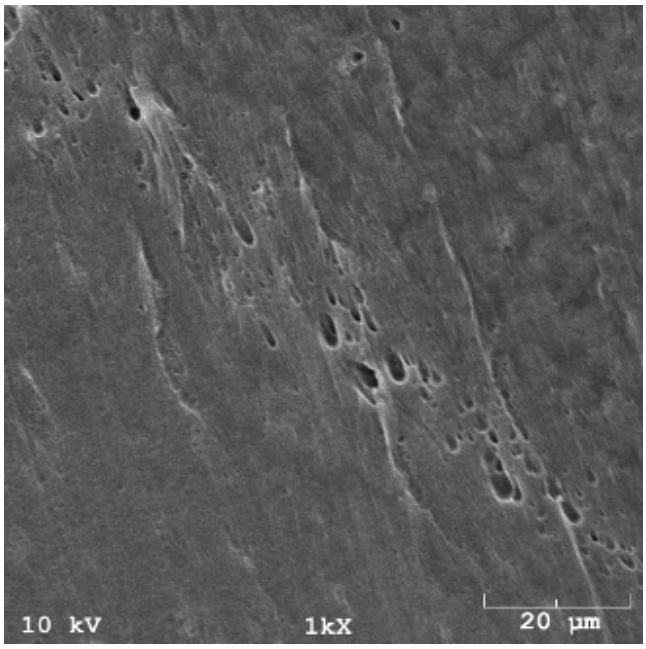

c) etching 2 h

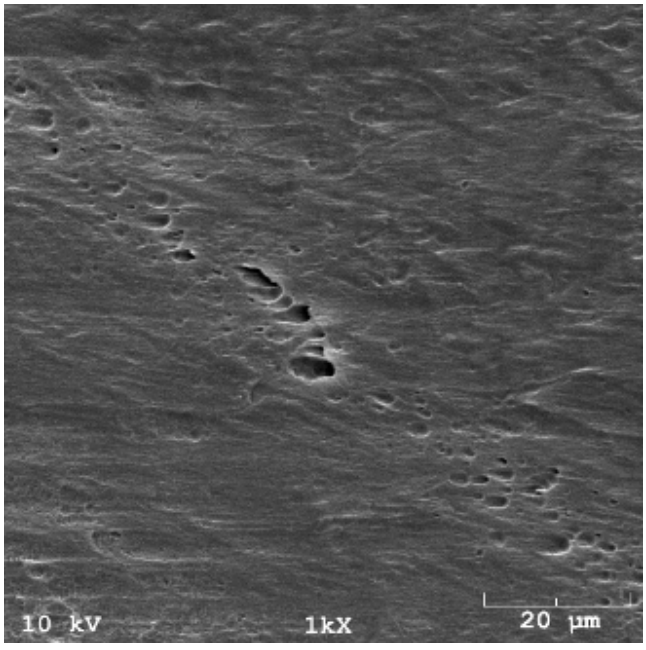

d) etching 3 h

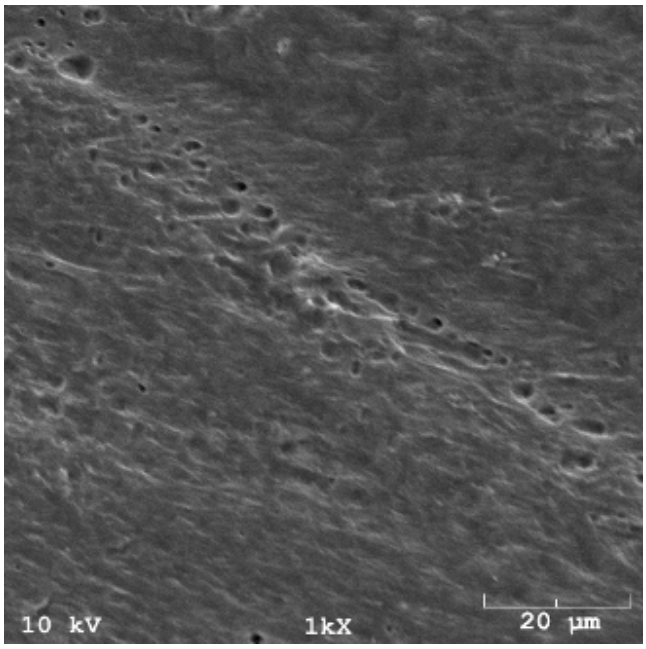

e) etching 4 h

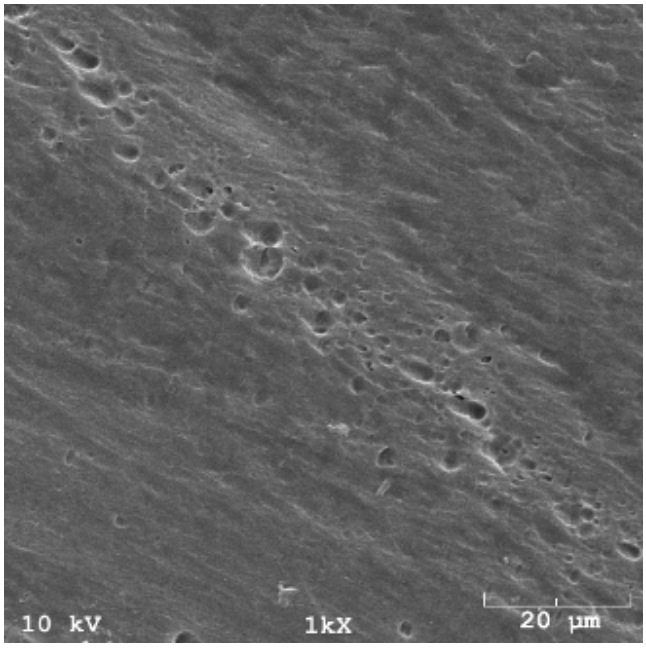

f) etching 5 h

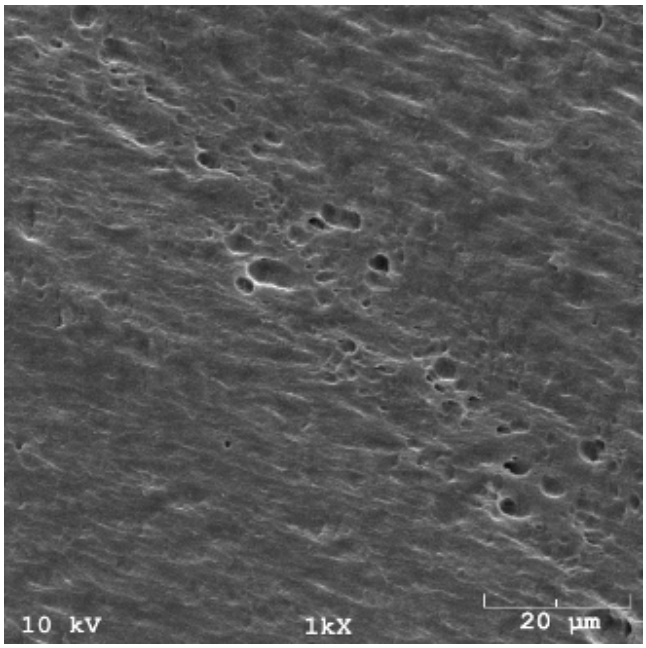

g) etching 6 h

Figure B.10 Interfacial bonding morphology of two crystallizable amorphous PET sheets etched by 2 wt% potassium hydroxide/isopropanol solution at heating temperature 210°C and heating time 90 s, a) etching time 30 min, b) etching time 1 h, c) etching time 2 h, d) etching time 4 h, e) etching time 5 h, f) etching time 6 h.

REFERENCES

1. W.T. Mead and R.S. Porter, J. Applied Polym. Sci., 22(11), 3249 (1978).
2. D.R. Salem, Structure Formation in Polymeric Fibers, Chapter 4, D.R. Salem, editor, Hanser Publishers, Munich (2001).
3. Mallick, P. K., Fiber-reinforced Composites: Materials, Manufacturing, and Design, Mechanical Engineering (Marcel Dekker, Inc.) ; 83, 74-81
4. J.D.Muzzy, Processing of advanced thermoplastic composites, The Manufacturing Science of Composites (T. G. Gutowski, ed.), ASME, New York (1988).
5. P.J. Hine, I.M. Ward, R.H. Olley and D.C. Bassett, J. Mater. Sci., 1993, 28, 316
6. Hine, P.J., Ward, I.M., J. Applied Polymer Science, Vol. 101, No. 2, July 2006, pp991-997.
7. Teishev, A., Incardona, S., Migliaresi, C., Marom, G., J. Applied Polym. Sci., Vol. 50, No. 3, October 1991, pp503-512.
8. Mosleh, M., Suh, N. P., Arinez, J., Composites Part A, Vol. 29, 1998, pp611-617.
9. Lacroix, F. V., Werwer, M., Schulte, K., Composites Part A, Vol. 29, 1998, pp371-376.
10. Barkoula, N.-M., Peijs, T., Schimanski, T., Loos, J., Polymer Composites, Vol. 26, 2005, pp114-120.
11. N Cabrera, B Alcock, J Loos and T Peijs, Processing of all-polypropylene composites for ultimate recyclability, Proc. Instn Mech. Engrs Vol. 218 Part: J. Material: Design and Applications

12. Devaux, E., Caze, C., Composites Sci. Techno., Vol. 59, No. 6, 1999, pp879-882.
13. www.lankhorst-indutech.nl
14. Peijs, T., et al., Comp. Sci. & Tech. (2003), to appear
15. Naitove, M. Hl, Schut, J. H., Plastics Technology, Vol. 51, No. 1, January 2005, pp31-32.
16. F.v. Lacroix, J.Loos, K. Schulte, Morphological investigations of polyethylene fiber reinforced polyethylene, Polymer 40 (1999) 843-847
17. T. Stern and G. Marom, Origin, morphology and crystallography of transcrystallinity in polyethylene-based single-polymer composites, Composites Part A 28A (1997) 437-444
18. S.Ratner, A.Weinberg, and G.Marom, Morphology and mechanical properties of crosslinked PE/PE composite materials, Polymer composites, June 2003, Vol.24, No.3, 422-427
19. Houshyar S., Shanks, R. A., Macromol. Mater. Eng., Vol. 288, No. 8, August 2003, pp599-606.
20. Hine, P. J., Ward, I. M., J. Appl. Polym. Sci., Vol. 91, No. 4, February 2004, pp2223-2233.
21. Ward, I. M., Hine, P. J., Polymer, Vol. 45, No. 5, March 2004, pp1413-1427.
22. X.Sun, H.Li, X. Zhang, J.Wang, D.Wang, and S.Yan, Effect of fiber molecular weight on the interfacial morphology of iPP fiber/matrix single polymer composites, Macromolecules 2006, 39, 1087-1092

23. Huihui Li, Shidong Jiang, Jijun Wang, Dujin Wang, and Shouke Yan, Optical Microscopic Study on the Morphologies of Isotactic Polypropylene Induced by Its Homogeneity Fibers, Macromolecules; 2003; 36(8) pp 2802 - 2807
24. Huihui Li, Xiuqin Zhang, Yongxin Duan, Dujin Wang, Lin Li and Shouke Yan, Influence of crystallization temperature on the morphologies of isotactic polypropylene single-polymer composite, Polymer, Volume 45, Issue 23, October 2004, Pages 8059-8065
25. P.Rojanapitayakorn, P.T.Mather, A.J.Goldberg, R.A.Weiss, Optically trnsparent self-reinforced poly(ethylene terephthalate) composites: molecular orientation and mechanical properties, Polymer 46(2005) 761-773
26. D.M.Rein, L.Vaykhansky, R.L.Khalfin and Y. Cohen, Controlling the properties of single-polymer composites by surface melting of the reinforcing fibers, Polym. Adv. Technol. 13, 1046-1054 (2002)
27. Puente Orench, F.J.Balta Calleja, P.J.Hine, I.M.Ward, A microindentation study of polyethylene composites produced by hot compaction, Journal of applied Polymer Science, Vol.100, 1659-1663 (2006)
28. M.J.Jenkins, P.J.Hine, J.N.Hay, I.M.Ward, Mechanical and acoustic frequency responses in flat hot compacted polyethylene and polypropylene panels, Journal of Applied Polymer Science, Vol.99, 2289-2796(2006)
29. P. J. Hine, A. Astruc, I. M. Ward, Hot compaction of polyethylene naphthalate, Journal of Applied polymer science, Vol. 93, 796-802 (2004)
30. Li, R., Nagarajan, P., Yao, D., American International Mechanical Engineering Congress, Accepted, 2006.

31. T.Niemelä, H.Niiranen, M.Kellomäki, P.Törmälä, Self-reinforced composites of bioabsorbable polymer and bioactive glass with different bioactive glass contents. Part I: Initial mechanical properties and bioactivity, Acta Biomaterialia 1 (2005) 235-242
32. Debra D. Wright-Charlesworth, Julia A.King, Darinda M. Miller, Cho Hui Lim, In vitro flexural properties of hydroxyapatite and self-reinforced poly(L-lactic acid), Journal of biomedical materials research. Part A, 2006, vol. 78, no3, pp. 541-549
33. T.Niemelä, Effect of β-tricalcium phosphate addition on the in vitro degradation of self-reinforced poly-L,D-lactide, Polymer Degradation and Stability 89 (2005) 492-500
34. Gilbert, J. L., Ney D. S., Lautenschlager, E. P., Biomaterials, Vol. 16, No. 14, September 1995, pp1043-1055.
35. Wright, D. D., Lautenschlager, E. P., Gilbert, J. L., J. Biomedical Materials Research, Vol. 36, No. 4, September 1997, pp441-453.
36. Wright, D. D. Gilbert, J. L., Lautenschlager, E. P., J. Mater. Sci.: Materials in Medicine, Vol. 10, No. 8, August 1999, pp503-512.
37. Nektaria-Marianthi Barkoula, Ton Peijs, Tilo Schimanski, Joachim Loos, Processing of single polymer composites using the concept of constrained fibers, Polymer Composites, Volume 26, Issue 1, 2005, Pages 114 - 120
38. R.J. Yan, P.J. Hine, I.M. ward, R.H. Olley and D.C. Bassett, J. Mater. Sci., 1997, 32, 4821.

39. J. Rasburn, P.J. Hine, I.M. Ward, R.H. Olley, D.C. Bassett and M.A. Kabeel, J. Mater. Sci, 1995, 30, 615.
40. I.M. Ward and P.J. Hine, Polym. Eng. Sci., 1997, 37, 1809.
41. P.J. Hine, I.M. Ward, N.D. Jordan, R. Olley and D.C. Bassett, Polymer, 2003, 44, 1117.
42. N.D. Jordan, D.C. Bassett, R.H. Olley, P.J. Hine and I.M. Ward, Polymer, 2003, 44, 1143.
43. Olley RH, Bassett DC, Hine PJ, Ward IM. J Mater Sci 1993;28:1107.
44. Kabeel MA, Bassett DC, Olley RH, Hine PJ, Ward IM. J Mater Sci 1994;29:4694.
45. Hine PJ, Ward IM, Jordan ND, Olley RH, Bassett DC. J Macromol Sci-Phys B 2001; 40:959.
46. Hine PJ, Ward IM. J Appl Polym Sci 2003; in press.
47. Hine PJ, Ward IM, Teckoe J. J Mater Sci 1998;33:2725.
48. www.curveonline.com
49. C.M.W. Bastiaansen and P.J. Lemstra, Macromolecular Chemistry, Macromolecular Symposium, 1989, 28, 73.
50. J. Loos, T. Schimanski, J. Hofman, T. Peijs, and P.J. Lemstra, Polymer, 2001, 42 (8) 3827.
51. Ton Peijs, Composites for recyclability, Materialstoday, April 2003, pp 30-35.
52. Lacroix, F. v., Werwer, M., Schulte, K,, A new technique for preparation of polyethylene matrix composite and resulting mechanical properties, ICCM-11, 1997, pp. VI, 279-287.

53. Schulz, E. and Hirte, R., Bildung strukturierter Polyethylen-Schichten auf hochgeordneten Polyethylen-Fäden. Acta Polym., 1988, 39, 177-183.

54. Jukkalapartio, K., Laitinen, O., Partio, E. K., Vasenius, J., Pohjonen, T., Tormala, P., Rokkanen, P., J. Orthopaedic Research, Vol. 15, No. 1, January 1997, pp124-127.

55. Hameed, T., Hussein, I. A., Macromol. Mater. Eng., Vol. 289, No. 2, February 2004, 198-203.

56. P.-E. Bourban, A. Bogli, F. Bonjour, and J.-A. E. Månson, Compos. Sci. Technol., 58, 633-637 (1998).

57. F.Yang and R. Pitchumani, Interlaminar contact development during thermoplastic fusion bonding, Polymer Engineering and Sceince, February 2002, Vol.42, No.2, 424-438

58. P. G. De Gennes, C. R. Acad Sc. Paris B, 291. 219-221 (1980).

59. H.-H. Kausch, Polymer fracture, Springer-Verlag (1987).

60. K. Jud and H. H. Kausch, Polym. Bull., 1, 697-707 (1979).

61. K. Jud, H. H. Kausch, and J. G. Williams, J. Mat. Sci., 16, 204-210 (1981).

62. S. Prager and M. Tirrell, J. C h a Phys., 76, 5194-5198 (1981).

63. Y. H. Kim and R. P. Wool, Macromolecules, 16, 1115-1120 (1983).

64. R. P. Wool, Polymer lnterfaces: Structure and Strength,Hanser (1995).

65. Kim, Y.H., Wool, R.P., 1983. A Theory of healing at a polymer-polymer interface. Macromolecules 16, 1115-1120.

66. Wool, R.P, O'Connor, K.M, 1981. A theory of crack healing in polymers. Journal of applied physics 52, 5953-5963

67. Wool, R.P, O'Connor, K.M, 1982. Time dependence of crack healing. Journal of polymer science: Polymer letters edition 20, 7-16.
68. C. Ageorges and L. Ye, Fusion bonding of polymer composites: from basic mechanisms to process optimization, London ; New York : Springer, c2002, Chapter 4.
69. Prager, S, 1981. The healing process at polymer-polymer interfaces. The journal of chemical physics 75, 5194-5198.
70. Dara, P.H., Loos, A.C., 1987. Processing of thermoplastic matrix composites, Review of progress in quantitative nondestructive evaluation 6B, 1257-1265.
71. Lee, W.I., Springer, G.S., 1987. A model of the manufacturing process of thermoplastic matrix composites. Journal of composite materials 21, 1017-1055.
72. Mantell, S.C., Springer, G.S., 1992. Manufacturing process model for thermoplastic composite materials, Journal of composite materials 26, 2348-2378.
73. Bastien, L.J., Gillespie Jr, J.W., 1991. A non-isothermal healing model for strength and touphness of fusion bonded joints of amorphous thermoplastics. Polymer engineering and science 31, 1721—1730.
74. De Gennes, P.G., 1971. Reptation of a polymer chain in the presence of fixed obstacles. Journal of chemical physics 55, 572-579.
75. Wool, R.P., Yuan, B.-L., McGAREL, O.J., 1989), Welding of polymer interfaces. Polymer engineering and science 29, 1340-1367.
76. Velisaris, C.N., Seferis, J.C., 1986. Crystallisation kinetics of polyetheretherketone (PEEP) MATRICES. Polymer engineering and science 26, 1574-1581.

77. Corrigan, E., Leach, D., McDaniels, T., 1989. The influence of processing conditions on the properties of PEEK matrix composites. In: Benson, S., Cook, T., Trewin, E., Turner, R.M. (Eds), Materials and processing-Move into 90's. Elsevier Science Publisher B.V., Amsterdam, 121-131.
78. Motz, H., Schultz, J.M., 1989a. The solidification of PEEK. Part I. Morphology. Journal of thermoplastic composite materials 2, 248-266.
79. Motz, H., Schultz, J.M., 1989b. The solidification of PEEK. Part II. Kinetics. Journal of thermoplastic composite materials 2, 267-280.
80. Avarami, M.K. Kinetics of Phase Change. I. General Theory. Journal of Chemical Physics 7, 1939, 1103-1112
81. Avaramim M.K. Kinetics of Phase Change. II. Transformation-Time Relations for Random Distribution of Nucei, Journal of Chemical Physics 8, 1940, 212-224.
82. Avrami, M.K., Kinetics of Phase Change. III. Granulation, Phase Change, and Microsturcture. Journal of Chemical Physics 9, 1941, 177-184.
83. Ozawa T. Kinetics of non-isothermal crystallization. Polymer 1971;12:150-8.
84. Franbourg A, Rietsch F. Crystallization Behaviour of PEEK as a Function of The Melt Temperature, Composes Macromoleculaires Organiques. Ann Chim Fr 1990;15:367-80.
85. LeeWI, Springer; GS. A model of the manufacturing process of thermoplastic matrix composites. J Compos Mater 1987;21:1017-55.
86. Mantell SC, Springer GS. Manufacturing process model for thermoplastic composite materials. J Compos Mater 1992;26:2348-78.

87. Velisaris CN, Seferis JC. Crystallisation kinetics of polyetheretherketone (PEEK) matrices. Polym Engng Sci 1986;26:1574-81.

88. Seferis JC, Velisaris CN. Modeling±processing±structure relationships of polyetheretherketone (PEEK) based composites. Proceedings of the 31st International SAMPE Symposium, 1986. p. 1236-52.

89. Choe CR, Lee KH. Non-isothermal crystallization kinetics of poly-(etheretherketone) (PEEK). Polym Engng Sci 1989;29:801-5.

90. Tobin MC. Theory of phase transition kinetics with growth site impingement. I. Homogeneous nucleation. J Polym Sci, Polym Phys Ed 1974;12:399-406.

91. Tobin MC. Theory of phase transition kinetics with growth site impingement. II. Heterogeneous nucleation. J Polym Sci, Polym Phys Ed 1976;14:2253-7.

92. Tobin MC. Theory of phase transition kinetics with growth site impingement. III. mixed heterogeneous-homogeneous nucleation and nonintegral exponents of the time. J Polym Sci, Polym Phys Ed 1977;15:2269-70.

93. D. D. Wright, J. L. Gilbert and E. P. Lautenschlager, J. Mater. Sci.: Materials in Medicine, 10, 503 (1999).

94. Icenogle RD. Temperature-dependent melt crystallization kinetics of poly(butene-1): a new approach to the characterization of the crystallization kinetics of semicrystalline polymers. J Polym Sci, Polym Phys Ed 1985;23:1369-91.

95. Maffezzoli AM, Kenny JM, Nicolais L. Welding of PEEK/carbon fiber composite laminates. SAMPE J 1989;25(1):35-9.

96. Maffezzoli AM, Kenny JM, Nicolais L. Modelling of thermal and crystallization behavior of the processing of thermoplastic matrix composites. Materials and Processing Ð Move into the 90's, 1989. p. 133-43.

97. Ahmed I. Abou-Kandil, Alan H. Windle, The morphology of 50% PET/PEN random copolymer as revealed by high resolution scanning electron microscopy and X-ray diffraction, Polymer 48 (2007) 4824-4836

98. Keller A, Martuscelli E, Priest DJ, Udagawa Y. Journal of Polymer Science Part A2 1807;9:1971.

99. Olley RH, Bassett DC. Polymer 1982;23:1707.

100. Olley RH, Bassett DC, Blundell DJ. Polymer 1986;27:344.

101. Starosta W, Wawszczak D, Sartowska B, Buckzkowski M. Radiation Measurements 1999;31:149.

102. Bartosiewick L, Mencik Z. Journal of Polymer Science, Polymer Physics Edition 1974;12:1163.

103. Bu HS, Cheng SZD, Wunderlich B. Polymer 1988;29:1603.

104. R. H. Olley and D. C. Bassett, Polymer, 23, 1707 (1982).

105. D. C. Bassett, in Comprehensive Polymer Science, Vol. 1 (G. Allen and J. C. Bevington, Eds.), Pergamon, Oxford, England, 1989, pp. 841–866.

106. S. D. Hudson and A. J. Lovinger, Polymer, 34, 1123 (1993).

107. M. J. Collins, S. H. Zeronian, and M. Semmelmeyer, J. Appl. Polym. Sci., 42, 2149 (1991).

108. Farrow G, Ravens DAS, Ward IM. Polymer 1962;3:17.

109. Duong DT, Bell JP. Journal of Polymer Science, Polymer Physics Edition 1975;13:765.
110. Arnett EM, Miller JG, Day AR. Journal of the American Chemical Society 1950;72:5634.
111. Li XH, Guo WH, Wu CF, The nucleation effect of grafted carbon black on crystallization of Poly(Ethylene terephthalate)/grafted carbon black composite, JOURNAL OF MACROMOLECULAR SCIENCE PART B-PHYSICS Volume: 46 Issue: 4 Pages: 761-774
112. Miyagi, A. and Wunderlich, B. J. Polym. Sci., Polym. Phys. Edn 1972, 10, 2072
113. Miyagi, A. and Wunderlich, B. J. Polym. Sci., Polym. Phys. Edn 1972, 10, 2085
114. Lang M, Glasmacher UA, Moine B, Neumann R, Wagner GA, Etch-pit morphology of tracks caused by swift heavy ions in natural dark mica, Journal of Polymer Science Part B: Polymer Physics, Volume 40, Issue 1 (p 124-133)
115. CAGIAO ME, CALLEJA FJB, VANDERDONCKT C, et al., Study of the morphology of semicrystalline poly(ethylene terephthalate) by hydrolysis etching, POLYMER Volume: 34 Issue: 10 Pages: 2024-2029 Published: 1993
116. Olley, R. H. Sci Prog Oxford 1986, 70, 17–43.
117. Chung JW, Son SB, Chun SW, et al., Nonisothermal crystallization behavior of exfoliated poly(ethylene terephthal ate)-layered silicate nanocomposites in the presence and absence of organic modifier, Journal of Polymer Science Part B: Polymer Physics, Volume 46, Issue 11 (p 989-999)

118. Hwang SY, Lee WD, Lim JS, et al., Dispersibility of clay and crystallization kinetics for in situ polymerized PET/pristine and modified montmorillonite nanocomposites, Journal of Polymer Science Part B: Polymer Physics, Volume 46, Issue 11 (p 1022-1035)

119. Gao X, Liu RG, Zhang J, et al., Crystallization behaviors of poly(ethylene 2,6-naphthalate) in the presence of liquid crystalline polymer, INDUSTRIAL & ENGINEERING CHEMISTRY RESEARCH Volume: 47 Issue: 8 Pages: 2590-2596

120. Li XH, Guo WH, Wu CF, The nucleation effect of grafted carbon black on crystallization of Poly(Ethylene terephthalate)/grafted carbon black composite, JOURNAL OF MACROMOLECULAR SCIENCE PART B-PHYSICS Volume: 46 Issue: 4 Pages: 761-774

121. Kawahara Y, Yoshioka T, Tsuji M, Ohara M, Kohjiya S, Kikutani T, Transmission electron microscopic investigation of the morphology of high-speed spun poly(ethylene terephthalate) fibers, Journal of Macromolecular Science, Part B, Volume 39, Issue 5 & 6 November 2000 , pages 701 – 710

122. N. J. Capiati, R. S. Porter, J. Mater. Sci., 10, 1671 (1975).

123. W. T. Mead, R.S. Porter, J. Applied Polym. Sci., 22, 3249 (1978).

124. M. Mosleh, N. P. Suh, J. Arinez, Composites Part A, 29A, 611 (1998).

125. M. Deng, S. W. Shalaby, Biomaterials, 18, 645 (1997).

126. F. V. Lacroix, M. Werwer, K. Schulte, Composites Part A, 29A, 371 (1998).

127. A. Teishev, S. Incardona, C. Migliaresi, G. Marom, J. Applied Polym. Sci., 50, 503 (1993).

128. E. Devaux, C. Caze, Composites Sci. Techno., 59, 879 (1999).

129. T. Hameed, I. A. Hussein, Macromol. Mater. Eng., 289, 198 (2004).

130. S. Houshyar and R. A. Shanks, Macromol. Mater. Eng., 288, 599 (2003).

131. P. J. Hine, I. M. Ward, R. H. Olley, D. C. Bassett, J. Mater. Sci., 28, 316 (1993).

132. P. J. Hine, I. M. Ward, N. D. Jordan, R. H. Olley, D. C. Bassett, J. Macromol. Sci. Phys., B40, 959 (2001).

133. P. J. Hine, I. M. Ward, N. D. Jordan, R. H. Olley, D. C. Bassett, Polymer, 44, 1117 (2003)

134. P. J. Hine, I. M. Ward, J. Appl. Polym. Sci., 91, 2223 (2004).

135. I. M. Ward, P. J. Hine, Polymer, 45, 1413 (2004).

136. F. Yang and R. Ritchumani, Polymer Composites, 24, 263 (2003).

137. Ming-Ya Tang, Soojaa L Kim, Poly(ethylene terephthalate)-solvent interaction: Gelation and melting point depression, Polymer Engineering and Science, Nov 1994; Vol.34, No.22, 1656-1663

138. Alexander, L. E. X-ray Diffraction Methods in Polymer Science; Wiley-Interscience: New York, 1969; p 137.

139. Daubney, R. P.; Bunn, C. W.; Brown, C. J. Proc R Soc London 1954, 226, 531.

140. Auriemma, F.; Guerra, G.; Parravicini, L.; Petraccone, V. J Polym Sci B 1995, 33, 1917.

141. Dumbleton, J. H.; Bowles, B. B. J Polym Sci A-2 1966, 4, 951.

142. Fontaine, F.; Ledent, J.; Groeninckx, G.; Reymaers, H. Polymer 1982, 23, 185.

143. Kitano, Y.; Kinoshita, Y.; Ashida, T. Polymer 1995, 36(10), 1947.

144. Makarewicz, P. J.; Wilkes, G. L. J Polym Sci Polym Phys Ed 1978, 16, 1529.

145. Jameel, H.; Noether, H. D.; Rebenfeld, L. J Appl Polym Sci 1982, 27, 773.

146. K. K. CHAWLA, On the Applicability of the "Rule-of-Mixtures" to the Strength Properties of Metal-Matrix Composites, Revista Brasileira de Física, Vol. 4, N.o 3, 411-418, 1974

147. Dae Hwan Cho, Woong-Ryeol Yu, Ji Ho Youk and Jae Heung Yoo, Formation of micro-crystals in poly(ethylene terephthalate) fiber by a short heat treatment and their influence on the mechanical properties, European Polymer Journal Volume 43, Issue 8, August 2007, Pages 3562-3572

148. S. Fakirov, Polyethylene terephthalate in: O. Olabisi (Ed.), Handbook of Thermoplastics, Marcel Dekker, New York, 1994, p. 451.

149. S.A. Jabarin, Crystallization kinetics of polyethylene terephthalate, I. Isothermal crystallization from the melt, Journal of Applied Polymer Science 34 (1987) 85–96.

150. Alexander, L. E. X-ray Diffraction Methods in Polymer Science; Wiley-Interscience: New York, 1969; p 137.

151. Daubney, R. P.; Bunn, C. W.; Brown, C. J. Proc R Soc London 1954, 226, 531.

152. Auriemma, F.; Guerra, G.; Parravicini, L.; Petraccone, V. J Polym Sci B 1995, 33, 1917.

153. Grimm RA. Welding processes for plastics. Adv Mater Process 1995;147:27-30.

154. Stokes VK. Joining methods for plastics and plastic composites: an overview. Polym Engng Sci 1989;29:1310-24.

155. P.-E. Bourban, A. Bogli, F. Bonjour, and J.-A. E. M h -son, Compos. Sci Technol., 58, 633-637 (1998).

156. Benatar, A. and Gutowski, T.G. (1986). Methods for Fusion Bonding Thermoplastic Composites, SAMPE Quarterly. 18(1): 35–42.

157. Stokes, V.K. (1989). Joining Methods for Plastics and Plastic Composites: An Overview, Polymer Engineering and Science, 29(19): 1310–1324.

158. Wedgewood, R. and Hardy, P.E. (1996). Induction Welding of Thermoset Composite Adherends using Thermoplastic Interlayers and Susceptors, 28th International SAMPE Technical Conference, pp. 850–861.

159. Ali Yousefpour, Mehdi Hojjati and Jean-Pierre Immarigeon, Fusion Bonding/Welding of Thermoplastic Composites, Journal of Thermoplastic composite materials, Vol. 17—July 2004

160. P. G. De Gennes, C. R. Acad Sc. Paris B, 291. 219-221 (1980).

161. H.-H. Kausch, Polymerfracture, Springer-Verlag (1987).

162. K. Jud and H. H. Kausch, Polym. Bull., 1, 697-707 (1979).

163. K. Jud, H. H. Kausch, and J. G. Williams, J. Mat. Sci.. 16, 204-210 (1981).

164. S. Prager and M. Tirrell, J. C h a Phys., 76, 5194-5198 (1981).

165. Y. H. Kim and R. P. Wool, Macromolecules, 16, 1115-1120 (1983).

166. R. P. Wool and K. M. O'Connor, J. Appl. Phys., 52, 5953-5963 (1981).

167. R. P. Wool, Polymer lnterfaces: Structure and Strength, Hanser (1995).

168. J. L. Gilbert, D. S. Ney and E. P. Lautenschlager, Biomaterials, 16, 1043 (1995).

169. R. B. Bird, W. E. Stewart, and E. N. Lightfoot, Transport Phenomena, pp. 354-357, John Wiley, New York, 1960.

170. H. S. Carslaw and J. C. Jaeger, Conduction of Heat in Solids, 2nd edition, p. 100, Clarendon Press, Oxford, 1959.

171. Gfeller B, Properzi M, Zanetti M, et al., Wood bonding by mechanically-induced in situ welding of polymeric structural wood constituents, JOURNAL OF APPLIED POLYMER SCIENCE Volume: 92 Issue: 1 Pages: 243-251 Published: APR 5 2004
172. SANG-GOOK KIM and NAM P. SUH, Performance Prediction of Weld line Structure in Amorphous Polymers, POLYMER ENGINEERiNG AND SCIENCE, SEPTEMBER, 1986, Vol. 26, No. 17, P1200-1207
173. S. C. Malguarnera and A. Manisali. Polym. Eng. Sci., 21, 586 (1981).
174. S. B. Hardenbrook and J. A. Schnall, Use of Tensile Test to Relate Melt Weldline Strength to Injection Molding Process Variables. M Eastman Kodak Report. MIDR-12-79.
175. E. M. Hagerman. Plastics Eng., 29, 67 (1973).
176. S. Y. Hobbs. Polym. Eng. Sci., 14, 621 (1974).
177. R. Li and D. Yao, “Preparation of single poly(lactic acid) composites”, J. Applied Polymer Science, 2007, Volume 107, Issue 5 , Pages 2909 - 2916
178. D. Yao, R. Li, and P. Nagarajan, "Single-Polymer Composites Based on Slowly Crystallizing Polymers", Polymer Engineering and Science, Vol. 46, No. 9, pp. 1223-1230 (2006).
179. R. L. Cormia, F. P. Price, and D. Turnbull, J. Chem. Phys. 37, 1333 (1962).
180. Ma Y, Zha LY, Hu WB, et al., Crystal nucleation enhanced at the diffuse interface of immiscible polymer blends, PHYSICAL REVIEW E 77, 061801 (2008)

181. Hatsuo Ishida and Philippe Bussi, Surface-Induced Crystallization in Ultrahigh-Modulus Polyethylene Fiber Reinforced Polyethylene Composites, Macromolecules 1991,24, 3569-3577

182. D. R. Norton and A. Keller, Polymer, 26,704 (1985).

183. Chi Wang and L. M. Hwang, Transcrystallization of PTFE Fiber/PP Composites (I) Crystallization Kinetics and Morphology, Journal of Polymer Science: Part B: Polymer Physics, Vol. 34, 47-56 (1996)

184. Chatterjee, A. M.; Price, F. P.; Newman, S. J. Polym. Sci. 1975, 13, 2369.

185. Weinhold, S.; Litt, M. H.; Lando, J. B. J. Appl. Phys. 1980,51, 5145.

186. Gray, D. G. J. Polym. Sci., Polym. Lett. Ed. 1974, 12, 509.

187. Hobbs, S. H. Nature Phys. Sci. 1971,234, 12.

188. Lovering, E. G. J. Polym. Sci., Part A-2 1970, 8, 1697.

189. M. J. Folkes and S. T. Hardwick, J. Mater. Sci. Letters, 6,656 (1987).

190. T. Hata, K. Ohsaka, T. Yamada, K. Nakamae, N. Shibata, and T. Matsumoto, Proc. 16th Annual Symposium, Adhesion Society, Williamsburg, VA, February 1993, pp. 180-183.

191. Kwei, T. K.; Schonhorn, H.; Frisch, H. L. J. Appl. Phys. 1967, 38,2512.

192. Matsuoka, S.; Daane, J. H.; Bair, H. E.; Kwei, T. K. J. Polym. Sa., Polym. Lett. Ed. 1968, 6, 87.

193. Bernhard Wunderlich, Macromolecular Physics, New York, Academic Press, Chapter IV, 1973

194. Kausch, H.-H. Polymer Fracture, 2nd ed.; Springer: Heidelberg, 1987.

195. Jud, K.; Kausch, H.-H. Polym Bull 1979, 1, 697.

196. Jud, K.; Kausch, H.-H.; Williams, J. G. J Mater Sci 1981, 16, 204.

197. Grewell D, Benatar A, Semi-empirical, squeeze flow and intermolecular diffusion model. I. Determination of model parameters, POLYMER ENGINEERING AND SCIENCE Volume: 48 Issue: 5 Pages: 860-867

198. J.H. Perepezko, K. Hildal, Metallic glass formation reactions and interfaces, Materials Science and Engineering B 148 (2008) 171–178.

199. M.H.Hartmann, Springer-Verlag, Berlin, 367-411 (1998).

200. M.Spinu, C.Jackson, M.Y.Kearing, and K.H.Gardner, Journal of Macromolecular Science- Pure and Applied Chemistry, A33 (10), 1497-1530 (1996).

201. H. Tsuji, Y. Ikada, Trends in Polym. Sci., 4, 27 (1999).

202. Y. Ikaka, K. Jamshidi, H. Tsuji, S. Hyon, Macromolecules, 20, 904 (1987).

203. H Tsuji, Res. Adv. in Macromolecules, 1, 25 (2000).

204. Eling, B.; Gogolewski, S.; Pennings, A. J. Polymer, 23, 1587(1982).

205. S. J. Holland, B. J. Tighe, ‘‘Biodegradable Polymers’’, in: Advances in Pharmaceutical Sciences, 1st edition, Academic Press London, London, 101–165(1992).

206. V. Gewin, PLoS Biol., 1, 15 (2003).

207. D. J. Sawyer, Macromol. Symp., 201, 271 (2003).

208. J. R. Dorgan, H. J. Lehermeier, L.-I. Palade, J. Cicero, Macromol. Symp., 175, 55 (2001).

209. J.-C. Bogaert, P. Coszach, Macromol. Symp., 153, 287 (2000).

210. N. Whiteman, ‘‘2000 Polymers, Laminations and Coatings Conference’’, Chicago, 631–635 (2000).

211. J. B. Snook, M.Sc. Thesis, Michigan State University, East Lansing, 130 (1994).

212. C. Migliaresi, A. De Lollis, L. Fambri, D. Cohn, Clin. Mater., 8, 111 (1991).

213. M. Hiljanen-Vainio, P. Varpomaa, J. Seppala, P. Tormala, Macromol. Chem. Phys., 197, 1503 (1996).

214. G. Perego, G. D. Cella, C. Bastioli, Polymer, 59, 37 (1996).

215. H. Cai, V. Dave, R. Gross, S. P. McCarthy, J. Polym. Sci., Part B: Polym. Phys., 34, 2701 (1996).

216. H. Tsuji, Y. Ikada, Macromol. Chem. Phys., 197, 3483 (1996).

217. J.-R. Sarasua, R. E. Prud’homme, M. Wisniewski, A. Le Borgne, N. Spassky, Macromolecules, 31, 3895 (1998).

218. H. Tsuji, Y. Ikada, Polymer, 36, 2709 (1995).

219. T. Miyata, T. Masuko, Polymer, 39, 5515 (1998).

220. Di Lorenzo, M. L. European Polymer Journal 2005, 41, 569.

221. Yasuniwa, M.; Tsubakihara, S.; Iura, K. Polymer 2006, 47, 7554.

222. Garlotta, D. J Polym Environ 2001, 9, 63.

223. Auras, R.; Harte, B.; Selke, S. Macromol Biosci 2004, 4, 835.

224. Farrington, D.W.; Lunt, J.; Davies, S; Blackburn, R. S. In Biodegradable and Sustainable Fibers, Blackburn, R. S., Ed.; Woodhead Publishing Limited: Cambridge, England, 2005, Chap. 6, pp. 191-220.

VITA

RUIHUA LI (JESSICA)

RUIHUA LI was born in China. She received a Bachelor degree in Applied chemistry from Harbin Institute of Technology, Harbin, China in 2000 and a Master degree in Materials from Harbin Institute of Technology, Harbin, China in 2002. She joined in Georgia Tech in the fall of 2004 and pursued a doctorate in Polymer.